TP 6308 E

THE EFFECT OF GEOGRID REINFORCEMENT ON THE STABILITY OF EMBANKMENTS ON A SOFT SENSITIVE CHAMPLAIN CLAY DEPOSIT

Prepared for

TRANSPORTATION DEVELOPMENT CENTRE

by

Library and Information Centre
Centre de Documentation (GSL)
RECEIVED – REÇU LE
NOV 25 1985
Government Publication Officielle
Transport Canada / Transports Canada

GOLDER ASSOCIATES
Consulting Geotechnical and
Mining Engineers

UNIVERSITÉ LAVAL
Faculté des Sciences
et de Génie

October 1985

PROJECT TEAM

The project team for this study comprised:

GOLDER ASSOCIATES

Mr. J. R. Busbridge
Mr. P. Chan
Dr. D. D. Dubois
Mr. V. Milligan
Ms. A. S. Poschmann

UNIVERSITE LAVAL

Prof. P. La Rochelle
Mr. D. LeFebvre

ACKNOWLEDGEMENTS

The authors wish to acknowledge and thank the four sponsoring agencies of the federal government who, collectively, made this study possible:

Supply and Services Canada, Unsolicited Proposals Fund
Transport Canada, Transportation Development Centre
National Research Council Canada, Division of Building Research
Energy, Mines and Resources Canada, Canadian Centre for Mineral and Energy Technology.

The authors also appreciate the assistance provided by the Steering Committee, particularly their comments on the draft final reports. Members included:

W.J. Eden, J.H.L. Palmer - NRC
Grant Feasby - CANMET
Wayne Rowan - TDC

"The contents of this report reflect the views of the contractor and not necessarily the official views or policies of the Transportation Development Centre".

REPORT DOCUMENTATION FORM

1. Transport Canada Report No.
TP 6308E

2. TDC Project No.
6159, 6160, 6161, 6162

3. Recipient's Catalogue No.

4. Title and Subtitle
The Effect of Geogrid Reinforcement on the Stability of Embankments on a soft sensitive Champlain Clay Deposit.

5. Report Date
October 1985

6. Performing Organization Report No.
841-1083

7. Author(s)
Busbridge, J.R., Chan, P., Milligan, V. (Golder Associates)
La Rochelle, P.R., Lefebvre, L.D. (Université Laval)

8. Transport Canada File No.
D1465-437

9. Performing Organization Name and Address

Golder Associates
3151 Wharton Way
Mississauga, Ontario
L4X 2B6

Université Laval
Faculté Des Sciences et de Génie
Cité Universitaire
Quebec, G1K 7P4

10. DSS File No.
11 SD.T8200-3-3586

11. DSS or Transport Canada Contract No.
1SD84-0029

12. Sponsoring Agency Name and Address
Transportation Development Centre (TDC)
1000 Sherbrooke St.W. Suite 2421, Montreal, Quebec H3A 2R3
Supply and Services Canada
Energy, Mines and Resources Canada
National Research Council Canada

13. Type of Report and Period Covered
Final

14. Sponsoring Agency Code
TDC 6159

15. Supplementary Notes
Summary Report is available in English and in French

16. TDC Project Officer
Wayne Rowan

17. Abstract

Three instrumented test embankments were constructed to failure at a site in St. Alban, Quebec, in order to study the effect of geogrid reinforcement on the stability of embankments on a soft sensitive clay deposit. The geogrid, Tensar SR-2, was incorporated in the base of two of the three embankments using different configurations. One of the embankments was reinforced with two horizontal layers (strips) of geogrid, while the other was reinforced with an equal quantity of geogrid, constructed to form a sand filled cellular structure. The interpretation of monitoring results provides a comparison of the foundation response, and the performance of the geogrid up to and immediately prior to failure. The forces mobilized at failure were examined by back analyses of the failed embankments using limit equilibrium methods. These analyses indicated that the reinforcement caused improvements in failure heights of about 34 and 17.5 per cent in the strip and geocell reinforced embankments, respectively. The significant effect of the crust strength in the prediction of failure heights of the test embankment is identified in the study. It is further concluded that there is no direct evidence to show that the geogrid has a beneficial effect on the redistribution of stresses in the foundation, nor in retarding the propagation of local failed zones prior to failure. Its apparent effect is to maintain the integrity of the fill and allow more extensive propagation of failed zones, before a general failure state is achieved in the foundation.

18. Key Words
Soil Stabilization, Earthfills, Field Tests, instrumentation, clays, sensitivity, Detailed Field Performance Data, Stability Analysis

19. Distribution Statement
A limited number of copies are available from the Transportation Development Centre.

20. Security Classification (of this report)
Unclassified

21. Security Classification (of this page)
Unclassified

22. No. of Pages
277

23. Price
-

FORMULE DE DOCUMENTATION POUR RAPPORT

1. Nº du rapport Transports Canada
TP 6308E

2. Nº de l'étude — CDT
6159, 6160, 6161, 6162

3. Nº de catalogue du destinataire

4. Titre et sous-titre
The Effect of Geogrid Reinforcement on the Stability of Embankments of a soft sensitive Champlain Clay Deposit.

5. Date du rapport
Octobre 1985

6. Nº du rapport de l'organisme exécutant
841-1083

7. Auteur(s)
Busbridge, J.R., Chan, P., Milligan, V. (Golder Associates)
La Rochelle, P.R., Lefebvre, L.D. (Université Laval)

8. Nº de dossier Transports Canada
D1465-437

9. Nom et adresse de l'organisme exécutant

Golder Associates
3151 Wharton Way
Mississauga, Ontario
L4X 2B6

Université Laval
Faculté Des Sciences et De Génie
Cité Universitaire
Quebec, G1K 7P4

10. Nº de dossier — ASC
11 SD.T8200-3-3586

11. Nº de contrat — ASC ou Transports Canada
1SD84-0029

12. Nom et adresse de l'organisme parrain
Centre de Développement des Transports (CDT)
1000 Ouest, Rue Sherbrooke, Suite 2421, Montréal, Québec H3A 2R3
Approvisionnements et Services Canada
Energie, Mines et Ressources Canada
Conseil National de Recherches Canada

13. Genre de rapport et période visée
Finale

14. Code de l'organisme parrain
CDT 6159

15. Remarques additionnelles
La rapport sommaire est disponible en français et anglais

16. Agent de projet — CDT
Wayne Rowan

17. Résumé

Trois remblais expérimentaux instrumentés ont été élevés jusqu'à rupture, à St-Alban (Québec), afin de connaître l'effet d'une armature en géotextile sur lar stabilité des remblais établis sur sol mou argileux. La géogrille utilisée, de marque Tensar SR-2, a été mise en place à la base de deux des trois remblais, selon deux configurations différentes. Le premier a reçu deux nappes horizontales de géogrille tandis que dans le deuxième, une même quantité de géogrille a servi à la réalisation d'une armature alvéolaire remplie de sable. L'interprétation des résultats des mesures a permis une appréciation comparative du comportement des assises et de l'action des armatures jusqu'à la rupture des remblais et immédiatement avant qu'elle ne survienne. Les forces en jeu à la rupture ont été analysées à posteriori par la méthode des états limites. On a pu constater que l'armature en nappe et l'armature alvéolaire ont permis d'augmenter la hauteur de rupture des remblais par environ 34 et 17,5%, respectivement. L'étude a mis en évidence l'importance de prendre en compte la résistance de la croûte d'argile dans la prédiction des hauteurs de rupture. Par contre, elle n'a pu trouver de preuve directe indiquant que la géogrille aurait une influence positive par la redistribution des contraintes dans l'assise des remblais, et qu'il retarderait la propagation des ruptures localisées jusqu'à la rupture finale. Il semble qu'il ait pour effet de retarder l'échéance de la rupture généralisée tout en autorisant une propagation plus étendue des zones de rupture localisées.

18. Mots-clés
Stabilisation des sols, remblais de terre, essais in situ, instruments de mesure, argile, sensibilité, comportement in situ, analyse de stabilité.

19. Diffusion
Le CDT dispose d'un nombre limité d'exemplaires.

20. Classification de sécurité (de ce rapport)	**21. Classification de sécurité (de cette page)**	**22. Nombre de pages**	**23. Prix**
Non classifié	Non classifiée	277	-

TABLE OF CONTENTS

Page No.

ABSTRACT iii

1.0 INTRODUCTION 1

2.0 BACKGROUND 7
- 2.1 LIMITATIONS OF CONVENTIONAL STABILITY ANALYSES 7
  - 2.1.1 Shearing Resistance 7
  - 2.1.2 Failure Mode 11
  - 2.1.3 Summary 11
- 2.2 SPECULATED EFFECT OF REINFORCING INCLUSIONS ON EMBANKMENT STABILITY 12
- 2.3 SITE SELECTION 15

3.0 GEOGRID REINFORCEMENT 17
- 3.1 SELECTION 17
- 3.2 PHYSICAL PROPERTIES 17

4.0 SITE DESCRIPTION AND SUBSURFACE INVESTIGATION 19
- 4.1 SITE DESCRIPTION 19
- 4.2 SUBSURFACE CONDITIONS 19
- 4.3 GEOTECHNICAL INVESTIGATION (1984) 22

5.0 EMBANKMENT DESIGN 24
- 5.1 METHODS OF SLOPE STABILITY ANALYSIS 24
- 5.2 SHEAR STENGTH PARAMETERS 26
- 5.3 DESIGN OF TEST EMBANKMENTS 28

6.0 INSTRUMENTATION 30
- 6.1 SUBSURFACE INSTRUMENTATION 31
  - 6.1.1 Piezometers 32
  - 6.1.2 Settlement Plates 34
  - 6.1.3 Monuments 34
  - 6.1.4 Inclinometers 35
  - 6.1.5. Vertical Extensometers 35
  - 6.1.6 Horizontal Extensometers 37
  - 6.1.7 Total Pressure Cells 38
- 6.2 GEOGRID INSTRUMENTATION 39
  - 6.2.1 Tensar Load Cell 39
  - 6.2.2 Bison Strain Gauges 41
  - 6.2.3 Differential Extensometer 43

7.0 CONSTRUCTION 44
- 7.1 STRIP REINFORCED EMBANKMENT 44
- 7.2 CONTROL EMBANKMENT 47
- 7.3 GEOCELL REINFORCED EMBANKMENT 47

TABLE OF CONTENTS (continued)

Page No.

8.0 MONITORING RESULTS 51
  8.1 CONTROL EMBANKMENT - TEST EMBANKMENT NO. 1 53
    8.1.1 Pore Pressures 53
    8.1.2 Vertical Deformations 55
    8.1.3 Horizontal Deformations 56
    8.1.4 Earth Pressures 58
  8.2 STRIP REINFORCED EMBANKMENT - TEST EMBANKMENT NO. 2 59
    8.2.1 Pore Pressures 59
    8.2.2 Vertical Deformations 60
    8.2.3 Horizontal Deformations 62
    8.2.4 Earth Pressures 63
    8.2.5 Geogrid Performance 64
  8.3 GEOCELL REINFORCED EMBANKMENT- TEST EMBANKMENT NO. 3 65
    8.3.1. Pore Pressures 65
    8.3.2 Vertical Deformations 66
    8.3.3 Horizontal Deformations 67
    8.3.4 Earth Pressures 68
    8.3.5 Geogrid Performance 69
  8.4 COMPARISONS OF EMBANKMENT BEHAVIOUR 70
    8.4.1 Pore Pressures 71
    8.4.2 Vertical Deformations 75
    8.4.3 Horizontal Deformations in Subsoil 75

9.0 OBSERVATIONS OF FAILURES 77
  9.1 STRIP REINFORCED EMBANKMENT 77
    9.1.1. Observations 77
    9.1.2 Post-failure Investigation 78
  9.2 CONTROL EMBANKMENT 79
    9.2.1 Observations 79
    9.2.2 Post-failure Investigation 80
  9.3 GEOCELL REINFORCED EMBANKMENT 81
    9.3.1 Observations 81
    9.3.2 Post-failure Investigation 82

10.0 PERFORMANCE OF THE REINFORCEMENT 83
  10.1 LIMIT EQUILIBRIUM ANALYSIS OF EMBANKMENT PERFORMANCE 83
  10.2 RATE OF STRAIN AND CAPACITY OF THE REINFORCEMENT UNDER EMBANKMENT LOADING 91
    10.2.1 Geocell Reinforced Embankment 92
    10.2.2 Strip Reinforced Embankment 95

TABLE OF CONTENTS (cont'd)

Page No.

11.0 DISCUSSIONS 97

In order following page 100

LIST OF REFERENCES

LIST OF SYMBOLS

FIGURES

APPENDIX A - Finite Element Analysis
APPENDIX B - Tensar Load Cell

LIST OF TABLES

No.		Page No.
3.1	Mechanical Properties of Tensar SR-2	18
6.1	Quantities of Installed Instrumentation	31
8.1	Number of Readings Taken During Construction	51
8.2	List of Figures Showing Data Recorded	52
10.1	Details of Failed Embankments	84
10.2	Factors of Safety for 1972 Embankment as Calculated by Stab	86
10.3	Factors of Safety for Unreinforced Embankments Assuming Mid-Depth Strength in Crust and $c_u = 0.9\ c_{u\ vane}$ Below Crust	89
10.4	Calculated Improvement in Failure Height and Force in Reinforcement at Failure	91

LIST OF FIGURES

1.1 Typical Stress-strain Behaviour of Clay (St. Alban)

1.2 Undrained Strength Stability Analysis

2.1 Basic Elements of Limit Equilibrium Stability Analysis

2.2 Factors Affecting Undrained Shear Strength

2.3 Definitions of Undrained Shear Strength at Failure

2.4 Speculated Effect of Geogrid on Shear Stress in Foundation

2.5 Speculated Effect of Geogrid on Shear Stress Distribution

2.6 Speculated Influence of Crust Thickness on Geogrid Effectiveness

3.1 Typical Dimensions of Tensar SR-2

3.2 Characteristic Strength of Tensar SR-2

4.1 Geographical Distribution of Sensitive Clays in Parts of Eastern Canada

4.2 Site Location Plan

4.3 Typical Soil Properties at St. Alban Test Site

4.4 Undrained Shear Strength Profiles

4.5 Field Test Location Plan

4.6 Embankment Layout and Site Contours

4.7 Field Vane Test Results (V-1 to V-10)

4.8 Field Vane Test Results (V-11 to V-15)

LIST OF FIGURES (cont'd)

4.9 Piezocone Test Results (P-1 and P-2)

4.10 Piezocone Test Results (P-3 and P-4)

4.11 Piezocone Test Results (P-5 and P-6)

5.1 Cohesion Circle Stability Analysis (BTENSAR)

5.2 Strength Profile and Assumptions

5.3 General Layout Plan

6.1 Instrumentation Layout, Control Embankment (No. 1)

6.2 Instrumentation Layout, Strip Reinforced Embankment (No. 2)

6.3 Instrumentation Layout, Geocell Reinforced Embankment (No. 3)

6.4 Sections of Piezometer Tips

6.5 Settlement Plate and Vertical Extensometer Assembly

6.6 Concrete Monument

6.7 Inclinometer Setup

6.8 Electrical Extensometer Sensor

6.9 Vertical and Horizontal Electrical Extensometers

6.10 Vertical Magnetic Extensometer

6.11 Specifications and Setup of Total Pressure Cell

6.12 Bison Strain Gauge Calibration Curve

6.13 Relative Location of Bison Strain Gauges

6.14 Details of Differential Extensometer

LIST OF FIGURES (cont'd)

7.1 Schedule of Field Work

7.2 Grain Size Distribution Curve of Fill Material

7.3 Placement and Instrumentation of Strip Reinforcement

7.4 Pictorials of Geocell Mattress and Bodkin Joint

7.5 Assembly of Geocell Mattress

7.6 Unit Weight Histograms, Embankments No. 1 and 2

7.7 Unit Weight Histogram, Embankment No. 3

7.8 Centreline Surcharge Versus Time

8.1 Pneumatic Piezometers No. 1, PN-2 to 8

8.2 Pneumatic Piezometers No. 1, PN-9 to 16

8.3 Hydraulic Piezometers No. 1, PN-1 to 10

8.4 Electrical Piezometer No. 1, PE-1

8.5 Settlement Plates No. 1, SP-1 to 11

8.6 Settlement of Monuments No. 1, MN-1 to 5

8.7 Settlement of Monuments No. 1, MN-1 to 14

8.8 Vertical Electrical Extensometers No. 1, VE-1 and 2

8.9 Vertical Electrical and Magnetic Extensometers No. 1, VE-3 and ME-1

8.10 Inclinometer Deflections No. 1, IN-1 and 2

8.11 Horizontal Displacement of Monuments No. 1, MN-2 to 10

8.12 Horizontal Displacement of Monuments No. 1, MN-11 to 14

8.13 Horizontal Extensometers No. 1, HE-1 and 2

8.14 Total Pressure Cells No. 1, TP-1 to 4

8.15 Pneumatic Piezometers No. 2, PN-1 to 8

LIST OF FIGURES (cont'd)

8.16 Pneumatic Piezometers No. 2, PN-9 to 16
8.17 Hydraulic Piezometers No. 2, PH-1 to 5
8.18 Electrical Piezometers No. 2, PE-1 and 2
8.19 Settlement Plates No. 2, SP-1 to 11
8.20 Settlement of Monuments No. 2, MN-6 to 14
8.21 Vertical Electrical Extensometers No. 2, VE-1 and 2
8.22 Vertical Electrical Extensometer No. 2, VE-3
8.23 Inclinometer Deflections No. 2, IN-1 and 2
8.24 Horizontal Displacement of Monuments No. 2, MN-1 to 10
8.25 Horizontal Displacement of Monuments No. 2, MN-11 to 14
8.26 Horizontal Extensometers No. 2, HE-1 and 2
8.27 Total Pressure Cells No. 2, TP-1 to 5
8.28 Tensar Load Cells No. 2, LC-1 and 2
8.29 Tensile Load Measured in Strip Reinforcements
8.30 Strain Measurements on Upper Layer of Strip Reinforcement
8.31 Pneumatic Piezometers No. 3, PN-1 to 8
8.32 Pneumatic Piezometers No. 3, PN-9 to 16
8.33 Hydraulic Piezometers No. 3, PH-1 to 10
8.34 Hydraulic Piezometers No. 3, PH-11 to 14
8.35 Electrical Piezometers No. 3, PE-1 to 4
8.36 Settlement Plates No. 3, SP-1 to 11
8.37 Settlement Plates No. 3, SP-12 to 18
8.38 Settlements of Monuments No. 3, MN-1 to 10

LIST OF FIGURES (cont'd)

8.39 Settlement of Monuments No. 3, MN-11 to 14

8.40 Vertical Electrical Extensometers No. 3, VE-1, and 2

8.41 Vertical Electrical Extensometer No. 3, VE-3

8.42 Inclinometer Deflections No. 3, IN-1 and 2

8.43 Horizontal Displacement of Monuments No. 3, MN-1 to 10

8.44 Horizontal Displacement of Monuments No. 3, MN-11 to 14

8.45 Horizontal Extensometers No. 3, HE-1 and 2

8.46 Total Pressure Cells No. 3, TP-1 to 4

8.47 Tensar Load Cells No. 3, LC-1 and 2

8.48 Tensile Loads in Geocell Reinforcement

8.49 Strain Measurements in Geocell Reinforcement

8.50 Strain Measurements in Geocell Reinforcement

8.51 Centreline Surcharge and Pore Pressure Response

8.52 Excess Pore Pressure Contours at Surcharge of 84 kPa

8.53 Excess Pore Pressure Contours at Surcharge of 90 kPa

8.54 Excess Pore Pressure Contours at Surcharge of 104 kPa

8.55 Pore Pressure Response of Piezometers PN-6 and 7

8.56 Pore Pressure Response of Piezometer PN-8

8.57 Comparison of Settlements at Centreline (SP-9)

8.58 Comparison of Deflection Profiles

8.59 Surcharge Versus Deflection at 5.5 m and 3 m Depths, IN-1

8.60 Surcharge Versus Deflection at 0.6 m Depth, IN-1

LIST OF FIGURES (cont'd)

9.1 Plan and Profiles of Failure, Strip Reinforced Embankment (No. 2)

9.2 Failure of Strip Reinforced Embankment (No. 2)

9.3 Piezocone Test Results (P-2.1 and P-2.2)

9.4 Piezocone Test Results (P-2.3 and P-2.4)

9.5 Piezocone Test Results (P-2.5)

9.6 Test Pit Log, Strip Reinforced Embankment

9.7 Plan and Profiles of Failure, Control Embankment (No. 1)

9.8 Failure of Control Embankment (No. 1)

9.9 Failure at Back of Control Embankment (No. 1)

9.10 Piezocone Test Results (P-1.1 and P-1.2)

9.11 Piezocone Test Results (P-1.3 and P-1.4)

9.12 Piezocone Test Results (P-1.5)

9.13 Piezocone Test Results (P-2.6 and P-2.7)

9.14 Post-Failure Vane Tests for Control Embankment (No. 1)

9.15 Plan and Profiles of Failure, Geocell Reinforced Embankment (No. 3)

9.16 Failure of Geocell Reinforced Embankment (No. 3)

9.17 Piezocone Test Results (P-3.1 and P-3.2)

9.18 Piezocone Test Results (P-3.3)

10.1 Average Vane Strength Profile in Failed Areas

10.2 Load-Strain Characteristics of Geocell Mattress

10.3 Summary of Stability Analyses

1.0 INTRODUCTION

Widespread areas in North America are underlain by soft clays. These materials are post-glacial, and of a lacustrine or marine origin. Because of varying depositional environments, there are significant differences in their composition and behavioural characteristics. For example, the marine clays are often highly sensitive and brittle and the lacustrine clays are generally varved or layered. The clays in the west central regions are often fissured and can contain a high proportion of swelling clay minerals.

Despite their varying compositions, most North American post-glacial soft clays are relatively sensitive, brittle soils which exhibit strain-softening behaviour. A marked example is the Champlain Sea clay in Eastern Canada. Natural processes such as aging, groundwater level changes and possibly cementation account for a light degree of overconsolidation, and their brittle/strain softening behaviour differentiates such soft clays from clays commonly occurring in many other areas of the world. These differences can be characterized by their stress-strain behaviour as shown on Figure 1.1. In the case of "brittle" clays, the response to loading in the field (i.e. porewater pressure response and dissipation rate, deformation and peak strength) is largely controlled by the small-strain behaviour of the soil.

Because of these behavioural characteristics, construction of embankment fills on these soils very often presents problems in terms of optimizing the geometry and construction costs. The need for flat side slopes and berms for stability of the foundation necessarily entails larger fill volumes, with consequent increased construction costs.

The rupture behaviour of soils can be reasonably represented by large strain criteria (eg. the Mohr-Coulomb criterion). In such cases, foundation performance and, hence, embankment geometry, can often be improved by stage loading techniques (in effect, the strength of the foundation soils can be measurably increased by decreasing the rate of load application). Unfortunately, time constraints on many projects preclude the use of stage loading.

Research efforts over the past 20 years have indicated that the fundamental technical issue in evaluating the stability and performance of embankments on brittle soft clays is the influence of the crustal materials, wherein natural weathering processes have increased the undrained shear strength. In natural deposits, this strength gain decreases with depth to a minimum value below the base of the crust. Preliminary work has suggested that the thickness and rigidity of these crustal soils influence the permissible embankment height and geometry. However, the effect of these parameters cannot be presently quantified since the specific problem has not been examined in any detail.

It is considered that the first step of any such examination should be an attempt to make as many variables as controllable as possible. Given that the crustal properties of natural soils will vary widely between locations, it would evidently be desirable to make the thickness and rigidity controllable variables. One way of doing this is to create an artificial crust by the use of synthetic inclusions in the embankment and in the near-surface soils. The synthetic material should have soil compatible rigidity, should be non-corrosive and, above all, should have well defined properties. Given these, the rigidity and/or thickness of the crustal zone can be rationally related to fill height.

However, creation of an artificial crust by means of synthetic inclusions is not the only reason for examining the effects of such inclusions. The entire concept of earth reinforcement has become topical within the past 10 years. The existing processes are largely proprietary and most commonly used in the form of tie-back strips for retaining walls. Nevertheless, review of these existing systems has suggested that it is highly likely that the use of inclusions could be shown to be a cost-effective means of improving embankment performance on soft soils. In such an event, the method can be readily adopted for widespread use in those circumstances where the natural crust is either too thin, or too soft, to allow for optimal embankment design. The resulting cost savings could prove to be truly substantial.

There are a number of approaches to evaluating the effect of fill reinforcement on the behaviour (e.g. stability) of an embankment on soft clay. An obvious approach is to modify conventional methods of stability analysis (e.g. limit equilibrium analysis) to include reinforcement as an additional force on the free body failure mass being analysed. This approach is apparently logical and can demonstrate mathematically some benefit occurring from reinforcing inclusions near the base of the embankment. However, it assumes, firstly, that free body forces or resistance are balanced at compatible strains, and secondly, that conventional limit equilibrium methods of analysis are, in themselves, correct.

Unfortunately, despite exhaustive research in the past 20 years, it is clear that there are still other unsolved problems associated with the prediction of stability of fills on soft clays. This situation is well illustrated by the predictions made by various researchers since 1960 (Figure 1.2). Bishop and Bjerrum (1960) established the validity of the $\phi_u = 0$ (short term-undrained strength) approach by back-analyzing a number of failures on clays; as shown on Figure 1.2a, this approach appeared to provide a reasonable solution for each of the cases studied and became a common method of analysis in geotechnical engineering. By the early 1970's, it became apparent that this approach did not always provide the correct prediction, as indicated on Figure 1.2b (Bjerrum, 1973). The magnitude of error in computed factor of safety increased with increasing plasticity when the strength was measured using the field vane. This trend led Bjerrum to propose an empirical correction factor to be applied to the measured vane strength. This modification was obviously compelling and was adopted widely. Again, however, numerous exceptions which did not conform with Bjerrum's correction factor were reported (Figure 1.2c), and considerable controversy developed as to the advisability of using Bjerrum's approach, based on both fundamental and practical considerations.

Some of the basic problems associated with conventional stability analyses for fills on soft clays will be discussed in Chapter 2. The conclusions drawn from this critical evaluation formed the basis of a hypothesis to explain the effect of reinforcement of such fills. The construction of a test embankment was considered to be an essential part of any research program, to obtain a better understanding of performance, and to check the validity of the hypothesis and the applicability of various methods of analysis, including the conventional limit equilibrium method.

Three test embankments were constructed at a site in St. Alban, Québec; two of which were reinforced using geogrids in different configurations. The embankments were constructed to heights which induced failure in the foundation soils and the behaviour of the embankment, geogrid and foundation, was monitored with in situ instrumentation. Included in the research program were:

- Analyses of the stability of reinforced and unreinforced test embankments at the site, using conventional limit equilibrium methods.

- Comparative mathematical modelling of the embankment and its foundation using the finite element method.

- Collection, interpretation of data and comparison of the analytical model with actual field performance and hence the calibration of the predictive model adopted.

- Development of conclusions and recommendations pertaining to rational design techniques and methods to be used in future construction incorporating reinforced embankments on soft, sensitive soils, as well as a comparison between the alternative geogrid configuration adopted.

The report on this research project is jointly prepared by Golder Associates and Université Laval. Chapters 2 to 7 describe the rationale for performing the trials, site conditions, design of the embankments and instrumentation, and the construction of the test embankments. In Chapters 8 to 10 the results of the monitoring, descriptions and back analyses of the failures, and comparison of the predicted and actual field performance are presented. Conclusions and recommendations for design of reinforced embankments including suggestions for further research in this area, are contained in Chapter 11.

2.0 BACKGROUND

2.1 LIMITATIONS OF CONVENTIONAL STABILITY ANALYSES

Current methods of predicting stability of embankments on clays basically involve establishing the limiting equilibrium of a free body failure mass as illustrated on Figure 2.1. Various trial failure surfaces are analysed and the failure surface which provides the minimum factor of safety is taken as the critical surface. Although many other factors are involved, the key components of the limit equilibrium method of analysis are the shearing resistance of the soil strata along the failure surface and the failure mode. These basic components are considered separately in the following sub-sections.

2.1.1 Shearing Resistance

The critical period with respect to fill stability on clay is generally immediately following construction. In this period, the soil is essentially undrained and in its weakest state. With time, by consolidation, water is expelled from the pores of the soil and its strength increases. It is common to measure soil shearing resistance in an undrained condition and to use this minimum design (undrained) strength in stability analyses. It is now recognized that many factors affect the design undrained strength and that, in fact, undrained strength is not a unique property of the soil deposit. Some of the major factors which affect undrained strength are as follows:

o Variation with depth - as shown on Figure 2.2a, the undrained strength of a soft clay deposit typically varies with depth. In the surface crust, which has been altered by natural weathering processes, the undrained strength is high but decreases with depth to a minimum below the base of the crust. Below this depth, the undrained strength generally increases in a uniform manner, with the rate of increase in strength dependent on the soil type. This variation in strength with depth is common in soft clay deposits.

- Weak layers - because of the nature of deposition, it is not uncommon for soft clay deposits to contain layers of weaker soils, (Figure 2.2a). These weak layers, if present, are difficult to detect and can control stability. Even if discrete weak layers are not present, it is obvious that the zone of minimum shear strength below the crust represents a weak zone.

- Rate of shearing - laboratory and field strength tests are often carried out at rates which are much more rapid than actual field loading (i.e. rate of fill construction). For example, field vane tests are carried out at rates which are about 10,000 times faster than actual fill construction. The undrained strength measured in common laboratory strength tests is dependent on strain rate and typically exhibits a 10 to 15 per cent increase in strength for each order of magnitude increase in strain rate.

- Anisotropy - as shown on Figure 2.2b, the undrained strength of soft clays depends on the direction of shearing (i.e. undrained strength is anisotropic). The degree of anisotropy decreases with increasing plasticity. The complex mode of failure associated with the common field vane tests results in a trend which does not reflect other tests in which the boundary conditions are better defined.

- Strain dependence - as stated previously, many soft clays are strain-softening, (Figure 1.1). In most situations, fills are designed such that the factor of safety against failure is low (in the order of 1.3). In this condition, a large portion of the foundation clay deposit is over-stressed (i.e. the imposed shear stress exceeds the shear strength of the soil). Therefore, if the soil is strain-softening, progressive failure will occur as some load is transferred from the over-stressed zones to adjacent under-stressed zones. As a result, at failure, the mobilized strength in large portions of the foundation soil will correspond to the lower "large strain" strength, so that the maximum shearing resistance does not apply throughout the failure surface.

Based on the above, it is obvious that the selection of undrained strength to be used in stability analysis is a complex issue. The problem of selecting the appropriate undrained shear strength for analysis has been addressed by a number of researchers using different approaches. Surprisingly, despite sometimes vigorous argument between the various protagonists, there is a consensus. Three of the more significant approaches are described below and are similar in one respect - the undrained strength proposed for use in analysis is related to the preconsolidation pressure (σ'_p) on the soil.

- Bjerrum/Mesri - Mesri (1975) reinterpreted Bjerrum's original data related to the strength at failure of soft clay deposits, (Figure 2.3a) and pointed out that when Bjerrum's correction factor was applied to c_u and σ'_p

plots, there was a unique ratio of undrained strength at failure to σ'_p (c_u/σ'_p) of 0.22. Later, Trak et al (1980) showed that this value of undrained strength corresponds to the strength mobilized at failure in the foundation of embankments built on inorganic soft clays.

- Ladd and Foott (1974) (MIT) - have recognized that direct simple shear strength (DSS) is the approximate average strength below an embankment on soft clay and have successfully used this strength value to explain failures (Figure 2.3b). As shown by Trak et al (1980) the ratio of c_u (DSS)/σ'_p equals 0.2 to 0.25.

- La Rochelle et al (1974) (Laval) - have suggested that the strength mobilized in the soft clay foundation would everywhere be the large strain strength. The ratio of undrained strength at large strains, c_u (USALS) to σ'_p is also equal to 0.2 to 0.25. (Trak et al 1980).

The above discussion has been confined to the question of the mobilized strength of the clay beneath the superficial zone of weathering. The deposition and stress history of the deeper material are better understood and reproducible in the laboratory. As a consequence, this material has attracted the attention of researchers at the expense of the more variable, inconsistent and elusive weathered zone; yet the properties of the weathered crust play a fundamental role in the stability of any embankment.

This is an obvious problem in the philosophy of modifying existing methods to account for the effects of geogrid reinforcement on embankment stability. If the incorrect undrained strength is adopted, then the design philosophy of soil reinforcement will not be rational.

2.1.2 Failure Mode

In the vast majority of stability analyses and back analyses of failures, it is assumed that the failure surface is circular - a kinematically admissible failure mode. However, there are many instances in which the assumption of a circular surface does not account for other important factors such as the presence of an obvious weak layer, or the zone of minimum shear strength being immediately below the crust. Attempts to fit circular failure surfaces passing through this zone can lead to unrealistic failure geometries within the fill and beyond the toe of the fill slope. This is particularly true when the surface crust is thin.

Analyses incorporating non-circular and translational failure modes do exist (e.g. wedge analyses) but are used less frequently than circular arc analyses. Further, many of the assumptions incorporated in the method of slices, which is common in both circular and non-circular analyses, are not applicable to analysis of translational failure modes.

2.1.3 Summary

Based on the above discussion, it is evident that there are a number of uncertainties associated with conventional limit equilibrium analyses of embankment stability on soft clays. In particular, the assumptions often made with respect to undrained strength and failure mode can be fundamentally erroneous. Therefore, it is considered that any program to provide a design method for the analysis of reinforced embankments must include some means of calibrating the strength of the foundation and observations of the failure mode.

2.2 SPECULATED EFFECT OF REINFORCING INCLUSIONS ON EMBANKMENT STABILITY

Based on limited experience and on instinct, reinforcement of fills with geogrids should improve their stability on soft clay foundations. An early example of reinforcement of fills on soft ground is the "corduroy" road in peat bogs where cut trees are laid side by side across the intended route and fill is placed on top of this "corduroy" arrangement. However, caution should be exercised in terms of inference drawn from this example, since the mode of failure associated with low road fills on peat is generally related to excessive deformation as opposed to rupture of the foundation soils - the case with soft clay foundations. The predominant effect of the corduroy is to keep the fill intact and to prevent distress to the road pavement as a result of spreading (lateral displacement) of the fill, in association with deformation of the underlying peat. It should also be appreciated that while corduroy (or geogrid) reinforcement of low road fills on peat may help to keep the fill intact, it will not reduce (and in some instances could increase) overall deformations.

There are probably a number of reasons why reinforcement of the base of fills enhances their stability on soft clay. For example, reinforcement would tend to reduce "splitting" of the fill and would therefore increase whatever contribution the fill strength makes to overall stability. It is considered that an effect of reinforcement could be to cause beneficial change in stress distribution in the soft clay foundation. The hypothesis is as follows:

Construction of fills on a flat ground surface induces movement and associated shear stresses at the fill/ground surface interface. The effect of incorporating reinforcement at the base of the fill is to reduce the magnitude of these shear stresses at the interface. Thus, as the fill tends to spread, the reinforcement is put into tension and, if sufficiently stiff, will reduce the magnitude of displacement, and, therefore, shear stresses at the fill/ground surface interface.

This change in external boundary stresses results in a significant change in the stress distribution in the foundation material by increasing the horizontal stress component and by preventing rotation of the principal stress directions due to application of shear at the ground surface. It is noted, however, that unless the lateral reinforcement is extremely rigid (i.e. flexurally stiff in a horizontal plane such as a rigid footing), the vertical stress distribution in the foundation would remain unchanged. To illustrate this hypothesis, Figure 2.4 shows typical stress conditions on an element of soil below reinforced and unreinforced fills. The combination of increased total horizontal stress and reduced boundary shear stress causes a reduction in the maximum shear stress on the soil element.

A more complete illustration of the change in stress conditions resulting from reinforcement is shown on Figure 2.5. This figure summarizes the maximum shear stress distributions below a typical fill for the extreme cases of perfectly stiff reinforcement and no reinforcement. These data suggest that very stiff reinforcement could result in a significant reduction in shear stress within a depth range below ground surface approximately equal to 1 to 1.5 times the embankment height. The magnitude of the reduction in shear stress associated with reinforcement decreases with depth. For a site where the surface crust is thin and a typical strength profile with depth exists (Figure 2.6a), the decrease in shear stress magnitude at shallow depth is important since, with the addition of reinforcement, the zone of highest shear stress moves to below the zone of minimum shear strength. This results in a deeper failure surface through more competent materials and as a result, a higher factor of safety (more stability) is obtained for a given fill height. The corollary is that on a given site, a higher fill can be constructed before failure occurs. It is apparent from the above that the effectiveness of the reinforcement in creating the required stress distribution is dependent on its relative stiffness.

Finite element analyses of a reinforced and an unreinforced embankment were carried out as part of this study. Details of the analyses and some of the results obtained are given in Appendix A of this report. The analyses adopted a hyperbolic stress-strain model for the soil and incorporated the soil parameters developed from laboratory and in situ tests by Trak (1974) for similar analyses of an unreinforced embankment on the St. Alban clay.

In summary, the analyses indicated that the effect of the reinforcement is to:

- Restrain the propagation of failure in the foundation under the embankment or conversely, allow a greater embankment height for the same extent of failure in the foundation.

- Reduce the excess pore pressure generated under the embankment.

- Reduce the magnitude of both horizontal and vertical displacements under the embankment.

2.3 SITE SELECTION

The present knowledge about the behaviour of soft sensitive clays under embankment loading has been added to significantly by the research carried out by the geotechnical group at Université Laval, Québec. The main focus of this work has been the construction of four test embankments at St. Alban, Québec, in 1972.

The same site at St. Alban was chosen as the site for the current research program. It is ideal for the test embankments because the previous test embankments provide considerable information on the performance of the subsoils. In addition, the topography is fairly flat with a uniform deposit of the soft, sensitive Champlain sea clay, overlain by a thin crust. The soft consistency of the clay means that only 4 to 6 m of fill has to be placed to induce failure.

One of the test embankments constructed in 1972 was built up until failure occurred and the results of this instrumented failure have been described by La Rochelle et al (1974). Reference to this failure was made by Trak et al (1980) as part of the development of new design approaches to the stability analysis of embankments on sensitive soils. From these studies, a shear strength approach corresponding to the undrained strength of the material at large strains (USALS) was suggested. This value was also shown to be related to the preconsolidation pressure of the foundation material and seems to approximate the average mobilized shear strength under failed embankments as given by back analyses. The significant effect of the thickness and strength assumptions of the weathered clay crust in the determination of the stability of embankments was also recognized in these studies. The pore pressure response of the foundation under loading for the failed embankment was also included as part of the study carried out by Leroueil et al (1978a) in the prediction of construction pore pressures. The geotechnical properties of the clay have also been extensively investigated in several other studies conducted by Université Laval in the past decade.

3.0 GEOGRID REINFORCEMENT

3.1 SELECTION

As discussed in Chapter 1, a geogrid suitable for the reinforcement of embankments on soft clays, should be environmentally inert and should have well defined physical properties. Based on these factors, the most appropriate geogrid available at the time was a high strength polyethylene geogrid, Tensar SR-2.

3.2 PHYSICAL PROPERTIES

The Tensar SR-2 geogrid is a uni-axial polymer based grid that was specifically designed as a reinforcing element within earthworks. The constituent polymer of the product is a high density polyethylene which has 2.5 per cent of finely divided carbon black added, to provide ultra violet protection to the polymer. The geogrid is produced by Tensar Incorporated, whose manufacturing facilities are situated in Atlanta, U.S.A. Distribution centres of the product in Canada are located in Montreal (Québec), Toronto (Ontario), and Calgary (Alberta).

The geogrid is produced, in a two-staged process, from polyethylene sheets. In the first stage a pre-determined regular array of holes is punched through the polyethylene sheet. The second stage controls the performance of the perforated sheet by the size, shape and position of the holes. The literature supplied by the manufacturer indicates that the resulting product has a service temperature range from -50°C to +80°C, and is inert to all chemicals naturally found in soils. It has no solvent at ambient temperatures and is resistant to attack by aqueous solutions of salts, acids and alkalis. The geogrid is also biologically inert as the base polymer is not a nutrient medium for micro-organisms.

The typical dimensions and mechanical properties of Tensar SR-2 are described in Figures 3.1 and 3.2 and in Table 3.1.

Longitudinal Direction	Mean
Single rib tensile strength*	1.72 kN
Peak strain*	10.5%
1 hour creep strain	6.8%
100 hour creep strain	8.6%
Quality control tensile strength*	79 kN/m-width
Peak strength - Index value **	68 kN/m-width

Table 3.1 Mechanical Properties of Tensar SR-2

---

* Based on quality control tests on single ribs at a high strain rate of 23 per cent/min, at 20°C.

** Peak strength - Index value based on index tests on 5 bars by 15 ribs at strain rate of 2 per cent/min, at 20°C.

4.0 SITE DESCRIPTION AND SUBSURFACE INVESTIGATION

4.1 SITE DESCRIPTION

St. Alban is located about 80 km west of Québec City, at the northern fringe of the St. Lawrence Lowlands. In 1894 the Municipality of St. Alban was the site of a massive flow slide. Soft, sensitive Champlain Sea clay deposits are distributed over flat lands between the north shore of the St. Lawrence River and the toe of the Laurentian mountains (Figure 4.1). The site of the test embankments is located outside the Town of St. Alban in the County of Portneuf, near the northern fringe of the Champlain clay deposits. This is about a kilometer from the toe of the Laurentian mountains (Figure 4.2). Relief across the relatively flat topography is introduced by a small stream marking the southeastern boundary of the site. Access is provided by a gravel road running along the west boundary of the site.

The bedrock underlying the overburden soils, at depths in excess of 24 m, is known to be a Trenton Limestone. The mountains to the north are composed of Precambrian granites and gneiss (Clarke 1949).

4.2 SUBSURFACE CONDITIONS

The subsurface conditions across the general site area were inferred from a detailed geotechnical investigation carried out in 1972 by Université Laval, as part of a site characterization program. This included 17 in situ vane tests, 8 static cone penetrometer tests, 9 borings with continuous pressuremeter tests and 5 boreholes within which 50 and 75 mm diameter tube samples were obtained by the NGI type stationary piston sampler. Most in situ testing and boreholes were terminated at depths of about 15 m below ground surface. Numerous routine laboratory tests were carried out on the recovered samples and the results have been reported by La Rochelle et al (1974), Tavenas and Chapeau (1973), Sarrailh and Tavenas (1972), and Juneau and Roy (1973). Since these early studies, many other research oriented investigations have been carried out at this site and have been reported in the literature.

The geotechnical investigation and the associated laboratory testing indicated that the original ground surface is covered by about 0.3 m of topsoil, which is underlain by a 1.5 m thick weathered clay crust. This is in turn underlain by a soft, grey to blue, marine clay deposit which is about 8 m thick. An approximately 4 m thick layer of soft, sensitive clayey silt underlies the marine clay deposit at about 9.7 m below ground surface. The clayey silt is in turn underlain by a dense fine to medium sand deposit which extends to the maximum depth investigated of 24.4 m. Bedrock was not encountered at these depths.

Studies have been focused upon the upper 9.7 m of the overburden soils. A typical profile of the geotechnical properties of the subsoils, reproduced from Trak et al (1980), is given in Figure 4.3.

In summary, the marine clay is of a low to medium plasticity with a plasticity index of about 37 per cent immediately below the crust at 1.8 m depth, decreasing to about 10 per cent at 9.0 m depth. The water content measured throughout the deposit was appreciably higher than the liquid limit. The measured liquidity index averaged 2.4.

The results of in situ vane and cone penetration tests carried out in 1972 indicated that the clay is fairly uniform across the site. The undrained shear strength of the clay, as inferred from these tests, increased linearly from a minimum value of 10 kPa at 1.8 m depth to about 33 kPa at 9.1 m. The maximum variation of undrained shear strength inferred from in situ vane testing was in the order of 20 per cent. The measured vane strength of the crust was as high as 48 kPa and averaged about 38 kPa. An averaged vane strength profile is shown on Figure 4.3. Conventional consolidated undrained and unconfined undrained triaxial testing of recovered tube samples generally gave strengths higher than those obtained from in situ vane tests. Unconfined undrained triaxial tests carried to strains large enough for a constant strength to be reached, typically at about 10 per cent strain (Figure 1.1), were also performed to examine the undrained strength at large strains of the clay. A well defined strain softening behaviour was demonstrated at strains beyond about 1 per cent in samples of the clay (Figure 1.1). In the fissured, crustal material, an elasto-plastic stress-strain curve, with the shear stress becoming constant at about 10 per cent strain, was confirmed by these large strain tests. These undrained strengths at large strains (USALS) are plotted with the average vane strengths in Figure 4.4 and indicated that the USALS strength is about 90 per cent of the vane strength below the crust.

The sensitivity of the clay, as measured by in situ vane testing, increased from 8 in the lower part of the crust, to 22 at a depth of about 6.4 m. An upward seepage gradient of 0.2 was found to prevail in the subsoils above the dense sand deposit.

The preconsolidation pressures σ'_p of the clay as determined by more than 40 oedometer tests gave a fairly consistent straight line, with σ'_p/σ'_{vo} (the ratio of preconsolidation pressure to effective overburden pressure) of about 2.0 and a c_u (vane)/ σ'_p ratio of about 0.24. These results indicated that the clay is preconsolidated over a pressure range of about 9.5 kPa under the crust.

4.3 GEOTECHNICAL INVESTIGATION (1984)

A geotechnical investigation was carried out between May 28 and June 21, 1984, to determine the subsurface conditions of the site over the proposed area of construction. This was carried out to ensure that subsurface conditions are consistent and can be directly compared to the 1972 investigation, especially in the area of the failed test embankment. The original plan was to construct the embankments within an area bounded by the fence to the north, the access road to the west and the creek to the south and east.

During the initial stage of the investigation, a total of ten in situ vane tests (Numbered V-1 to V-10, inclusive) and five piezocone tests (Numbered P-1 to P-5, inclusive) were carried out at locations as shown on Figure 4.5. These results indicated that the site for the proposed test embankments was fairly consistent with the exception of an area near the east end of the site (Vanes No. V-3 and V-4). In this area very low shear strengths were obtained below 4 m depth. The results of these tests are shown on Figures 4.7 and 4.8 for vane tests, and on Figures 4.9 to 4.11a, inclusive, for piezocone tests.

Because of these inconsistencies, it was decided to explore the area north of the fence (i.e. east of the 1972 failed embankment) in search of more consistent subsoils. Five additional in situ vane tests (Numbered V-11 to V-15, inclusive) and one piezocone test were carried out in the neighbouring field (Figure 4.5). The results of these latter tests confirm that the vane strengths of the clay below the crust in that area is fairly consistent with the rest of the site. The additional vane and piezocone tests are plotted on Figures 4.8 and 4.11b, respectively. The layout of the three proposed test embankments was therefore rearranged as shown on Figure 4.6. The embankments would differ in the form of reinforcements to be incorporated at the base. The unreinforced control embankment (No. 1) would be constructed furthest from the 1972 failed embankment. Embankment No. 2 which would be reinforced with two horizontal layers of Tensar SR-2 was to be constructed first. The Geocell Reinforced Embankment (No. 3) would be built last and would be located east of the 1972 failed embankment.

The thickness of the crust throughout the proposed construction area is about 1.5 m, as inferred by in situ vane and piezocone testing. The strengths obtained in the crust by the vane tests varied significantly between the sites of the three proposed embankments. The "strongest" crust was located in the area of the control embankment, with the "weakest" in the area of the geocell reinforced embankment. This will be discussed later when considering the performance of the embankments.

At the time of the investigation it could not be determined if the variation in strength of the crust indicated a true difference in strength between the various sites, or was merely a reflection of the normal data scatter which can be obtained in these fissured materials.

5.0 EMBANKMENT DESIGN

This section of the report describes the design of the test embankments. Limit equilibrium analyses were carried out to back-analyse the 1972 failed test embankment constructed to failure on the same site. The results of these analyses were used to calibrate methods of stability analyses, the assumption of shear strength profile, and hence the design of the proposed test embankments.

5.1 METHODS OF SLOPE STABILITY ANALYSES

The study of the 1972 failure allows the calibration of several methods of slope stability analyses, as well as an assumption of the shear strength profile in the fill and the foundation subsoil (described in Section 5.2). Brief descriptions of three computer programs written for different methods of stability analyses, but all based on a state of limiting equilibrium on a circular failure surface, are as follows:

a) STAB - The program was developed by Université Laval and was used extensively for analysis of the 1972 test embankments. The program is based on the Bishop Simplified method of slope stability analysis (Bishop 1955). The shear strength parameters of the foundation can be represented by a varying strength profile. Moment equilibrium conditions are satisfied on all slices.

b) BTENSAR - The program was developed by Golder Associates for assessments of the stability of embankments on clay foundations in the undrained condition. The method represents the failure conditions in the fill with the active force Pa. This is effectively an assumption that there are no shear forces on vertical interslice planes through the fill (as assumed in the Bishop Simplified method). A circular arc failure through the clay foundation is assumed (Figure 5.1). Global moment equilibrium is satisfied. Successive iteration is carried out to locate the centre of the critical arc. The program was modified to include a stabilizing moment induced by a horizontal reinforcing force acting at the base of the embankment. The strength of the foundation is represented by discrete layers and the average shear strength along the circular arc passing through the bottom layer is calculated, as shown in Figure 5.1.

c) SARMA - The program was developed by Golder Associates for general stability analyses. It is based on the method of slope stability analysis proposed by Sarma (1973). Static equilibrium is satisfied for both force and moment on every slice on the slip surface. The strength of the foundation is represented by discrete layers.

5.2 SHEAR STRENGTH PARAMETERS

The assumption of shear strength parameters for analysis has been discussed in detail by La Rochelle et al (1974). Several shear strength profiles were considered in their back-analysis (Figure 5.2). Two profiles were assumed for the material beneath the weathered crust. These were the profile obtained from in situ vane tests and that from unconsolidated undrained triaxial tests at strains of about 15 per cent. The latter shear strength was designated "the undrained strength at large strains" (USALS).

In the weathered crust five profiles were considered as shown in Figure 5.2. These are:

(1) Full Strength; the full measured vane strength in the crust being used.

(2) Mid-depth Strength; the strength of the upper half of the crust was assumed equal to the vane strength measured at half the full depth of the crust, and the strength of the lower half of the crust assumed equal to the average vane strength measured in that layer.

(3) Minimum Strength; the shear strength of the crust being assumed equal to the minimum shear strength measured in the profile.

(4) USALS A; the strength at large strains as measured in laboratory samples of the crust being used, with the strength profile being extrapolated to a maximum value at ground surface.

(5) USALS B; the strength at large strains as measured in laboratory samples being used but the strength assumed to be constant in the upper 0.6 m of crust.

In addition to the above, six different assumptions about the strength mobilized in the fill were made. These included: a full depth fissure, three different distributions of earth pressure, a zero shear strength condition and limit equilibrium as calculated by STAB for $\phi' = 44°$.

In a subsequent paper, Trak et al (1980) included a shear strength profile in which the Bjerrum (1972) correction was applied to the vane strength measured in the material below the crust and a shear strength profile corresponding to $c_u = 0.22 \;\; '_p$ which was shown to be in good agreement with the USALS profile. (Figure 4.4).

Factors of safety ranging from 0.59 to 1.72 were obtained for the back analysis. Using a measured $\phi' = 44°$ in the fill, the USALS profile, which included the USALS A profile in the crust, gave a factor of safety of 0.94 for the failed embankment. This profile does not involve the arbitrary assumptions for the strength of the crust, necessary in those profiles based on the vane strength, and it was concluded that the USALS method gave a fairly close approximation to the average strength mobilized under an embankment. The results will be discussed in more detail in a later section of this report.

Following the results of the 1972 test embankment, the USALS profile was used to design the test fill.

5.3 DESIGN OF TEST EMBANKMENTS

The program used for the calculation of force in the reinforcement (BTENSAR) was first calibrated against the other programs. The factors of safety (F_s) obtained for the 4 m high fill with unit weight, $\gamma = 18.9$ kN/m^3 for the the three computer programs are:

METHOD	F_s
STAB	0.94
BTENSAR	0.97
SARMA	0.96

This was considered to be satisfactory agreement and BTENSAR was adopted for design of the reinforced embankments.

The program was extended to include a horizontal stabilizing force placed at the base of the embankment to simulate the reinforcement. For design, an USALS shear strength profile as discussed above was assumed. Based on this, and provided that a tensile force equivalent to the quality control tensile strength of two layers of the proposed Tensar SR-2 (158 kN/m-width) could be mobilized, a failure height of 5.2 m was calculated for a state of limiting equilibriuim (factor of safety of unity). The design of the two reinforced fills was thus based on this failure height of 5.2 m. The base of all test embankments was similar and the dimensions of the control embankment were identical to the 1972 embankment. The geocell mattress was designed using the same quantity of geogrid as was used in providing 2 horizontal continuous layers of reinforcement (the arrangement for the reinforcement in Embankment No. 2).

In both the strip reinforced and the geocell reinforced embankments, the geogrid was to be laid out across the width of the embankment. The reinforcing strength available in the longitudinal direction in the embankment would be small in the case of the geocell and zero in the case of the strips laid end to end. Berms were therefore necessary at both ends to ensure that failure would not occur in this "unreinforced" direction. An additional berm was required along the back of all the embankments to encourage failure on the preferred side, where the instrumentation was concentrated.

For the berm along the back of the embankment, a factor of safety of 1.3, taking into account the reinforcement, was taken as the design criterion. Calculations using both circular arc and translational wedge type failures indicated that a 1.5 m high berm extending to 13 m from the eventual embankment crest would be required.

The berms at the end were designed to a lower factor of safety of 1.2, since end restraints make this an unlikely mode of failure for a "long" embankment. However, the factor of safety had to be based on an unreinforced embankment; reinforcement being negligible in that direction, and a required berm length of 19 m from the embankment crest was calculated.

Based on the results of the 1984 site investigation (described in Chapter 4) the embankments were positioned as shown in Figure 5.3. A drainage trench just east of the access road was filled to ensure that the discontinuity in ground surface profile would not affect the behaviour of Embankment No. 2 (strip reinforced embankment) located about 10 m east of the trench.

6.0 INSTRUMENTATION

A variety of geotechnical instruments were utilized to monitor the behaviour of the three test embankments. As each of the embankments were dimensioned to approximate a plane strain condition, most of the instruments were concentrated near the axis of the proposed embankment. The side of the embankment where failure would occur (opposite to the berm side) was heavily instrumented. The layout of the instruments in each embankment was similar, so that direct comparisons of the behaviour under different configurations of reinforcement could be made.

Assembly and calibration of the subsurface instruments, and their subsequent installation were carried out by the staff at Université Laval, using their own drilling equipment. The design and assembly of the geogrid instrumentation were the responsibility of the staff of Golder Associates, with some technical input provided by Tensar Incorporated. These are discussed in the following sections. The layout plans of the instrumentation for the control, strip reinforced and geocell reinforced embankments are provided on Figures 6.1, 6.2 and 6.3, respectively. The type and quantity of instrumentation installed is listed in Table 6.1.

	Quantities of Instrumentation		
Type of Instruments	Control (No. 1)	Strip Reinforced (No. 2)	Geocell Reinforced (No. 3)
Pneumatic piezometers	14	16	16
Hydraulic piezometers	10	5	14
Electrical piezometers	1	2	4
Settlement plates	11	11	18
Monuments (settlement)	14	14	14
Vertical extensometers	4	3	3
Inclinometers	2	2	2
Horizontal extensometers	2	2	2
Monuments (horizontal displacement)	14	14	14
Total pressure cells	4	5	4
Tensar load cells	-	2	2
Bison strain gauges	-	16	10
Differential extensometers	-	2	-

Table 6.1 Quantites of Installed Instrumentation

6.1 SUBSURFACE INSTRUMENTATION

The installation of subsurface instruments usually preceeded embankment construction by at least 4 weeks, to allow for stabilization of the installed instruments. This stabilization period was also necessary for the consolidation of the model material: a mixture of kaolinite, bentonite and cement, used as backfill for borings made to install the instruments. The stress-strain characteristics of the consolidated model material have been shown to be similar to those of the Champlain clay (Tavenas et al, 1973). Instruments which required a period of stabilization include piezometers, vertical extensometers, inclinometers, and monuments. Horizontal extensometers and total pressure cells were installed in the fill during construction.

6.1.1 Piezometers

The monitoring of pore water pressure provides a good indication of the response of the clay, under relatively rapid loading in an approximately undrained condition. The excess pore pressure also provides an insight into the extent of over-stressed zones in the foundation. Pneumatic, hydraulic and electrical piezometers were used throughout the study.

a) Pneumatic Piezometers

Pneumatic piezometers work on the balance of pressures across a diaphragm, and offer a fast response time and a moderate dynamic response. The pneumatic Petur P-105 piezometer, produced by Petur Instruments Limited of Vancouver, British Columbia, was used throughout the three test embankments. These piezometers have a low capacity of 0 to 400 kPa which makes them suitable to react to small changes of pressure under low pressure conditions; this explains that the small dissipations of pore pressure between loadings observed in the present case were not recorded in 1972, when much less sensitive piezometers were used. The piezometers were installed through BW casings advanced to the designated depth of installation by wash boring. The casings were withdrawn in steps to allow installation of the piezometer.

A layer of fine sand, 200 mm thick, was placed in the bottom of the hole, to form a permeable cushion. The piezometer was then placed on top of this sand cushion, with a weight attached to the top of the piezometer tip to hold it in place at the bottom of the hole. More fine sand was placed around the piezometer to form a 350 mm layer of permeable material above the tip. Bentonite pellets were then placed on top to form a seal of at least 300 mm thickness. Backfill to original ground surface was provided by the model material. To ensure that all pneumatic piezometers were hydraulically isolated, only one installation was permitted in a borehole. Details of the piezometer tip are shown on Figure 6.4a.

b) Hydraulic Piezometers

Hydraulic piezometers respond to a change in pore water pressure in the surrounding ground by migration of water in or out of the measuring standpipe. Their response time is therefore dependent on the flow rate of a relatively large amount of water and as a consequence is inherently slower than pneumatic and electrical piezometers. The Geonor M-206 hydraulic piezometer used in this study consists of a hollow metal tube, on the bottom of which is mounted a conical tip. Three sintered bronze filters are mounted on the hollow stem with chamferred brass rings sealing and supporting the filters. The measuring standpipe is a plastic tube, protected by a steel pipe which is connected to the top of the piezometer tip and extends to ground surface. The whole assembly is pushed into the ground by hand. Details of the hydraulic piezometer are given on Figure 6.4b.

c) Electrical Piezometers

The Geonor M-600 piezometer used is an electrical instrument containing a vibrating wire strain gauge transducer connected to a diaphragm on one end and fixed on the other. Changes in diaphragm pressure produce a variation in wire tension which is recorded as a change in the frequency of the vibrating wire. The entire assembly is housed within a hollow steel tube with a porous end section which is fitted with a conical tip. Installation procedures are similar to those for the hydraulic piezometers. Details of the Geonor M-600 electrical piezometer are given in Figure 6.4c.

6.1.2 Settlement Plates

The settlement plates are made from two pieces of 0.6 m square plywood boards, each 250 mm thick and nailed together. A steel pipe is fitted on the centre of the plywood board and settlement readings are taken from the top of the steel pipe. The pipe is extended in 1 m sections as construction proceeds. The settlement plates are installed in a shallow excavation about 150 mm below original ground surface, and are seated on a thin sand cushion. Where vertical extensometers were installed at the same location, the plates act as the reference ground level and the steel pipe provides an access for the sensor.

A total of 11 settlement plates was installed in each of the control and strip reinforced embankments. Eighteen of these devices were installed in the geocell reinforced embankment. Details of the settlement plates are given on Figure 6.5.

6.1.3 Monuments

A total of 14 monuments were installed at the front of each of the three embankments. These consisted of 19 mm diameter steel rods placed in a 150 mm diameter hole, 750 mm deep and filled with concrete. The top of the steel rod extends about 150 mm above ground surface. Settlement and horizontal displacement readings of the top of the steel rod were taken by precision level and theodolite, respectively. A typical section of the concrete monument is given in Figure 6.6.

6.1.4 Inclinometers

Standard 76 mm internal diameter SINCO inclinometer casings were installed at two locations in each of the three test embankments. The inclinometers were installed to at least 16 m below original ground surface into the very dense sand stratum, to ensure that a stationary reference could be made to the bottom of the casing. The inclinometer casings were installed within H casings driven and wash bored to the designated depths. After installation, the annular space between the casing and the borehole was filled with the model material. Readings of the inclination of the casing were taken by a Digitilt Model 5030 readout unit. The initial set of reference readings was taken after the model material had consolidated, and just prior to construction. Where necessary, the top of the casings were extended in 1.6 m sections to above ground level. A typical inclinometer set-up is shown in Figure 6.7.

6.1.5 Vertical Extensometers

The vertical strain of the subsoils under the test embankments was monitored by three electrical extensometers in each of the embankments. To confirm their accuracy a magnetic extensometer was installed adjacent to an electrical extensometer in the control embankment.

a) Electrical Extensometers

The electrical extensometer was developed by the staff at Université Laval. It consists of 50 mm long, 25 mm diameter, thin copper rings spaced approximately 1 m apart and fixed inside a corrugated flexible plastic tubing (of the type commonly used as floats in swimming pools).

A sensor probe fitted with 4 external copper wires (Figure 6.8) travels within the tubing. The position of the copper rings can be determined by electrical contacts causing a change in voltmeter reading. Vertical strains can be calculated from relative displacements of the copper rings.

The flexible tubing was installed to between 14 and 18 m depths below ground surface, to provide adequate fixity into the more competent subsoils. Installation procedures were similar to those for the inclinometer casings. The top of the extensometer was connected to the underside of a settlement plate. Access to the extensometer was provided by the hollow steel pipe extending from the settlement plate. The set-up is illustrated in Figure 6.9a.

b) Magnetic Extensometers

The magnetic extensometer works on a similar principle to its electrical counterpart, but employs non-contacting magnetic induction to detect the position of the targets. Ring magnets are used instead of copper rings. A bottom sealed rigid plastic pipe, called the access tube, was installed within H casings to the designated depth and the annular space between the access tube and the casing was filled to ground surface with the model material. The casing was then withdrawn in stages to allow the installation of ring magnets outside the access tube, by a larger diameter installation tube pushing onto the magnet. The ring magnets were fitted with three spring loaded metal strips which anchor into the surrounding soil as they clear the tip of the casing. Readings of the relative distance between magnets were taken by a sensor probe travelling inside the access tube, which was kept above ground surface by 1 m long extensions as embankment construction proceeded. The magnetic extensometer set-up is illustrated on Figure 6.10.

6.1.6 Horizontal Extensometers

The lateral deformations of the base of the fill were monitored by two horizontal extensometers installed along the axis of each of the three embankments. In each embankment the lower extensometer was installed at not more than 150 mm below original ground surface and extended from the preferred failure side to the back of the stabilizing berm. Both ends of the extensometer were left open. The upper extensometer was installed at 1.5 m above original ground surface, level with the tops of the stabilizing berm.

The principle of operation of the horizontal extensometer is identical to that of the vertical electrical extensometer. A 200 mm square and 25 mm thick piece of plywood is fixed at right angles to each of the copper rings as the horizontal extensometer is installed in a shallow trench, to ensure that lateral ground movements are directly transferred to the copper rings. Prior to installation, a steel wire is threaded through the flexible tubing and serves as the lead for the sensor probe. Readings of the copper rings are taken by feeding the sensor wire from one end and pulling the lead wire from the other. Details of the copper ring connection for the horizontal extensometer are illustrated in Figure 6.9b.

6.1.7 Total Pressure Cells

The total pressure cell TP-101, manufactured by Petur Instruments Limited, was used to measure the vertical and horizontal stresses in the embankment fill during construction. Typically 2 or 3 pressure cells were installed in the horizontal plane along the axis at the original ground surface in each of the three test embankments. In addition, 2 or 3 pressure cells were installed in a vertical plane (to measure horizontal stresses) at different levels in the fill at the centre of the embankment.

The TP-101 total pressure cell consists of two circular stainless steel plates heli arc welded together around their periphery. The annular space between the plates is filled with an incompressible fluid. The cell is connected via a stainless steel tube to a pneumatic transducer, forming a closed hydraulic system. A change in the fluid pressure is reflected by a change in the reading of the pneumatic transducer. Prior to field installation, the pressure cell was calibrated to read a pressure range of 0 to 400 kPa in a laboratory concrete compression machine. The specifications and a photograph illustrating the set-up of the total pressure cell are given on Figure 6.11.

6.2 GEOGRID INSTRUMENTATION

The effect of the reinforcing geogrid on the behaviour of the reinforced test fills can be better assessed by understanding the mobilized load and strain in the material. The tensile load in the geogrid (Tensar SR-2) was measured by a load cell assembly, and strain of the geogrid was measured by Bison strain gauges. A description of these devices are given in the following sections. The monitoring results are presented in Chapter 8 of this report.

6.2.1 Tensar Load Cells

Within the intended working environment it is necessary that the load cell be capable of measuring a tensile load of up to 80 kN which is the quality control tensile strength of Tensar SR-2 (refer to Chapter 3). It has to form a complete replacement of the geogrid so that it will record the total load in the strip, and it has to be sufficiently small and stiff so that it will not significantly disturb the soil-geogrid interaction. It was designed to be robust to withstand normal construction activities so that it could later be recovered and re-used.

Considerable difficulty was experienced in designing a satisfactory load cell. The originally proposed load cell was connected to the reinforcement by bolts and this arrangement failed at the bolts under testing because of the directional non-homogenuity of the geogrid. Alternatives which involved machined clamps or non-machined clamps with the geogrid embedded in a plastic mould were investigated. Although the latter is significantly more expensive than the originally proposed bolted connection, it is more economical than machined clamps and proved to be satisfactory under load testing.

Details of the load cell and its calibration curves, together with the method of assembly, are given in Appendix B.

During the development of the clamping arrangement, a set of 0.3 m wide prototype test clamps were manufactured. These clamps were then fitted to a length of Tensar SR-2, 0.3 m wide and 0.36 m long. The whole assembly was subjected to destructive tensile testing. Two tests to breakage were carried out and in both the geogrid failed across a row of ribs which were not adjacent to any of the clamps. The results of these tests indicated that the clamping arrangement was at least as strong as the geogrid and failure was not initiated by stress concentration at the moulded connections with the geogrid.

The first test was carried out at an approximately constant strain rate of 0.7 per cent/minute and failure was noted at a tensile load of 16.3 kN. A faster rate of 1.4 per cent/minute was maintained in the second test, and a failure load of 18.0 kN was observed at a failure strain of about 19 per cent. Extrapolating these test results over a metre width of Tensar SR-2 give failure loads of 62 kN and 69 kN, for strain rates of 0.7 per cent and 1.4 per cent/minute, respectively. These are in general agreement with the manufacturer's quoted values.

The connection between the clamps is facilitated by three load bridges, each mounted with double T-rosette electrical resistance strain gauges to form a full wheatstone bridge. These instrumented load bridges were then protected and subsequently calibrated.

The two components of the Tensar load cell (i.e. the clamps and the load bridges) were prefabricated under laboratory conditions and then assembled in the field. In total, two complete Tensar load cells were manufactured and one redundant bridge was assembled to be installed as a temperature control for the loaded bridges. The load cells were successfully recovered after the failure of the strip reinforced embankment and were subsequently re-installed in the geocell reinforced embankment.

6.2.2 Bison Strain Gauges

The use of Bison strain gauges for measurement of small soil strains has been developed by Truesdale et al (1962, 1965) and described by Selig (1971) and Paterson (1972). Recently they have been used, with success, to monitor the behaviour of Tensar SR-2 when incorporated into retaining walls and embankments in the United Kingdom.

The Bison strain gauge system consists of two basic components: a pair of embedded sensors and an external instrument readout unit. The sensors consist of a pair of 50 mm diameter flat coil discs attached to adjacent ribs of the Tensar SR-2 geogrid by plastic fasteners. The principle of operation is based on electromagnetic induction to measure the relative movement between a pair of sensor coils on a plane. A 50 kHz 20 volt (peak to peak) signal is established by the readout unit in one of the coils (the primary). The alternating magnetic field produced by the excited primary coil induces a current in the secondary coil. The magnitude of this current is directly related to the physical separation of the sensor coils. A calibration chart can be produced by measuring the magnitude of this induced current over a range of known separation between sensor coils. A calibration chart typical of the batch of sensors purchased for this study is shown on Figure 6.12.

The sensor coils purchased for this study came with 0.3 m of leads which were extended by RG-58-C/U coaxial cables to the readout unit. These sensor coils were all found to give inconsistent readings after being installed in the strip reinforced embankment. After a detailed examination of the sensor assembly, the lead wires were considered to be the most probable source of error. These were subsequently removed and the coaxial cables were directly connected to the sensor coils. The connection was then doubly sealed with shrink-wraps and silicon rubber. Performance of these strain gauges were found to be satisfactory in the geocell reinforced embankment.

A total of 28 sensor coils were installed in the strip reinforced embankment. Twenty-four of the coils were fastened onto the geogrid for direct strain measurements. Four of the coils were placed, but not fastened, on the geogrid in an attempt to measure the relative movement of the soil-geogrid interface.

After the failure of the strip reinforced embankment, a total of 8 sensor coils were recovered for use in the geocell reinforced embankment. These were subsequently dried, sealed and recalibrated. A total of 19 sensor coils, generating 10 strain readings, were installed in the geocell reinforced embankment.

A sketch of the relative locations of the Bison strain gauges for the strip and geocell reinforced embankments is shown in Figure 6.13.

6.2.3 Differential Extensometers

The relative movement of the soil-geogrid interface was also measured by means of two differential extensometers installed on each of the geogrid layers in the strip reinforced embankment. These extensometers consist of an aluminum angle resting on the geogrid and joined to a hollow protective pipe which extend to the slope surface. A steel wire was tied to the geogrid and threaded through the protective pipe. A movement along the soil-geogrid interface would be indicated by a relative displacement between the end of the protective pipe and the steel wire.

Details of the differential extensometers are shown on Figure 6.14. The results of monitoring on the strip reinforced embankment during construction and after failure indicated that no slip occurred at the soil-geogrid interface and hence their installation in the geocell reinforced embankment was discontinued.

7.0 CONSTRUCTION

The construction procedures for the three test embankments are outlined in this section of the report. The construction, including site preparation, lasted for 7 months from mid May to November, 1984. To maintain construction on a relatively flat site, the area was mowed and cleared of large shrubs prior to the installation of subsurface instruments. The construction of the test embankments is summarized in a bar schedule in Figure 7.1. The embankments are described in the following subsections in their order of construction, namely, the strip reinforced section, the control section and the geocell reinforced section.

7.1 STRIP REINFORCED EMBANKMENT (No. 2)

Installation of subsurface instrumentation for the strip reinforced embankment commenced on June 29 and was completed on July 9, 1984. After allowing four weeks for the installed instruments to stabilize, the construction of the embankment commenced on August 13, 1984. An existing drainage trench for the access road just west of the embankment was filled with sand from a local borrow on the same day. The main contractor for the field work was Les Excavations Lu-Cau Ltee. A few local contractors were also retained on an as-required basis.

The equipment mobilized included a Liebherr 925 excavator, a Caterpillar D-6 bulldozer, and 2 to 4 tandem trucks. The sand used for the construction of the embankment was taken from two of the three remaining test embankments constructed in 1972. When that source was exhausted, a local borrow producing a very similar sand fill was used.

Grain size analyses on 25 samples of the fill material, carried out in the 1972 study and reported by La Rochelle et al (1974), indicated that it is a uniform medium to coarse sand, with a uniformity coefficient of about 3.0. The envelope of grain size distribution curves of the sand is reproduced in Figure 7.2. The sand was placed in lifts of about 0.3 m thickness, with minimal compaction from the weight and spreading action of the bulldozer. The sloping surface was carefully hand trimmed to maintain a gradient of 1.5 horizontal to 1 vertical, especially at the the preferred failure side. The height of the berm at 1.5 m was reached in 4 days and from then on, 2 lifts (0.6 m) per day were placed until the final day when failure occurred*. An access ramp was built along the north end of the embankment to bring in the fill, and its alignment was kept away from the area of the preferred failure. This rate of construction was generally maintained throughout the construction of the three embankments.

A 450 mm layer of sand was placed over the vegetated ground surface to level the site. The first layer of Tensar SR-2 was laid on this levelled surface on the first day of construction and the placement operation took about 3 hours to complete. The geogrid arrived in 25 m long pre-cut rolls and each strip was pegged to the ground surface by 200 mm long steel pins (Figure 7.3a). Adjacent strips were tied by plastic fasteners to hold the strips together during fill placement. A layer of fill, 300 mm thick, was placed over the geogrid after the instruments at that level had been installed.

---

* Three lifts each 0.3 m thick were placed on the 11th day before failure of the strip reinforced embankment occurred.

These instruments included two horizontal extensometer and three total pressure cells near the base of the embankment, as well as load-displacement sensors (load cells and Bison strain gauges) on the geogrid. Figure 7.3b illustrates some of the instrumentation on the strip reinforcements. The sand was placed along the longitudinal axis of the geogrid in an effort to tighten the reinforcement as filling proceeded. A minimum thickness of 150 mm of fill over the geogrid was required before construction equipment could travel on it. Similarly, the second layer of Tensar SR-2 was placed on the third day of construction. At the end of the fourth day the berm height of 1.5 m was reached, and from the fifth day on, the rate of construction was maintained at 0.6 m per day.

Measurements of the unit weight of the placed sand were made on each layer by means of a portable nuclear density apparatus. An average of 10 to 12 tests were carried out per day. A total of 119 tests were carried out for this embankment. The average total unit weight of the placed fill was 16.9 kN/m^3 and the average water content was 5.4 per cent.

Readings of most of the instrumentation installed were taken before and after the placement of each layer. The more time consuming readings on the extensometers and inclinometers were usually taken at least twice a day.

Failure of the embankment occurred on August 23, 1984, at a height of about 6.0 m above original ground surface. Those instruments which were not damaged were continuously monitored for a week, after which period the failure surface was studied by a local excavation at the toe of the failure and by piezocone testing. Some instruments were recovered for use in the second and third embankments.

7.2 CONTROL EMBANKMENT

Subsurface instrumentation was completed in 3 weeks from August 1 to August 20, 1984. After allowing three weeks for instrument stabilization, the construction work commenced on September 10, 1984. The sand fill used for the construction of the first embankment was taken to build the control embankment. Initially a bulldozer was used to push the fill over the area of the control embankment. When the embankment reached a height of 1.5 m, the bulldozer was used to push the fill to a point where the excavator could pick up and place the material. The same rate of construction as that adopted in building the strip reinforced embankment was maintained. As the bulldozer was used to transport the fill, the stabilizing back face of the embankment took the shape of an access road at a gradient of about 3.5 horizontal to 1 vertical. In an attempt to recover as much sand as possible, some overexcavation at the base of the strip reinforced embankment created a ditch of about 1.4 m depth below general ground surface during the final stages of the construction.

The density of the placed fill was measured by 78 in situ density tests, which indicated an average total unit weight of 18.1 kN/m^3 and an average water content of 6.3 per cent.

The embankment failed on September 19, 1984, at a height of about 5.1 m above original ground surface. Two failures occurred almost simultaneously; one in the anticipated direction of failure and another on the side of the stabilizing berm, into the ditch which had been created by over-excavation of the first embankment.

7.3 GEOCELL REINFORCED EMBANKMENT

Installation of subsurface instrumentation for the geocell reinforced embankment started on August 23, 1984 and took about 4 weeks to complete. During the stabilization period, the geocell mattress was assembled from September 24 to October 3, 1984.

The geocell mattress consisted of interconnected cells of Tensar SR-2 geogrid, 1 m in height and filled with sand. Within the geocell mattress a right angled triangular arrangement of cells was used. The spacing of the transverse members was 1.2 m centres and this resulted in a finished mattress with a total quantity of geogrid equivalent to the two layers of geogrid used in the strip reinforced embankment. A diagram of the cell structure is shown on Figure 7.4.

The geocells were erected over a 150 mm layer of sand which was used to level the site. In order to construct the geocells accurately and quickly, it was necessary that some of the transverse members be tensioned in position. Two screw-in anchors 1.5 m in length were hand augered to about 1 m below ground surface and secured temporarily to the ends of a transverse member. Tension was applied at one end, the berm side, by means of an 18 kN capacity wire winch. Four of these winches (commonly called come-along jacks) were used to erect successive 25 m long transverse members in an upright position. To complete the cell structure, adjacent transverse members were connected by diagonal strips. The connection between panels was facilitated by "bodkin" joints. A typical bodkin joint was formed by bending the ribs on a diagonal strip and the knuckles thus formed were inserted through apertures on the transverse strip at the designated position (Figure 7.4a). A steel rod, 8 mm in diameter and 1.1 m long with a 0.1 m long hook at one end, was inserted through the knuckles to complete the connection (Figure 7.4b). In normal construction practice, the cells are filled after the diagonal panel is installed.

The tension on the two adjacent transverse panels is then released and the procedure of tensioning, stitching and filling progresses along the length of the embankment. In the St. Alban application, the cells were erected but most of them were left unfilled until the mattress was fully erected, to keep the rate of loading on the foundation consistent with that adopted in the other two embankments (Figure 7.5). Only the last row of cells at the south and back (west) ends of the mattress were filled to secure the geocells in position.

Filling of the geocells started on October 9, 1984, after the subsurface instrumentation had had about 4 weeks to stabilize. An access ramp approached the site from the south end and the geocells were filled by backhoe without compaction, with sand used for the construction of the control embankment. Re-tensioning of the transverse panels from the front was necessary during filling to maintain the shape of the mattress. The geocells were filled in about 3 days and the berm height of 1.5 m was reached in 4 days, as planned. The rate of construction was then maintained consistent with the two completed embankments, at 0.6 m per day.

The density of the placed fill was measured by a total of 118 in situ density tests, which indicated an average total unit weight of 18.2 kN/m^3 and an average water content of 9.1 per cent.

The difference in average total unit weights of the three embankments was due to the variation in water contents of the material. No direct compaction was carried out and the compactive effort on the fill for the three embankments from the bulldozer stayed fairly constant, as indicated by the variation in dry unit weight of the material of only 16 to

17 kN/m^3. The bulk unit weight histograms of the three embankments are shown in Figures 7.6 and 7.7. The increase in centreline surcharge for the three embankments with respect to time is shown in Figure 7.8.

Failure of the geocell reinforced embankment occurred overnight between 22:00 hours on October 17 and 7.00 hours on October 18, 1984, at a height of about 4.5 m above original ground surface. The surviving instruments were continuously monitored for a week, during which period some additional field vane and piezocone testing were carried out.

Detailed descriptions of the failures and the inferred locations of the slip surfaces are presented in Chapter 9.

8.0 MONITORING RESULTS

Periodic readings of the installed subsurface instruments were taken prior to the construction of each of the three embankments, to ensure that the readings had stabilized. Initial readings of these subsurface instruments were taken daily during the week preceding the start of construction. During construction, most of the instrumentation were read before and after the placement of each layer of fill. Instruments reading requiring more time and manpower for readings, including the extensometers and inclinometers, were monitored at least twice a day. Horizontal displacements of the monuments were taken by theodolite on a daily basis. The frequency of readings on some of the critical instruments was increased as the embankments approached failure.

In all, a total of 21360 readings in 728 installations were taken during construction of the three test embankments. These figures, together with the number of field tests carried out, are shown in Table 8.1.

	Control Embankment (No. 1)	Strip Reinforced Embankment (No. 2)	Geocell Reinforced Embankment (No. 3)	Total
No. of Installations	218	246	264	728
No. of Readings	6780	8365	6215	21360
No. of Field Tests	34*	5	6	45

Table 8.1 Number of Readings Taken During Construction

* Including site investigation

The results of the monitoring obtained during embankment construction are presented in the following sections. Sections 8.1, 8.2 and 8.3 provide descriptions of the actual data measured in the control, strip reinforced and geocell reinforced embankments. Comparisons of the monitored behaviour of the embankments for the most significant measurements are discussed in Section 8.4. A total of 50 figures (numbered 8.1 to 8.50, inclusive) have been prepared to illustrate the response of the instruments to embankment construction. These figures contain graphs with selected readings plotted against time, from the start of construction to just before or just after failure. Table 8.2 provides a breakdown of the figures in this report which illustrate the data recorded.

		Figure Number	
Type of Instrument	Control	Strip Reinforced	Geocell Reinforced
Pneumatic piezometers	8.1, 8.2	8.15, 8.16	8.31, 8.32
Hydraulic piezometers	8.3	8.17	8.33, 8.34
Electrical piezometers	8.4	8.18	8.35
Settlement plates	8.5	8.19	8.36, 8.37
Monuments (settlement)	8.6, 8.7	8.20	8.38, 8.39
Vertical extensometers	8.8, 8.9	8.21, 8.22	8.40, 8.41
Inclinometers	8.10	8.23	8.42
Monuments (horizontal displacement)	8.11, 8.12	8.24, 8.25	8.43, 8.44
Horizontal extensometers	8.13	8.26	8.45
Total pressure cells	8.14	8.27	8.46
Tensar load cells	-	8.28, 8.29	8.47, 8.48
Bison strain gauges	-	8.30	8.49, 8.50

Table 8.2 - List of Figures Showing Data Recorded

8.1 CONTROL EMBANKMENT - TEST EMBANKMENT NO. 1

Initial readings of the instrumentation were taken on September 10, 1984 at the start of embankment construction. Failure of the embankment occurred on the 10th day of construction, on September 19, 1984. Periodic rain showers occurred during the construction period.

8.1.1 Pore Pressures

The measured pore pressure in the pneumatic, hydraulic and electrical piezometers (Figures 8.1 to 8.4) built up slowly in the first 4 days to a maximum excess head of 1.3 m under the centreline, for a surcharge of about 28 kPa or an equivalent fill height of 1.5 m. During this period, a slight dissipation of pore pressure, in the order of 0.1 to 0.2 m head of water, generally occurred overnight. From the 5th day until the 7th day (equivalent centreline surcharge of 62 kPa) the pore pressure head under the centreline (Piezometers PN-14 to 16) built up more rapidly at a maximum rate of about 1 m per day and no dissipation of pore pressure was observed overnight. From the 7th day until failure, the maximum daily rise in pore pressure head was up to 1.7 m for a rate of increase in surcharge of about 11 kPa/day. The pore pressure continued to build up at this stage by as much as 0.3 m head of water overnight. The maximum excess pore pressure was recorded under the centreline in piezometers located at 3.0 m and 5.0 m below original ground surface (PN-15 and 14, Figure 8.2). The next row of piezometers which was 3.5 m to 5.0 m away from the centreline showed pressure buildups of 60 to 70 per cent of those under the centreline. The response of the piezometers installed further away from the centreline near the toe was less pronounced. At hydraulic piezometers PH-1 to 6, which acted as control points, the water level stayed practically constant throughout the construction.

Hydraulic standpipe piezometers typically recorded values of about 80 to 90 per cent of the excess pore pressures recorded by pneumatic piezometers, for installations at the same depth and offset from the centreline (PH-8 and PN-10, PN-9; Figures 8.2 and 8.3). The difference was only obvious during the last stages of filling. In addition, the dissipation of pore pressures overnight could not be observed in the hydraulic piezometers. This is considered to be due to the slower response time for hydraulic standpipe piezometers.

The electrical piezometer PE-1 which was installed at the same depth and offset from the centreline, as pneumatic piezometer PN-7, showed very similar response during most of the construction period (Figure 8.4). The difference between the readings of the two installations was generally less than 10 per cent. The electrical piezometer showed some reduction in pore water pressure for one day before failure.

It is interesting to note that all the piezometers, with the exception of the electrical piezometer, which were located within a 5 m deep circular segment outcroping at the toe of the observed failure, showed an increase in pressure after failure.

8.1.2 Vertical Deformations

The settlement or heave of the original ground surface was monitored by vertical movements of the settlement plates and monuments (Figures 8.5, 8.6 and 8.7). From the readings of settlement plates installed along the centreline (Settlement Plates SP-7 to 11), it is apparent that the settlements increased uniformly at a maximum rate of about 7.5 mm per day for the first 4 days. From the 5th day on (at a centreline surcharge of about 28 kPa), the rate of settlement under the centreline increased to between 35 mm per day and 40 mm per day. This rate was maintained until just before failure. The maximum settlement was about 240 mm at the location of Settlement Plate SP-7 just prior to failure. Settlement plates installed on a row offset by 5 m from the centreline (SP-3 to 6) showed vertical movements of between 83 and 86 per cent of those at the centreline. At the toe, the settlement or heave was generally about 10 mm prior to failure (MN-11 to 14). The two rows of monuments furthest from the embankment at about 8 m and 3 m from the toe (MN-1 to 6, and MN 6 to 10) indicated insignificant vertical movements prior to failure; these were typically about 5 mm.

The vertical strains in the foundation were measured by 3 electrical extensometers installed to about 16 m depth below original ground surface. A magnetic extensometer (ME-1) was also installed to about 17 m depth at the centreline beside electrical extensometer VE-3 for cross reference (Figure 6.1). The other two electrical extensometers, VE-1 and VE-2, were installed at offset distances of 10 m and 7.5 m from the centreline, respectively. The results of the monitoring (Figures 8.8 and 8.9) indicate that the maximum vertical strains occurred at about 1.5 m depth below original ground level. Significant straining of up to 4.5 per cent was noted at 0.5 m depth within the weathered crust. At a depth of 2.5 m to 3.5 m the vertical strains were noted to be considerably smaller than those in the overlying layer.

The maximum vertical strains in the subsoil measured under the centreline on the morning of the 10th day (equivalent centreline surcharge of about 84 kPa) were 6.2 and 9.3 per cent in the magnetic and electrical extensometers, respectively. It should be noted that fewer measuring points were installed in the magnetic extensometer than in the electrical extensometer; the result being that the strains are the average values over a longer length and therefore the magnetic extensometer installation is less able to record local large strains. Indeed the shape of the strain curve plotted for the magnetic extensometer (Figure 8.9b) suggests that the maximum strain might not have been measured at that location. The readings of the electrical extensometers were therefore taken as the reference for other vertical extensometers. These indicate that the maximum vertical strains for extensometers installed at offsets of 7.5 m and 10 m were about 70 and 15 per cent of those measured at the centreline, respectively.

8.1.3 Horizontal Deformations

The horizontal deformations of the foundation were monitored by two inclinometers installed at offsets of 7.5 m and 10 m from the centreline (Figure 6.1). These were installed to about 17 m below original ground surface. Only the lateral displacements in the anticipated direction of the failure were plotted as the transverse movements were insignificant. The maximum deflections in the inclinometer casings were measured on the 9th day at an equivalent centreline surcharge of 84 kPa. The results indicated that 59 mm and 73 mm of lateral movements had occurred at a depth of 3 m below original ground surface in inclinometers IN-1 and IN-2, respectively (Figure 8.10). Movements in excess of 36 mm were noted down to a depth of 5.5 m below original ground surface. Readings of the inclinometers after the 9th day were impossible because of the excessive curvature of the casing which jammed the sensor probe.

The lateral movements of the ground were also monitored by monuments installed on 3 rows: one at the toe and two at offsets of 3 m and 8 m from the toe of the embankment. Consistent with the behaviour of most of the instrumentation, the lateral movements of the monuments were insignificant until the 5th day (Figures 8.11 and 8.12). From then on the movements increased, to a maximum rate of about 8 mm per day at monument MN-13 near the toe. From the 9th day (centreline surcharge of 73 kPa) until failure, a maximum movement of 32 mm was recorded in 1.5 days at the same monument (Figure 8.12). Horizontal ground movements at monuments installed at offsets of 3 m and 8 m from the toe were typically between 47 and 50 per cent, and between 12 and 21 per cent of those measured at the toe, respectively.

The horizontal strains in the fill were measured by two horizontal extensometers installed at original ground level and at 1.4 m above original ground level (designated HE-1 and HE-2, respectively). Difficulty was experienced in reading extensometer HE-2 on the 6th day. The last reading on this extensometer was taken on the 7th day when the maximum horizontal strain measured was about 0.5 per cent at 12.5 m from the toe (Figure 8.13). In the lower extensometer, a maximum horizontal strain of about 1.8 per cent was recorded at about 13 m from the toe of the embankment on the 10th day, at a centreline surcharge of 84 kPa. The slope of the displacement curve is the average strain measured over the 1 m distance between the rings. A positive slope indicates tensile strain while a negative slope indicates compressive strains which are unlikely at the base of the embankment. The compressive strains measured increase with the distance from the point of measurement. They are considered to reflect inaccuracy in the readings, and the strains have been generally interpreted from a smoothed-out curve.

8.1.4 Earth Pressures

The total vertical earth pressure exerted on the foundation by the fill was measured by two pressure cells, TP-1 and TP-2, installed horizontally at offsets of 10 m and 7.5 m from the centreline, respectively. In addition, two pressure cells were installed on a vertical plane at the centreline (TP-3 and TP-4) to measure the horizontal earth pressure at 1.5 m and 3 m above the original ground surface.

The readings obtained from the horizontally installed pressure cells TP-1 and TP-2 showed similar trends to the construction activity (Figure 8.14).

TP-2 which was located 7.5 m from the centreline or 4 m from the toe, recorded pressures equal to the calculated surcharge until the embankment height reached 1 m. From 1 m to 2 m embankment height, when the crest of the embankment was approaching the axis of the pressure cell, the reading was 30 per cent higher than the maximum surcharge. Above a height of 2 m, the recorded pressure continued to increase. While the magnitude of pressure recorded is not necessarily accurate, the trend of increasing pressure clearly indicates that some degree of arching was taking place. A greater pressure is exerted on the foundation under the slope than is calculated by the weight of fill directly over the cell.

TP-1 under 1.0 m of fill near the toe generally recorded the weight of direct surcharge until day 7 when it increased by about 50 per cent to the time of failure.

Pressure cells TP-3 and TP-4 confirm the trend observed in previous studies, that the horizontal pressure at the centreline of an embankment on soft soil is very small (Bozozuk, 1963).

8.2 STRIP REINFORCED EMBANKMENT - TEST EMBANKMENT NO. 2

This section describes the monitoring results obtained from the strip reinforced embankment. Descriptions are briefer than in the previous section since the results are in many ways similar.

Initial readings of the installed subsurface instruments were taken on August 13, 1984 at the start of embankment construction. Failure of the embankment occurred on the 11th day of construction, on August 23, 1984. No significant precipitation occurred during this period. The results of the monitoring are shown on graphs plotted against time on Figures 8.15 to 8.30, inclusive.

8.2.1. Pore Pressures

The measured pore pressures in the piezometers built up slowly in the first 6 days to a maximum head of 2.8 m. The average rate of pore pressure head increase was about 0.5 m per day and slight dissipation of pore pressure was observed under constant load during this period. The centreline surcharge to the end of this period was about 46 kPa as the fill was lighter than that for the control embankment; the average unit weight being 16.9 kN/m^3. From the 7th day on, the pore pressure head built up more rapidly at a rate of up to 1.5 m per day in pneumatic piezometer PN-15 installed at 3 m depth under the centreline. A rise of pore pressure head of up to 0.4 m was also observed overnight under constant load. This trend continued for 2 days until the evening of the 9th day (centreline surcharge of 78 kPa) when a dissipation of pore pressure of up to 0.2 m was observed overnight in piezometer PN-15. On the 10th day the pore pressure head rose by up to 1.2 m during construction, but remained constant, or dissipated slightly, overnight. On the 11th day the pore pressure head rose by a maximum of 1.8 m (PN-10) before embankment failure occurred. On that date an extra lift of fill (0.3 m) was placed prior to failure.

The distribution of pore pressure across the foundation, when adjusted for the difference in the unit weight of the fill, is very similar to that under the control embankment. The behaviour of hydraulic and electrical piezometers were also similar.

All the piezometers under the main body of the embankment with the exception of PN-16, showed a rise in pore pressure after failure. All piezometers at shallow depths under the toe showed a reduction.

8.2.2 Vertical Deformations

The rate of settlement of the foundation was very uniform in the first 4 days and averaged about 4 mm per day under the centreline (Figure 8.19). A slight increase was noted on the

5th day and an increase in rate of about 20 mm per day was noted in the morning reading on the 6th day. The rate of settlement then further increased to an approximately constant rate until failure, when a maximum total settlement of 223 mm was measured at settlement plate SP-11 at the centreline. In the period from the 6th day until failure, the rate of settlement under the centreline averaged 35 mm per day. At an offset of 5 m the corresponding rate was 26 mm per day (about 75 per cent of the rate at the centreline). Along the toe the measured heave of the monuments reached a maximum of 25 mm prior to failure. The heave of the ground along a line 3 m outside the toe was greater than that at the toe, by as much as 65 mm just prior to failure in monument MN-9.

The vertical strains in the foundation were measured by 3 electrical extensometers installed at the same relative locations as those in the control embankment. Consistent with the behaviour of the same devices in the control embankment, the maximum vertical strains occurred at a depth of about 1.5 m below original ground level, and reduced significantly at a depth of 2.5 m to 3.5 m. The maximum vertical strain measured at the centreline (VE-3) was 8.5 per cent and, as recorded in the control embankment, significant vertical strains of about 5.5 per cent were recorded between 0.5 m and 1.5 m depth, which constitutes the lower zone of the weathered crust.

Maximum strains measured in extensometers installed at offsets of 7.5 m (VE-2) and 10 m (VE-1) from the centreline were typically 85 and 40 per cent of the centreline readings, respectively.

8.2.3 Horizontal Deformations

In general, the deflected shapes of the inclinometer casings IN-1 and IN-2 showed a similar trend to those in the control embankment. The maximum deflections measured, on the 10th day, at a centreline surcharge of 89 kPa, were 108 mm in both installations but occurred at 3 m in IN-1 and at 2.5 m in IN-2. Significant lateral deformation of up to 74 mm was observed down to 5.5 m below ground surface at this surcharge (Figure 8.23). Readings could not be taken in the inclinometers beyond the 10th day because of the pronounced curvature of the casing.

Measurements of the horizontal displacement of the monuments installed in front of the toe, indicated a maximum movement of about 68 mm under a centreline surcharge of 89 kPa. Monuments installed near the axis at offsets of 3 m and 8 m from the toe typically measured lateral movements of about 65 and 20 per cent of those at the toe, respectively (Figures 8.24 and 8.25).

Measurements of the upper horizontal extensometer (HE-2) within the fill are quite scattered, but indicate that the distribution of horizontal strain in the embankment fill was at a maximum near the centreline. The last reading on the 11th day, at a centreline surcharge of 89 kPa, as determined from the slope of the plot in Figure 8.26b, was about 2.2 per cent. The results from the lower extensometer (HE-1) are less scattered and indicate that the horizontal strain was about 2.3 per cent under the centreline, at the same surcharge.

8.2.4 Earth Pressures

The vertical total earth pressure recorded in pressure cell TP-1, at the base of the embankment and located 1.5 m from the toe, followed the surcharge loading until the surcharge became equal to about 26 kPa (Figure 8.27). Thereafter the pressure reading progressively dropped to about 15 kPa and then increased just before failure to 23 kPa. The maximum vertical surcharge directly over the pressure cell was about 17 kPa from the 5th day on and so it appears that some arching took place in the fill, just prior to failure, causing an increase in earth pressures at the location of TP-1.

At the location of TP-2, 4 m from the toe, the recorded pressure also diverged from the surcharge line at about 26 kPa . This reading continued to increase, although at a lesser rate than the loading, until it reached a maximum value of 58 kPa. At the location of TP-2 the maximum vertical surcharge over the pressure cell was about 34 kPa; so some degree of arching can be inferred.

The horizontal total pressure recorded in the fill in TP-4 and TP-5, 1.5 m and 3 m above the base of the embankment at the centreline, respectively, indicated very low pressures, as were noted in the control embankment. However, TP-3 installed in a vertical plane at the base of the embankment under the centreline, indicated a horizontal pressure of about 35 kPa during most of the period of loading. From this it could be inferred that the reinforcement maintained some horizontal pressure in the embankment after initial loading and so provided some resistance to spreading of the fill.

8.2.5 Geogrid Performance

The performance of the geogrid (Tensar SR-2) during embankment construction was monitored by load cells and Bison strain gauges, details of which have been described in Section 6.2. In the strip reinforced embankment, one load cell was installed in each of the upper and lower geogrid layers, at an offset of 5 m from the centreline. Due to a calibration problem in one of the strain gauge readout units, the load cell readings are not considered to be reliable in the first 3 days of construction. This explains why the load-time plots do not intercept the lower axis at the proper day of installation of the geogrids. Tension induced by the fill to the geogrid is expected to be very small during this period.

Similar to the behaviour of many of the instruments in this embankment, the load measured in the load cells stayed at a low level of less than 3 kN/ strip (1 m wide) until the 7th day of construction (Figure 8.29). Under a centreline surcharge of 46 kPa, the measured load started to increase at an approximately constant rate of about 1.5 kN/strip per day until failure occurred. During this period, the upper load cell was measuring about 70 per cent of the load in the lower layer. The measured loads just prior to failure were 9.1 and 6.4 kN/strip, and increased to 15.4 and 11.8 kN/strip just after failure, for the lower and upper load cells, respectively. This is about 30 per cent of the failure load of the geogrid (see Section 10.2). The actual maximum load in the geogrid was almost certainly much higher at failure, as cracking noises were heard in the embankment moments before failure, and this is inferred to indicate tensile breakage of the geogrids.

Bison strain gauges were also mounted in the upper and lower strips of Tensar SR-2 at 3 different offset distances from the centreline. Due to a lead wire problem, described in Section 6.2, all of the strain gauges in the lower layer, and many of those in the upper layer did not function properly. Those which remained in an apparent working order were located in the upper layer at the centreline and at an offset of 3 m from the centreline. These strain gauges indicated that the horizontal strain induced in the geogrid just prior to failure was about 1 per cent under the crest and about 2 per cent at the centreline (Figure 8.30).

Two differential extensometers mounted on the upper and lower layers of Tensar SR-2 indicated that no slip occurred between the fill and the upper surface of the geogrid throughout construction and during the failure of the embankment.

8.3 GEOCELL REINFORCED EMBANKMENT - TEST EMBANKMENT NO. 3

Initial readings of the installed instrumentation were taken on October 9, 1984, at the start of the construction. Failure of the embankment occurred 9 days later, during the night between October 18 and 19, 1984. During the period of construction no significant precipitation was recorded. The monitoring results are shown generally as a function of time in Figures 8.31 to 8.50, inclusive.

8.3.1 Pore Pressures

The response of the pore pressure reflected the particular construction procedure of this embankment which involved the filling of the geocell mattresses. Many of the piezometers showed very little response until the 2nd day of construction, by which time fill had been placed over the area of most of the piezometers.

Continuing from this stage the behaviour of the piezometers was very similar to the two previously built embankments. A noticeable increase in the rate of pore pressure rise, with no overnight dissipation, was observed on the 6th day at a centreline surcharge of 39 kPa (Figure 8.32b). From then on the increase in pore pressure head were observed to be as much as 1.4 m in the pneumatic piezometer PN-15 installed at 3 m below the centreline. The pore pressure at this stage continued to increase by as much as 0.4 m overnight. On the day prior to the embankment failure, the rise in pore pressure head in PN-15 was noted to be as much as 1.7 m.

The distribution of pore pressure, as well as the response of hydraulic and electrical piezometers, was similar to those observed in the other two embankments. After failure most piezometers showed an increase in pore pressure.

8.3.2. Vertical Deformations

The behaviour of the settlement plates and monuments were very similar to those encountered in the two previously built embankments. In the first 4 days, the average settlement along the centreline was about 25 mm. A slight increase was noted on the 5th day; in the next morning an average settlement of about 20 mm was observed on the centreline. The rate of settlement then further increased at an approximately constant rate of about 25 mm per day until failure occurred. The maximum settlement recorded was about 230 mm at settlement plate SP-9 on the centreline (Figure 8.36b). At an offset of 5 m, the settlement was typically about 75 per cent of that on the centreline. West of the centreline at an offset of 6 m on the berm side, the settlement was about 70 per cent of the value at the centreline, suggesting that the settlement profile of the foundation is symmetrical about the centreline. The heave of the ground along a line 3 m from the toe was greater than that at the toe, being as much as 29 mm at MN-8 (Figure 8.38b) compared to 14 mm at the location of MN-13 at the toe (Figure 8.39). Settlements of the row of monuments furthest from the toe, MN-1 to MN-5, were negligible.

The distribution and response of vertical strain in the foundation were also similar to those observed in the other two embankments. By the 9th day of construction, two of the vertical extensometers were inaccessible because of large deformations. The only surviving vertical extensometer VE-3 recorded a vertical strain of 13 per cent under the centreline. The centreline surcharge corresponding to this reading was 85 kPa. The measured maximum strains at offset distances of 7.5 m and 10 m were typically 50 and 10 per cent of the centreline readings, respectively.

8.3.3. Horizontal Deformations

In general the deflected shapes of the inclinometer casings were similar to those in the other two test embankments. The last set of deflection readings were taken at a centreline surcharge of 85 kPa on the 9th day of construction (Figure 8.42). The maximum horizontal displacements were noted to be 110 mm and 76 mm for inclinometers IN-1 and IN-2, respectively. Displacements in excess of 60 mm were noted down to 6 m below ground surface.

Horizontal ground movements as measured in the concrete monuments averaged 62 mm at the toe near the axis. At offsets of 3 and 8 m from the toe, movements were about

70 and 20 per cent, respectively, of those measured at the toe (Figures 8.43 and 8.44).

Some difficulty was experienced in taking readings of the two horizontal extensometers. This could be due to the readjustment of the geocell structure on loading which caused localized misalignment of the flexible extensometer tubing. A few local excavations carried out to repair the extensometers revealed that some of the plywood boards supporting the copper rings were pushed out of their perpendicular alignment to the extensometer tubing. Consequently, the readings were quite scattered (Figures 8.45). However, the distribution of horizontal strains could still be identified to be near maximum at the centreline of the embankment, in the order of 2 per cent in the lower extensometer (HE-1) and between 2 and 3 per cent in the upper installation (HE-2).

8.3.4 Earth Pressures

Vertical total earth pressure recorded by earth pressure cells TP-1 and TP-2 just prior to failure were about 20 kPa and 50 kPa, respectively, which, when compared with the surcharge of 18 kPa and 36 kPa at their respective locations, could infer some arching at TP-2. The pressure at the location of TP-1 diverged from the surcharge after the fill reached its maximum height over the pressure cell (i.e. when the centreline surcharge pressure exceeded 36 kPa), and progressively increased to its maximum value of 50 kPa.

The horizontal total earth pressures recorded were negligible and the high horizontal pressure recorded at the centreline of the fill in the strip reinforced embankment was not repeated in the geocell reinforced embankment.

8.3.5 Geogrid Performance

The load in the geocell structure was monitored by two Tensar load cells, LC-2 and LC-1, installed on a transverse member of the geocell mattress; at the centreline and at an offset of 4.5 m from the centreline, respectively. They did not register a load increase until the 2nd day when the filling of the geocell mattress approached the centreline (Figures 8.47 and 8.48).

When the cell was filled, a load of about 5 kN/strip was recorded in both of the load cells. This could have introduced a prestressing load in the geocell structure which might explain a slight drop in measured load on subsequent days, even when additional load was applied to the foundation. An increase in load was noted on the 6th day and the load continued to increase until failure. On the night before the failure, the last set of readings indicated loads of 19 and 8 kN/strip in the geogrid, in load cells LC-2 and LC-1 under the embankment centreline and crest, respectively.

Bison strain gauges were mounted at 5 locations on the geocell mattress (Figure 6.13). In each location, usually 2 pairs of coils (generating 2 readings) were mounted; one pair at 10 mm from the top and the other pair at a similar distance from the bottom of the assembled geogrid. Two of these locations (BG-1 and BG-5) were on the tranverse members within 0.6 m of the centreline; two others were installed at offsets of 4.4 m (BG-2) and 8.9 m (BG-3). Only 1 pair of coils was installed at mid-depth of the cell at the location of BG-3. A diagonal member on the centreline was also monitored by 2 pairs of Bison coils (BG-4).

Contrary to the observation on the load cell, an equivalent prestressing strain was not readily observed from reading the Bison gauges. The strains recorded on the filling of the geocell mattress were less than 1 per cent, and remained so until the 6th day. Under centreline surcharges in excess of 39 kPa, the strains under the centreline increased at a greater rate. The average strain measured in the transverse members on the centreline just prior to failure, at a centreline surcharge of 85 kPa, was 3.4 per cent. The corresponding average readings at offsets of 3.5 m and 8.4 m were 1.8 and 0.6 per cent, respectively. At the same time, the readings on the diagonal member (BG-4) indicated an average strain of 2.7 per cent.

8.4 COMPARISONS OF EMBANKMENT BEHAVIOUR

The height of the test embankments was increased at the same rate in an effort to maintain the same rate of loading on the foundation. However, the unit weight of the fill in each of the embankments varied because of different water contents. Therefore the surcharge pressure of the fill at the centre of the embankment has been taken as a basis for comparison of embankment behaviour. The settlement of the embankment has to be taken into account in calculating the surcharge pressure, as more fill was actually placed to maintain a constant level at the top of the embankment. The same reasoning could be applied to the heave at the toe. The surcharge pressure is thus calculated from the fill height plus the average of the settlement under the centreline and the shoulder, minus the heave at the toe. This height is multiplied by the average total unit weight of the embankment to obtain the surcharge pressure. A plot of surcharge pressure against the number of days from the start of construction for the three embankments (Figure 7.8), demonstrates that the rates of loading of the foundation were very similar. The average loading rate was in the order of 7 kPa per day for the first 4 days, and increased to about 10.5 kPa per day thereafter. The variation of surcharge pressure is within 5 per cent of the average.

8.4.1. Pore Pressures

The behaviour of the pneumatic piezometer PN-15 is taken to illustrate the build up of pore pressures under the centre of the embankments (Figure 8.51b). This piezometer was placed at an offset of 1.5 m from the centreline and at a depth of 3 m below the original ground level. For all of the embankments it showed the largest response. It can be seen from Figure 8.51b that the pore pressure build-up is very similar in all three test embankments. The conventional pore pressure coefficient ($\bar{B} = \Delta\mu/\Delta\sigma_1$) is given by the gradient of this figure since under the embankment centre, $\Delta\sigma_1$ equals $\Delta\sigma_V$. A $\bar{B}$ value of about 0.5 was observed for surcharge pressures up to between 37 and 41 kPa. These values are very close to the results reported by La Rochelle et al (1974) for the 1972 failed embankment.

The initial low values of $\bar{B}$ could be due to the slight overconsolidation of the St. Alban clay, as demonstrated by Tavenas and Leroueil (1980). The coefficient of consolidation of the clay in this stress range is relatively high and during initial loading some consolidation (dissipation of pore pressure) will take place. Due to this consolidation the $\bar{B}$ value is less than unity. According to Tavenas and Leroueil, the value of $\bar{B}$ can be predicted from the equation:

$$\bar{B} = 0.6 - 2.4 \left(\frac{z}{D} - 0.5\right)^2$$

where z is the depth of the piezometer, which for PN-15 is equal to 3 m, and D is the thickness of the deposit, equal to 9.7 m in this case.

The calculated $\bar{B}$ value of 0.5 is identical to the value observed in this piezometer.

The effective stress in the clay increases as a result of pore pressure dissipation. When the vertical effective stress σ_v' exceeds the preconsolidation pressure σ_p' of the material, the clay becomes normally consolidated and its coefficient of consolidation reduces by a factor of 10 to 50. From then on the undrained condition prevails in the clay and the $\bar{B}$ value should approach unity. Typical pore pressure response under the embankment centre is shown in Figure 8.51a.

Figure 8.51b shows the pore pressure response at PN-15, 3 m under the centre of the three test embankments. The increase in total vertical stress at which $\bar{B}$ becomes unity is in the range of 37 to 41 kPa for the three embankments. The increase in effective vertical stress at this point is the preconsolidation range for the clay ($\sigma_p' - \sigma_{vo}'$) and this can be obtained by subtracting the excess pore pressure from the increase in total vertical stress. From Figure 8.51b, the preconsolidation range for the clay at 3 m below ground surface is in the range of 18 kPa to 20 kPa.

$\bar{B}$ of unity was observed to persist until the increase in total vertical stress reached a value equal to about 60 kPa. Above 60 kPa the slope of the pore pressure response line further increased to about $\bar{B} = 1.3$, and thereafter remained virtually constant until failure occurred.

The increase in $\bar{B}$ at a surcharge of 60 kPa is taken to represent the onset of local failure in the clay at the location of PN-15. Further increase in surcharge causes a reduction in effective stress with $\bar{B} > 1$.

Because of the problem of the orientation of principal stresses at locations other than under the centre of the embankment, the same simple determination of yield and the onset of plasticity cannot readily be made at other locations. However, excess pore pressure response can serve as a good relative measure between the various embankments to indicate the spread of failed zones within the subsoil. For this purpose, the excess pore pressure contours under the axis of the embankments, when subjected to surcharges from 84 to 104 kPa are shown in Figures 8.52, 8.53 and 8.54. In Figure 8.52 the excess pore pressure contours for a centreline surcharge of 84 kPa, are shown for all three embankments. The agreement between them is remarkable; the only differences being a higher pore pressure at 1.5 m depth under the centre of the reinforced embankments and a higher pore pressure at depth under the toe of the strip reinforced embankment. This could be an indication of the strip reinforcement driving the failure deeper but it is not substantiated by the readings under the geocell reinforced embankments which are in close agreement with those under the control embankment. The geocell reinforced embankment failed at a centreline surcharge of 86 kPa.

At a centreline surcharge of 90 kPa, the control embankment and the strip reinforced embankment showed very similar pore pressure response with slightly higher values being recorded at depth under the centre and the toe of the reinforced embankment (Figure 8.53). The control embankment failed at a surcharge of 96 kPa.

Further increase in the height of the strip reinforced embankment caused a greater increase in pore pressure, with the higher values apparently developing along a zone at 5 to 6 m below ground surface. Figure 8.54 shows the pore pressures in the subsoil measured at the failure surcharge of 104 kPa, about 1 hour before failure.

It has been postulated in Chapter 5 that one of the effects of reinforcement inclusions at the base of an embankment on soft clay is to reduce the magnitude of shear stresses in the foundation. This was supported by the finite element analyses carried out. Since failure initiates under the centre of both reinforced and unreinforced embankments and then propagates outwards, the examination of pore pressure response under the embankment toe can help in determining if the reinforcement had any effect on the propagation of failure in the foundation (Figures 8.55 and 8.56).

The excess pore pressures at 5 m under the toe (PN-6, Figure 8.55) of all three embankments were similar at the same centreline surcharge. The geocell reinforced embankment and the control embankment failed at surcharges of 86 kPa and 96 kPa, respectively. Thereafter the pore pressure under the toe of the strip reinforced embankment continued to increase at the same rate until it also failed, at 104 kPa.

At a depth of 3 m under the toe in pneumatic piezometer PN-7 (Figure 8.55), the pore pressure responses of the strip reinforced and the control embankment were virtually identical. A higher pore pressure response for the same surcharge was noted at 3 m under the toe of the geocell reinforced embankment.

At 1.5 m depth under the toe (PN-8, Figure 8.56), the response was again identical in the case of the control embankment and the strip reinforced embankment. At this location a significantly lower response was obtained under the geocell reinforced embankment.

No definitive evidence was obtained that the reinforcement is effective in reducing pore pressure response in the foundation.

8.4.2 Vertical Deformations

The settlements under the centreline of the three embankments show identical trends with a gradual increase in rate of settlement with respect to surcharge loads (Figure 8.57). It is interesting to note that the geocell reinforced embankment, which failed at the lowest height, had the largest settlement for a given surcharge; while the strip reinforced embankment, which achieved the greatest height, had the least settlement. The settlements of all three embankments at failure were in the very narrow range of 220 mm to 235 mm.

8.4.3 Horizontal Deformations in Subsoil

An indication of the ability of the reinforcement to restrain the development of failure in the foundation is the horizontal deformation in the subsoil under the embankment. Figure 8.58 shows the horizontal deflection profiles under the embankments, at 2.5 m from the toe, and under the toe, for a centreline surcharge of 77 kPa. Under the toe of the embankments more horizontal deflection developed in the foundation of the reinforced embankments, where in both cases very large shear distortions develop at between 5 m and 6 m depth.

The horizontal defections measured under the toe of all three embankments at depths of 5.5 m, 3 m and 0.6 m are shown in Figures 8.59 and 8.60.

The trend of deformation is very similar in all of the embankments, except that at high surcharges the deformations below the weathered crust (at 3 m and 5.5 m depth) are significantly greater in the case of the reinforced embankments. The rate of horizontal deformation below the weathered crust increases quite dramatically when the centreline surcharge exceeds about 74 kPa under the geocell reinforced embankment and about 78 kPa under the strip reinforced embankment. A similar increase in the rate with respect to surcharge was noted at 0.6 m depth under the toe of the geocell reinforced embankment and this could reflect the weakness of the crust at that location.

The comparison of horizontal deformations under the embankments provided no evidence that the reinforcement had a beneficial effect on the distribution of stresses in the subsoil under the weathered crust, nor did it help to retard the propagation of failed zones in the foundation. It would appear that the main effect of the reinforcement is to hold the embankment together while deformations develop to a greater extent than would have occurred at failure under an unreinforced embankment.

9.0 OBSERVATIONS OF FAILURES

9.1 STRIP REINFORCED EMBANKMENT

9.1.1 Observations

Failure of the strip reinforced embankment occurred on August 23, 1984 at 16:47. On that day (the 11th day of construction) an extra lift of 0.3 m of fill was placed. The total height of fill placed at the time of failure was 6.0 m above original ground surface. Fifteen minutes after the placement of the last fill layer the failure occurred while a bulldozer was levelling the top of the embankment. Several witnesses working on top of the fill at that time, heard cracking noises in the embankment seconds before the failure. No sign of instability was observed prior to failure.

The failure was sudden; it took place within half a minute and occurred as a massive rotational slip which initiated from the centreline. The crest moved down about 2.0 m and the toe heaved to form a sheared face of approximately the same height. The entire embankment was involved in the failure, as the sidescarps extended to the stability berms on the sides. The backscarp of the failure was noted to be tight, indicating that the frictional resistance of the fill had been mobilized during failure. Numerous tension cracks opened up behind the backscarp, some were even noted on the backside of the embankment.

A sketch of the pattern of cracks and profiles of the failure as surveyed on 5 sections, are shown in Figure 9.1. Photographs showing the top and front view of the failures are presented in Figure 9.2.

9.1.2 Post-failure Investigation

The angle between the base of the fill and the natural ground surface maintained its pre-failure value of 33 degrees after failure; indication that the embankment and the foundation moved as a solid body. From this and the displacement patterns of reference points at the toe and on the fill surface, it is evident that the failure surface had developed along an approximately circular arc. This was further confirmed by a total of 5 piezocone tests (P-2.1 to P-2.5 inclusive) concentrated along the original toe of the embankment. The results of these tests are presented in graphical form in Figures 9.3 to 9.5, inclusive. The location of these field tests have been shown on the in situ test location plan in Figure 4.5. These tests indicated that the failure surface could be located between elevations 94.3 m to 95 m, i.e. at 3.4 m to 4.1 m below the original ground surface. The depth of the failure surface, obtained by averaging the results of tests close to the axis, was at about 4.0 m below the original ground surface.

In addition, a trench excavation was carried out in front of the toe of the failed mass, to a depth of about 1 m below ground surface. The failure surface could be identified as a 0.55 m thick layer of markedly softened material, located at about 0.2 m below the original ground surface. The excavation stayed open just long enough to allow logging of the position of the failure surface (Figure 9.6).

The location at which the maximum deflection of an inclinometer casing occurs is frequently used to identify the depth of slip surface. Measurements taken in the installed inclinometers of this embankment suggested that the failure surface could occur at depths of 3 m to 5.5 m in IN-1 and at 2.5 m to 5.5 m in IN-2 (refer to Section 8.2.3).

The location and depth of the failure surface, as revealed by the results of the monitoring and field testing, are shown on the centreline Profile C in Figure 9.1.

9.2 CONTROL EMBANKMENT

9.2.1 Observations

The embankment failed on September 19, 1984 at about 16:15 when it was at a height of 5.1 m above original ground surface. The failure was witnessed by the excavator operator while the bulldozer was placing more fill to stabilize the backside of the embankment. The excavator had just finished placing the last lift of the day. Two simultaneous failures took place; one towards the front in the intended direction of failure and the other to the back, moving the entire berm. No sign of instability was observed prior to failure. The entire failure lasted about 30 seconds.

The backscarps of the front and back failures were clearly identified along the centreline. In the front, the crest settled about 2.5 m with a roll at the toe about 1.5 m high. As in the case of the strip reinforced embankment, the angle between the fill and the natural ground did not change as a consequence of front fracture and the geometry of the slip suggests that the failure mechanism is rotational. The sidescarps of the front failure extended to the stabilizing berms at the north and south extremities, but appeared to be more confined than the failure in the strip reinforced embankment. The pattern of cracks is shown on Figure 9.8, while photographs of the front slip are shown on Figure 9.9.

At the back of the embankment the crest had settled to about 0.5 m below the backscarp of the front slip. Prior to failure, some over-excavation at the base of the adjacent strip reinforced embankment created a ditch about 1.4 m deep through the weathered crust. The toe of the back slip was clearly emanating from the ditch and an estimated translational movement of 2.5 m squeezed the sidewall of the ditch to roll up to a height of about 1 m. The patterns of cracks suggests a three part wedge, translational type failure. The longitudinal crack at the centreline was noted to be tight. Photographs of the back slip are shown on Figure 9.10.

9.2.2 Post-failure Investigation

A total of 7 piezocone tests (Numbered P-1.1 to 1.5, and P-2.6 and P-2.7) were carried out to locate the slip surface at the front and back of the failed embankment. The results of these tests were plotted on Figures 9.11 to 9.13, inclusive. The results of the piezocone tests P-1.1 and 1.2 indicated that the slip surface at the toe of the embankment could be located at elevation 94.9 m, or at 3.95 m below the original ground surface. The piezocone tests P-1.3, 1.4 and 1.5 were unsuccessful in identifying a slip plane. At the back of the control embankment, the location of the slip surface could be inferred at elevations 94.3 and 94.0 m (4.1 and 4.4 m depths) at the location of piezocone tests P-2.6 and 2.7, respectively.

In addition, seven in situ vane tests (V-20 to V-26, inclusive) were conducted at the locations shown on Figure 4.5. This testing was carried out to further examine the ground around the two failed embankments to detect any inconsistent subsoils. The results of these vane tests are shown on Figure 9.14. The vane strengths obtained from these tests were similar in value and distribution to those carried out in the area prior to construction.

The deflected shape of inclinometers installed near the toe of the control embankment indicated that the slip surface could be located at between 3 m and 5.5 m below the original ground surface in both installations.

The location and depth of the failure surface as revealed by interpretation of these field data are shown in Profile C of Figure 9.8.

9.3 GEOCELL REINFORCED EMBANKMENT

9.3.1 Observations

Failure of the geocell reinforced embankment occurred unwitnessed between 22:00 October 16 and 7:00 on October 17, 1984. The height of the fill above the original ground surface at failure was 4.5 m.

The extent of this failure was the least dramatic of the three embankments, which could be expected as the height was the lowest.

The backscarp of the slip was initiated along the centreline of the embankment, but numerous tension cracks were noted behind the centreline. The settlement at the crest was in the order of 1.5 m while the heave measured at the toe of the failure was also about 1.5 m.

A sketch of the pattern of cracks and profiles of the failed embankment is shown on Figure 9.15. Photographs showing the failure are presented on Figure 9.16.

9.3.2. Post-failure Investigation

The angle between the fill and the natural ground was maintained during the failure and this together with the geometry of the failed mass suggested that the mode of failure was rotational. To locate the slip surface three piezocone tests (Numbered P-3.1, P-3.2 and P-3.3) were carried out along the toe of the unfailed embankment. The results of these tests are shown in Figures 9.17 and 9.18. These indicate that the slip surface could be located at depths between 3.1 m to 3.6 m below the original ground surface. The locations of these tests have been shown in Figure 4-5. Along the axis at the location of piezocone test P-3.1, the slip surface can be inferred to be at a depth of 3.1 m.

Similar to observations made in the other embankments, the failure surface at the location of the inclinometers could be inferred to be between 3 m and 6 m below the original ground surface. The location and depth of these inferred slip surfaces are shown in Profile C of Figure 9.15.

10.0 PERFORMANCE OF THE REINFORCEMENT

The purpose of installing reinforcement in an embankment is to increase the failure height of the embankment. Prior to construction of the test embankments it was postulated that the reinforcement, by controlling strains at the fill/foundation interface, could have some effect on the distribution of stresses in the foundation and hence on the development of kinematically admissible failure surfaces. As has been discussed in the preceding section, a comparison of strains in the foundation and of the development of critical pore pressures in the foundation of the reinforced and unreinforced embankments has failed to indicate an improvement in the foundation response. This section presents back analyses of the failures, using limit equilibrium methods, to determine the effect of the reinforcement on the failure heights. In addition, the strains in the reinforcement are compared with the measured performance of the reinforcing geogrid in order to assess the capacity of the reinforcement under the embankment loading.

10.1 LIMIT EQUILIBRIUM ANALYSES OF EMBANKMENT PERFORMANCE

For the St. Alban site, details are available of two unreinforced embankments constructed to failure, one built in 1972 and the other constructed as part of this study. Against these controls the performance of the reinforced embankments can be compared.

For the four test embankments the data relevant to the limit equilibrium analyses is shown in Table 10.1

EMBANKMENT	Height at Failure (h_c) (1) (m)	Depth of Failure (2) (m)	Fill Parameters Unit wt.(γ) (kN/m^3)	Fill Parameters Surcharge (γh_c) (kPa)	Fill Parameters ϕ' (degrees)
1972 Unreinforced	4.0	4.0	18.9	75.6	44
1984 Unreinforced	5.3	4 to 5.5	18.1	95.9	34
1984 Strip Reinforced	6.2	4 to 5.5	16.9	104.8	34
1984 Geocell Reinforced	4.7	3 to 6	18.2	85.5	34

Table 10.1 Details of Failed Embankments

In all of the failures observed during this study and in the failure monitored in 1972, the mode of failure was clearly rotational and consequently circular arcs have been used in all the analyses.

---

(1) The height at failure is taken as the height above the original ground surface plus the average of the settlement of the base under the centreline and the shoulder of the embankment, and minus the heave of the toe.

(2) Depth of failure inferred from piezocones after failure and inclinometers readings during construction.

The average shear strength profiles measured by in situ vane tests in the areas which eventually experienced the foundation failure are shown in Figure 10.1. Also shown in the figure is the equivalent profile for the site of the 1972 failure.

Any proper comparison between the failed embankments must include some consistent treatment of the weathered crust. It is in the crust that the greatest divergence of measured shear strength occurs when the three profiles under the 1984 embankments are compared.

As discussed in the introduction, a great deal of valuable data has been acquired in the past decade on the strength and performance of soft clay deposits below the surficial zone of weathering. It has been shown by Mesri (1975), Ladd and Foott (1974), and Trak et al (1980) that the available shear strength at failure is uniquely related to the maximum past vertical stress in the soil (σ'_p) and that the ratio of these two parameters c_u/σ'_p is in the range of 0.2 to 0.25 for many soils.

Trak et al (1980) have shown that for the St. Alban site, the strength profile given by $c_u/\sigma p' = 0.22$ is close to the USALS profile, which has been demonstrated by back analyses to be consistent with the strength mobilized under the 1972 embankment at failure (La Rochelle et al 1974).

For the material below the weathered crust at the St. Alban site, the USALS profile has been shown to be close to 0.9 times the profile obtained from the in-situ vane tests (La Rochelle et al 1974). No such simple relationship can be derived for the weathered crust, and in order to carry out a reliable comparison between the various embankments, a consistent approach for the treatment of this layer has to be adopted. For the appropriate choice of methods, reference is made to the back analyses of the 1972 embankment as reported by La Rochelle et al (1974) and Trak et al (1980).

The various assumptions made on the shear strength of the crust have been explained in Chapter 5 of this report and illustrated in Figure 5.2. For a fill with a shear strength defined by $\phi' = 44°$, the factors of safety calculated by back-analysis of the 1972 embankment, using STAB, are shown in Table 10.2

Strength Profile Below Crust	Assumptions of Crust Strength Based on Measured Vane Strength			Crust Strength From USALS	
	FULL	MID-DEPTH	MINIMUM	A	B
USALS				0.94	0.89
c_u Vane	1.2	1.14	0.85		
μc_u Vane* [$\mu = 0.96$]	1.15	1.09	0.82		

Table 10.2 Factors of Safety for 1972 Embankment as calculated by STAB

Based on these results it would appear that the most appropriate assumption for the crust strength based on measured vane strength would be the mid-depth assumption.

---

* Bjerrum 1972 (correction as reported by Trak et al (1980)).

In all of the boreholes put down as part of the confirmatory investigation for the 1984 test embankments, the shallowest vane tests were carried out between 0.8 m and 1 m below ground surface. The thickness of the crust as established by the vane tests and the piezocones can be taken as 1.5 m. The crust has been divided into 2 equal layers and the average value obtained from the shallowest test is taken as the strength of the top layer of crust. The strength of the lower layer is assumed equal to the average of the vane strengths measured in the shallowest vane tests and the vane tests carried out between 1.3 m and 1.5 m depth.

Having established this procedure for defining the strength of the crust, the question of whether or not to apply a correction to the measured vane strength below the crust was addressed. This was done by back analyzing the 1984 unreinforced control embankment. Since the program BTENSAR was to be used for the calculation of forces in the reinforcement at failure, this program was adopted for the back analyses.

The embankment fill placed in 1972 had been compacted during placement to an average unit weight (γ) of 18.9 kN/m^3 and triaxial tests on compacted samples indicated that for this condition, $\phi' = 44°$. In 1984, the sand was placed loose and the different unit weights measured were a consequence of different water contents during construction of the three test embankments. For this loose condition the angle of internal friction was estimated to be 34°.

No cracks developed in the embankment prior to failure and based on a fully mobilized shear strength in the fill ($\phi' = 34°$) and the average unit weight of 18.1 kN/m^3 measured during construction, the factor of safety of the 1984 unreinforced embankment was calculated to be 1.0 when a correction factor of 0.9 was applied to the measured vane strength profile below the crust (mid-depth strength being assumed in the crust). This agrees with the USALS profile and therefore seemed to be appropriate for the analyses.

Using the same method of determining the shear strength profile, a factor of safety of 0.99 was obtained for the 1972 unreinforced embankment at its failure height of 4.0 m using BTENSAR [$\gamma = 18.9\ kN/m^3$ and $\phi' = 44°$].

The sensitivity of the answer to the value assumed for ϕ' for the fill was then checked by calculating the factors of safety for $\phi' = 44°$ for the 1984 fill and $\phi' = 34°$ for the 1972 fill without changing any of the other parameters. This resulted in factors of safety of 1.03 and 0.96, respectively, which confirms that, for a frictional fill within the range of strength considered, the answer is not sensitive to the assumed value for the angle of internal friction of the fill.

The failure of the back of the 1984 unreinforced control embankment was analysed using the same foundation strength profile as used for the analyses of the failure of the front of the embankment. For this analysis the SARMA program was used in order to take account of the trench which had been excavated down to the lower part of the crust at the end of the berm and to investigate non-circular translational type failures. A factor of safety of 1.23 was obtained (Figure 10.3) which does not satisfactorily explain why failure took place in this direction simultaneously with failure towards the front of the embankment. No shear strength measurements were made under the berm prior to construction and it can be speculated that the foundation soil was weaker in this area. It is possible that previous construction of the berm of the strip reinforced embankment in this area had some effect in reducing the strength of the foundation but no evidence is available to support this hypothesis.

The results of the limit equilibrium stability analyses of the unreinforced fills are presented on Table 10.3. Details of the critical surfaces calculated and observed, and the shear strength profiles adopted in the analyses, are given in Figure 10.3.

		BTENSAR		SARMA	
	ø' Fill	Factor of Safety	Depth of Critical Arc	Factor of Safety	Depth of Critical Surface
1972 Embankment	34 44	0.96 0.99	4.0 4.0		
1984 Control Embankment	34 44	1.00 1.03	4.0 4.5	0.97	4.6
1984 Control Embankment Back Failure	34	-	-	1.23	5.0*

Table 10.3 Factors of Safety for Unreinforced Embankments Assuming Mid-Depth Strength in Crust and $c_u = 0.9\ c_{u\ vane}$ Below Crust

* Composite slip surface analysis used only for the back slope

The method so calibrated against both the 1984 and the 1972 unreinforced embankments was then used to analyse the reinforced fills. For the subsoil strength at each failure location, as defined above, and with $\phi' = 34°$ for both embankments and the measured average unit weights, failure heights of 4.6 m and 4.0 m were calculated for the strip reinforced and the geocell reinforced embankments, respectively, if no reinforcement had been included. Since these embankments reached the respective heights of 6.2 m and 4.7 m, it is concluded that the inclusion of the reinforcement caused an improvement in failure heights by 34 per cent and 17.5 per cent, respectively. Using the same computer program (BTENSAR) it was calculated that the total force in the reinforcement at the failure heights, was 123 kN and 64 kN per metre of embankment length for the strip and the geocell reinforced embankment, respectively.

It is interesting to note that the calculated failure heights of 4.0 m and 4.6 m for unreinforced embankments constructed on the sites of the geocell reinforced and the strip reinforced embankments correspond to centreline surcharges of 73 kPa and 78 kPa, respectively. These surcharges are the values at which there was an abrupt increase in the rate of horizontal deformations under the toe of the embankments with respect to surcharge (Figures 8.58 and 8.59).

The improvement in embankment height due to the inclusion of reinforcement as calculated by the limit equilibrium method is summarized in Table 10.4.

	ø' Fill (degrees)	Calculated Failure Height for Equivalent Unreinforced Fill (m)	Observed Failure Height (m)	Improvement (percent)	Calculated Force in Reinforcement at Failure (kN/m)
1984 Strip Reinforced	34	4.6	6.2	34	123
1984 Geocell Reinforced	34	4.0	4.7	17.5	64

Table 10.4 Calculated Improvement in Failure Height and Force in Reinforcement at Failure

10.2 RATE OF STRAIN AND CAPACITY OF THE REINFORCEMENT UNDER EMBANKMENT LOADING

The stress-strain properties of geotextiles and geogrids vary significantly with temperature and strain rate. Manufacturer's literature commonly quotes stress-strain characteristics and strengths for a particular "reference" temperature, strain rate and general test conditions. Not all manufacturers use the same testing technique or reference criteria.

The mechanical properties of Tensar SR-2 commonly included in any technical description have been listed in Table 3.1. Further information and details on testing techniques for Tensar SR-2 have been reported by McGown et al (1984).

The variation of properties with strain rate and, in particular, the tendency for polymer based materials to creep under load and to rupture at stresses above a certain level cause concern to the design engineer. The stress in the reinforcement is a direct function of strain (for a given strain rate) and the strain, in turn, will be controlled by the strains induced in the reinforced soil mass. It has been shown in Chapter 8 that for the case studied, where reinforcement is placed at the base of embankments, the reinforcement has a minimal effect on the strains in the subsoil but it is these strains which will control the strains at the base of the embankment and hence the stress level and creep potential in the reinforcement.

Until now there has been a scarcity of data on the strains which develop at the base of an embankment built on a soft clay foundation; yet it is important to quantify the magnitude and the rate of these strains so that a proper assessment can be made of the capacity of the reinforcement under embankment loading.

Figure 3.2a shows the creep characteristics of Tensar SR-2. In Figure 3.2b the load-strain curves for loads sustained for periods ranging from 1 hr to 10,000 hrs. are shown. Also shown in these figures is the "Performance Limit Strain" for Tensar SR-2 which is defined as the tensile strain below which there is no possibility of failure of the geogrid occurring within the life of the structure (shown in the illustration as 10 per cent for a 120 year design life - McGown et al 1984).

10.2.1 Geocell Reinforced Embankment

Strains in the geocell reinforcement were measured by the Bison gauges as described in Chapter 3. The maximum average strain of 3.4 per cent was recorded in the three gauges on the transverse strip under the centreline of the embankment in the last reading before failure. The corresponding reading on the diagonal member at the centreline was 2.7 per cent.

Figure 10.2 shows a plot of the strain recorded in the Bison gauges (Figures 8.49 and 8.50) against the load recorded in the load cells positioned in the adjacent transverse members of the geocell (Figures 8.47 and 8.48) under both the crest and the centreline of the embankment. From this the overall stiffness of the transverse member, up to a strain of 3.4 per cent was 5.6 kN/per cent strain/strip. Just before failure the load in the transverse member was 19.2 kN/strip. If the diagonal member was operating at the same stiffness, the load in the diagonal member at the same location was 15.2 kN/strip. Resolving the forces, the total resistance being offered by the geocell mattress per unit cell width in the last reading before failure was $19.2 + 15.2 - \sqrt{2} = 29.9$ kN which is equivalent to 25 kN/m length of embankment. It is interesting to note that the instruments on the longitudinal member under the crest gave a similar stiffness and a load of 9 kN at a strain of 1.7 percent.

The load and strain in the reinforcement under the crest was therefore some 50 per cent of the load under the centreline of the embankment in the reading taken just before failure. An examination of the load cell readings during construction indicates that the load at the centreline was increasing at a faster rate as failure approached. The strains recorded in the fill by the horizontal extensometers immediately below and above the geocell mattress indicated maximum strains of 1.6 to 2 per cent at 7.7 days from the start of construction. At that time the surcharge pressure was 74 kPa and the Bison gauges were recording a strain of about 1.8 per cent under the centreline of the embankment (Figure 8.50). There is therefore good agreement between the strain measuring instruments.

The average straining of the reinforcement, calculated over the period of construction, was about 0.26 per cent/day (equivalent to 1.8×10^{-4} per cent/min.). Reference to Figure 3.2a indicates that at this strain rate and load, the reinforcement was in a stable state under the maximum load of 19.2 kN/strip. Details of test results supplied by the manufacturer indicate that the ultimate tensile capacity of Tensar SR-2 when strained at a rate less than 10^{-3} per cent/min. is 60 per cent* of the Peak Load (index value). Taking the ambient temperature in the ground as 10°C a correction factor of 1.1 should be applied and the ultimate tensile capacity, if the above strain rate was sustained, would have been:

$$0.6 \times 68 \times 1.1 = 45 \text{ kN/strip}$$

Higher rates of strain give greater capacity and it must be emphasized that the strain rate was increasing in the period just before failure so that the failure load in the reinforcement would have been greater than 45 kN.

To increase from 19.2 kN as measured just before failure, to some value in excess of 45 kN in the short period between the last reading being taken and the onset of failure, a rapid increase in load must have taken place and since this was ineffective in resisting the failure, it is concluded that there was a significant reduction in the strength of the foundation in the period immediately preceding failure.
It is interesting to note that at the conservatively

---

* 60 per cent is the minimum capacity which is applicable for all strain rates less than 10^{-3} per cent/min.

extrapolated rupture load of 45 kN in the transverse member of the geocell, the total resistance available in the geocell mattress was: 45 x 25 + 19.2 = 58 kN/m. This is in agreement with the force in the reinforcement back-calculated for the geocell mattress at failure (64 kN/m) by limit equilibrium methods. Since the estimated failure load of 45 kN is likely to be conservative, it is concluded that the limit equilibrium analysis has probably under-estimated the load in the reinforcement to some degree.

10.2.2 Strip Reinforced Embankment

The same detailed comparison of the stress-strain performance of the strip reinforcement cannot be made because of failure of the Bison gauges attached to the reinforcement in this embankment.

The load cells were installed under the embankment crest and the loads recorded about 1 hour before failure were 9.1 and 6.4 kN/strip (1 m wide) in the lower and upper layers, respectively. In the horizontal extensometers, installed just under the lower layer, a maximum strain of about 2.3 per cent was measured under the centre of the embankment and about 1 per cent under the crest at 10.4 days from the start of construction. At that time, the measured loads in the lower and upper layers of reinforcement under the crest were 8.5 and 6.0 kN/strip, respectively. This indicates an overall stiffness of the reinforcement of 600 kN/m to 850 kN/m. While the horizontal extensometers do not directly measure the strain in the reinforcement, the stiffness of the reinforcement inferred from the readings agree with the value of 560 kN/m obtained from the load cells and also with the Bison gauges on the geocell mattress.

The load cells were not located under the centreline of the embankment at the point of maximum strain and so the loads measured were not the maximum load in the reinforcement at the time of reading. From the strain measurements it is considered that the total maximum load in the two layers at the centre of the embankment about 1 hour before failure was about 40 kN/m of embankment length. As discussed above, the ultimate failure load of Tensar SR-2 even for very slow strain rates is about 45 kN/strip. For the two strips, the rupture load is likely to be about 2.5 times the load measured just prior to failure. It is therefore apparent, as in the case of the geocell mattress, that the sudden failure which occurred must have been precipitated by some loss in strength of the foundation prior to failure.

Given that the estimated failure load of 45 kN/strip (90 kN/m for two layers) is recognized to be an underestimation of the true failure load under the rapid straining which must have led to failure, it is considered that the value of 123 kN/m calculated for the total force in the two layers of reinforcement at failure is a reasonable value.

11.0 DISCUSSION

The analysis of the results from the instrumented test embankments has led to a number of important observations. Some of these relate to the general problem of design and construction of embankments on soft clays, while others are concerned with the performance and design of reinforced embankments.

The pore pressure responses and deformations of the St. Alban clay measured under the three test embankments were very similar to those reported in previous studies on the clay. Pore pressure response under the centre of all the embankments indicate that yielding of the clay under the weathered crust at a depth of 3 m takes place at an increase in vertical effective stress of 18 to 20 kPa. When the increase in total vertical stress increases to above about 60 kPa, the soil exhibits strain softening characteristics with the pore pressure increases induced by each stage of loading in excess of the increase in applied load ($\bar{B} > 1$).

The site was chosen because of its well known and consistent subsoil properties and apart from some local variations in shear strength profiles, the consistency of the material below the weathered crust was confirmed by the monitoring results. Given this apparent consistency in the performance of the St. Alban clay, it is at first sight surprising that embankment failure heights varied so erratically.

The strength mobilized under the weathered crust at St. Alban during an embankment failure is defined by an USALS profile which agrees closely with the profile given by: $c_u = 0.22\ \sigma'_p$. This profile is close to 0.9 times the average shear strength as measured by in-situ vane tests.

A much greater problem is to determine the strength of the crust which is mobilized during embankment failure. No reliable prediction of the failure height of an embankment on soft clay can be made until reliable data on the crust is obtained and the applicability of this data to stability analyses is demonstrated.

The limit equilibrium analyses described in this report made use of the four known test embankment failures on the same site in order to calibrate a method of analysis and the interpretation of strength data available for the foundation. The crust strength assumed was the "mid-depth" strength and although this is not considered to be necessarily the actual strength mobilized in the crust, it gave the correct answer in the back-analysis of the two unreinforced fills (1972 and 1984). When this crust strength is consistently applied to the reinforced embankments, the improvement in failure height due to the inclusion of the reinforcement can be determined. From the analysis, it appears that the strip reinforcement allowed a 34 per cent increase in the failure height, while the geocell reinforcement allowed the embankment to be built 17.5 per cent higher than its "unreinforced" failure height.

The relative lack of effectiveness of the geocell mattress is considered to be due to the members not all being orientated along the direction of maximum destabilizing force as were the strips in the other embankment. Any increase in flexural stiffness at the base of the embankment provided by the geocell does not appear to affect the stress distribution in the foundation sufficiently to compensate for the reduction in tensile capacity. The flexural stiffness could possibly have been increased by compacting the sand fill in the cells. Compaction was considered to be impractical at reasonable cost on a full scale project and for this reason it was not carried out. For the conditions of the test embankments it is concluded that the geocell mattress is inferior to the simple horizontal strip layout which is far easier to place and construct.

Based on the results of this study it would appear that the simple method of limit equilibrium stability analysis presented in this report can be used to predict the failure height of a reinforced, embankment provided that the strength of the crust is known.

The study has shown that even on an "ideal" site, significant differences in the strength depth profile occur over short distances. More importantly, the strength of the crust can be so variable that details of it must be known at close spacings if an accurate prediction of failure height is to be made. For embankment design, the probable failure at any location must be investigated and therefore the location where the embankment is likely to fail should provide the relevant profile for design. For this a conservative estimate of the crust strength is required. Further, care must be taken not to disturb the crust during or after construction.

The tensile stress at which the Tensar SR-2 geogrid failed in the reinforced embankments was at least 45 kN/strip which is consistent with the value back calculated by limit equilibrium analyses. For embankments on soft clay foundations, forces in the reinforcement are a direct consequence of the strains induced in the foundation. The maximum strain in the test embankments was about 3.5 per cent up to and immediately before failure in the test embankments. Creep failure of the reinforcement would not be a problem at a strain of 3.5 percent.

Relatively low loads were observed in the reinforcements a few hours before failure, and these would have to have increased significantly for failure of the reinforcement to occur. It therefore appears that at failure, the resistance of the soil was significantly less than had been available a few hours earlier. This confirms a strain softening effect in the foundation during failure as indicated by laboratory tests (Figure 1.1).

Comparison of the pore pressure response and the lateral deformations under the embankment suggest that the reinforcement does little to restrain the foundation. Instead, its effect is to hold the embankment together and allow more extensive propagation of failure and consequent deformations in the foundation soil before overall failure is initiated.

At the present state of knowledge, simple limit equilibrium analysis with realistic properties for the reinforcing elements and some conservative estimate for the strength of the crust, offers the most reliable method of design.

LIST OF REFERENCES

BISHOP, A.W. (1955). The Use of the Slip Circle in the Stability Analysis of Slopes. Geotechnique 5. No. 1.

BISHOP, A.W. AND BJERRUM, L. (1960). The Relevance of the Triaxial Test to the Solution of Stability Problems. N.G.I. No. 34, Oslo.

BJERRUM, L. (1972). Embankments on Soft Ground. Proceedings of the ASCE Specialty Conference on Performance of Earth and Earth-Supported Structures, Purdue University, West Lafayette, IN, Vol. 2, pp. 1-54.

BJERRUM, L. (1973). Problems of Soil Mechanics and Construction on Soft Clays, Proc. 8 Int. Conf. on SMFE, Moscow.

BOZOZUK, M. (1963). The Modulus of Elasticity of Leda Clay from Field Measurements. Canadian Geotechnical Journal Vol. 1, No. 1, pp. 43-51.

CLARK, T.H. (1949). Les Terrains paleozoques, Rapport Preliminaire Sur la Region De Grondines, Ministere des Mines, Quebec, R.P. 237.

JUNEAU, R. and ROY M., (1973). Etude Pressiometrique du site de Saint-Alban. Departemente de genie civil. Faculte des Sciences. Universite Laval, Quebec, Quebec, Rap. Int. No. GCN-73-04-04 (MS-N6).

LA ROCHELLE, P., TRAK, B., TAVENAS, F. and ROY, M. (1974). Failure of a Test Embankment on a Sensitive Champlain Clay Deposit. Canadian Geotechncial Journal 11, No. 1.

LADD, C.C., and FOOTT, R. (1974). New design procedure for stability of soft clays, ASCE Journal of the Geotechnical Engineering Divison, 100(GT7) pp. 763-786.

LEROUEIL, S., TAVENAS, F., TRAK, B., LA ROCHELLE, P., and ROY, M. (1978a). Construction pore pressures in clay foundations under embankments. Part I: the Saint-Alban test fills. Canadian Geotechnical Journal, 15, pp. 54-65.

MESRI (1975). Discussion on Ladd and Foott (1974), Journal of the Geo. Eng. Div., ASCE, Vo. 101, No. GT 4.

McGOWN, A., ANDRAWES, K.Z., YEO, K.C., and D. DUBOIS (1984). The Load-Strain-Time Behaviour of Tensar Geogrids. Proc. Symposium on Polymer Grid Reinforcement in Civil Engineering, Inst. Civ. Eng., London, England, 1984.

LIST OF REFERENCES (cont'd)

PATERSON, W.D.O. (1972). The Measurement of Pavement Deformations using Induction Coils, KKU Bulletion No. 13, National Roads Board, New Zealand.

SARRAILH, J., and TAVENAS, F.A. (1972). Etude geotechnique preliminare du site de Saint-Alban-Essais vane et penetrometre. Departement de Genie Civil, Faculte des Sciences, Universite Laval, Quebec. Quebec. Rap. Int. No. GCN-72-09-02 (MS-N2)

SARMA, S.K., (1973). Stability Analysis of Embankment and Slopes. Geotechnique, Vol. 23, No. 3.

SELIG (1971). Soil Compaction Evaluation with Strain Measurement. New York State Dept. of Transportation. Engineering Research and Development. Report No. FLDGP8M14B13B.

TAVENAS, F.A., and CHAPEAU, C., (1973). Etude en laboratoire des proprietes geotechniques de l'argile de Saint-Alban, Department de Genie Civil Faculte des Sciences, Universite Laval, Quebec, Quebec. Rap. Ing. GCN-73-040-03(MS-N5).

TAVENAS, F.A., CHAPEAU, C., La ROCHELLE, P. and ROY M. (1974). Immediate settlement of three test embankments on Champlain clay. Canadian Geotechnical Journal 11 (1), pp. 109-141.

TAVENAS, F. and LEROUEIL (1980). The behaviour of Embankments on Clay Foundations. Canadian Geotechnical Journal 17, No. 2.

TAVENAS, F.A., ROY, M. and LA ROCHELLE, P. (1973). An Artificial Material for Simulating Champlain Clays. Canadian Geotechnical Journal Vol. 10, No. 3, pp. 489-503.

TRUESDALE, W.B.(1963). Development of a Small Soil Strain Gauge. Air Force Special Weapons Centre Report No. AFSWC-TDR-63-3, New Mexico.

TRUESDALE, W.B. and ANDERSON, H.E. (1964). A New Device for Soil Strain Measurement. Proceedings of the Symposium Soil Structure Interaction, University of Arizona.

LIST OF SYMBOLS

I. GENERAL

$\pi = 3.1416$

e = base of natural logarithms 2.7183

$\log_e a$ or $\ln a$, natural logarithm of a

$\log_{10} a$ or $\log a$, logarithm of a to base 10

t	time
g	acceleration due to gravity
V	volume
W	weight
M	moment
F	factor of safety

II. STRESS AND STRAIN

u	pore pressure
σ	normal stress
σ'	normal effective stress ($\bar{\sigma}$ is also used)
τ	shear stress
ϵ	linear strain
ϵ_{xy}	shear strain
ν	Poisson's ratio (μ is also used)
E	modulus of linear deformation (Young's modulus)
G	modulus of shear deformation
K	modulus of compressibility
η	coefficient of viscosity

III. SOIL PROPERTIES

(a) *Unit weight*

γ	unit weight of soil (bulk density)
γ_s	unit weight of solid particles
γ_w	unit weight of water
γ_d	unit dry weight of soil (dry density)
γ'	unit weight of submerged soil
G_s	specific gravity of solid particles $G_s = \gamma_s/\gamma_w$
e	void ratio
n	porosity
w	water content
S_r	degree of saturation

(b) *Consistency*

w_L	liquid limit
w_P	plastic limit
I_P	plasticity index
w_S	shrinkage limit
I_L	liquidity index $= (w - w_P)/I_P$
I_C	consistency index $= (w_L - w)/I_P$
e_{max}	void ratio in loosest state
e_{min}	void ratio in densest state
D_r	relative density $= (e_{max} - e)/(e_{max} - e_{min})$

(c) *Permeability*

h	hydraulic head or potential
q	rate of discharge
v	velocity of flow
i	hydraulic gradient
k	coefficient of permeability
j	seepage force per unit volume

(d) *Consolidation (one-dimensional)*

m_v	coefficient of volume change $= -\Delta e/(1+e)\Delta\sigma'$
C_c	compression index $= -\Delta e/\Delta \log_{10} \sigma'$
c_v	coefficient of consolidation
T_v	time factor $= c_v t/d^2$ (d, drainage path)
U	degree of consolidation

(e) *Shear strength*

τ_f	shear strength	
c'	effective cohesion intercept	in terms of effective stress $\tau_f = c' + \sigma' \tan \phi'$
ϕ'	effective angle of shearing resistance, or friction	
c_u	apparent cohesion*	in terms of total stress $\tau_f = c_u + \sigma \tan \phi_u$
ϕ_u	apparent angle of shearing resistance, or friction	
μ	coefficient of friction	
S_t	sensitivity	

---

*For the case of a saturated cohesive soil, $\phi_u = 0$ and the undrained shear strength $\tau_f = c_u$ is taken as half the undrained compressive strength.

SECTION 1

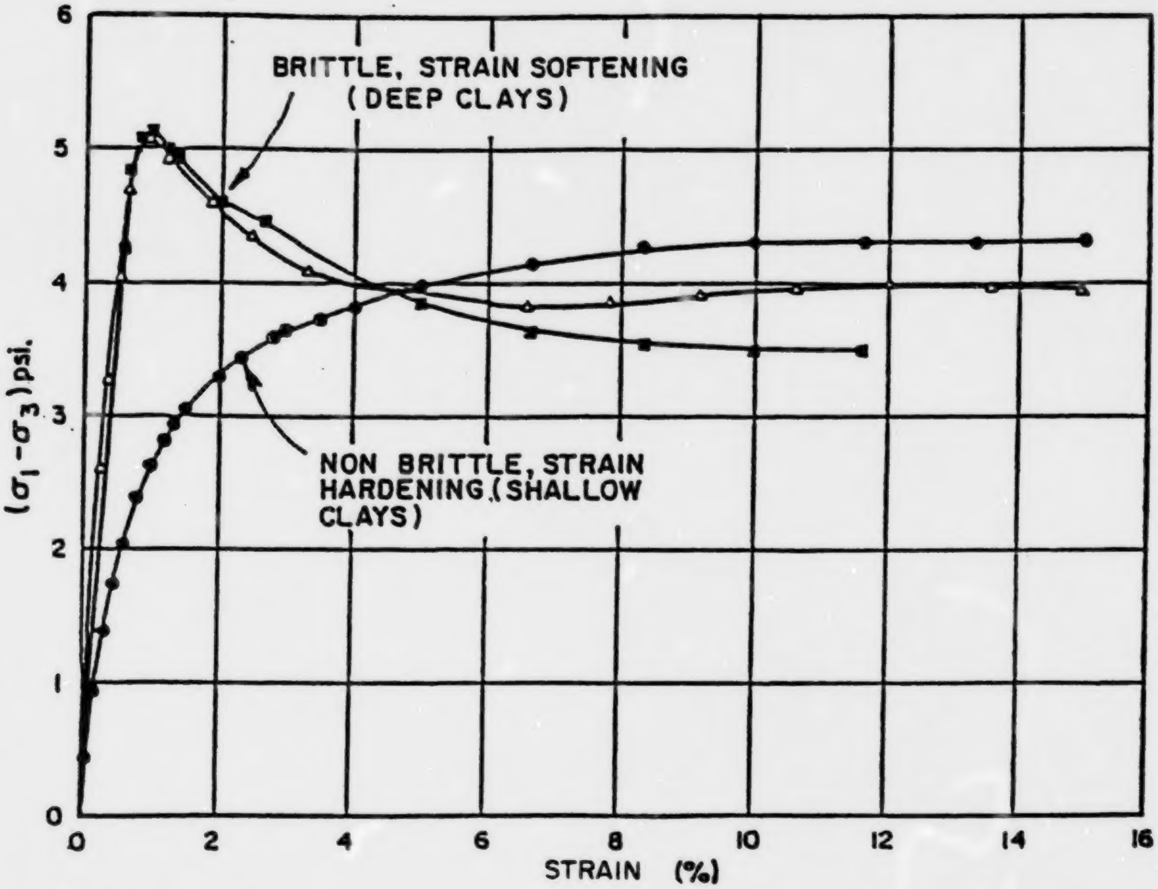

(AFTER LAROCHELLE ET AL, 1974)

FIGURE 1.1 TYPICAL STRESS-STRAIN BEHAVIOUR OF CLAY (ST. ALBAN)

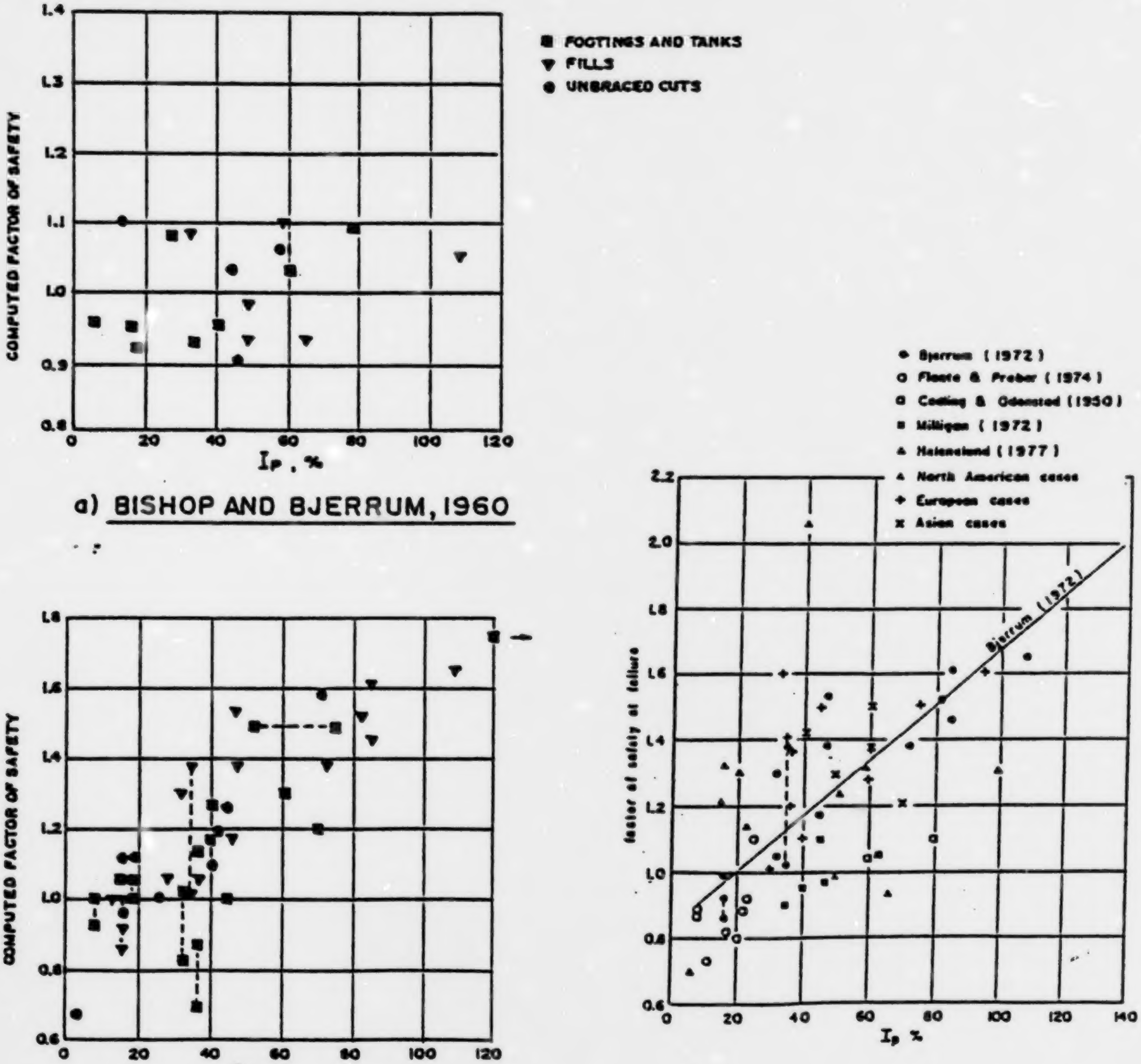

a) BISHOP AND BJERRUM, 1960

b) BJERRUM, 1973

c) TAVENAS, 1980

FIGURE 1.2 UNDRAINED STRENGTH STABILITY ANALYSIS

SECTION 2

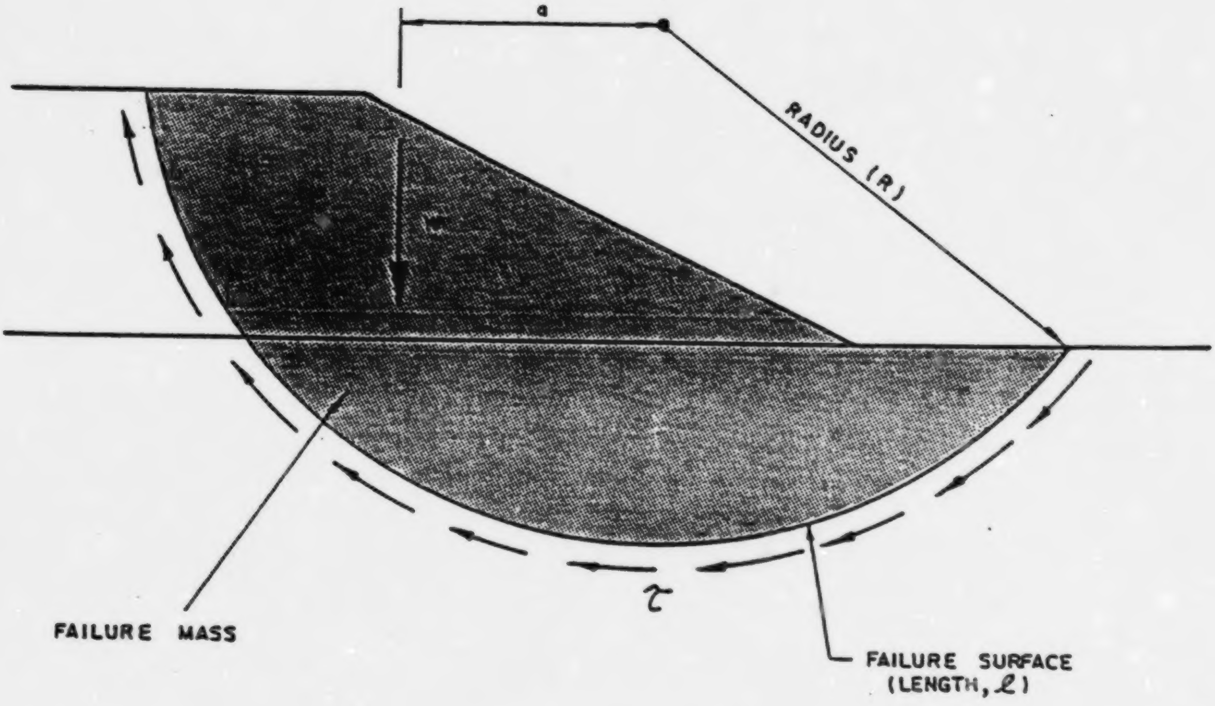

FACTOR OF SAFETY, (FS) = $\frac{\tau . \ell . R.}{W. a.}$ $\frac{\text{(RESISTING MOMENT)}}{\text{(DISTURBING MOMENT)}}$

FIGURE 2.1 BASIC ELEMENTS OF LIMIT EQUILIBRIUM STABILITY ANALYSIS

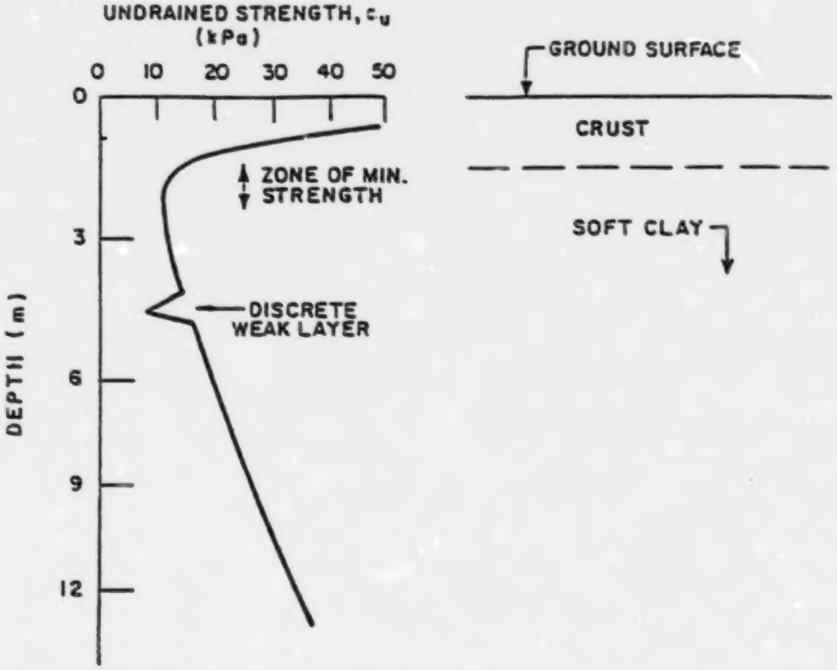

a) STRENGTH VARIATION WITH DEPTH

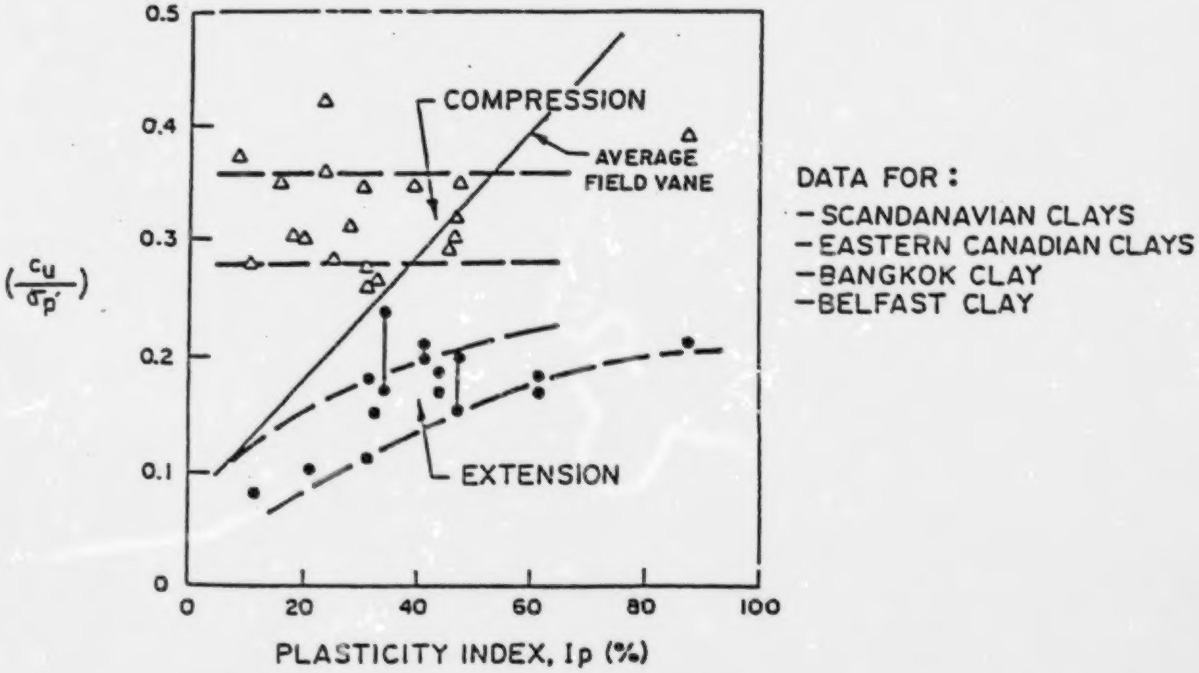

b) UNDRAINED STRENGTH ANISOTROPY

FIGURE 2.2 FACTORS AFFECTING UNDRAINED SHEAR STRENGTH

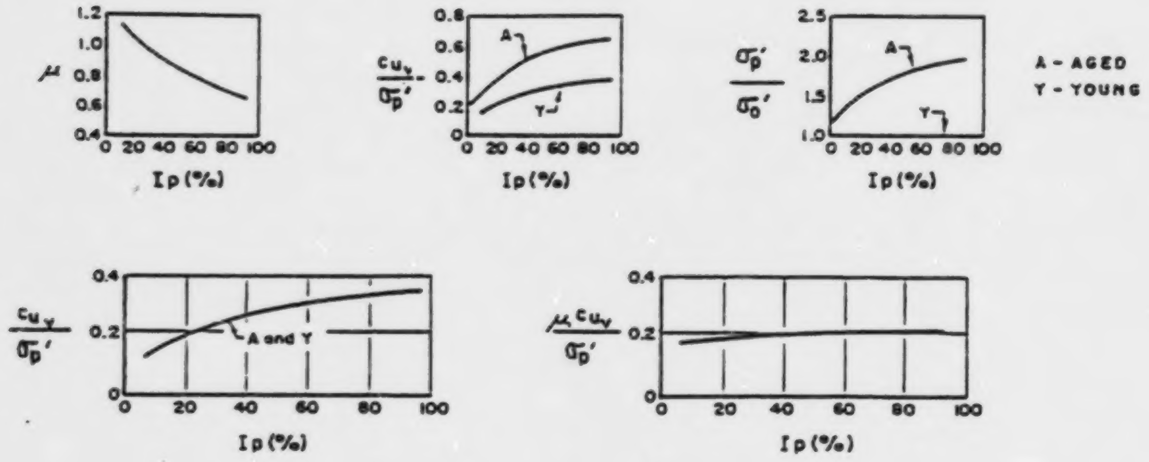

a) MESRI'S INTERPRETATION OF BJERRUMS DATA

(MESRI, 1975)

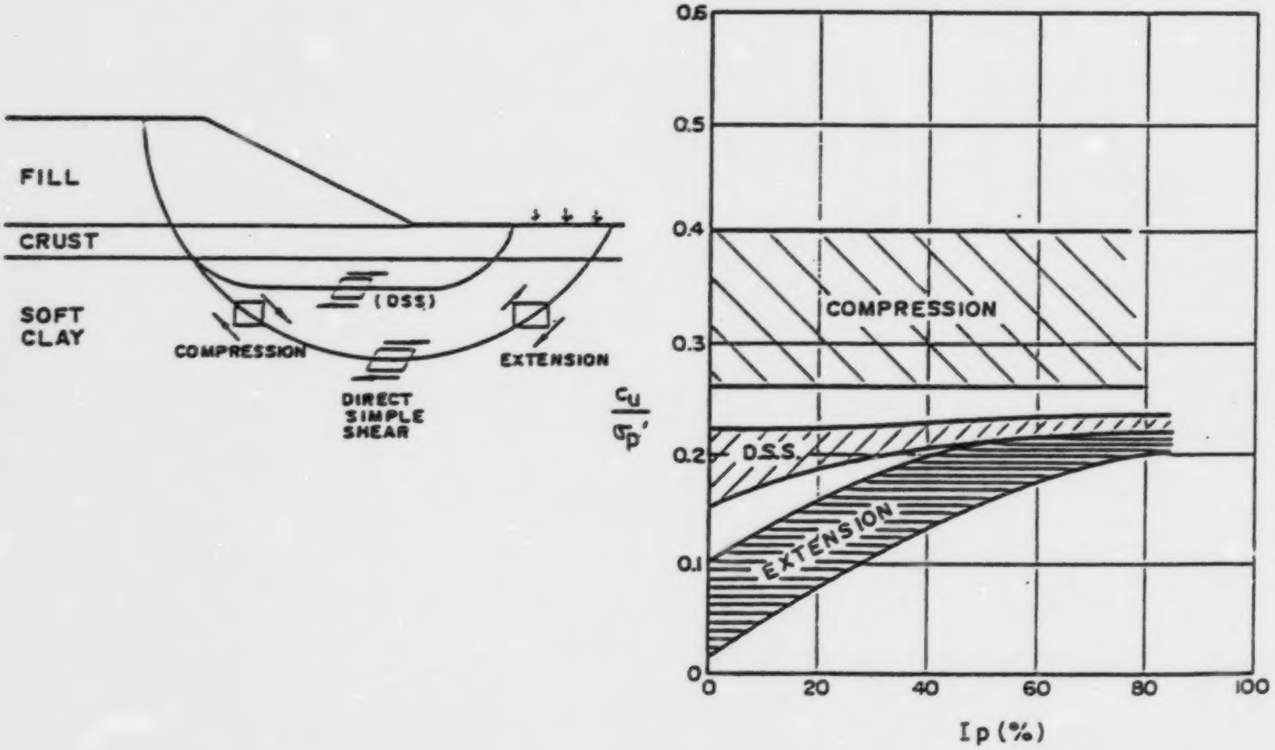

b) LADD- cu (D.S.S.) APPROACH

(LADD AND FOOTT, 1974)

FIGURE 2.3 DEFINITIONS OF UNDRAINED SHEAR STRENGTH AT FAILURE

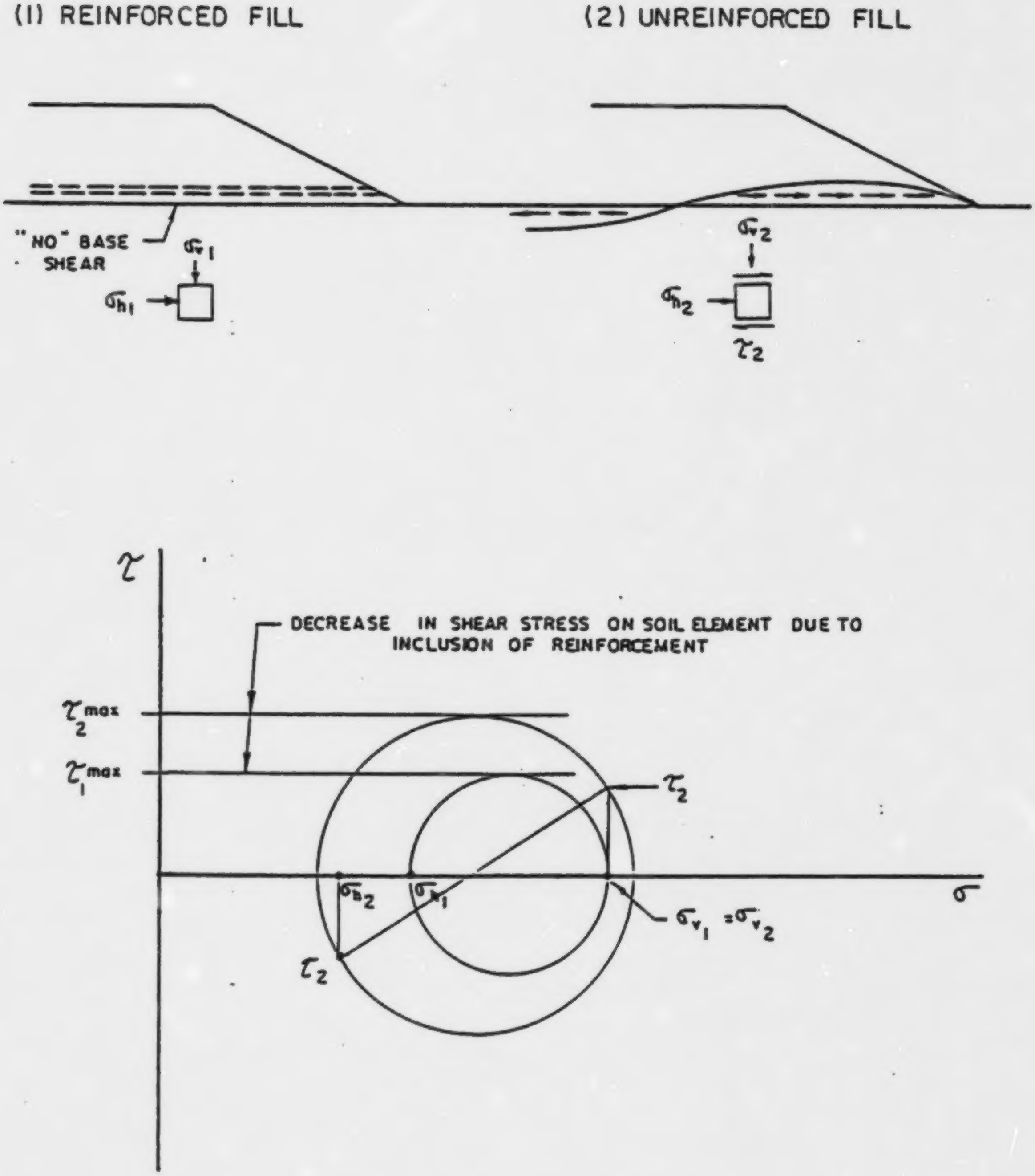

FIGURE 2.4 SPECULATED EFFECT OF GEOGRID ON SHEAR STRESS IN FOUNDATION

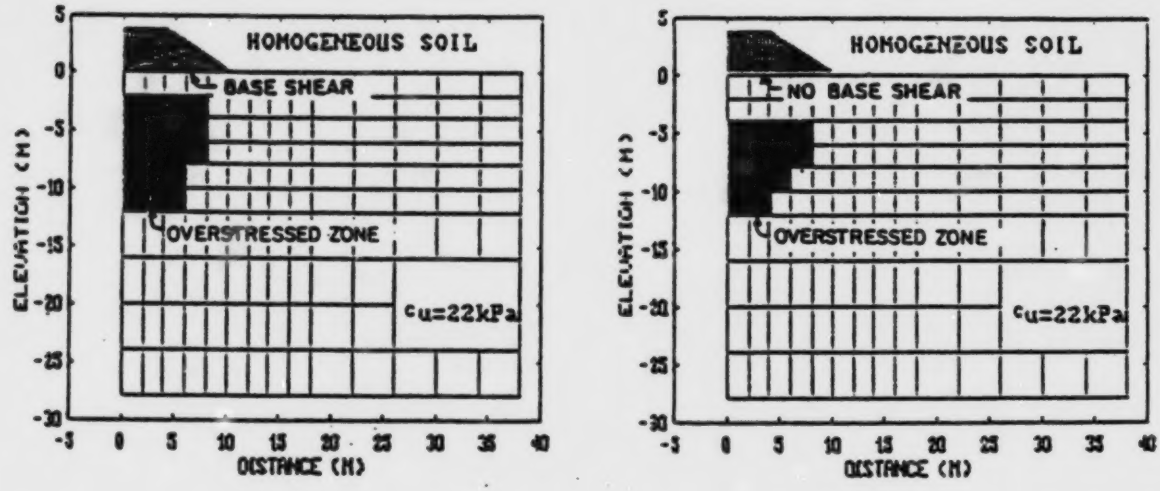

UNREINFORCED FILL

REINFORCED FILL

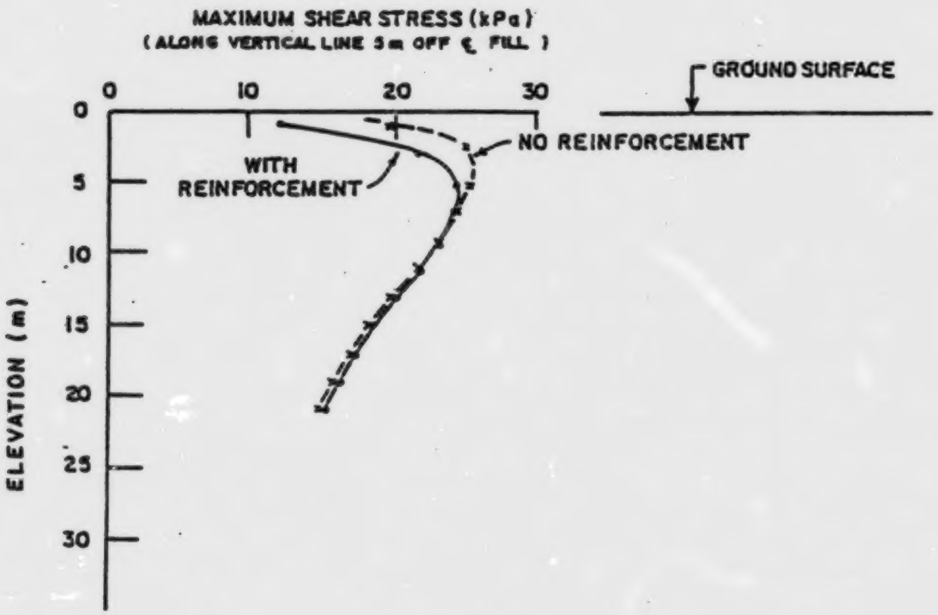

FIGURE 2.5 SPECULATED EFFECT OF GEOGRID ON SHEAR STRESS DISTRIBUTION

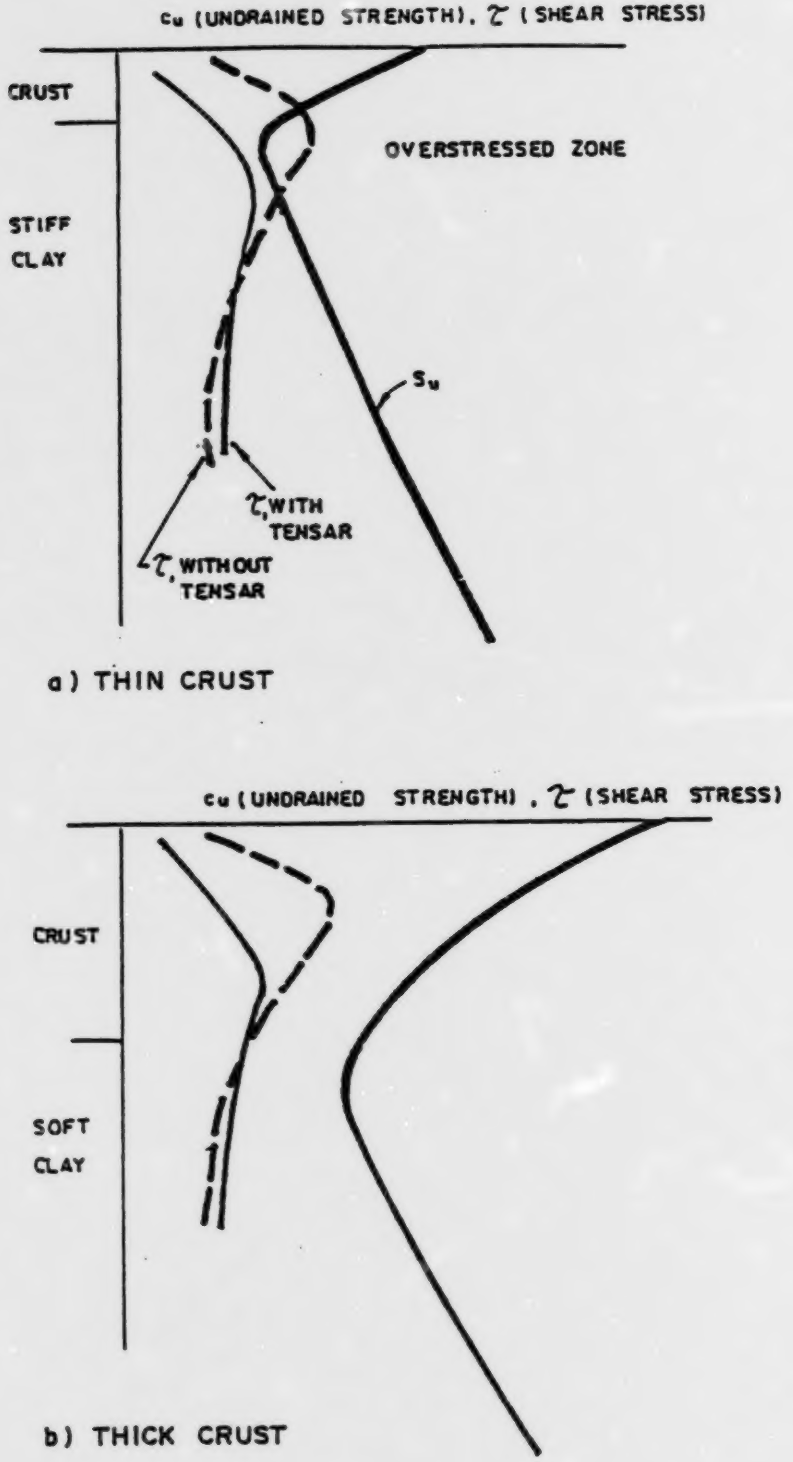

FIGURE 2.6 SPECULATED INFLUENCE OF CRUST THICKNESS ON GEOGRID EFFECTIVENESS

SECTION 3

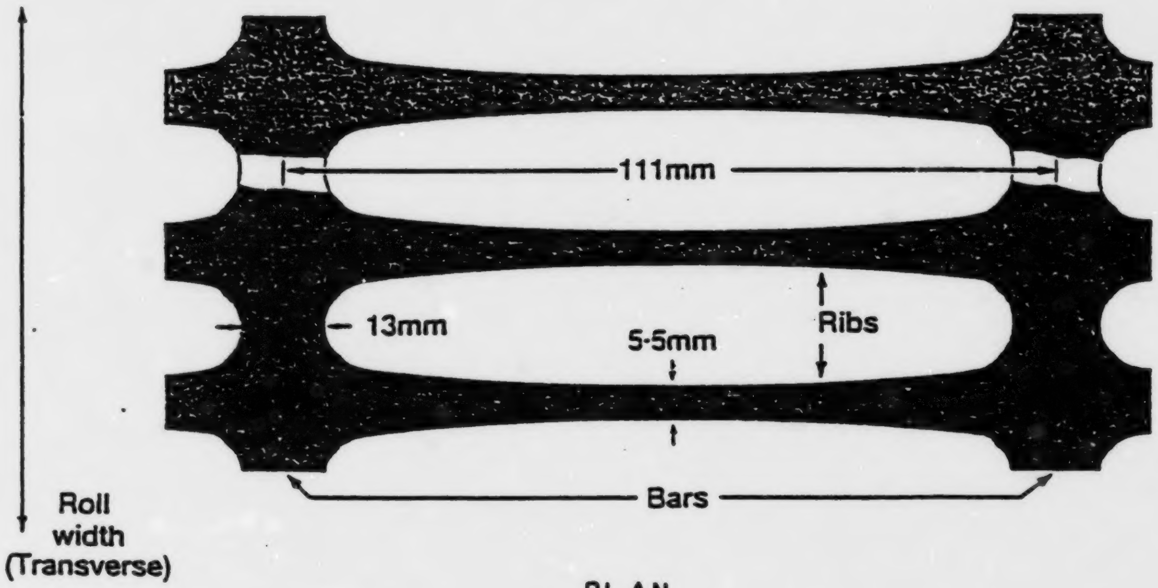

PLAN

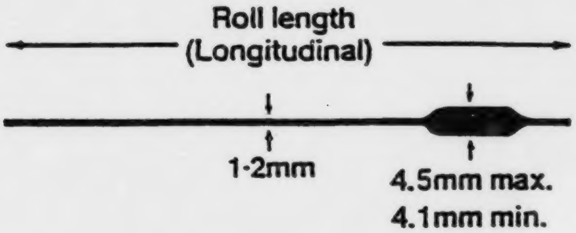

TYPICAL SECTION

TYPICAL DIMENSIONAL PROPERTIES

PRODUCT WIDTH	: 1 m
PRODUCT LENGTH	: 30 m
NUMBER OF RIBS	: 46 / UNIT WIDTH
WEIGHT (APPROX.)	: 28 kg / ROLL
COLOUR	: BLACK

FIGURE 3.1 TYPICAL DIMENSIONS OF TENSAR SR-2

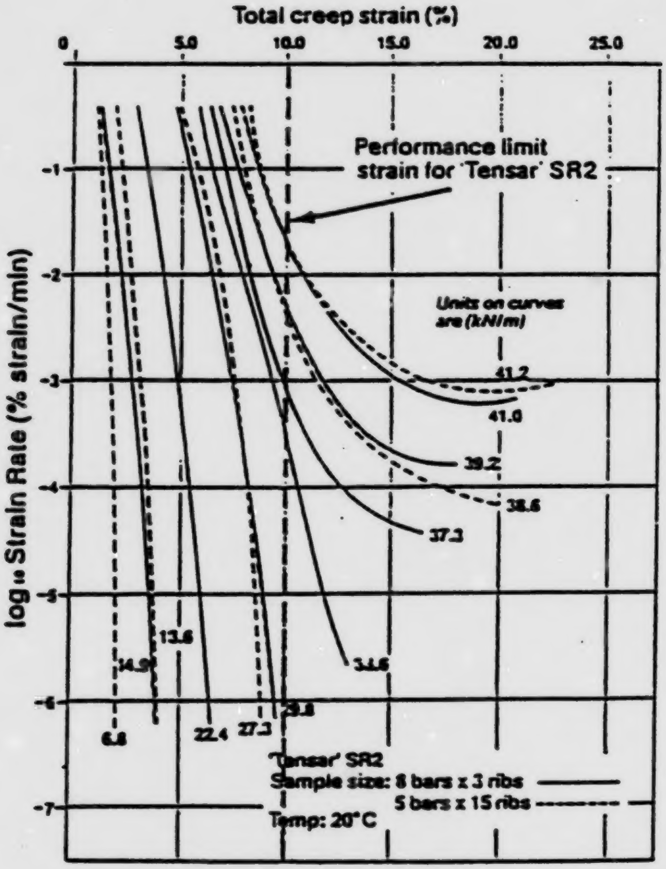

a) CREEP STRAIN RATE VS STRAIN

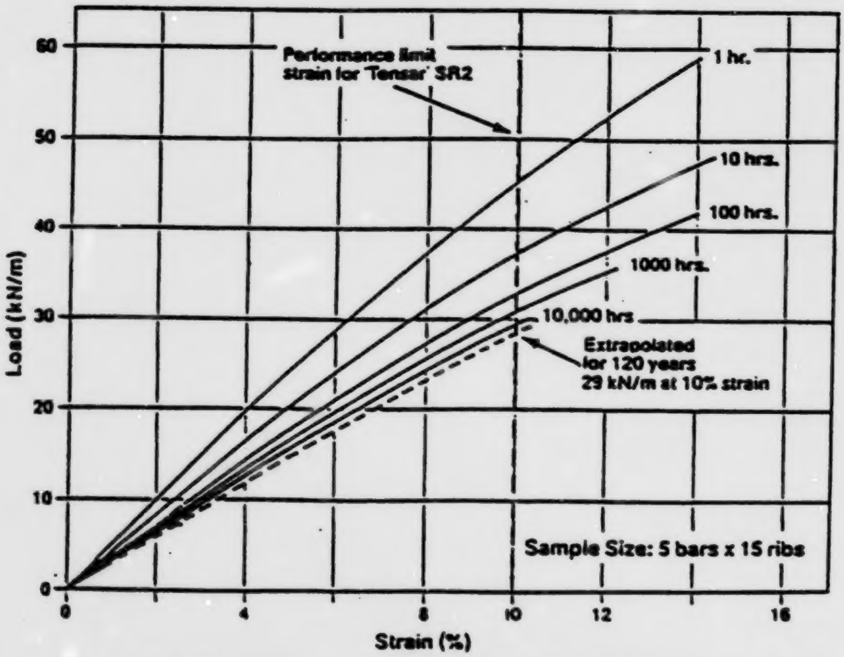

b) ISOCHRONOUS LOAD STRAIN CURVES

FIGURE 3.2 CHARACTERISTIC STRENGTH OF TENSAR SR-2

SECTION 4

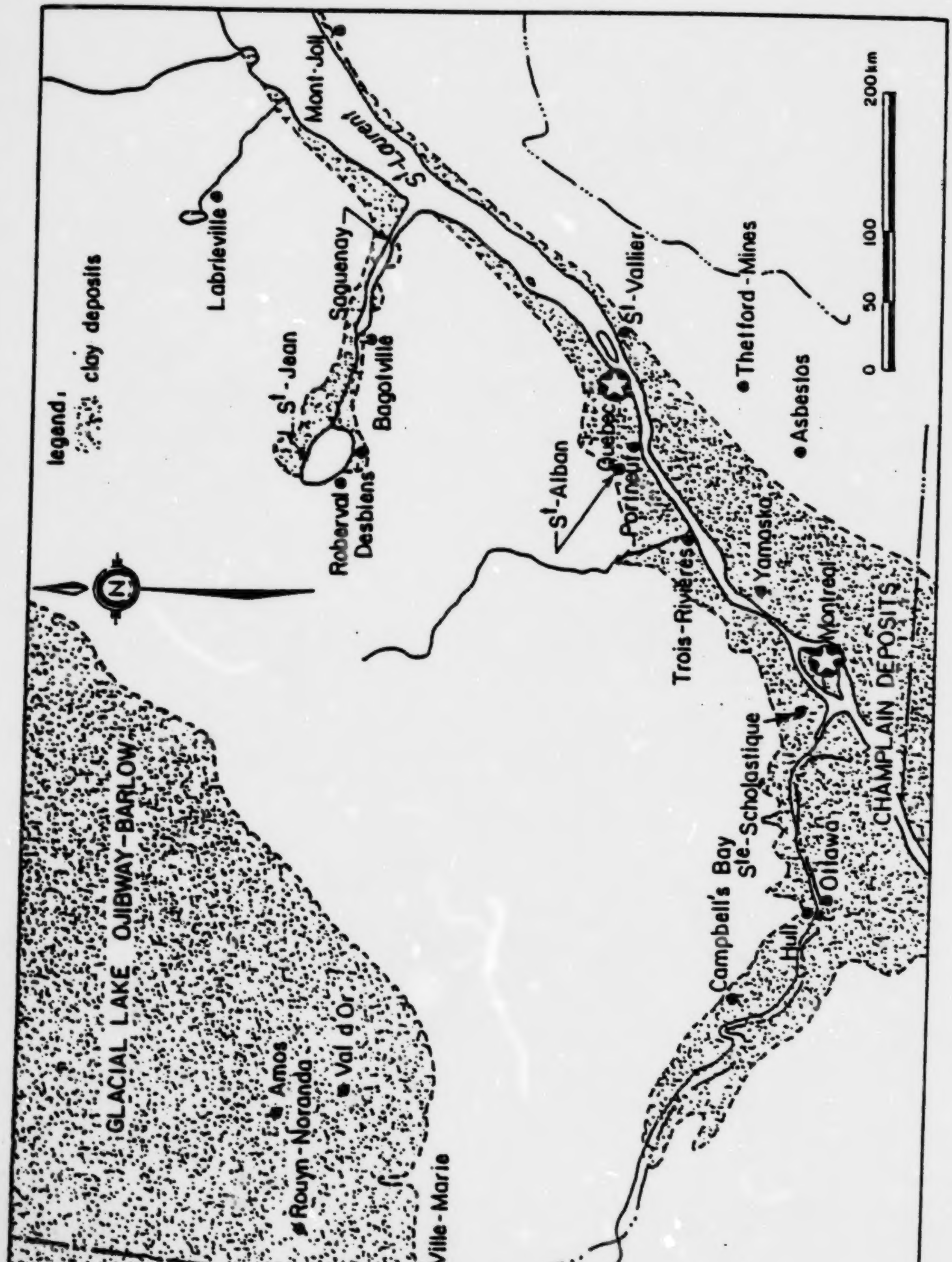

FIGURE 4.1 GEOGRAPHICAL DISTRIBUTION OF SENSITIVE CLAYS IN PARTS OF EASTERN CANADA

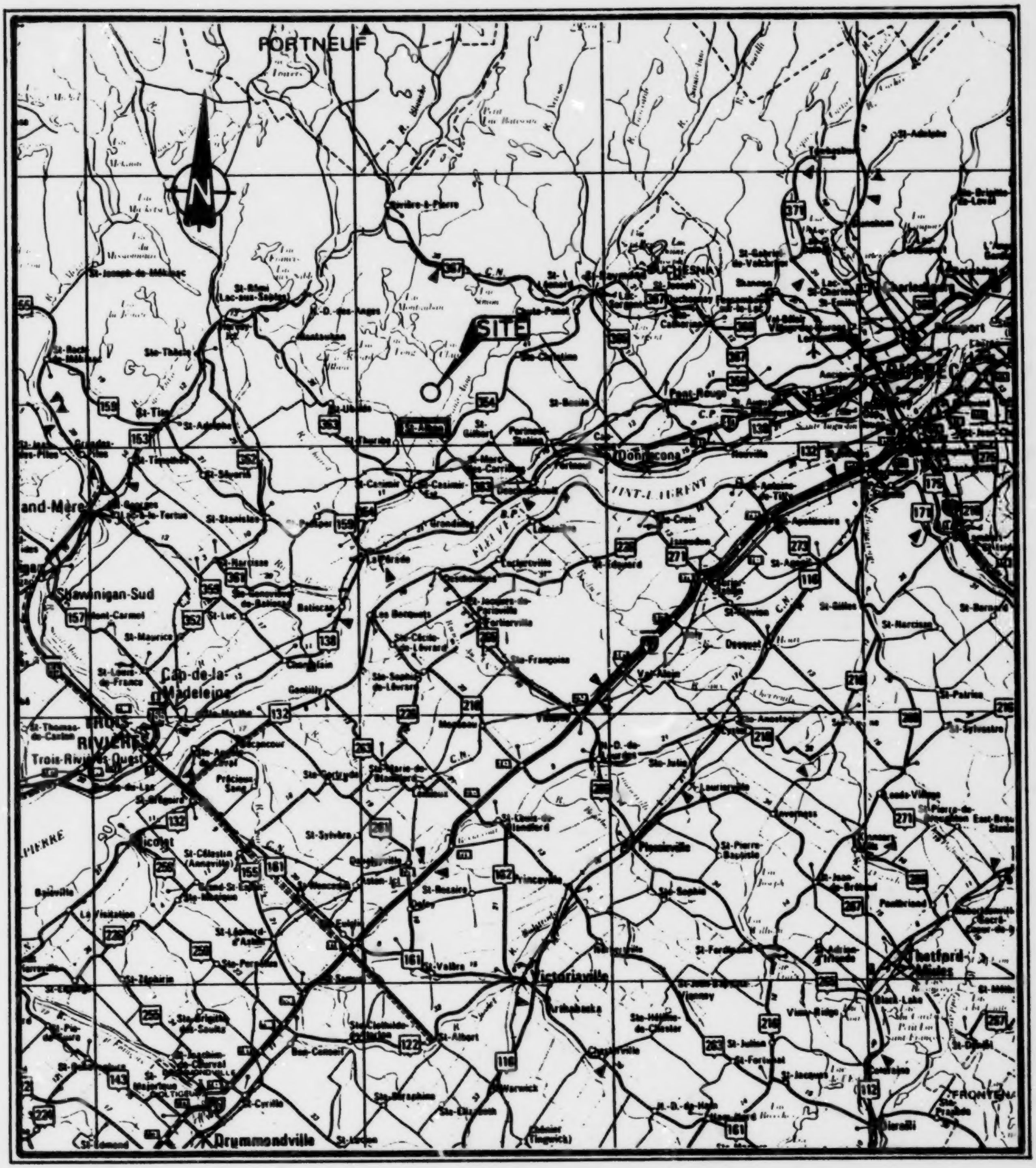

SCALE 1:750

FIGURE 4.2 SITE LOCATION PLAN

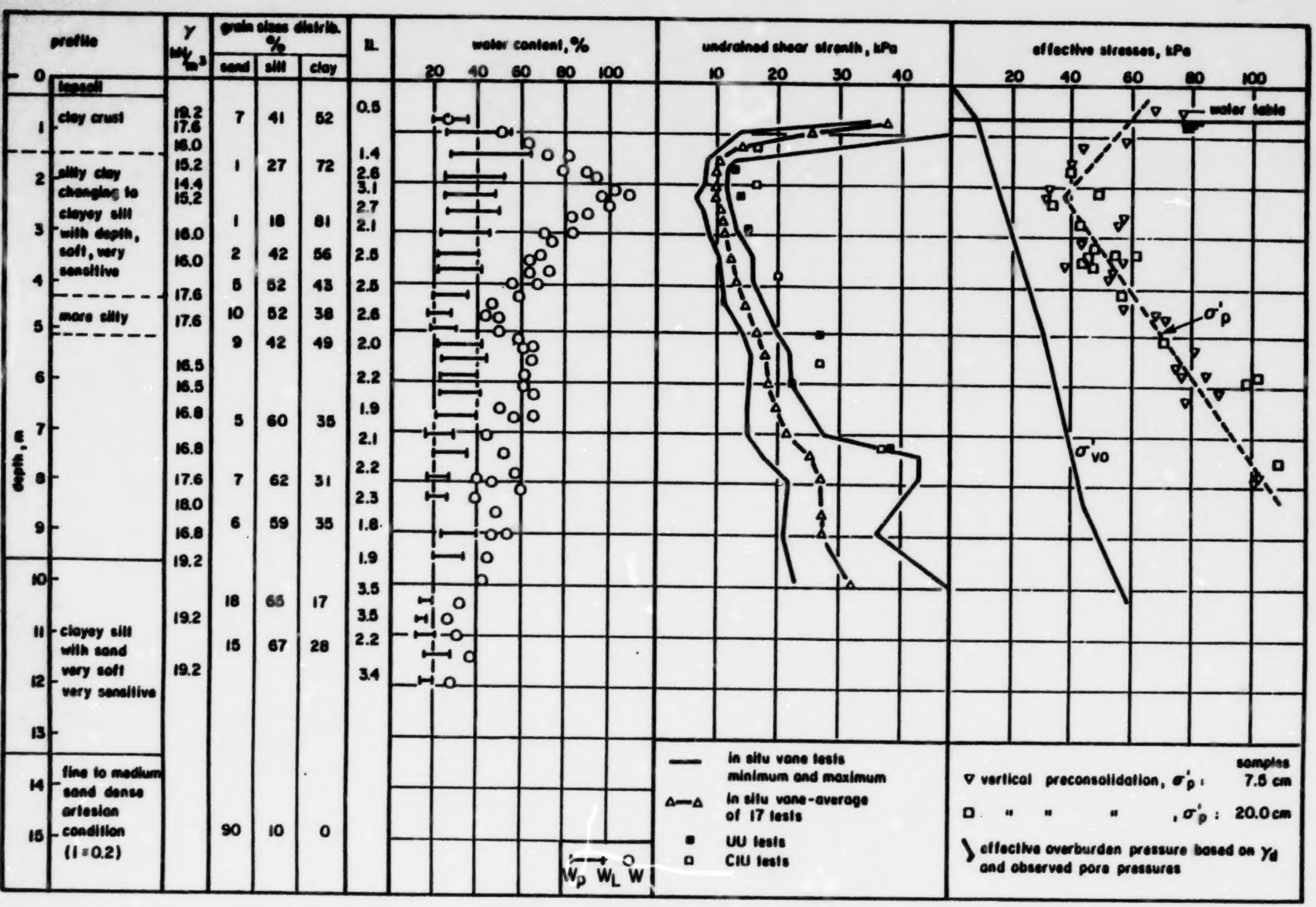

FIGURE 4.3 TYPICAL SOIL PROPERTIES AT ST. ALBAN TEST SITE, 1972 INVESTIGATION

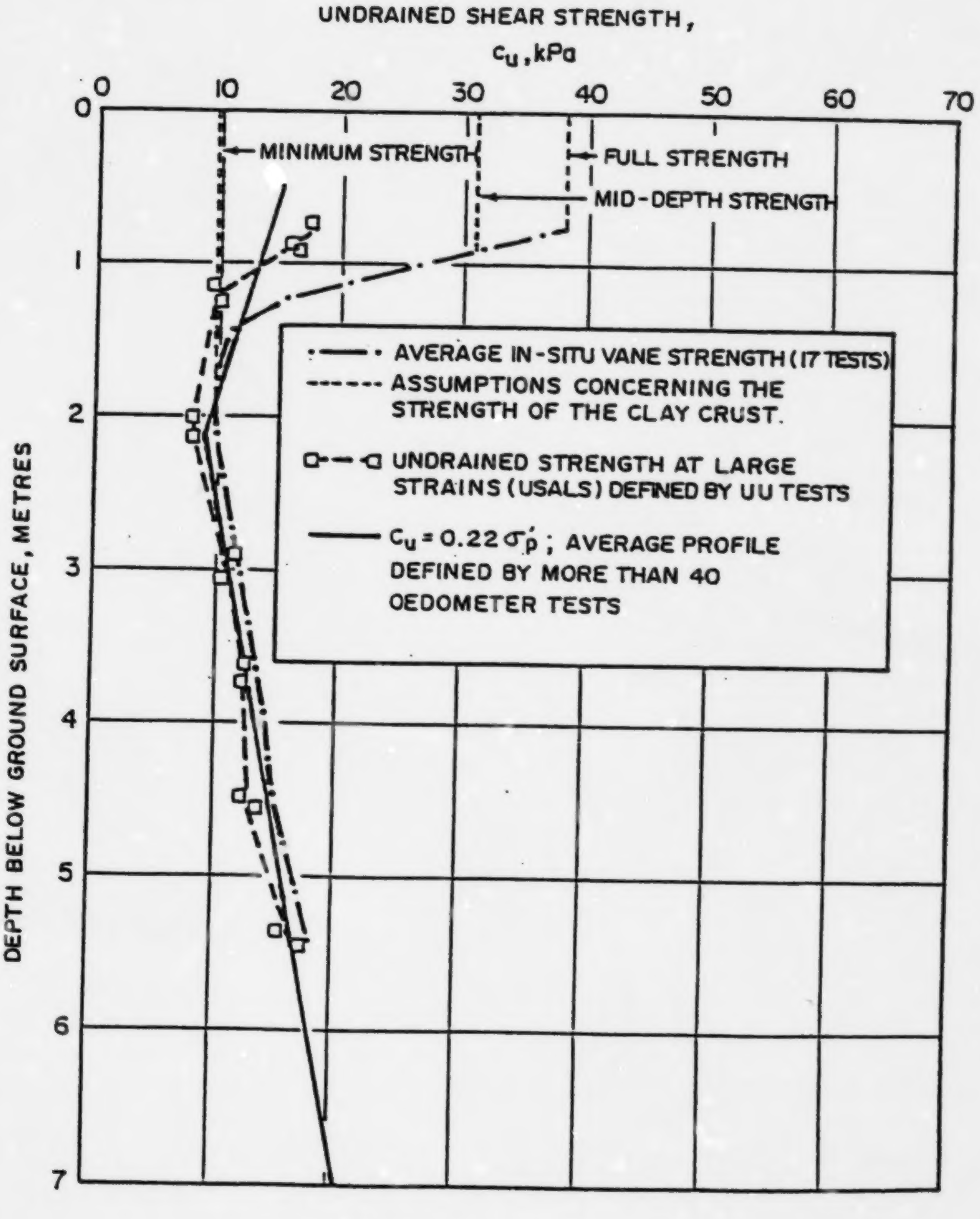

FIGURE 4.4 UNDRAINED SHEAR STRENGTH PROFILES, AFTER TRAK ET AL (1980)

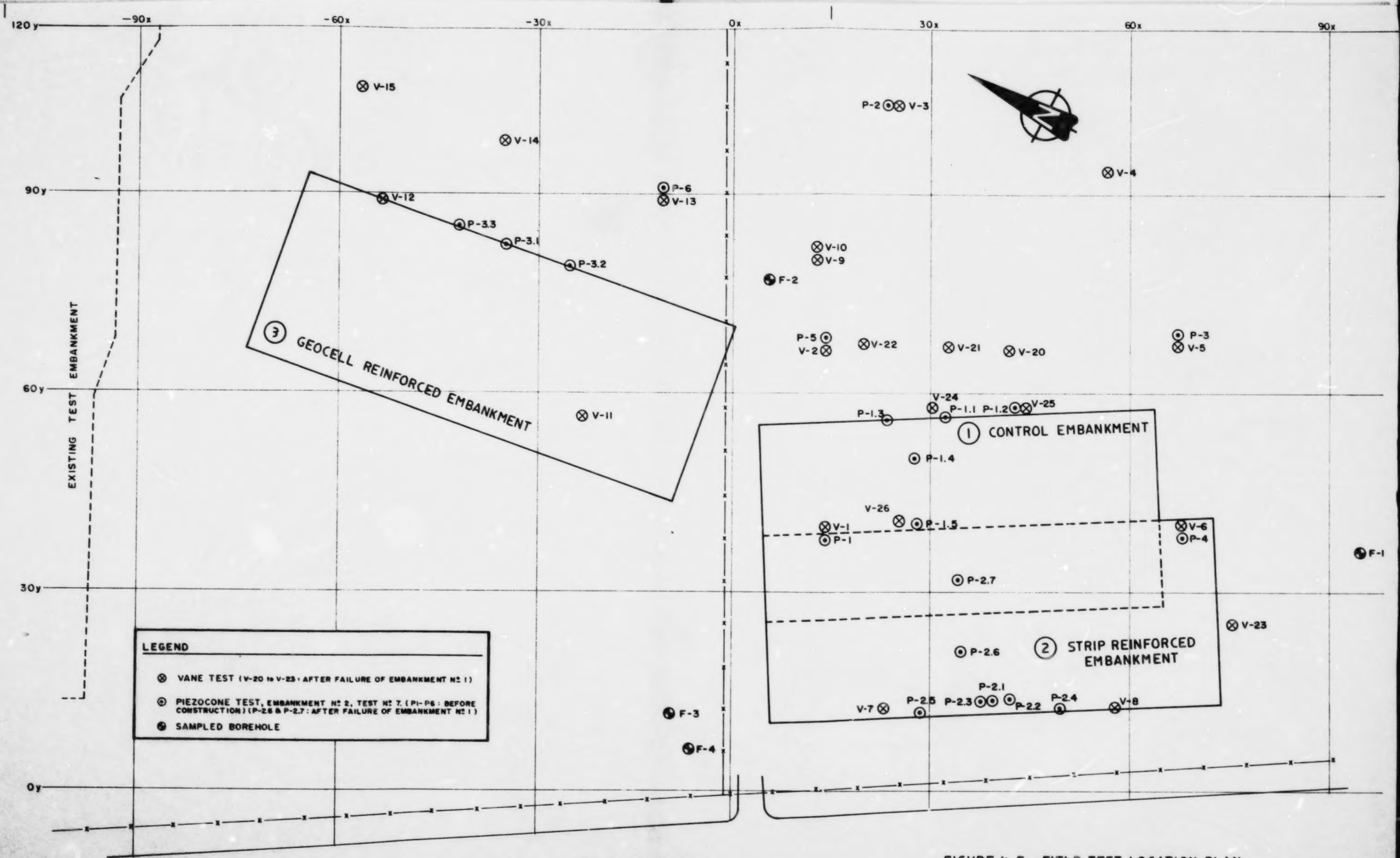

FIGURE 4·5 FIELD TEST LOCATION PLAN

Golder Associates - Université Laval

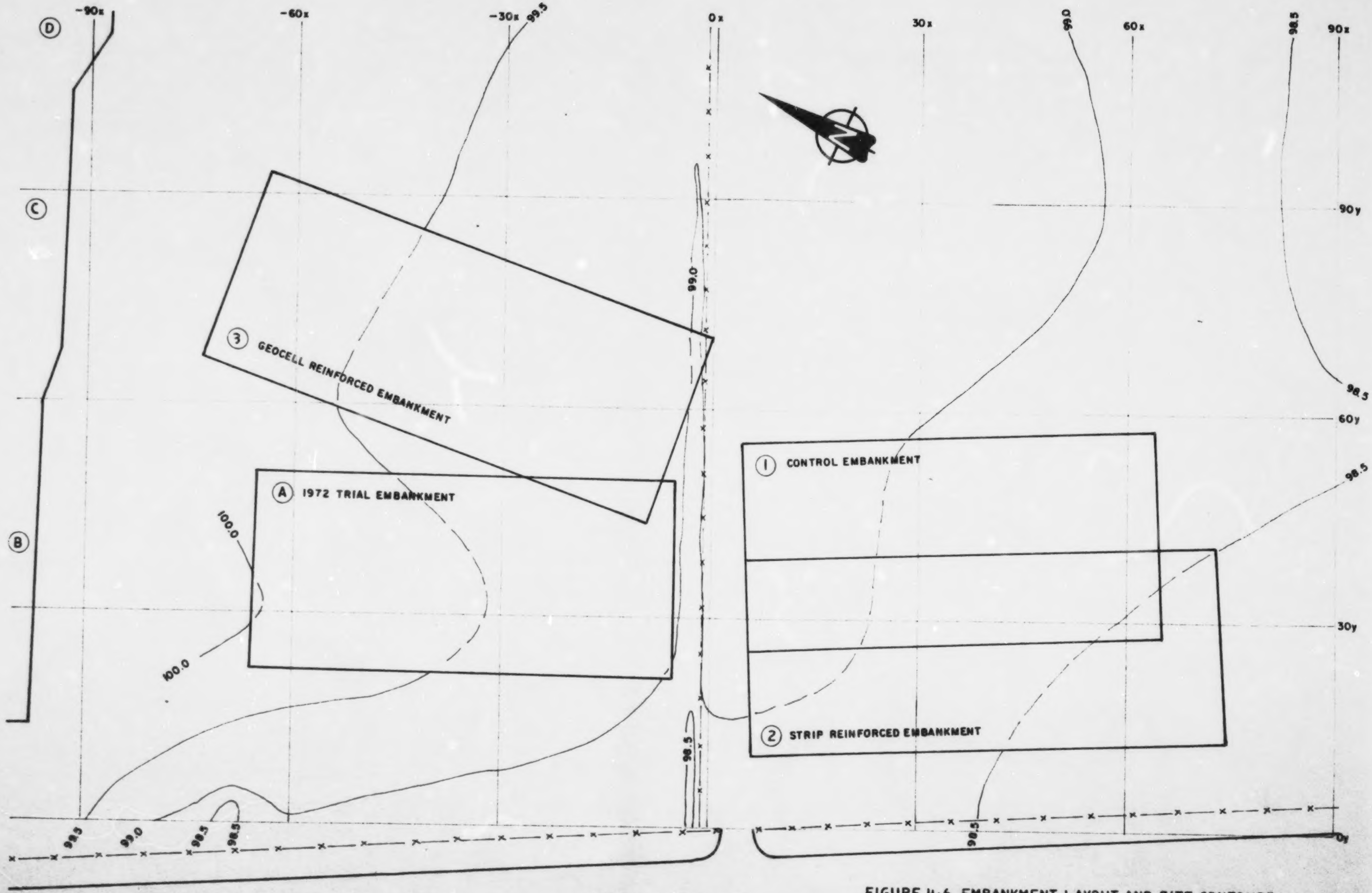

SCALE 1 : 500 (APPROX.)

FIGURE 4-6 EMBANKMENT LAYOUT AND SITE CONTOURS

Golder Associates - Université Laval

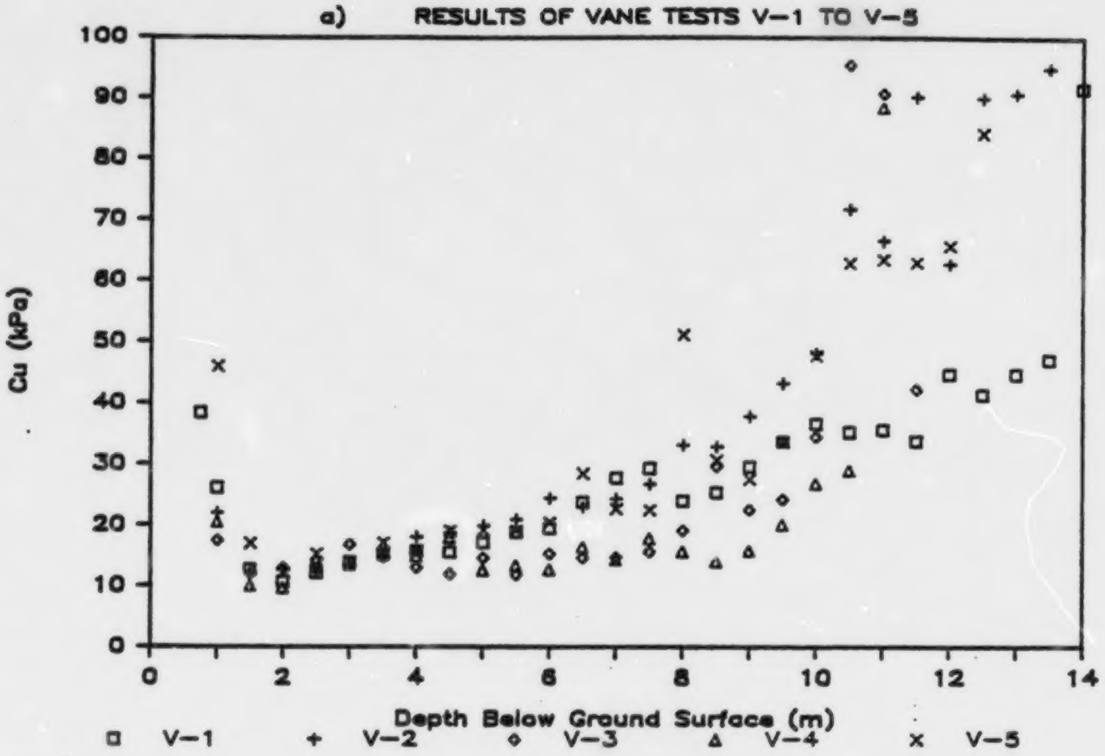
a) RESULTS OF VANE TESTS V-1 TO V-5

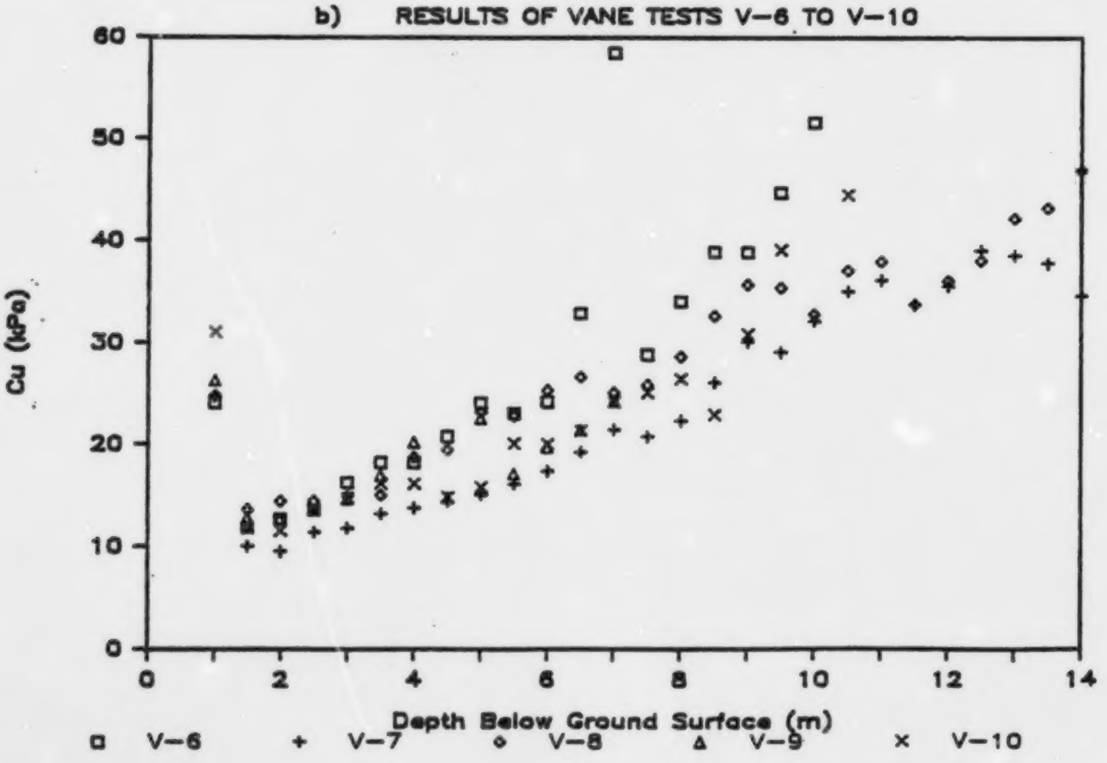
b) RESULTS OF VANE TESTS V-6 TO V-10

FIGURE 4.7 FIELD VANE TEST RESULTS (V-1 TO V-10)

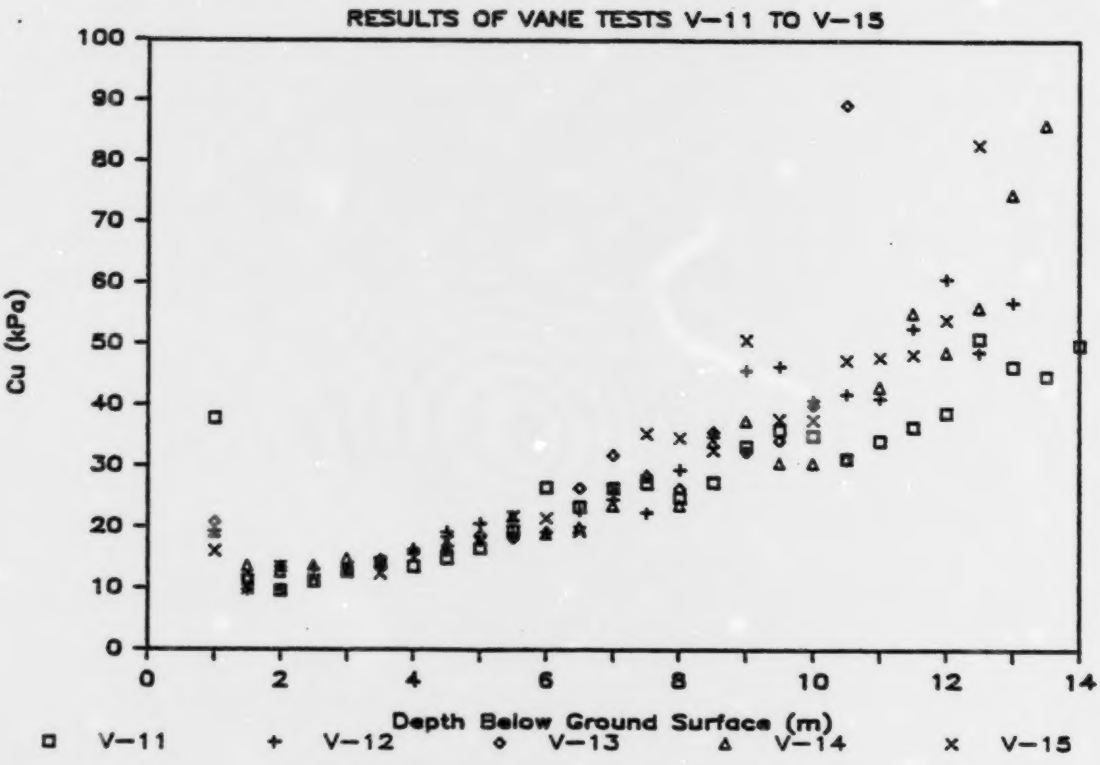

FIGURE 4.8 FIELD VANE TEST RESULTS (V-11 TO V-15)

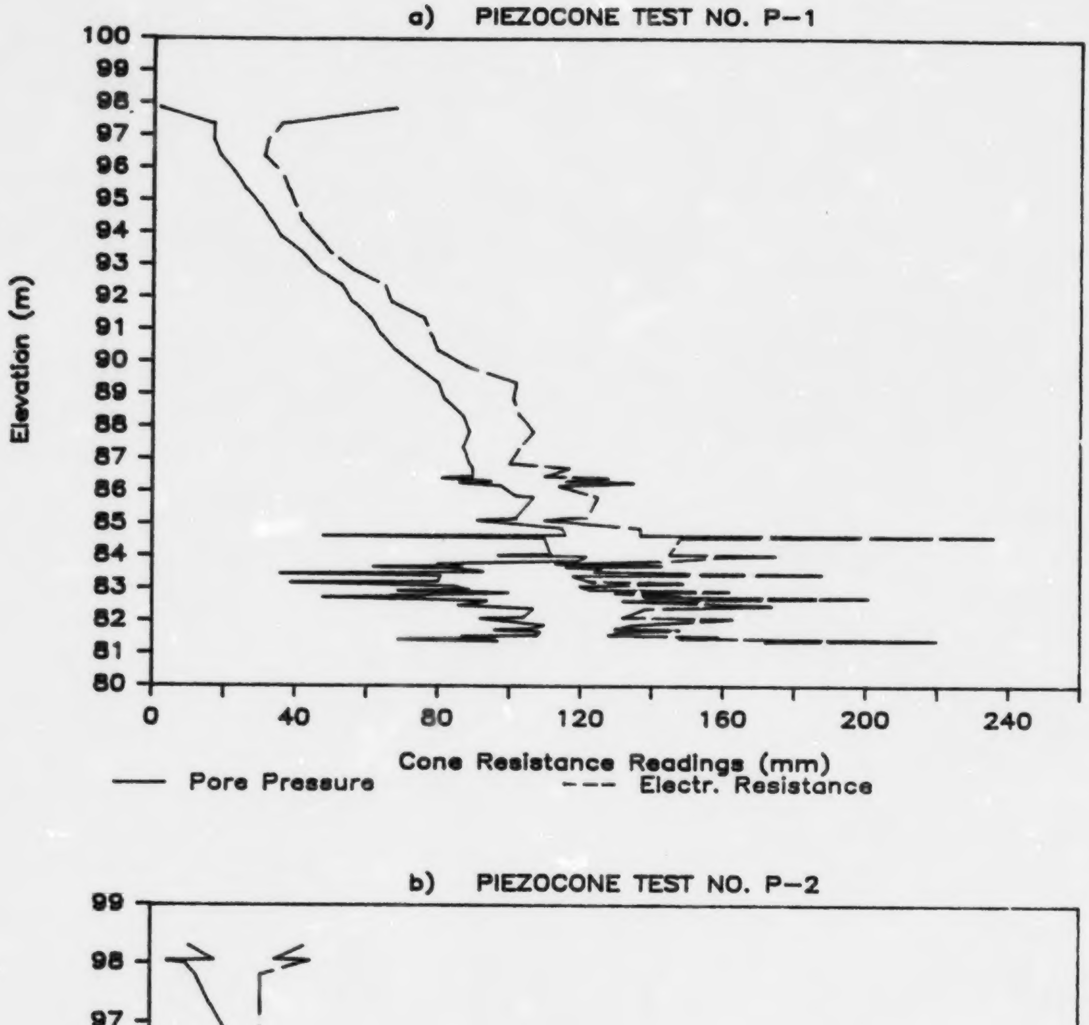

FIGURE 4.9 PIEZOCONE TEST RESULTS (P-1 AND P-2)

a) PIEZOCONE TEST NO. P-3

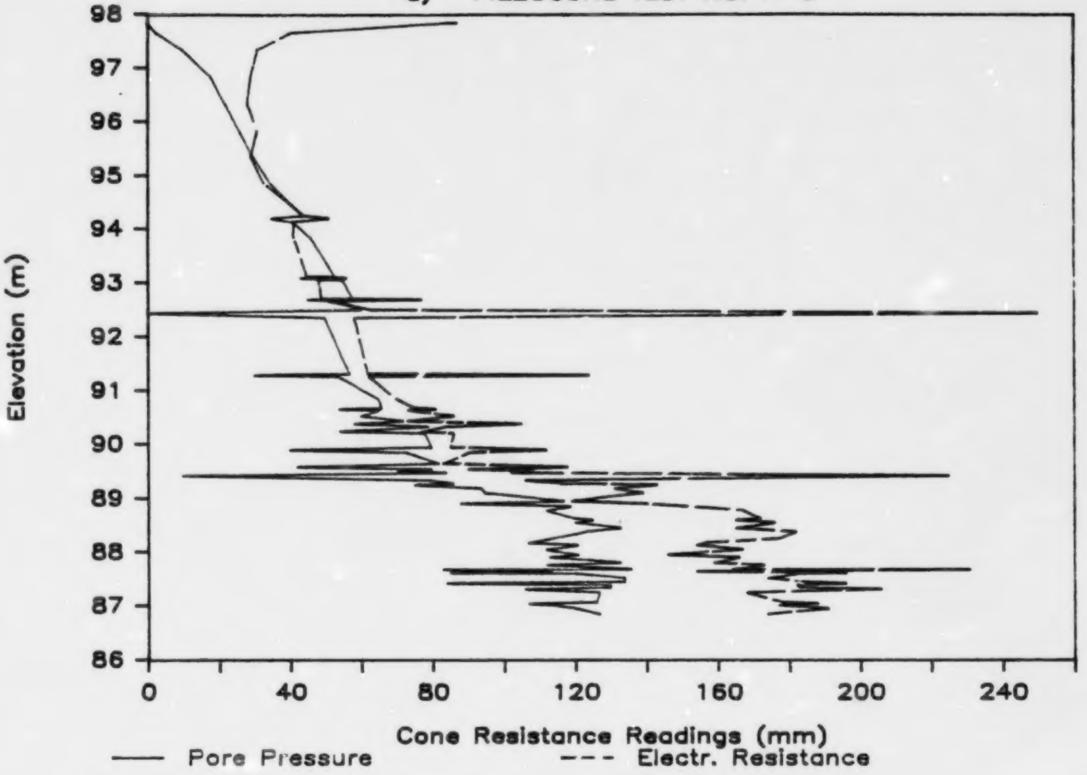

b) PIEZOCONE TEST NO. P-4

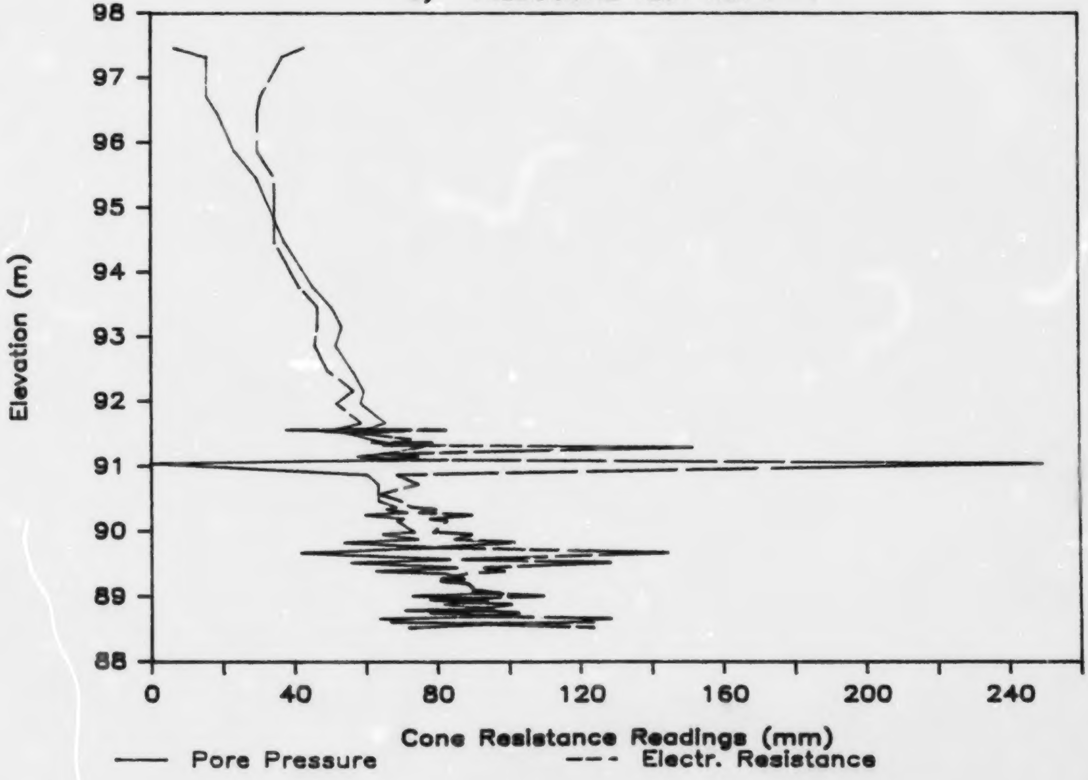

FIGURE 4.10 PIEZOCONE TEST RESULTS (P-3 AND P-4)

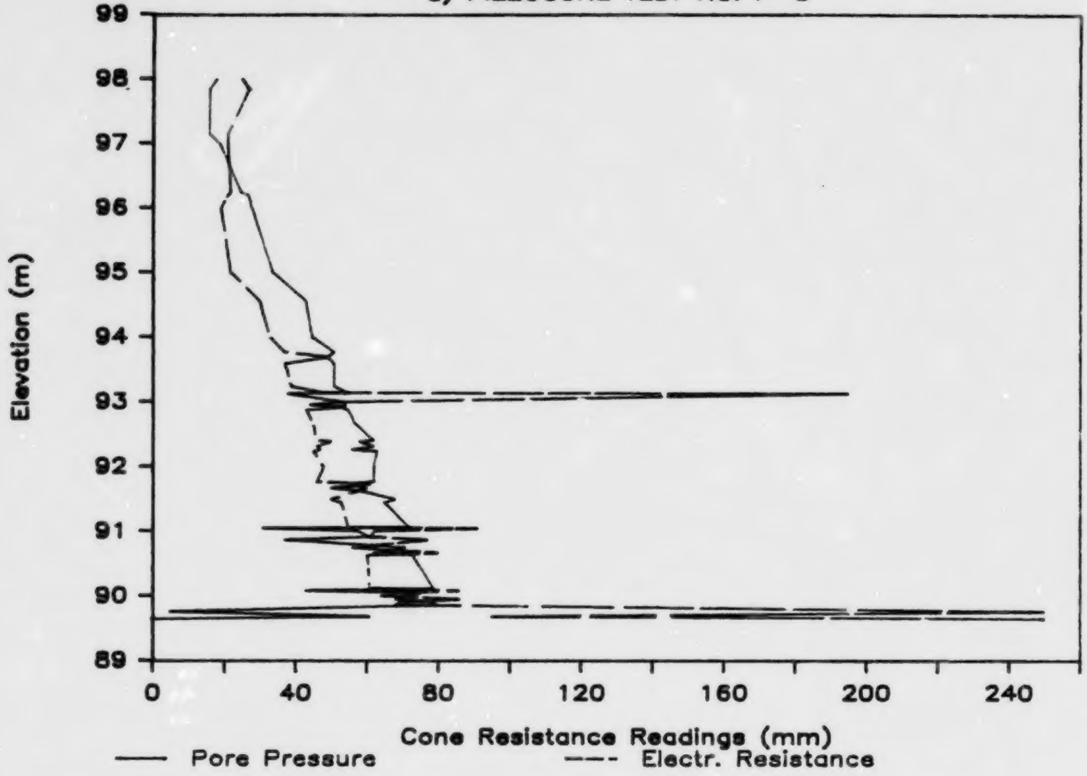
a) PIEZOCONE TEST NO. P-5

b) PIEZOCONE TEST NO. P-6

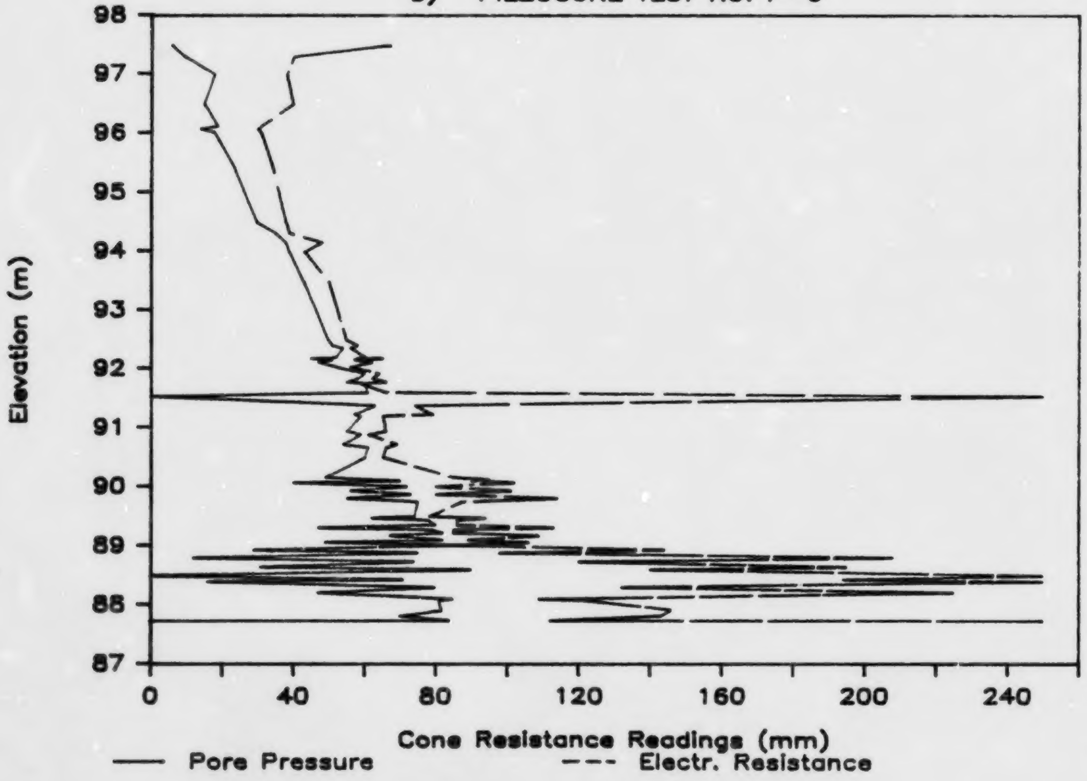

FIGURE 4.11 PIEZOCONE TEST RESULTS (P-5 AND P-6)

SECTION 5

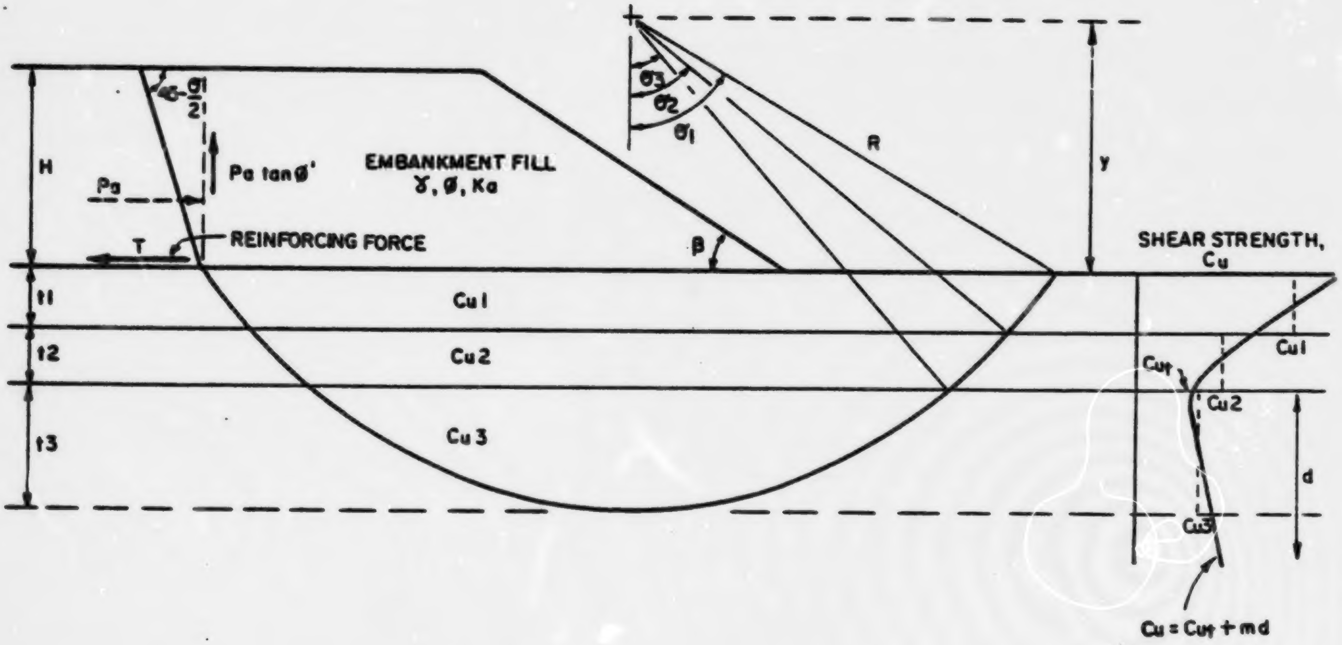

FACTOR OF SAFETY, F.S. $= \dfrac{R^2\left[\sigma_1 - \sigma_2\,Cu_t + (\sigma_2 - \sigma_3)\,Cu2 + \sigma_3\,Cu3\right] + T_y}{\frac{\gamma h}{2}\left[R^2 \sin^2\sigma_1 \frac{\cot^2\beta}{12} + Ka\,H\left(y - \frac{H}{3}\right)\right]}$

AVERAGE SHEAR STRENGTH ALONG CIRCULAR ARC IN BOTTOM LAYER,

$$Cu\,3 = m\left[\frac{\sqrt{R^2 - (y + t1 + t2)^2}}{\cos^{-1}\frac{y + t1 + t2}{R}} - y\right] + Cu_t$$

FIGURE 5.1 COHESION CIRCLE STABILITY ANALYSIS (BTENSAR)

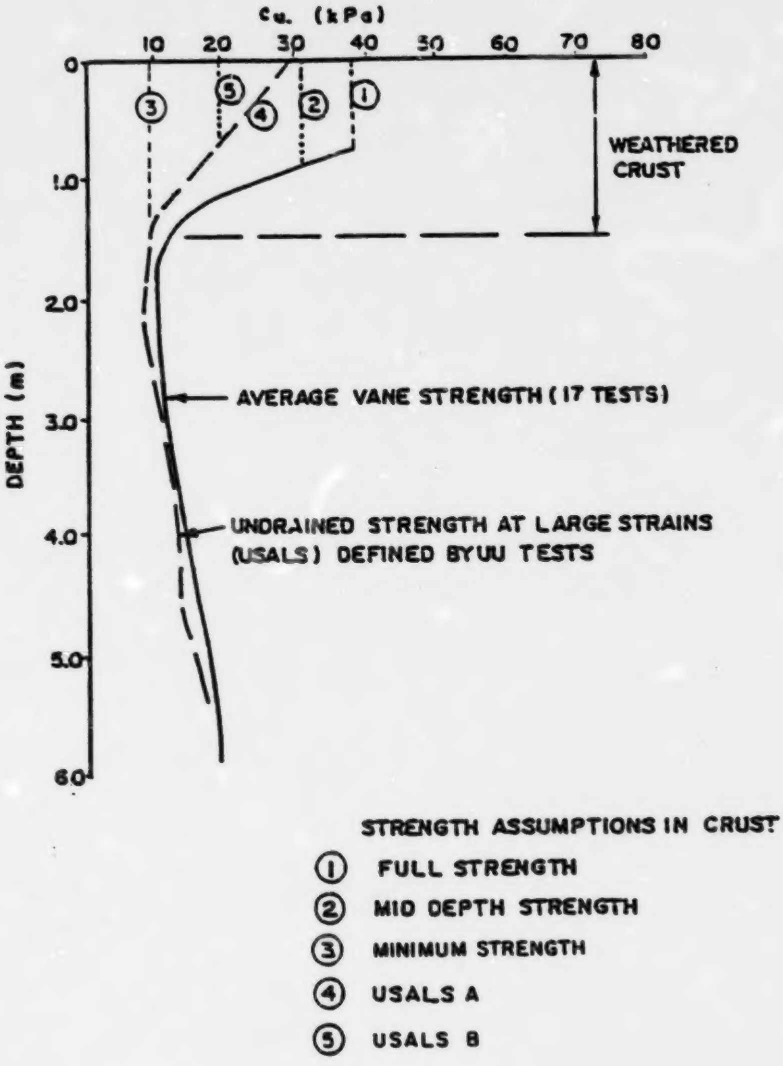

REFERENCE: La Rochelle et al (1974)

FIGURE 5.2 STRENGTH PROFILE AND ASSUMPTIONS

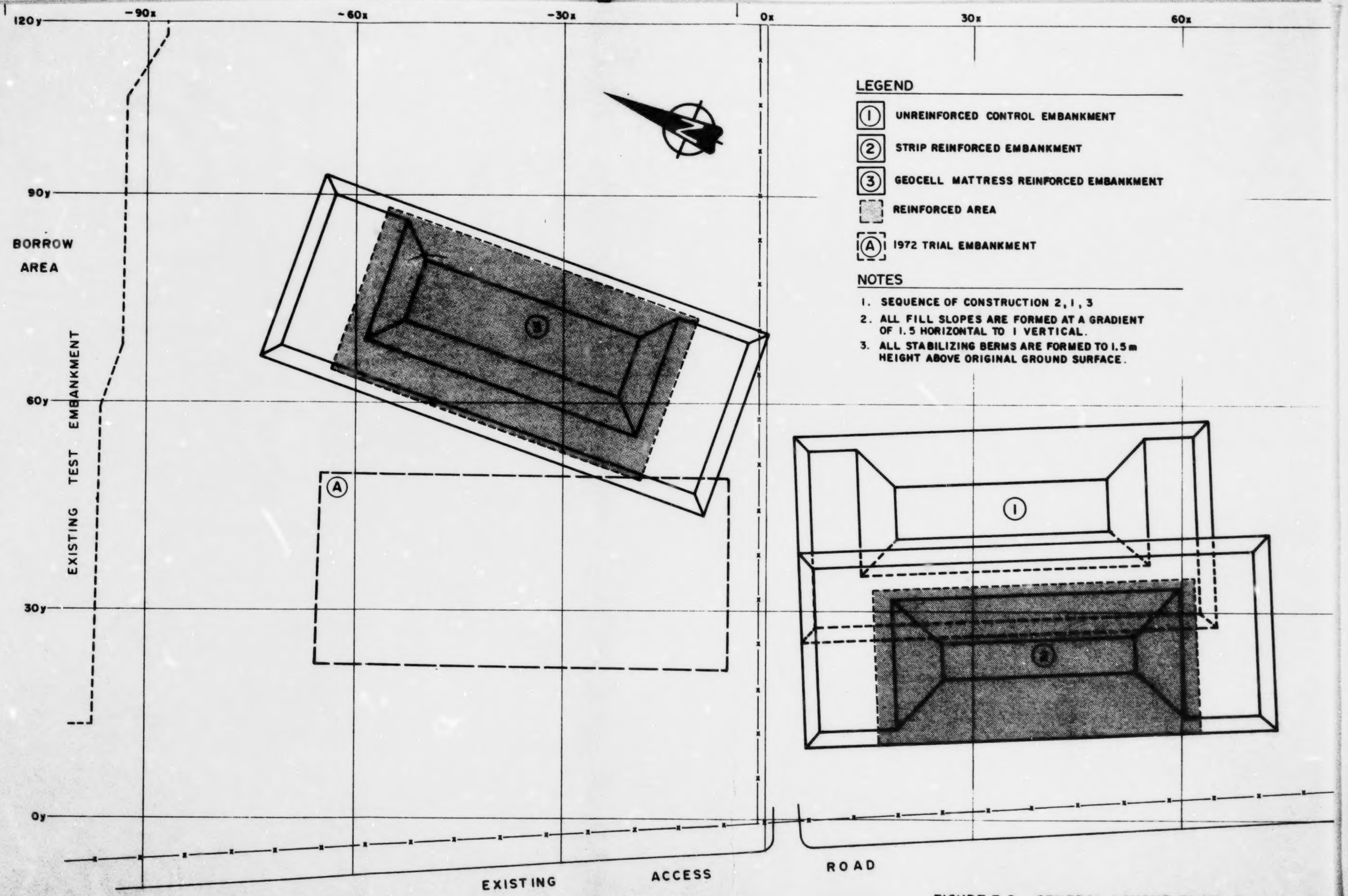

NOTES

1. SEQUENCE OF CONSTRUCTION 2, 1, 3
2. ALL FILL SLOPES ARE FORMED AT A GRADIENT OF 1.5 HORIZONTAL TO 1 VERTICAL.
3. ALL STABILIZING BERMS ARE FORMED TO 1.5 m HEIGHT ABOVE ORIGINAL GROUND SURFACE.

SCALE 1 : 500 (APPROX.)

FIGURE 5·3 GENERAL LAYOUT PLAN

Golder Associates - Université Laval

SECTION 6

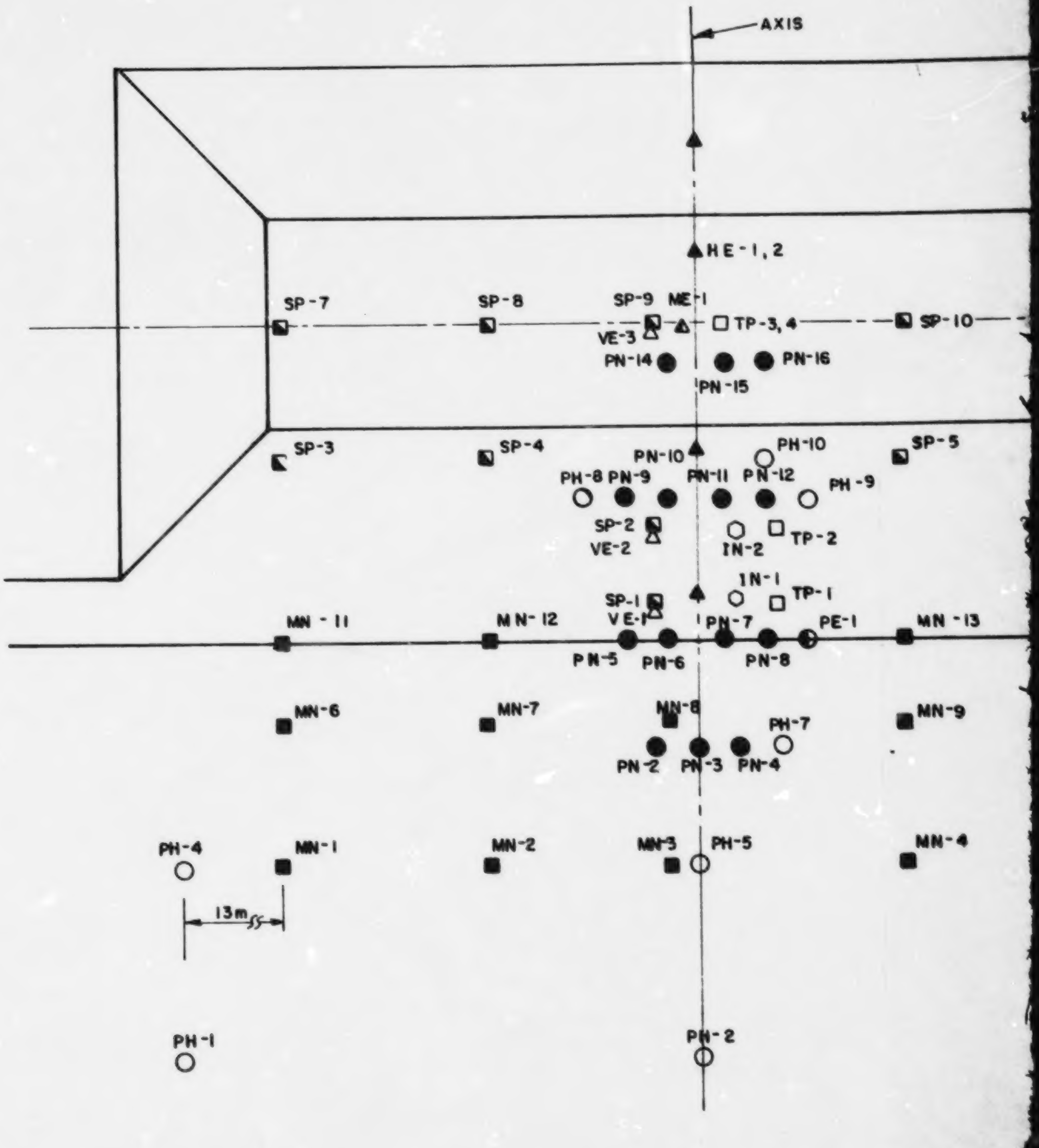
AXIS
HE-1,2
SP-7
SP-8
SP-9
ME-1
VE-3
TP-3,4
SP-10
PN-14
PN-15
PN-16
SP-3
SP-4
PN-10
PH-10
SP-5
PH-8
PN-9
PN-11
PN-12
PH-9
SP-2
VE-2
IN-2
TP-2
IN-1
SP-1
TP-1
VE-1
MN-11
MN-12
PN-7
PE-1
MN-13
PN-5
PN-6
PN-8
MN-6
MN-7
MN-8
MN-9
PH-7
PN-2
PN-3
PN-4
PH-4
MN-1
MN-2
MN-3
PH-5
MN-4
13m
PH-1
PH-2

PLAN

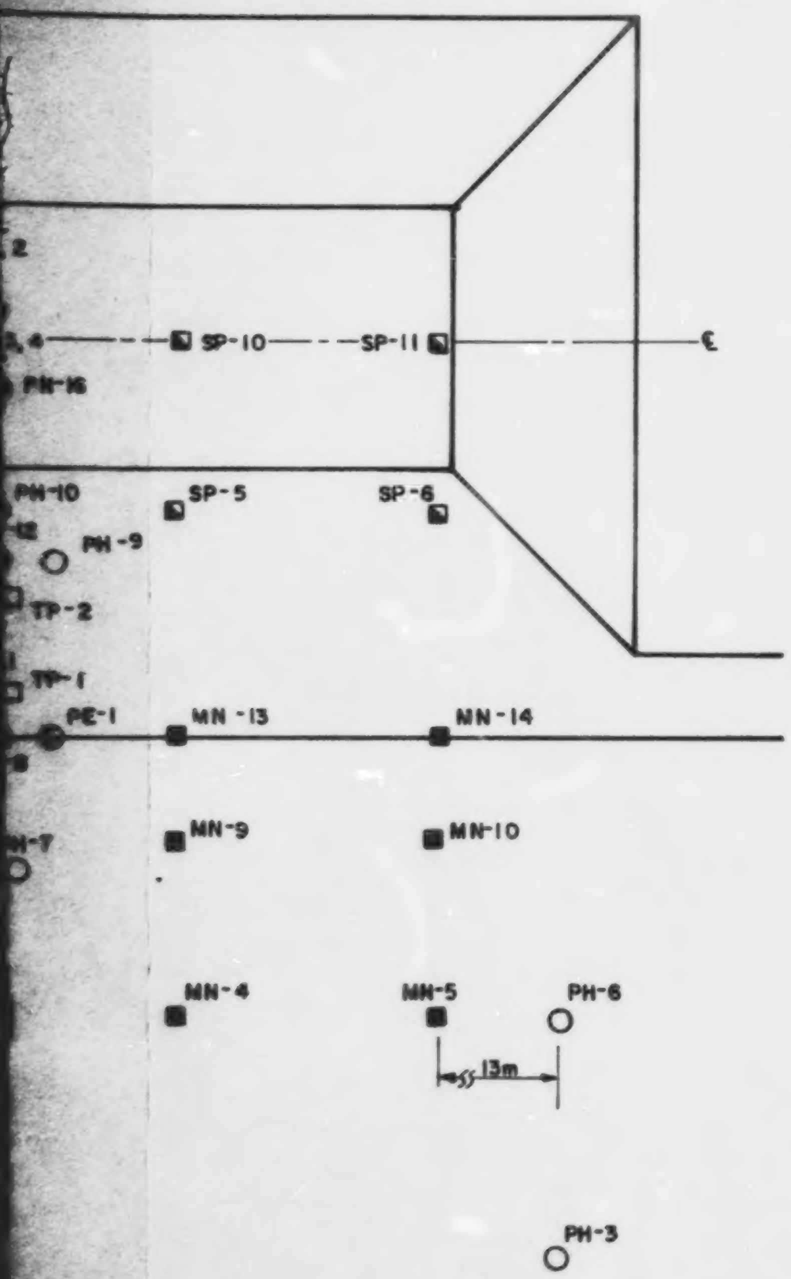

SCALE 1 : 200

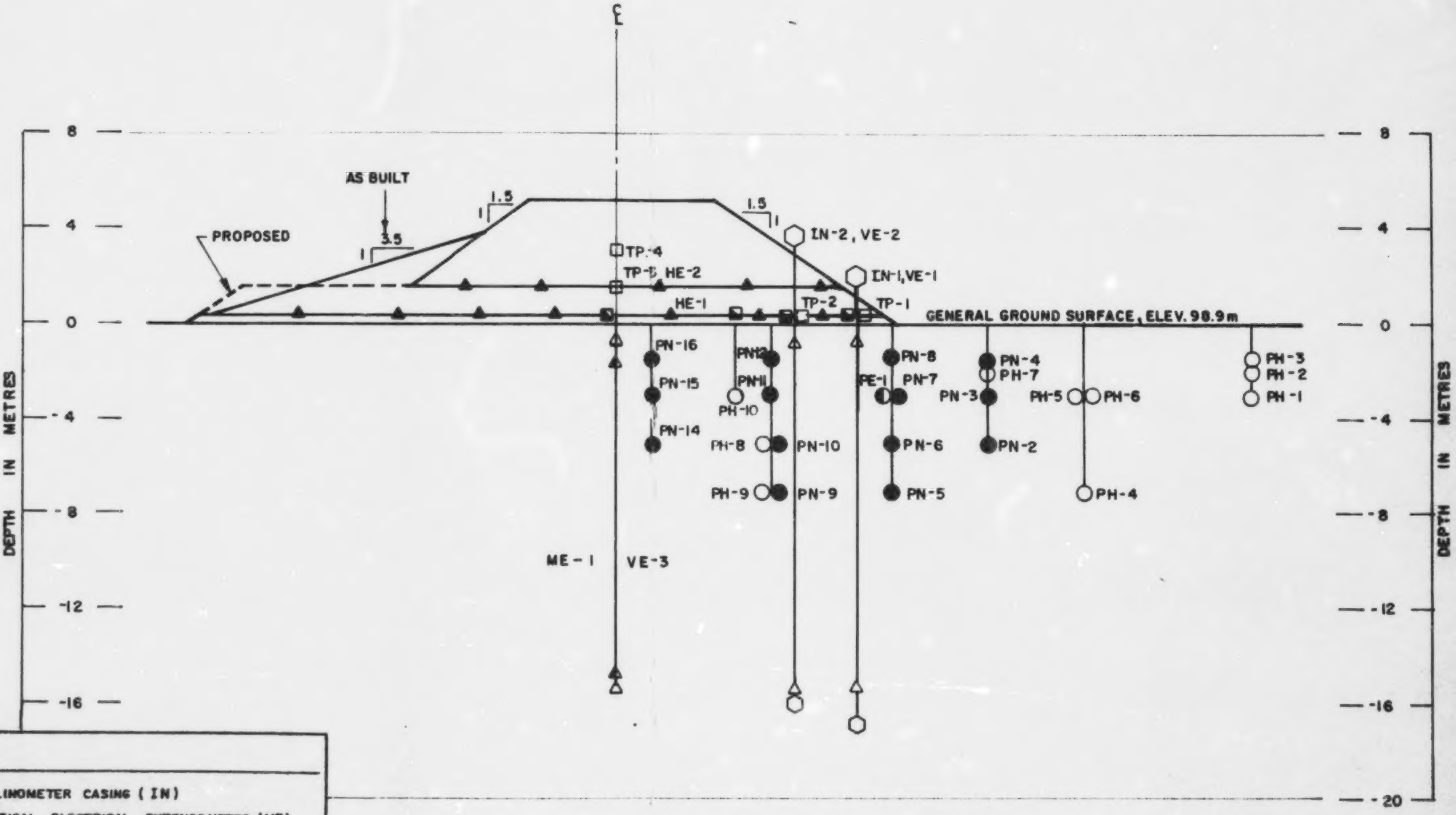

SECTION

LEGEND

- ○ INCLINOMETER CASING (IN)
- △ VERTICAL ELECTRICAL EXTENSOMETER (VE)
- ▲ VERTICAL MAGNETIC EXTENSOMETER (ME)
- ▲ HORIZONTAL ELECTRICAL EXTENSOMETER (HE)
- ● PNEUMATIC PIEZOMETER (PN)
- ◐ ELECTRICAL PIEZOMETER (PE)
- ○ HYDRAULIC PIEZOMETER (PH)
- □ TOTAL PRESSURE CELL (TP)
- ▣ SETTLEMENT PLATE (SP)
- ■ MONUMENT (MN)

FIGURE 6·1 INSTRUMENTATION LAYOUT,
CONTROL EMBANKMENT (No. 1)

Golder Associates - Université Laval

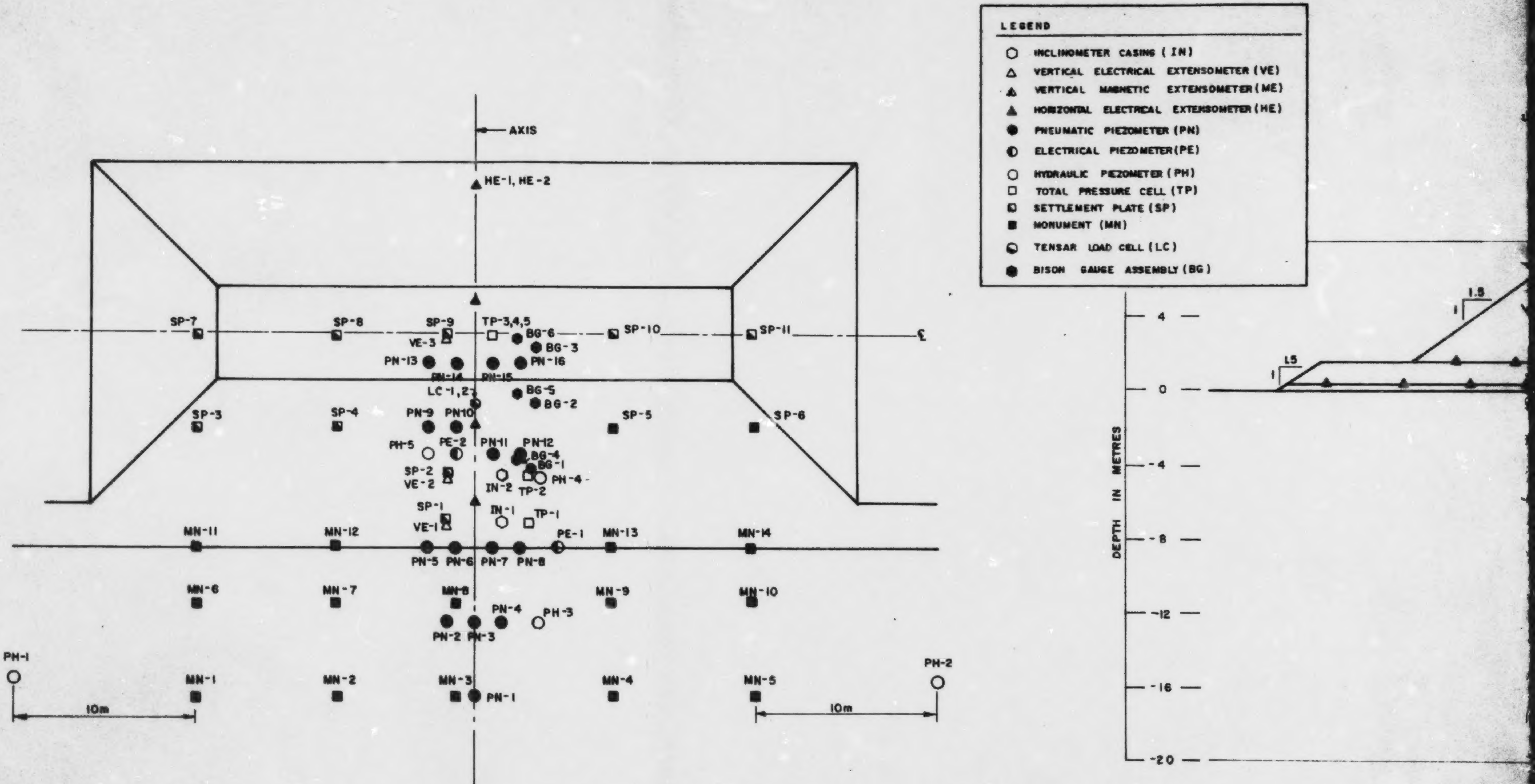

PLAN

SCALE 1 : 200

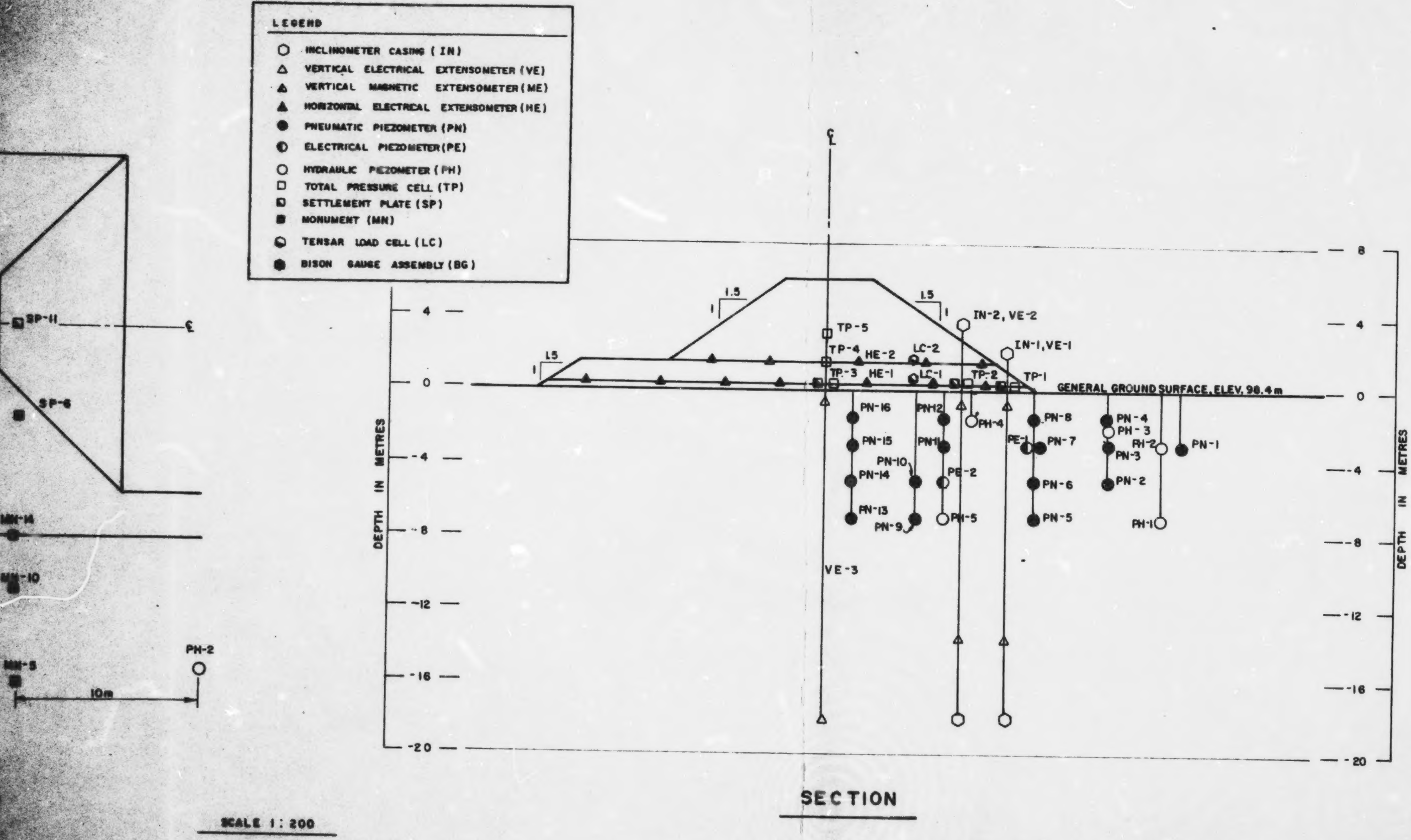

FIGURE 6·2 INSTRUMENTATION LAYOUT, STRIP REINFORCED EMBANKMENT (No. 2)

Golder Associates - Université Laval

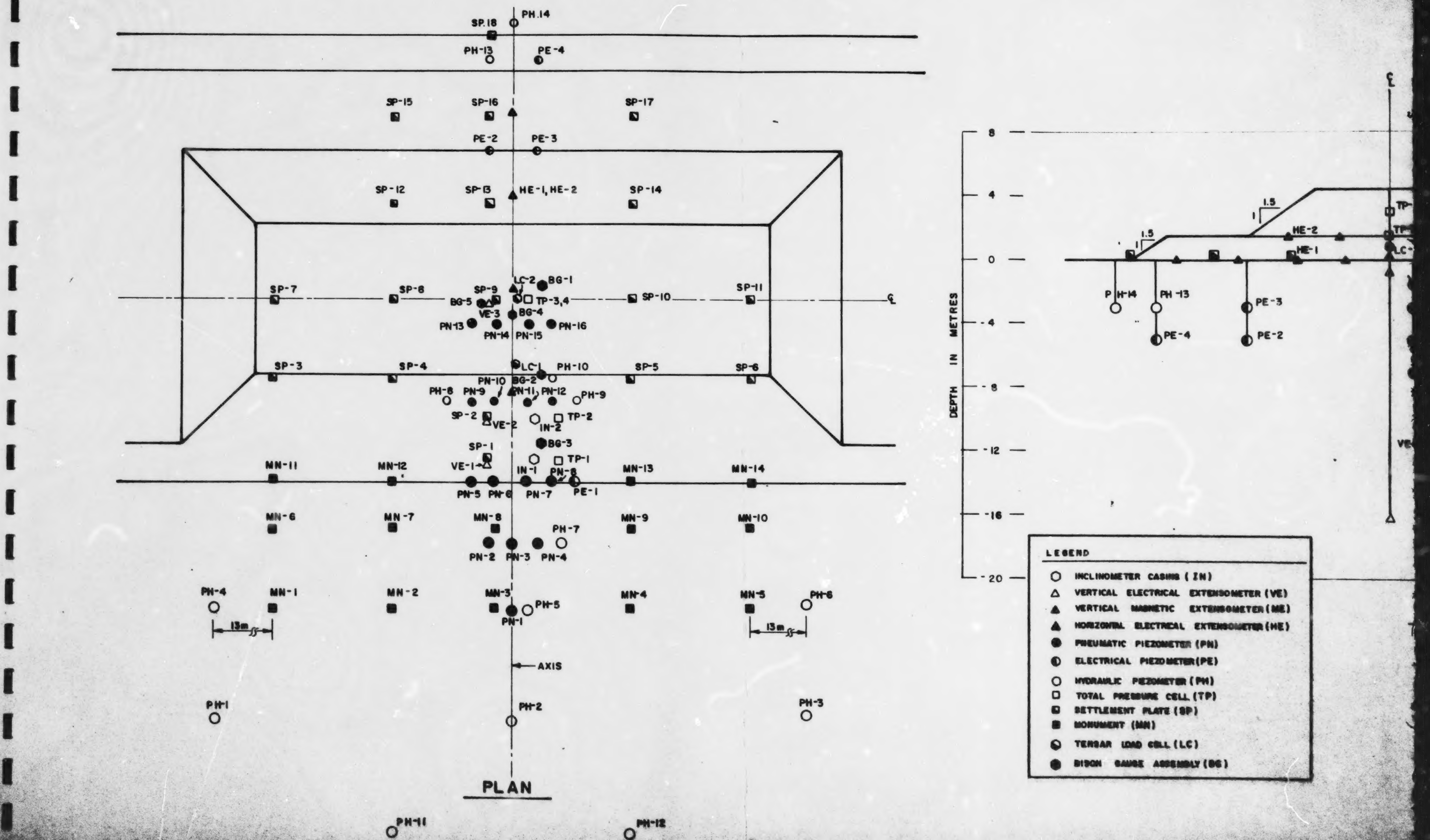
SP.18
PH.14
PH-13
PE-4
SP-15
SP-16
SP-17
PE-2
PE-3
SP-12
SP-13
HE-1, HE-2
SP-14
SP-7
SP-8
SP-9
LC-2
BG-1
BG-5
TP-3,4
SP-10
SP-11
VE-3
BG-4
PN13
PN-14
PN-15
PN-16
LC-1
PH-10
SP-3
SP-4
SP-5
SP-6
PN-10
BG-2
PH-8
PN-9
PN-11
PN-12
PH-9
SP-2
VE-2
IN-2
TP-2
BG-3
SP-1
TP-1
MN-11
MN-12
VE-1
IN-1
PN-8
MN-13
MN-14
PN-5
PN-6
PN-7
PE-1
MN-6
MN-7
MN-8
PH-7
MN-9
MN-10
PN-2
PN-3
PN-4
PH-4
MN-1
MN-2
MN-3
PH-5
MN-4
MN-5
PH-6
PN-1
13m
13m
AXIS
PH-1
PH-2
PH-3
PLAN
PH-11
PH-12
DEPTH IN METRES
8
4
0
-4
-8
-12
-16
-20
1.5
1
1.5
1
HE-2
HE-1
TP
LC
PH-14
PH-13
PE-3
PE-4
PE-2
VE
LEGEND
○ INCLINOMETER CASING (IN)
△ VERTICAL ELECTRICAL EXTENSOMETER (VE)
▲ VERTICAL MAGNETIC EXTENSOMETER (ME)
▲ HORIZONTAL ELECTRICAL EXTENSOMETER (HE)
● PNEUMATIC PIEZOMETER (PN)
◐ ELECTRICAL PIEZOMETER (PE)
○ HYDRAULIC PIEZOMETER (PH)
□ TOTAL PRESSURE CELL (TP)
▣ SETTLEMENT PLATE (SP)
■ MONUMENT (MN)
◔ TENSAR LOAD CELL (LC)
● BISON GAUGE ASSEMBLY (BG)

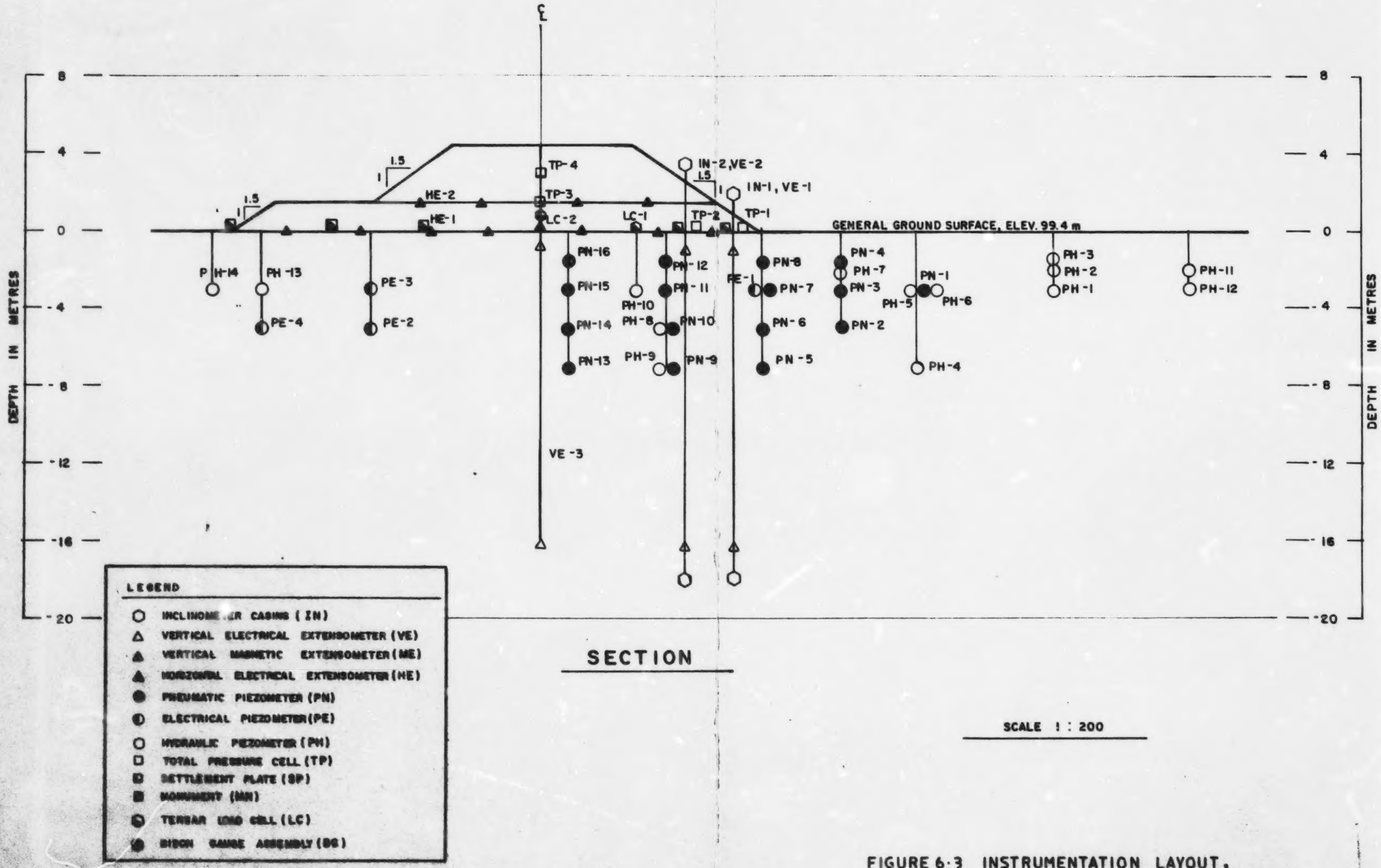

FIGURE 6·3 INSTRUMENTATION LAYOUT,
GEOCELL REINFORCED EMBANKMENT (No. 3)

Golder Associates - Université Laval

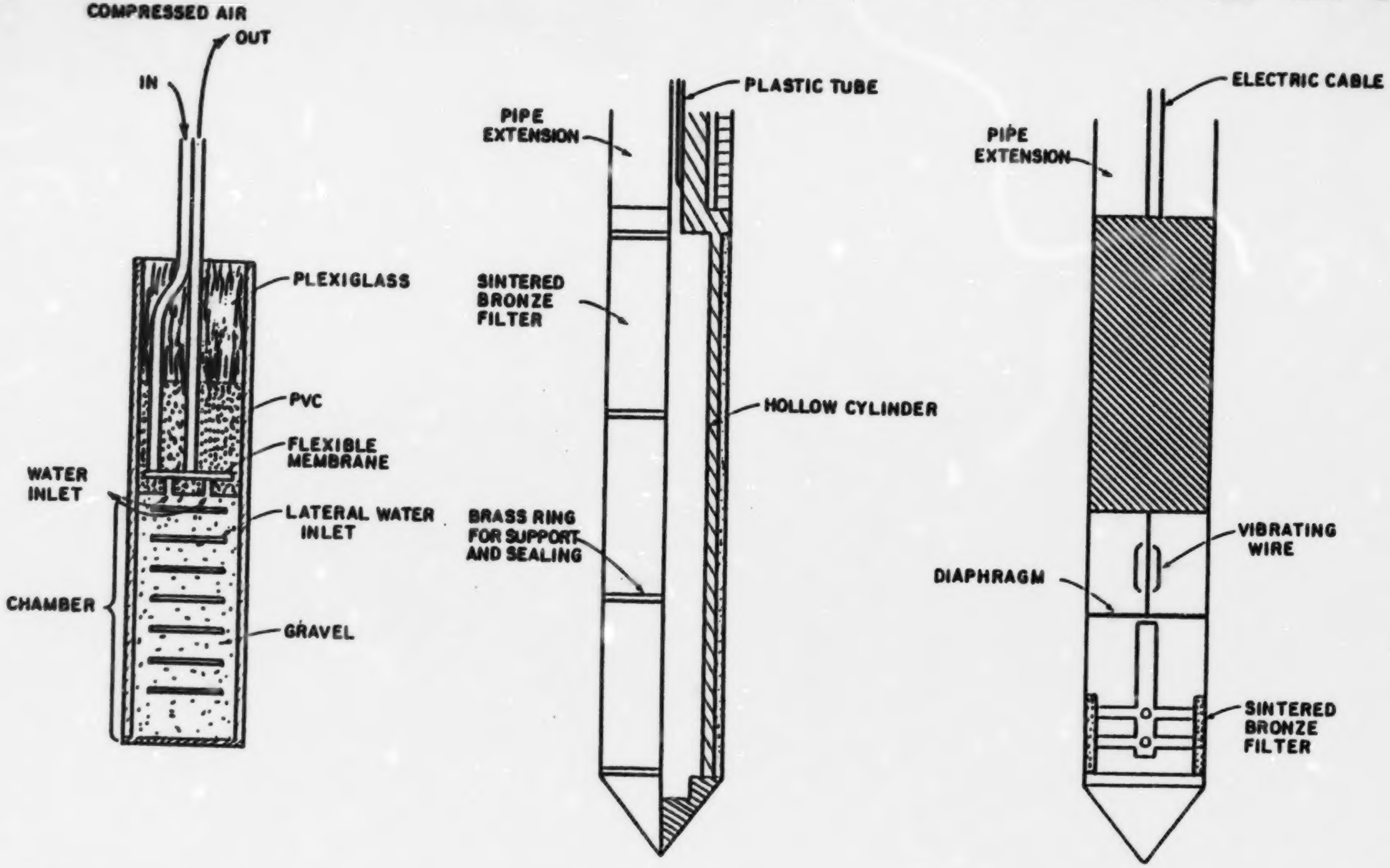

a) PNEUMATIC PETUR

b) HYDRAULIC GEONOR

c) ELECTRIC GEONOR

FIGURE 6.4 SECTIONS OF PIEZOMETER TIPS

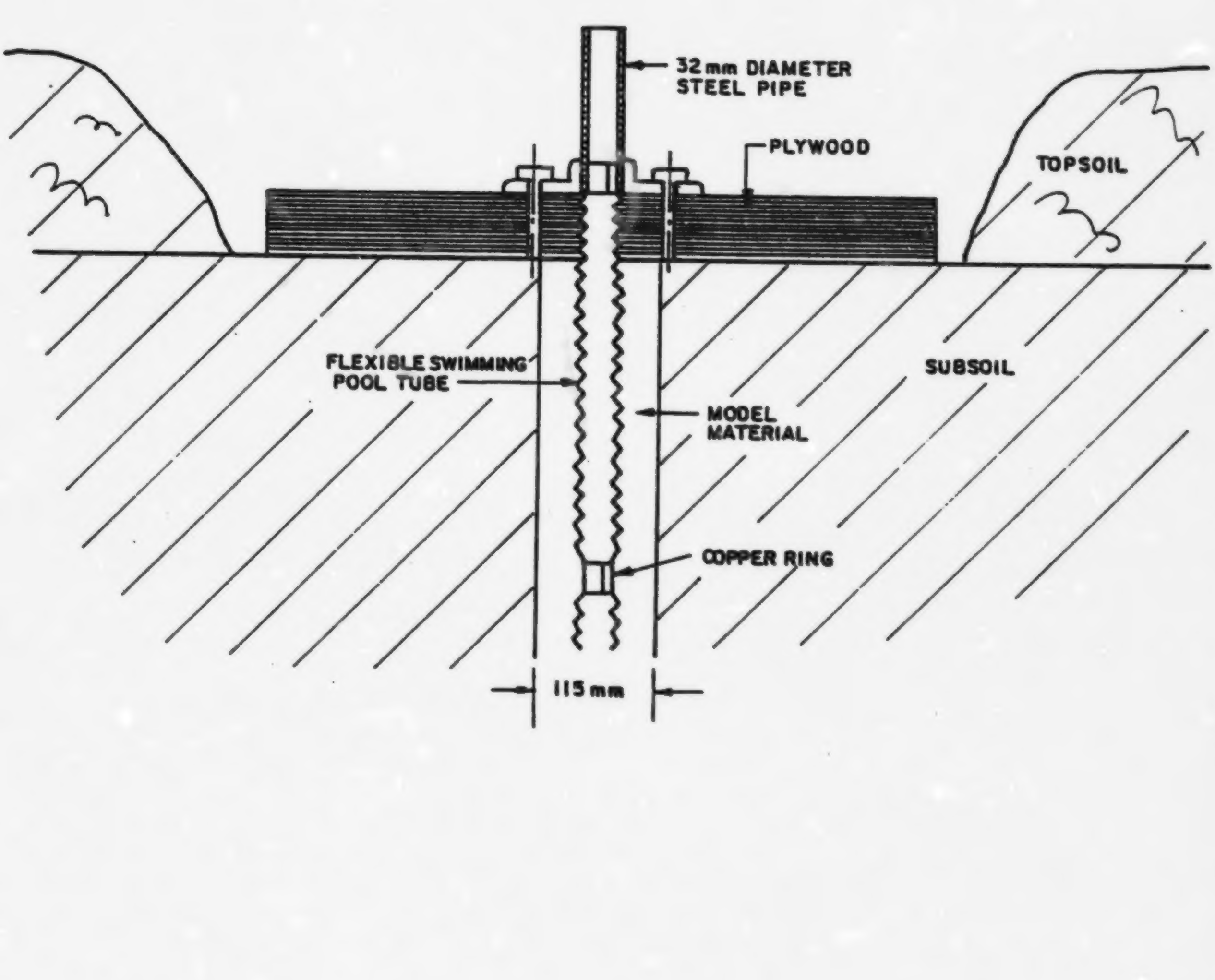

FIGURE 6.5 SETTLEMENT PLATE AND VERTICAL EXTENSOMETER ASSEMBLY

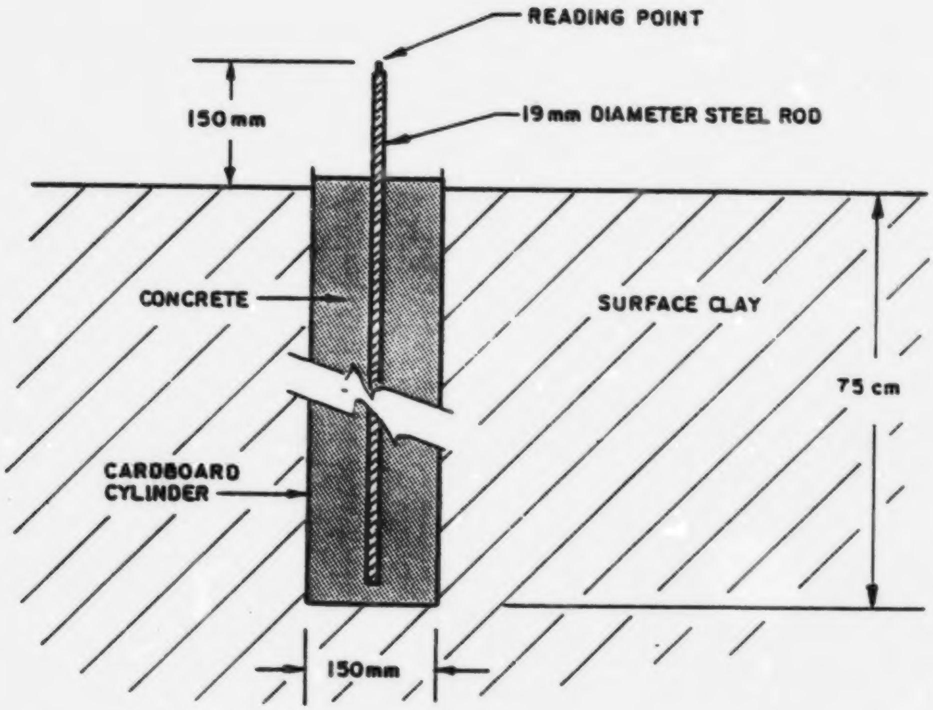

FIGURE 6.6 CONCRETE MONUMENT

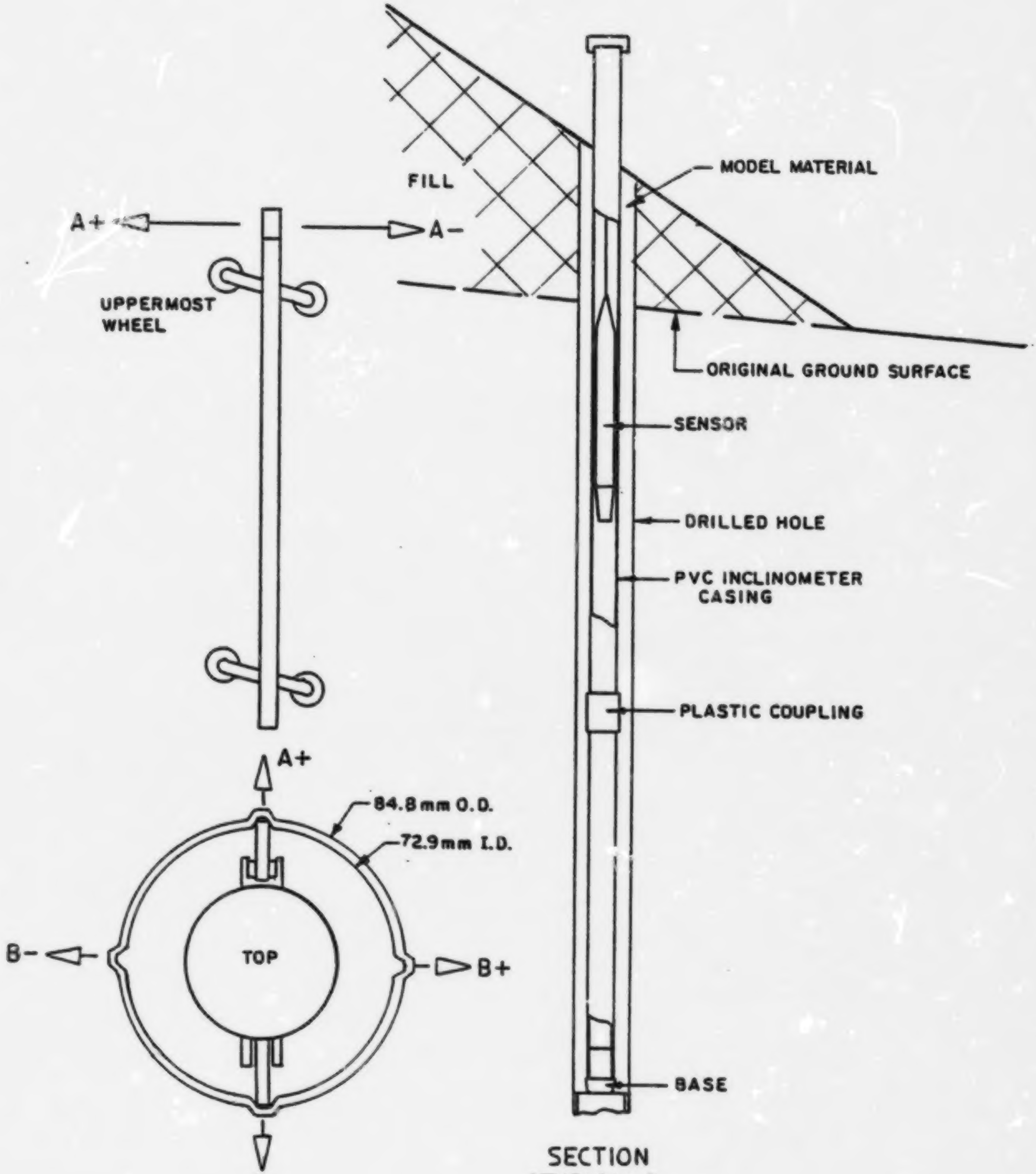

PLAN OF
INCLINOMETER CASING

SECTION
(TYPICAL)

FIGURE 6.7 INCLINOMETER SETUP

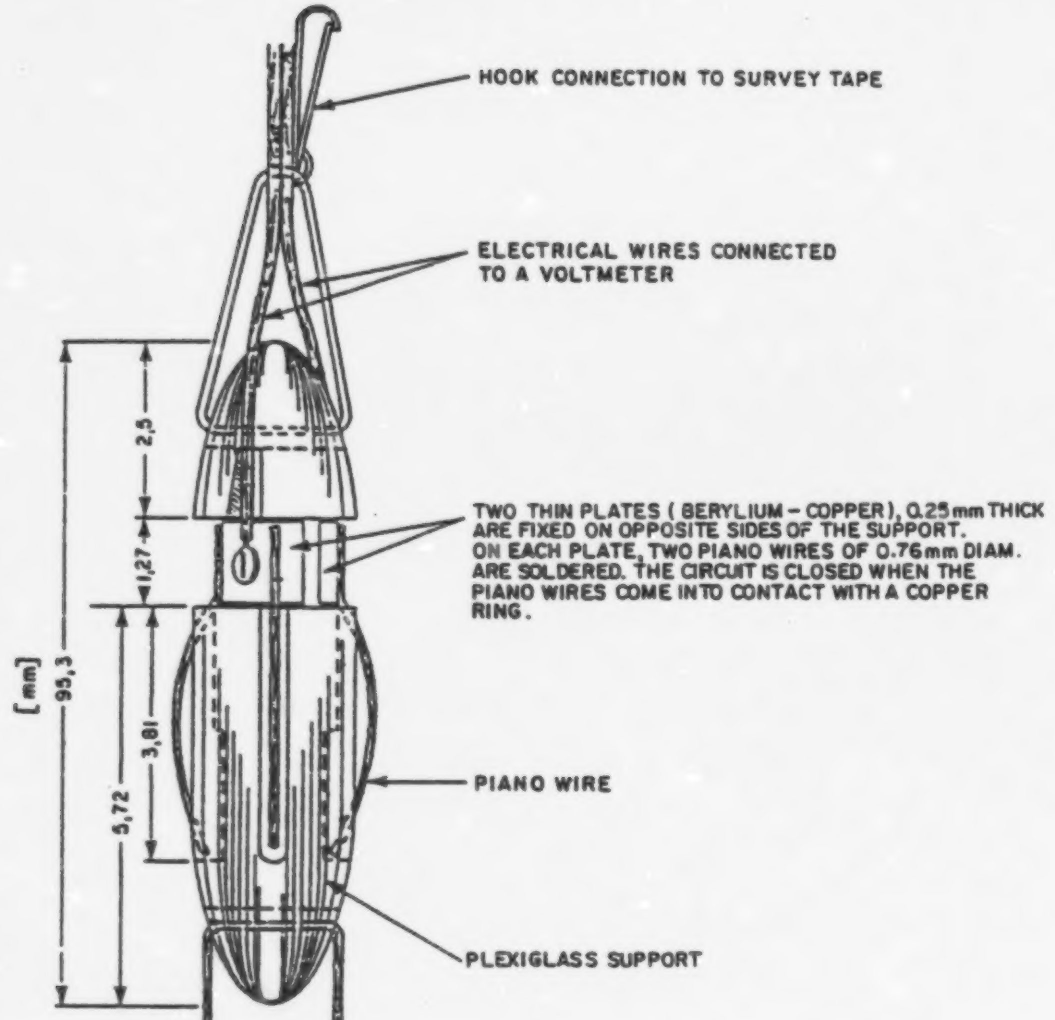
HOOK CONNECTION TO SURVEY TAPE
ELECTRICAL WIRES CONNECTED TO A VOLTMETER
TWO THIN PLATES (BERYLIUM - COPPER), 0.25 mm THICK ARE FIXED ON OPPOSITE SIDES OF THE SUPPORT. ON EACH PLATE, TWO PIANO WIRES OF 0.76 mm DIAM. ARE SOLDERED. THE CIRCUIT IS CLOSED WHEN THE PIANO WIRES COME INTO CONTACT WITH A COPPER RING.
PIANO WIRE
PLEXIGLASS SUPPORT
SMALL WEIGHTS
2,5
1,27
[mm]
95,3
3,81
5,72

FIGURE 6.8 ELECTRICAL EXTENSOMETER SENSOR

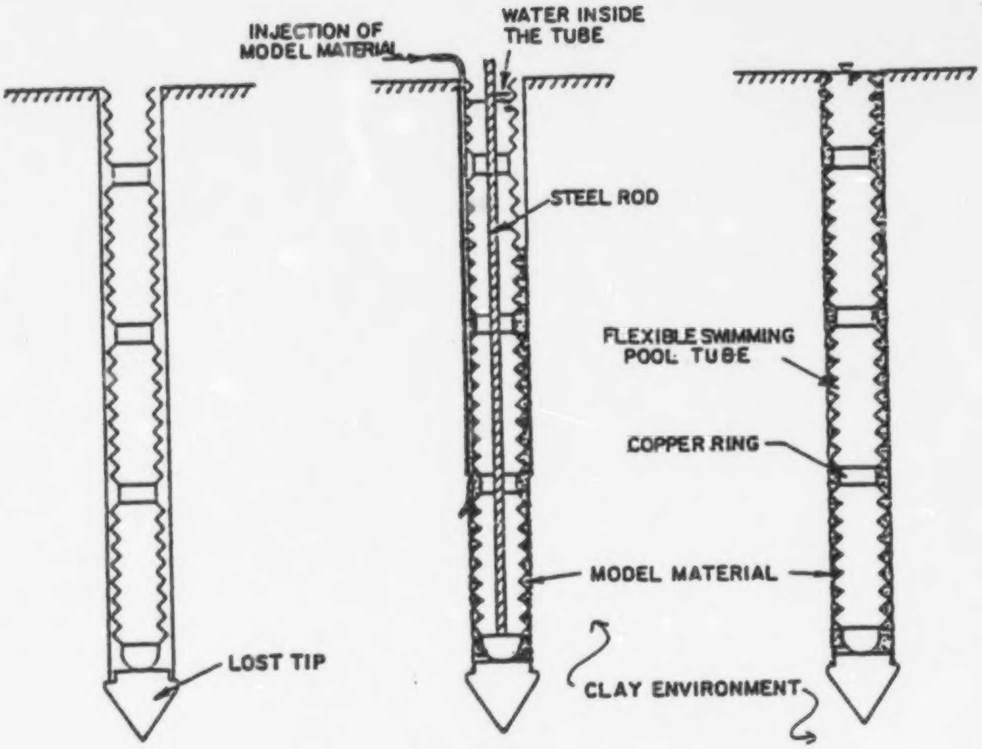

A. CASING PUSHED DOWN WITH SWIMMING POOL TUBE INSIDE.

B. PULLING OUT THE CASING

C. FINAL CONDITION

MODEL MATERIAL: WATER ; 120 l
KAOLIN ; 23 kg
REGULAR CEMENT ; 10 kg
BENTONITE; 7 kg

UNDRAINED STRENGTH (C_u) : 9.6 TO 14.4 kPa after 15 days

a) INSTALLATION OF A VERTICAL EXTENSOMETER

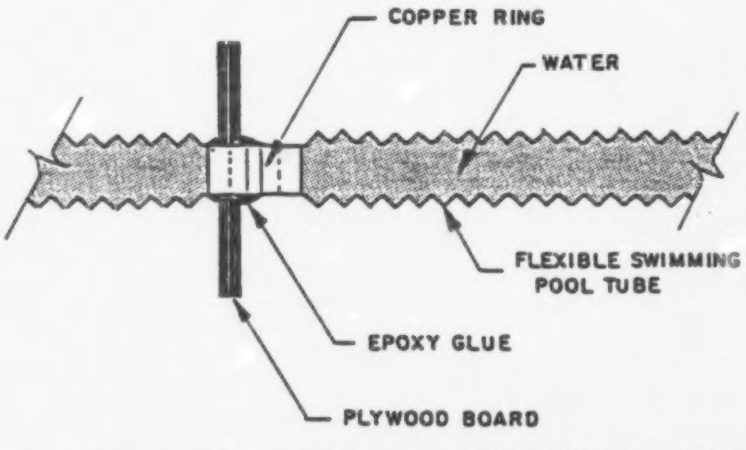

b) COPPER RING CONNECTION IN HORIZONTAL EXTENSOMETER

FIGURE 6.9 VERTICAL AND HORIZONTAL ELECTRICAL EXTENSOMETERS

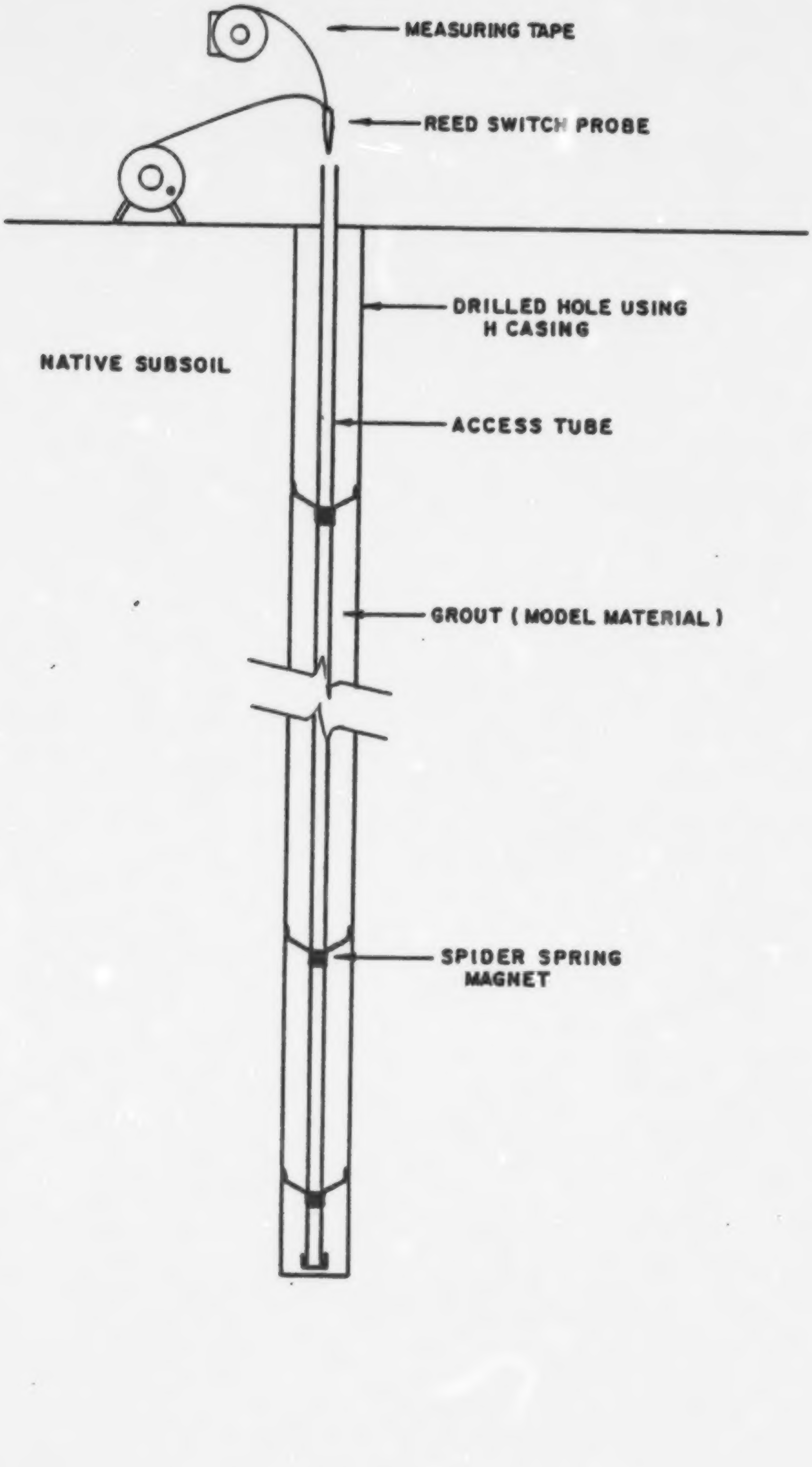

FIGURE 5.10 VERTICAL MAGNETIC EXTENSOMETER

SPECIFICATIONS FOR TOTAL PRESSURE CELL

MODEL NUMBER	TP-101
DIMENSIONS	9.0 in. 229 cm. } DIA. BY .438 in. 1.11 cm. } THICK Other sizes available on special order basis.
PLATE MATERIAL	304 STAINLESS
DIAPHRAGM	Nitrile Rubber (Buna-N)
RANGE	0-60 psi 0-4.2 bars 3-200 psi .2-14 bars 3-2000 psi .2-140 bars
DISPLACEMENT	.002cc

Sensing Element: Petur P-100 Pneumatic Transducer

MAXIMUM OPERATING PRESSURE	MATERIALS BODY	DIAPHRAGM	FILTER	LINEAR RANGE	SENSITIVITY*	ACCURACY	DIAPHRAGM DISPLACEMENT	MAX. TUBING LENGTH
2000 psi 138 bars	Glass filled Nylon-12	Nitrile rubber (Buna-N)	Porous (20μ) 316 Stainless	3-2000 psi 0.2-138 bars	±0.1% at constant flow rate 20 CCM	Exceeds readout gauge	0.002 cc	3000 ft. 1000 M

*The P-100 can detect changes in pressure as small as .10" of water, which in normal applications exceeds the capabilities of the readout equipment. Write Petur Instruments Ltd. for test information.

Contact us for prices, additional information and warranty.

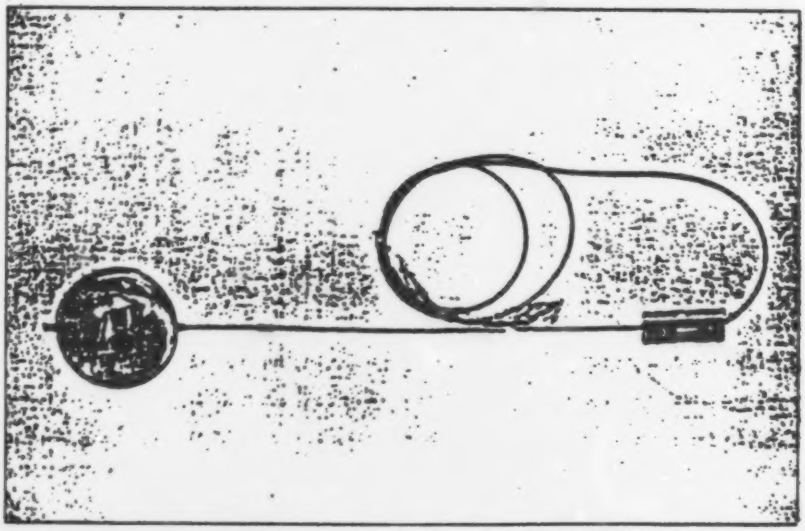

FIGURE 6.11 SPECIFICATIONS AND SETUP OF TOTAL PRESSURE CELL

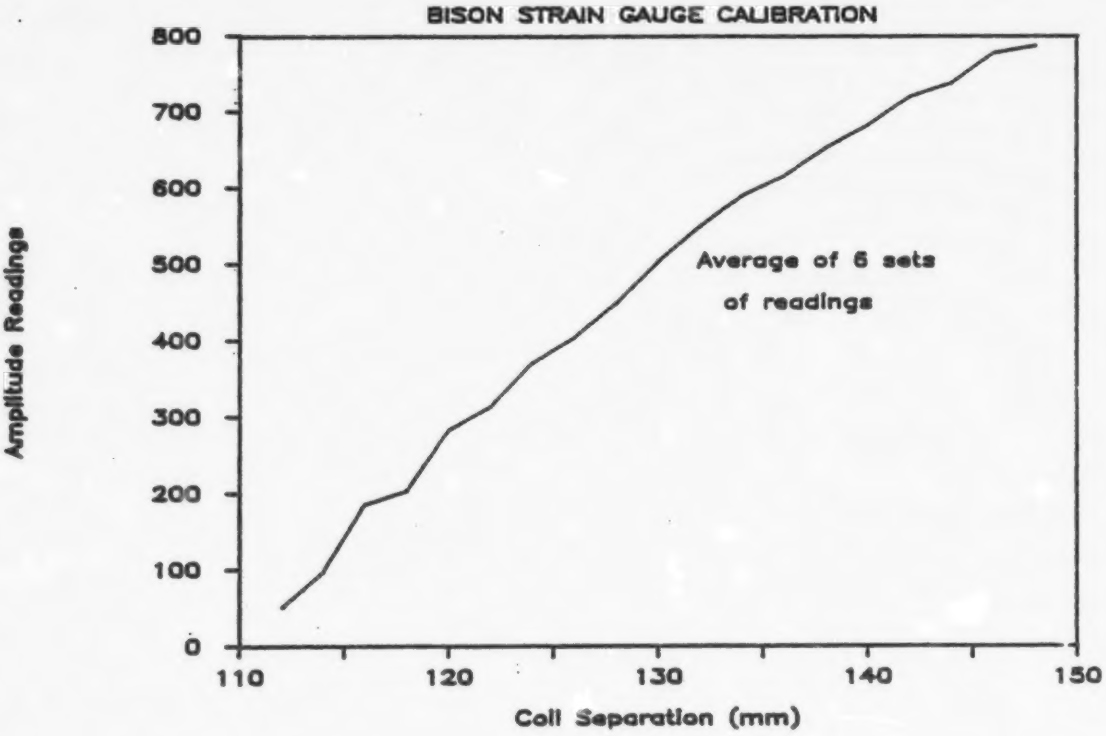

FIGURE 6.12 BISON STRAIN GAUGE CALIBRATION CURVE

a) LOCATION OF BISON STRAIN GAUGES, STRIP REINFORCED EMBANKMENT (No. 2)

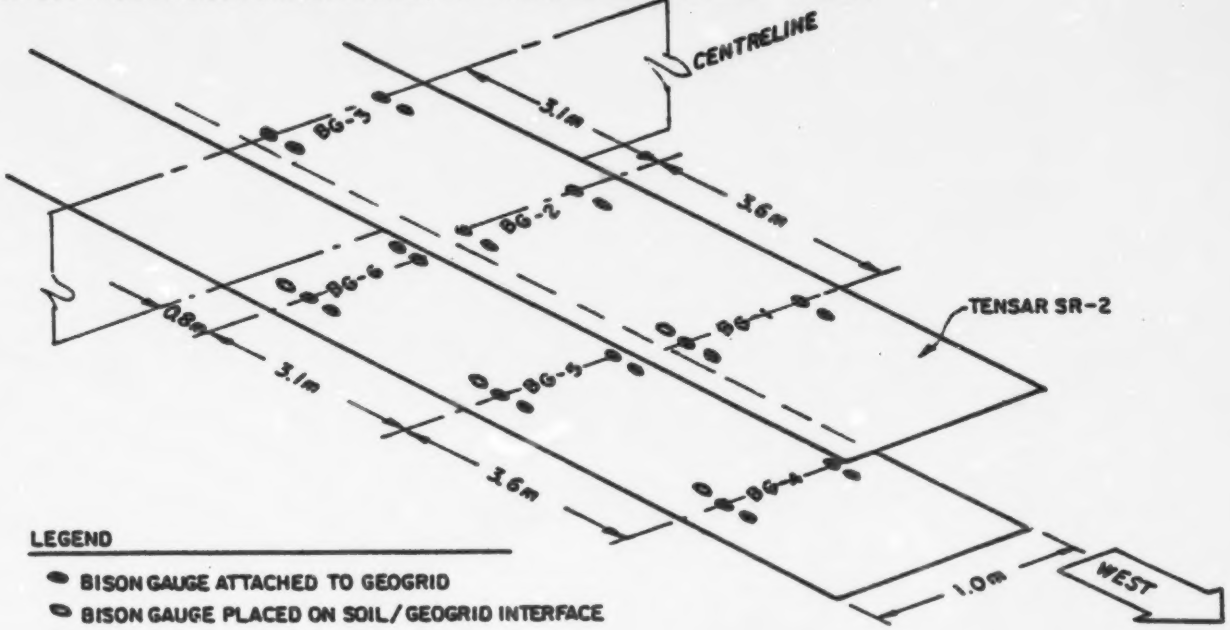

b) LOCATION OF BISON STRAIN GAUGES, GEOCELL REINFORCED EMBANKMENT (No. 3)

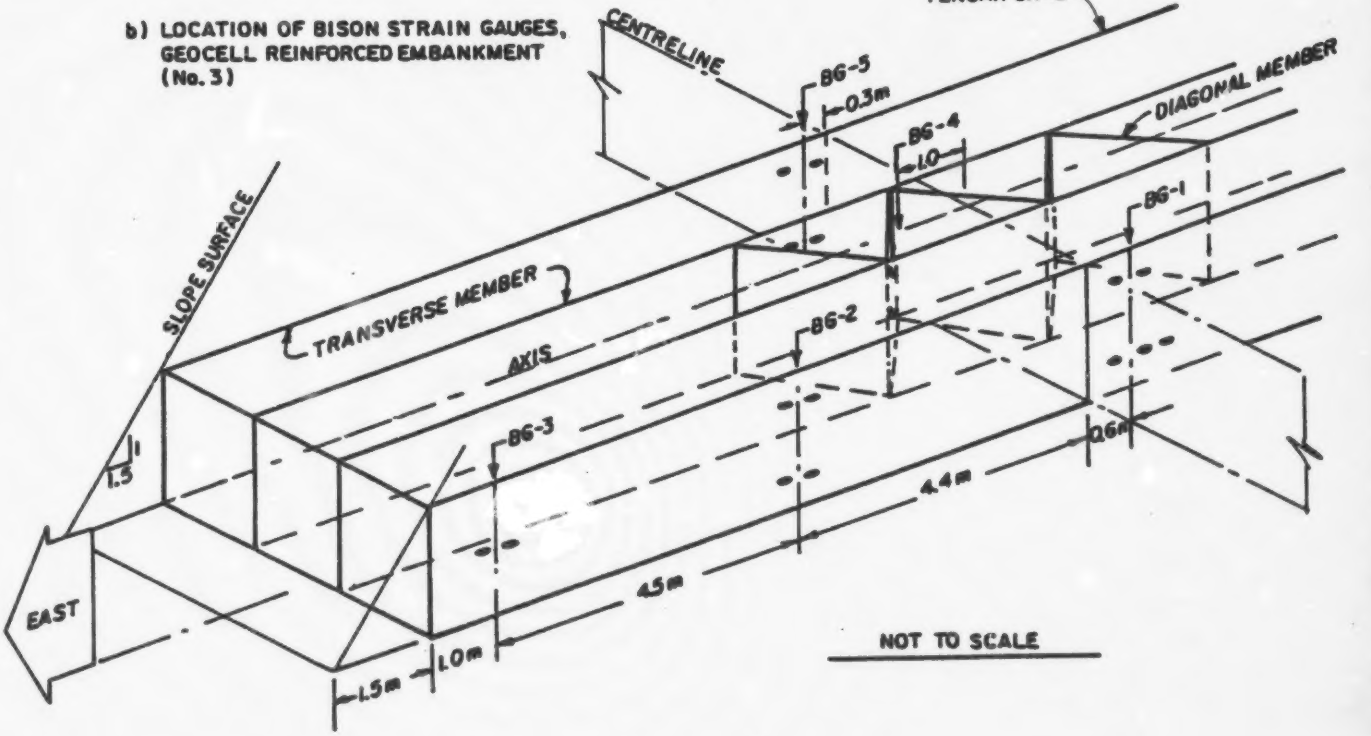

FIGURE 6.13 RELATIVE LOCATION OF BISON STRAIN GAUGES

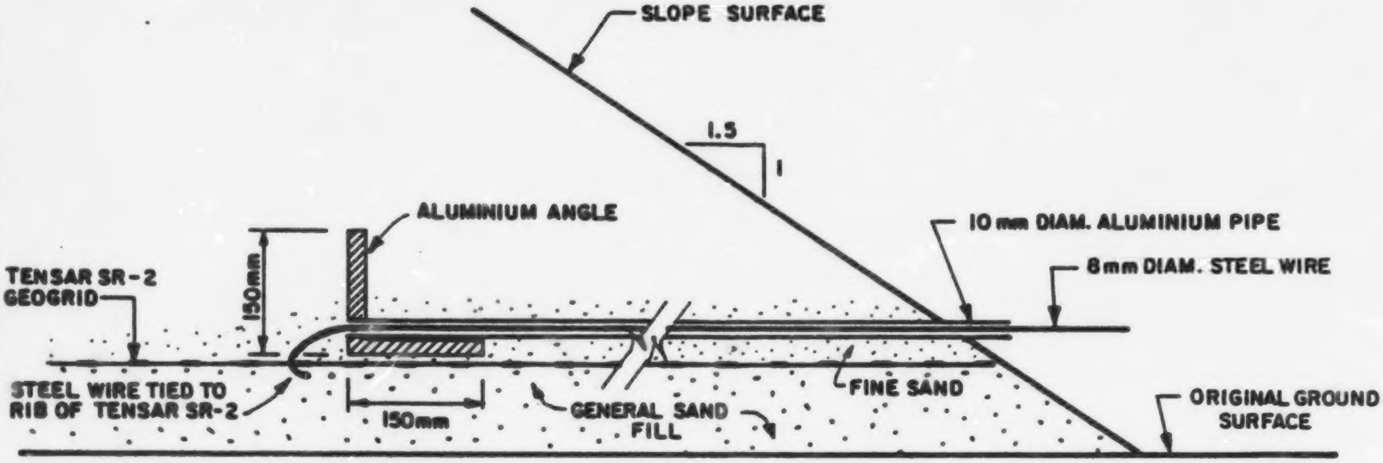

FIGURE 6.14   DETAILS OF DIFFERENTIAL EXTENSOMETER

SECTION 7

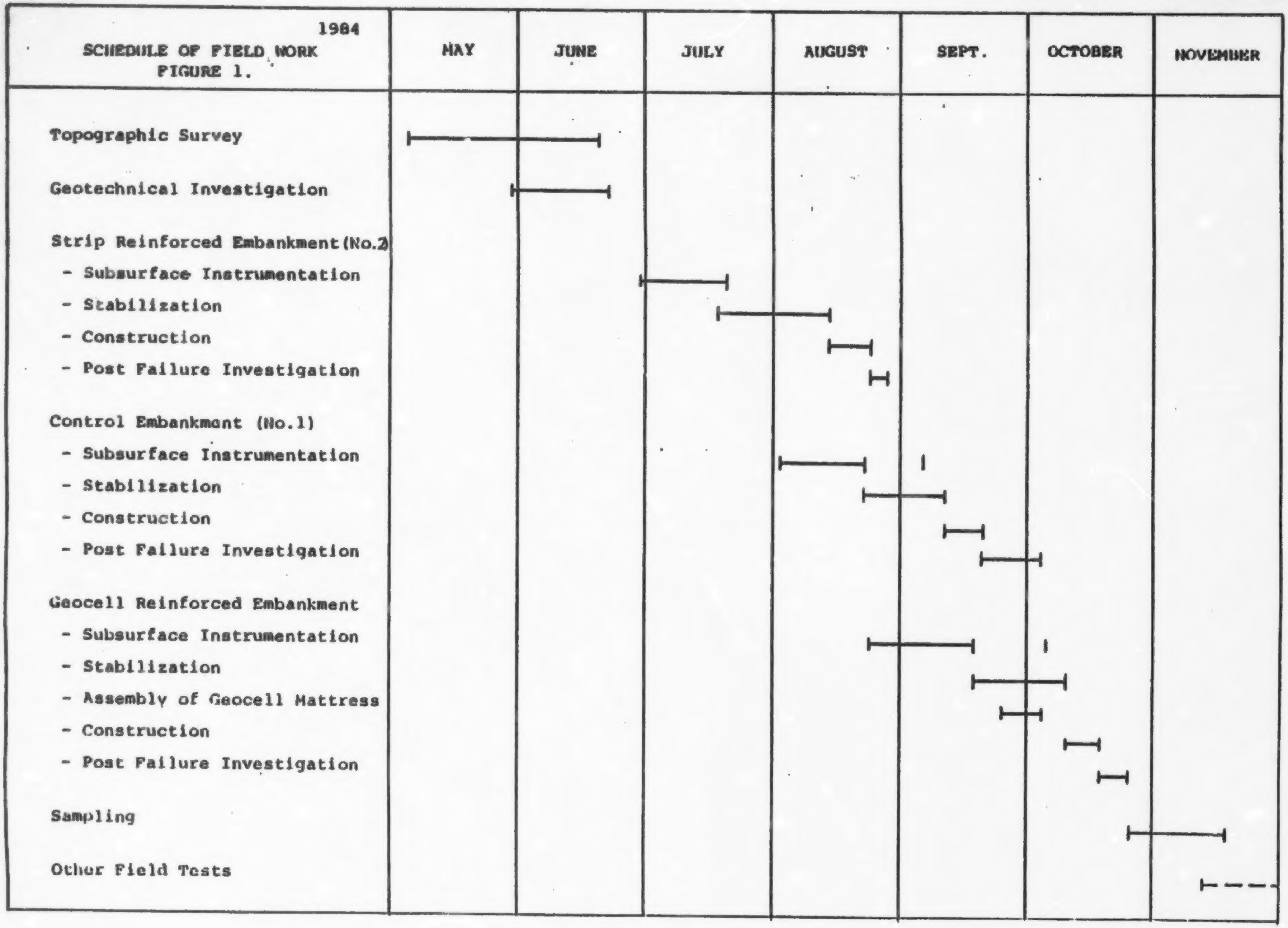

FIGURE 7.1 SCHEDULE OF FIELD WORK

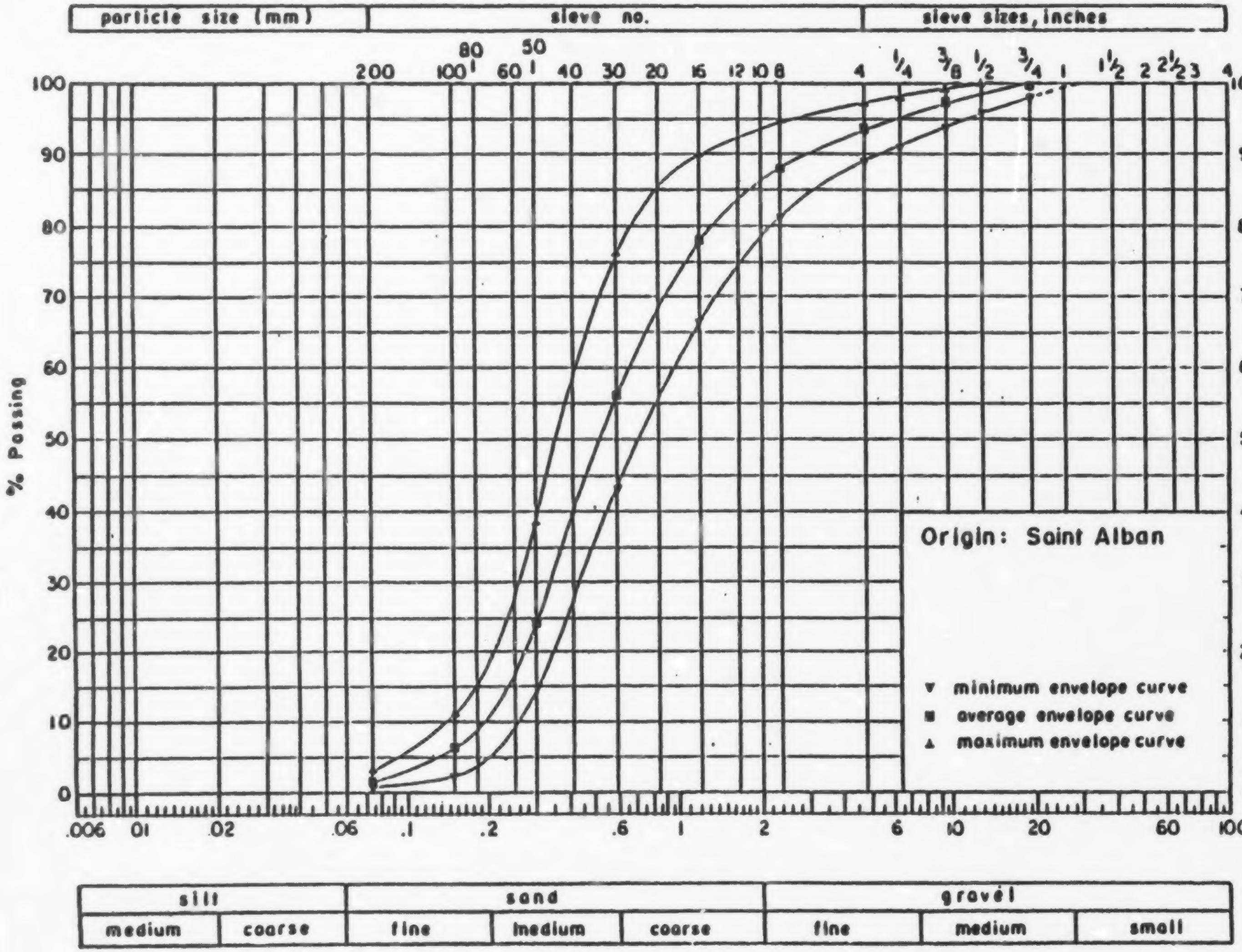

FIGURE 7.2 GRAIN SIZE DISTRIBUTION CURVE OF FILL MATERIAL

a) PLACEMENT OF GEOGRID REINFORCEMENT

b) GEOGRID INSTRUMENTATION

FIGURE 7.3 PLACEMENT AND INSTRUMENTAION OF STRIP REINFORCEMENT

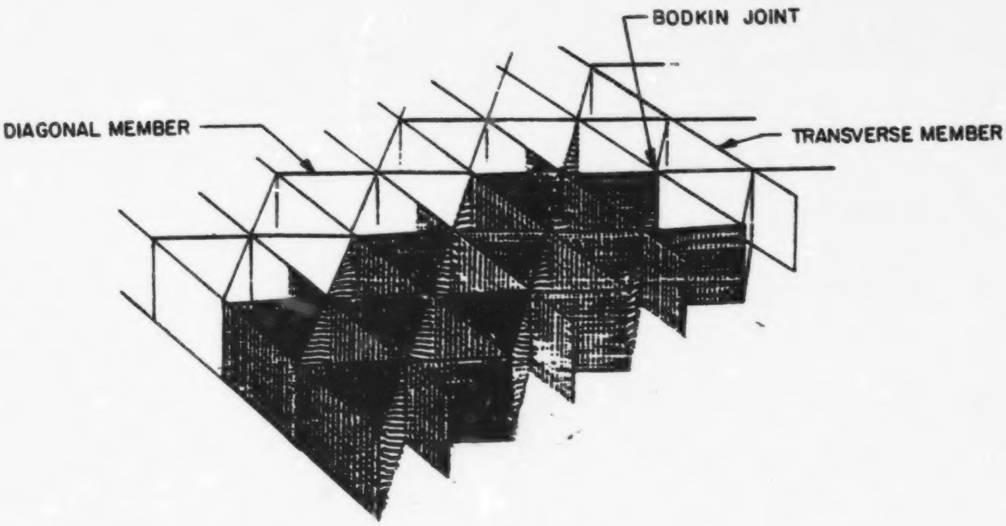

a) ASSEMBLED GEOCELL MATTRESS

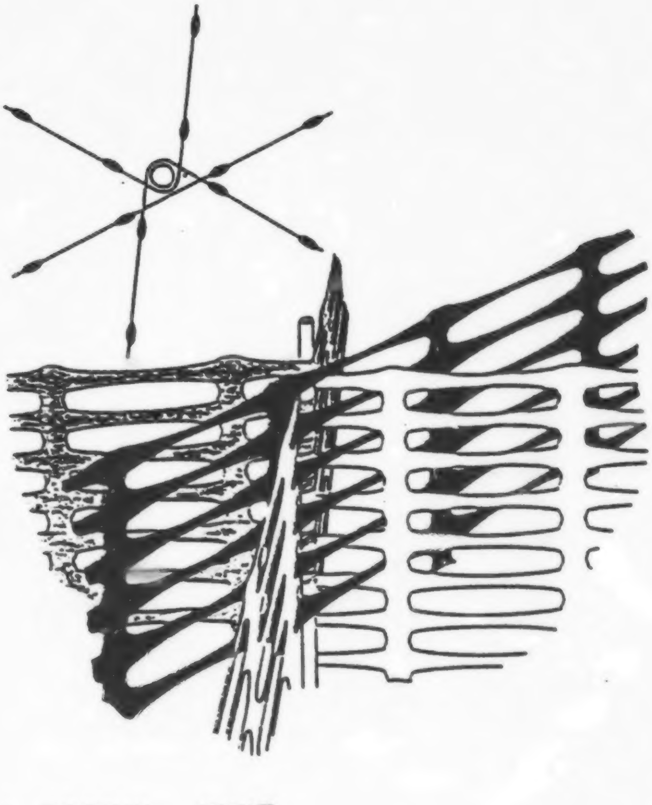

b) BODKIN JOINT

FIGURE 7.4 PICTORIALS OF GEOCELL MATTRESS AND BODKIN JOINT

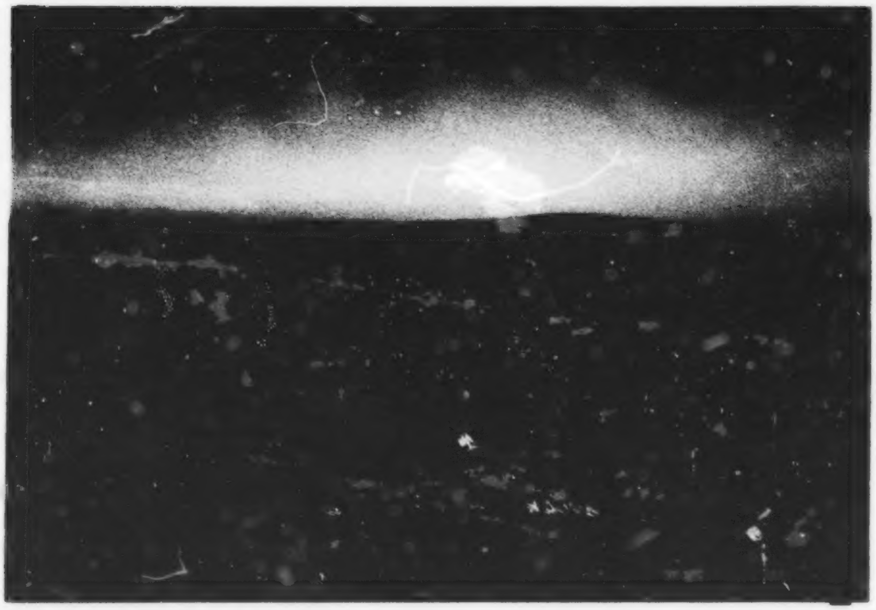

FIGURE 7.5 ASSEMBLY OF GEOCELL MATTRESS

a)UNIT WEIGHT HISTOGRAM,CONTROL (NO. 1)

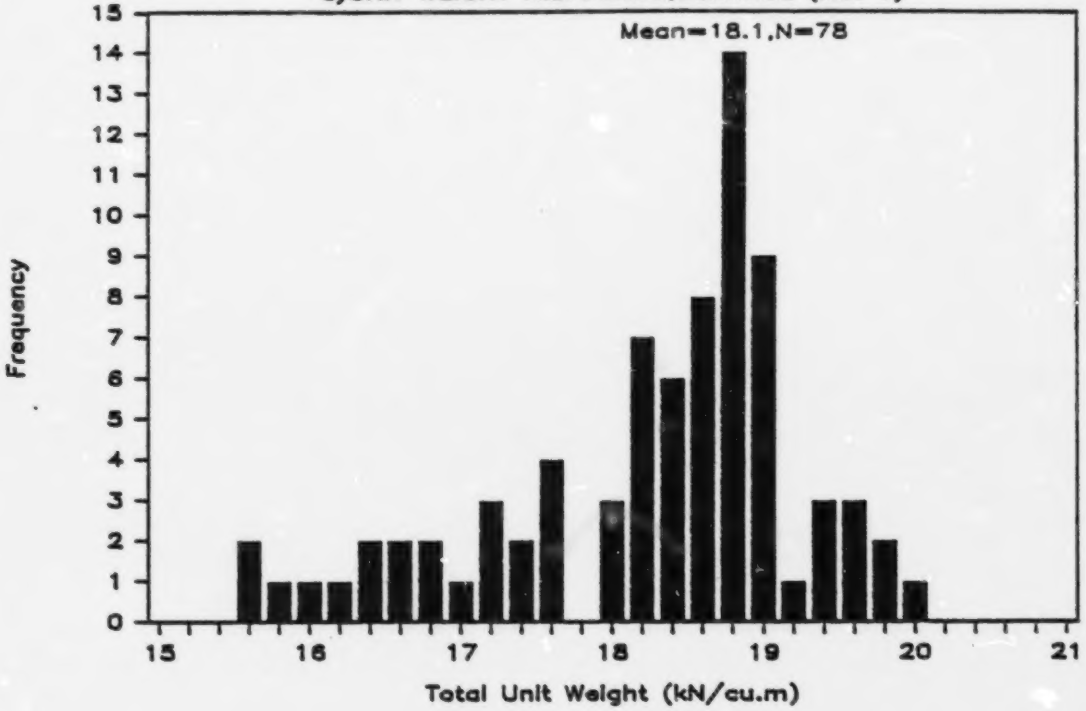

b) UNIT WEIGHT HISTOGRAM, STRIP (NO. 2)

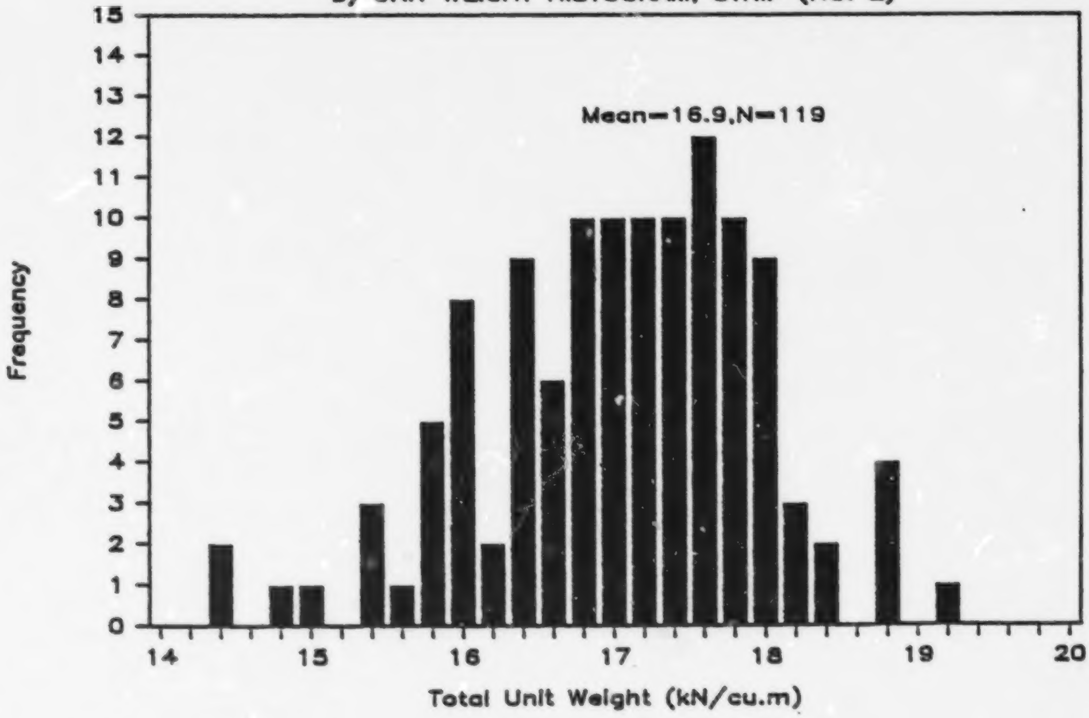

FIGURE 7.6 UNIT WEIGHT HISTOGRAMS, EMBANKMENTS NO. 1 AND 2

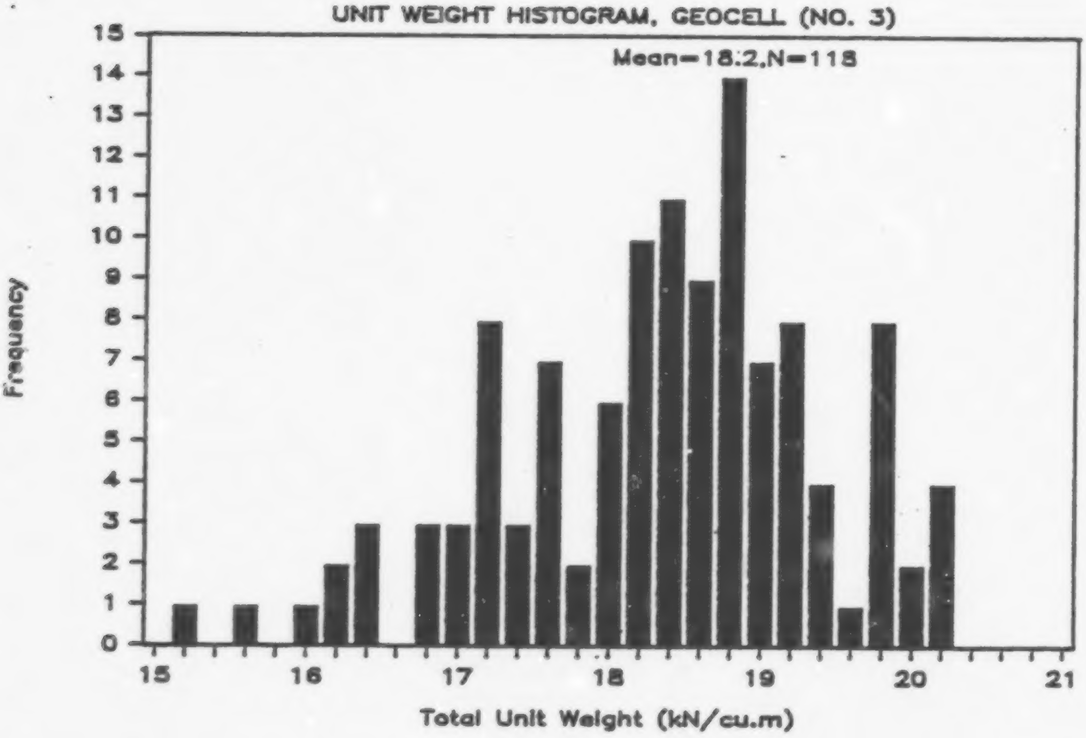

FIGURE 7.7 UNIT WEIGHT HISTOGRAM, EMBANKMENT NO.3

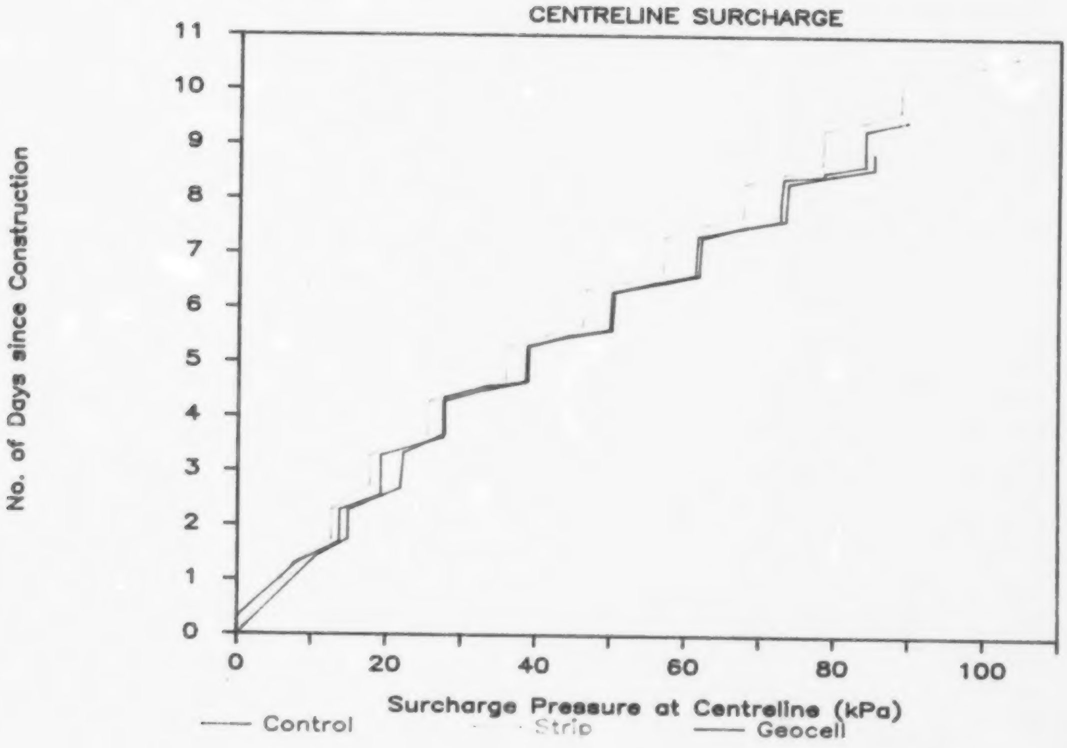

FIGURE 7.8 CENTRELINE SURCHARGE VERSUS TIME

SECTION 8

a)PNEUMATIC PIEZOMETERS NO.1,PN–2,3 &4

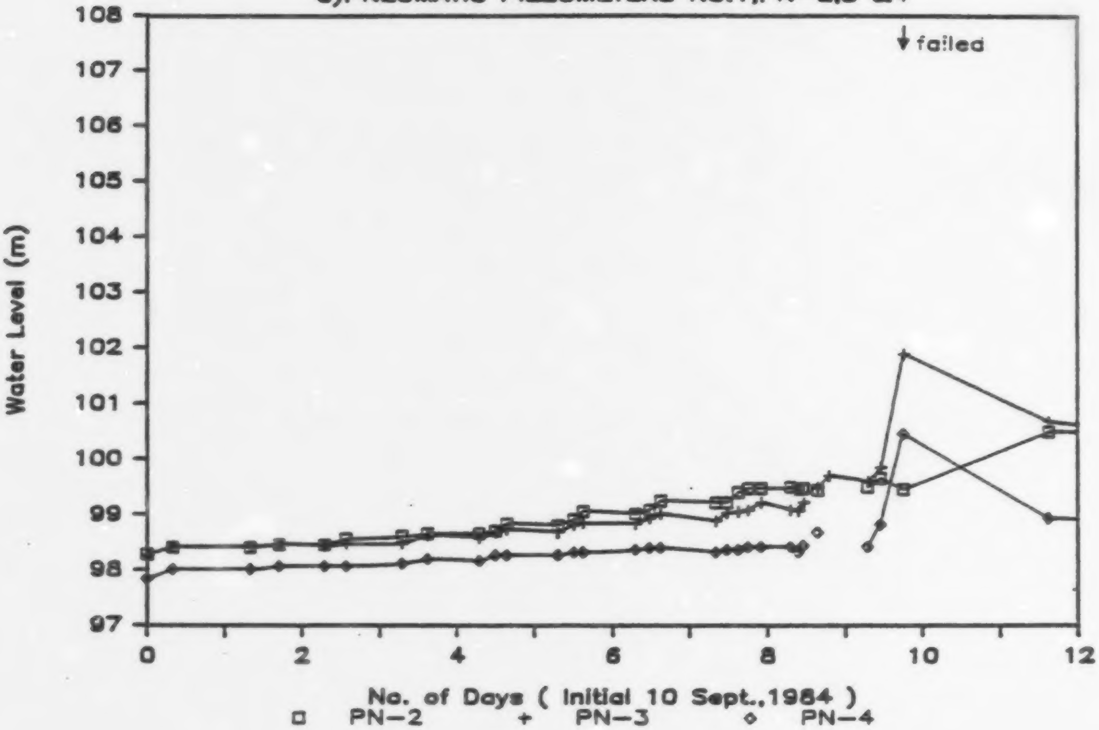

b) PNEUMATIC PIEZOMETERS NO.1,PN–5 TO 8

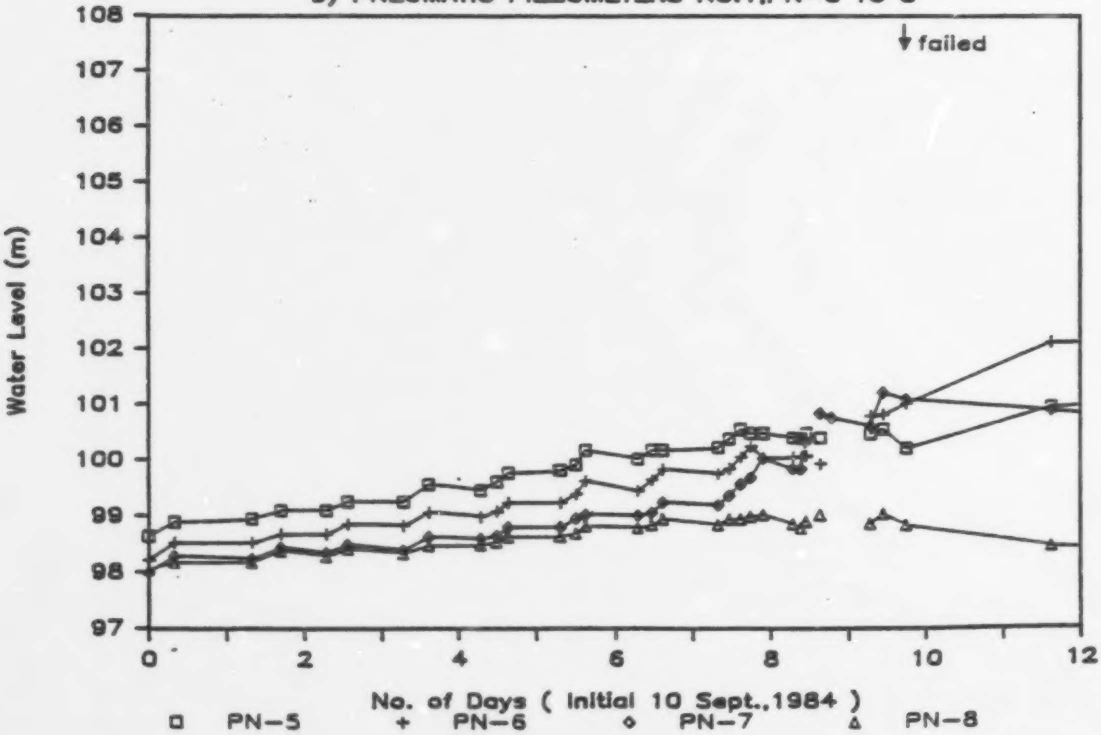

FIGURE 8.1 PNEUMATIC PIEZOMETERS NO.1, PN–2 TO 8

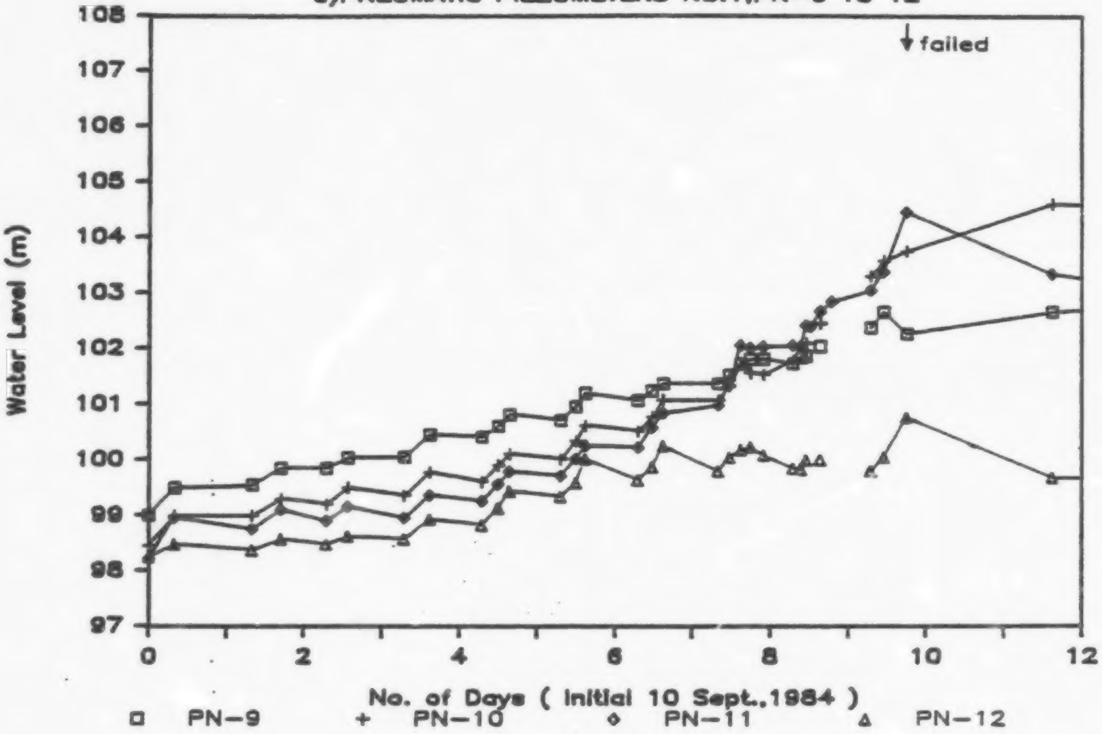

a)PNEUMATIC PIEZOMETERS NO.1,PN-9 TO 12

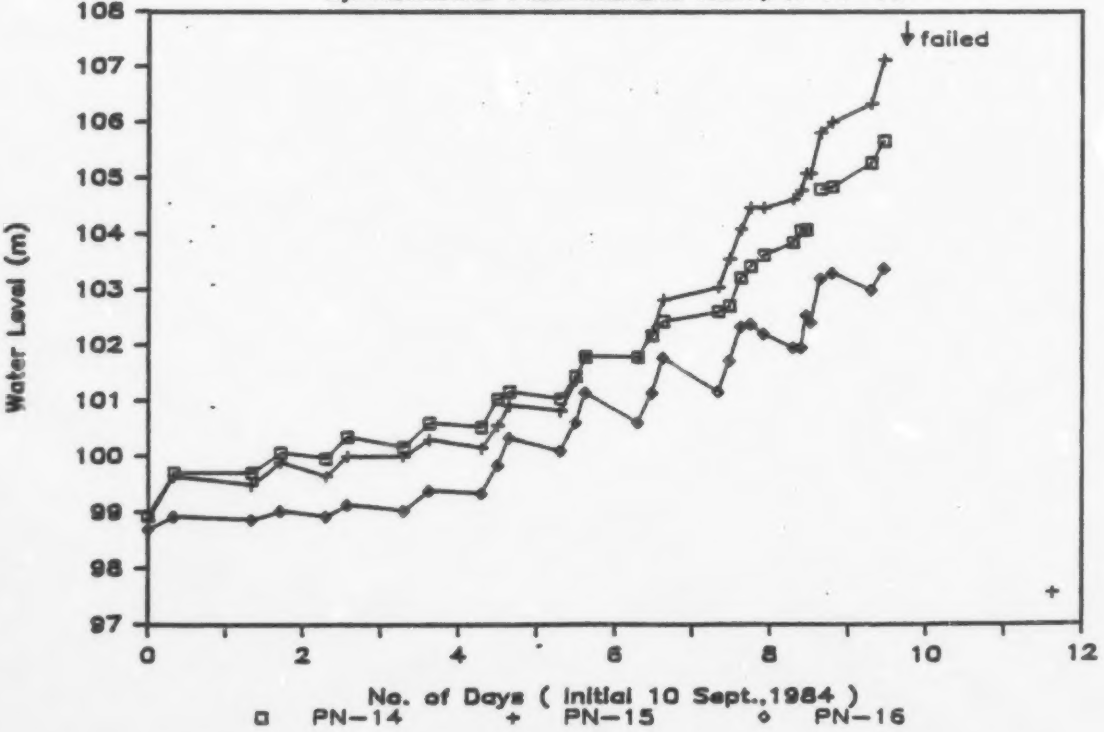

b)PNEUMATIC PIEZOMETERS NO.1,PN 14-16

FIGURE 8.2 PNEUMATIC PIEZOMETERS NO.1. PN-9 TO 16

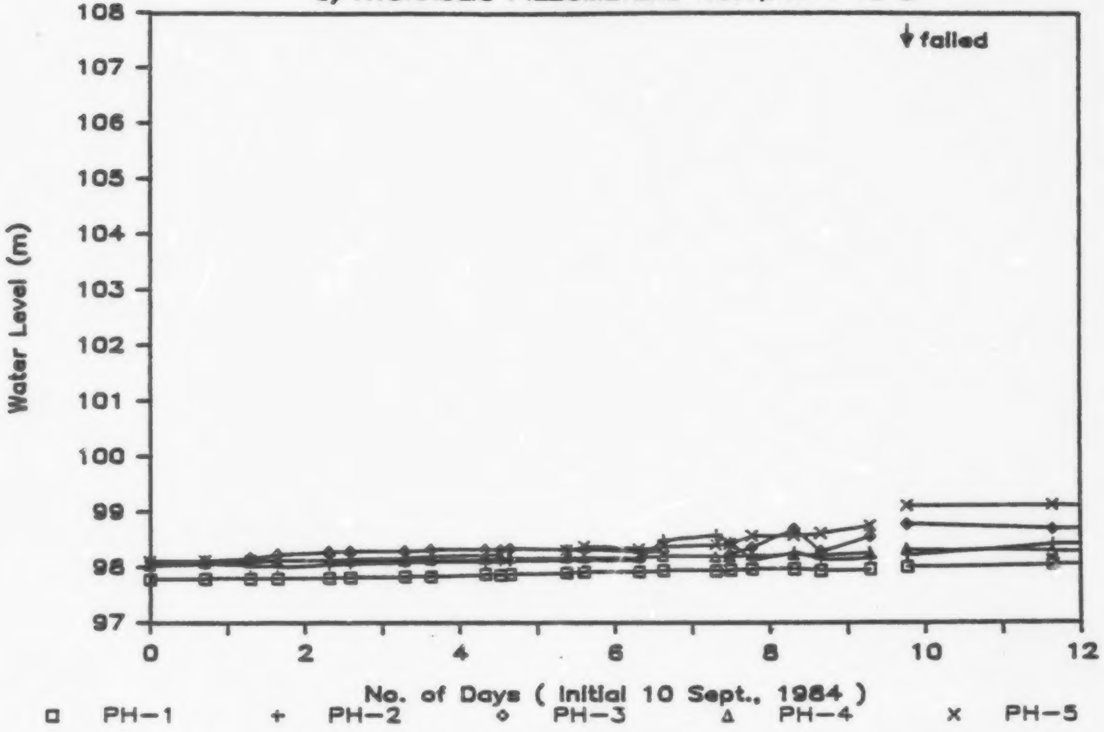

a) HYDRAULIC PIEZOMETERS NO.1,PH-1 TO 5

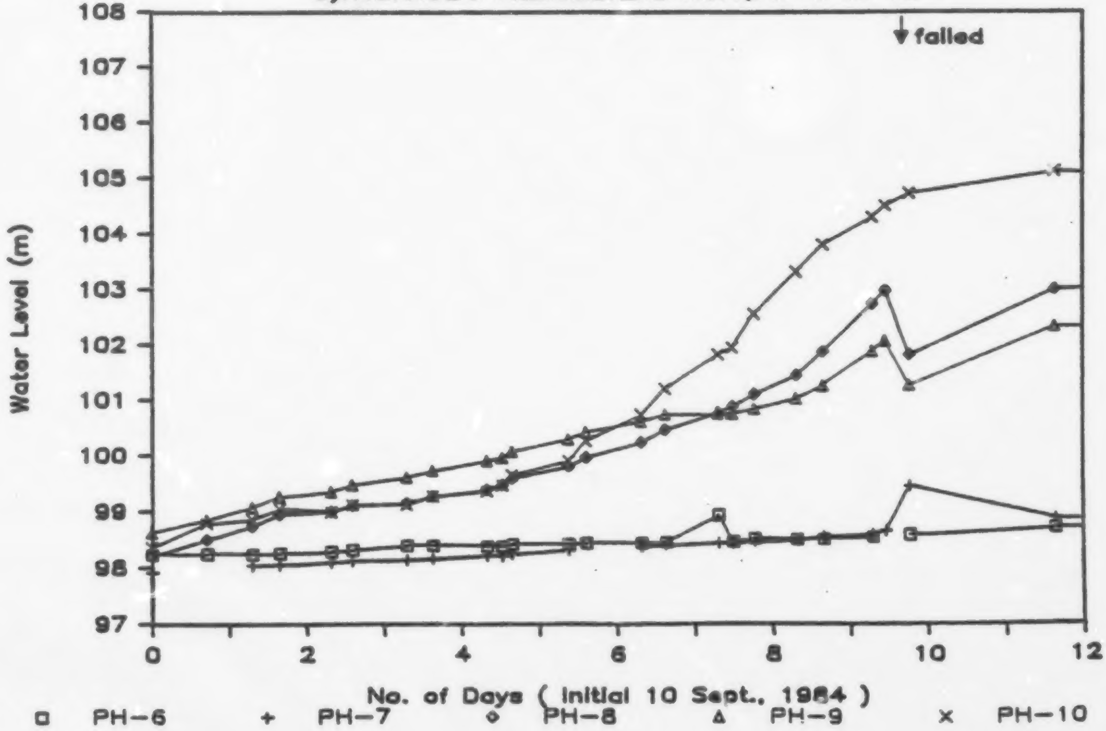

b)HYDRAULIC PIEZOMETERS NO.1,PH-6 TO 10

FIGURE 8.3 HYDRAULIC PIEZOMETERS NO.1, PN-1 TO 10

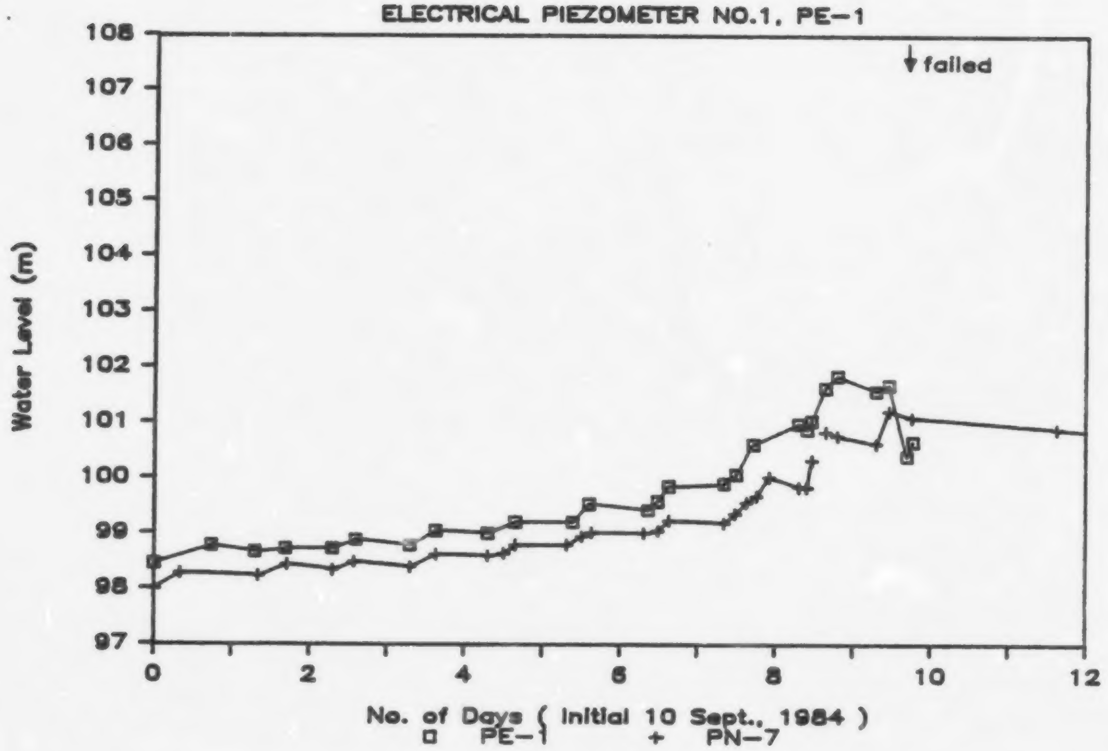

FIGURE 8.4 ELECTRICAL PIEZOMETER NO.1, PE-1

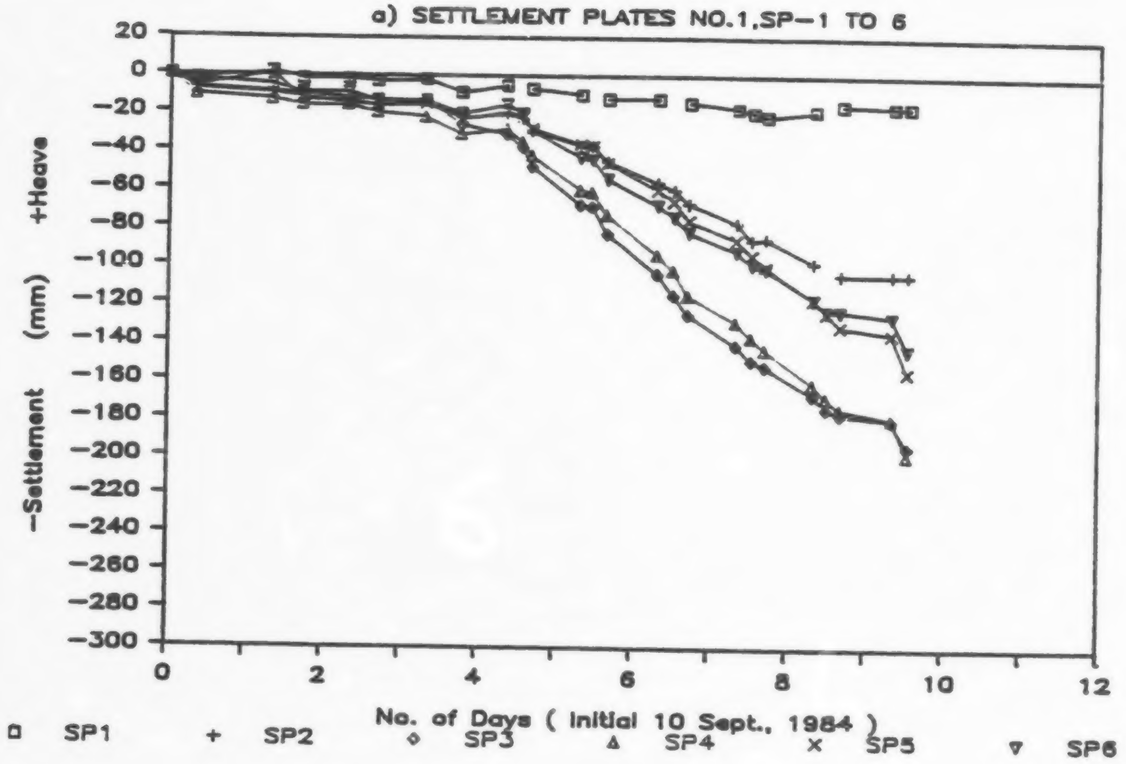

a) SETTLEMENT PLATES NO.1,SP-1 TO 6

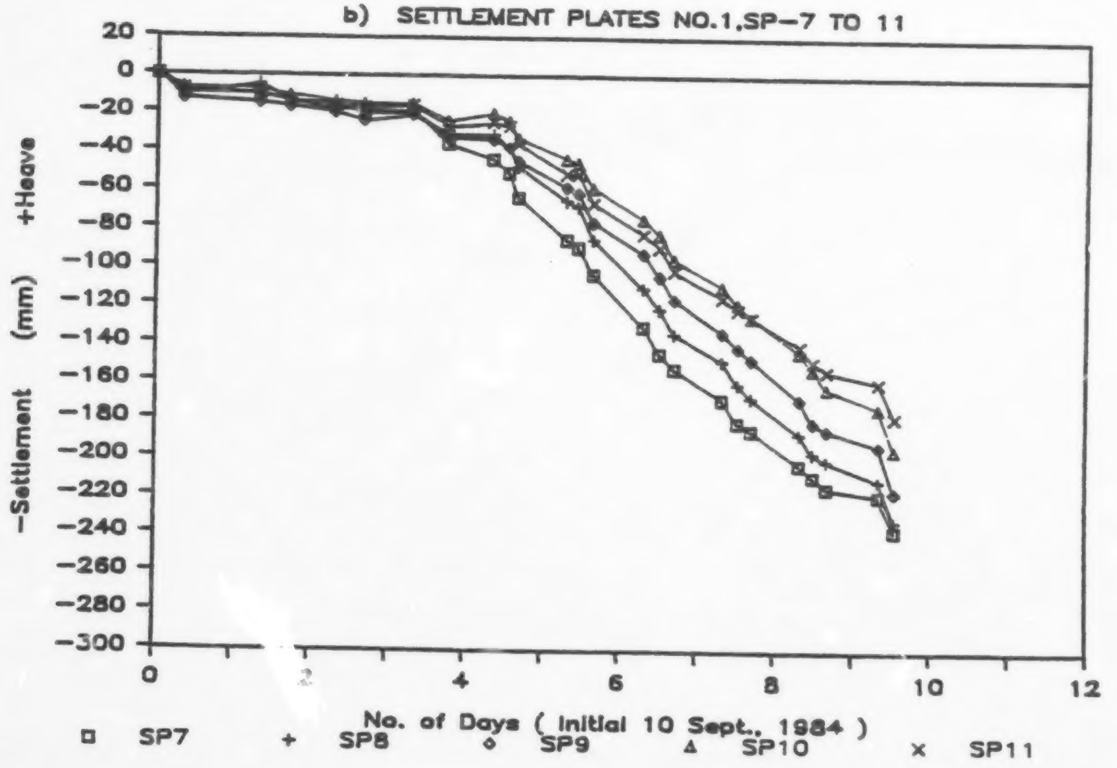

b) SETTLEMENT PLATES NO.1,SP-7 TO 11

FIGURE 8.5 SETTLEMENT PLATES NO.1, SP-1 TO 11

a) SETTLEMENT OF MONUMENTS NO.1,MN 1–5

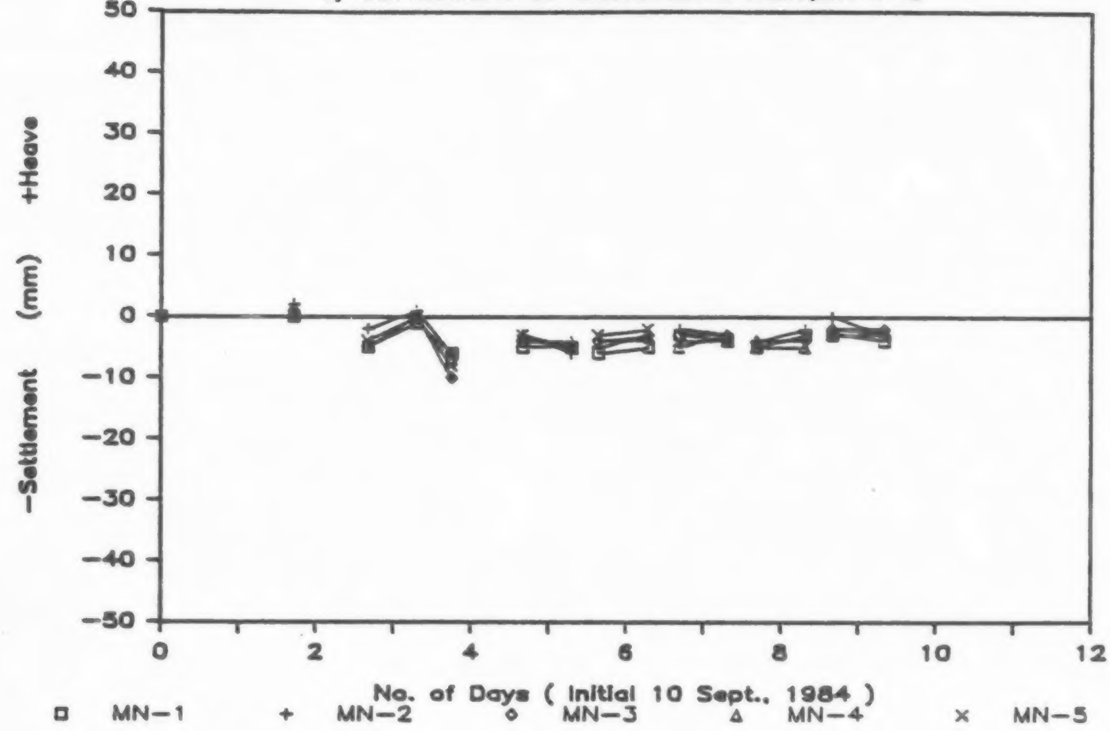

b) SETTLEMENT OF MONUMENTS NO.1,MN 6–10

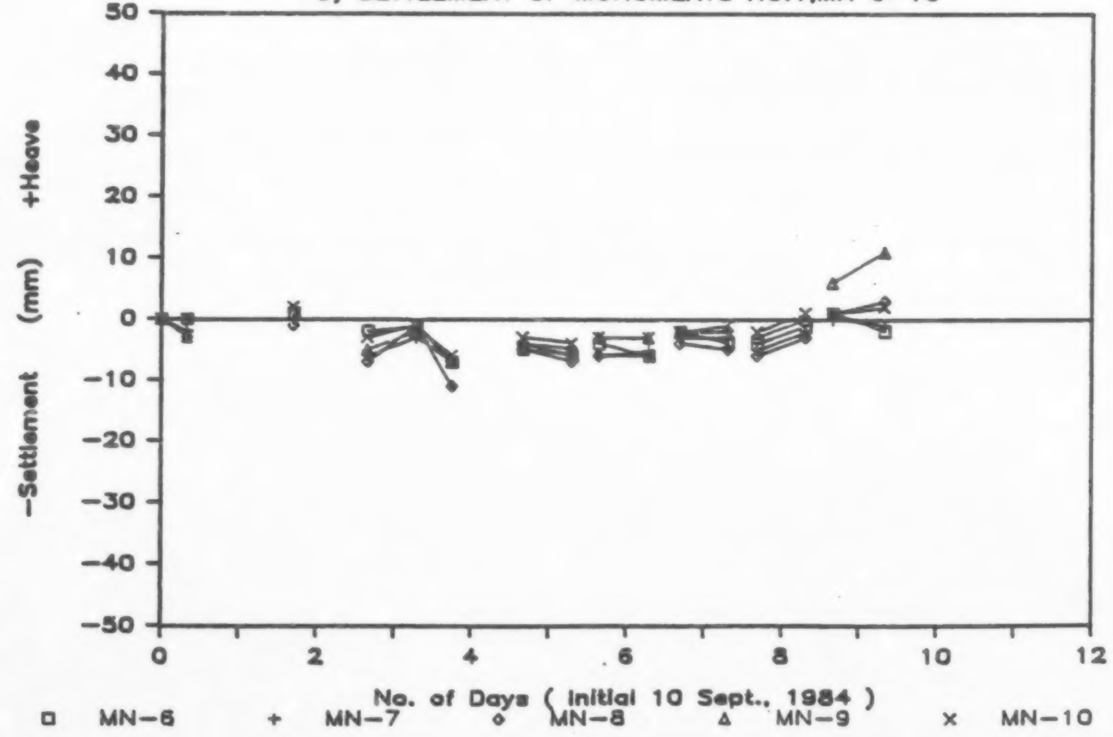

FIGURE 8.6 SETTLEMENT OF MONUMENTS NO.1, MN-1 TO 5

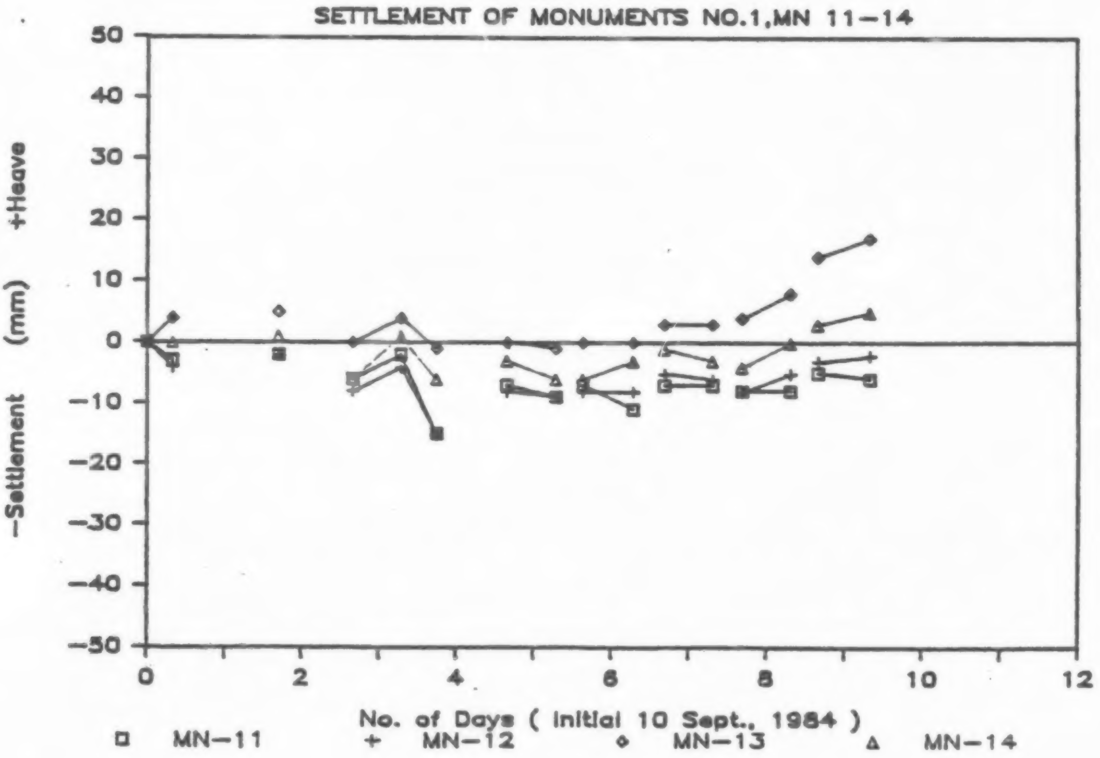

FIGURE 8.7 SETTLEMENT OF MONUMENTS NO.1. MN-11 TO 14

a) VERT. ELECTR. EXTENSOMETER NO.1,VE–1

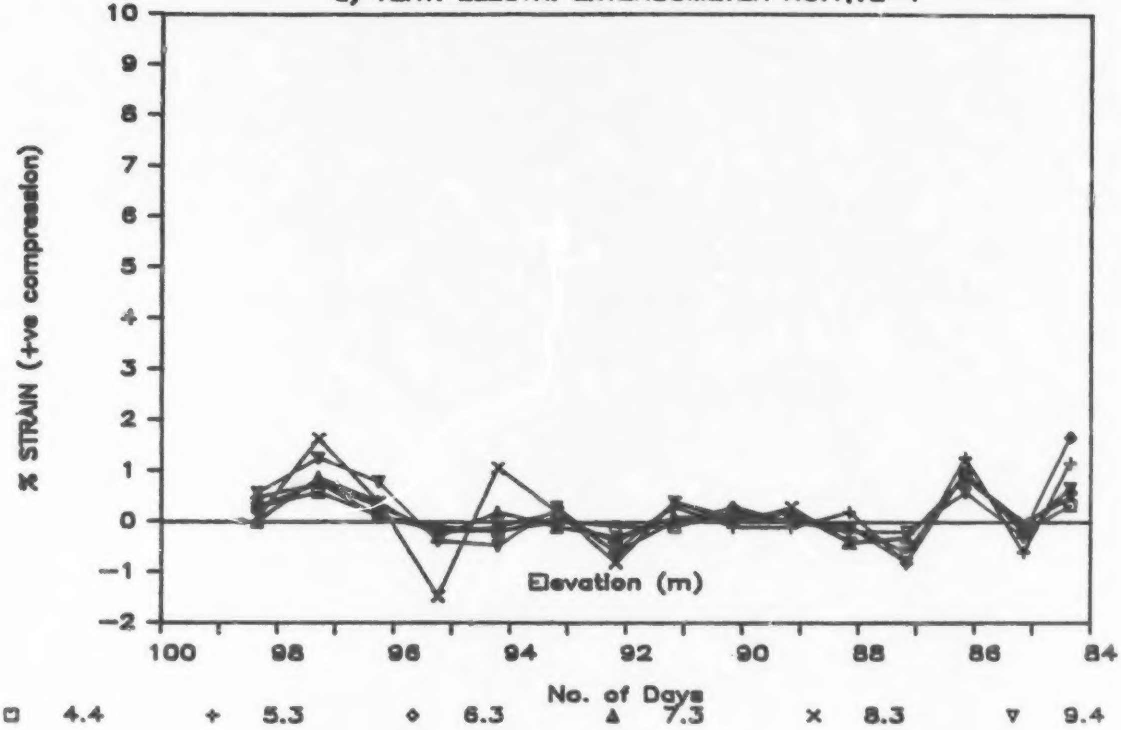

b) VERT. ELECTR. EXTENSOMETER NO.1,VE–2

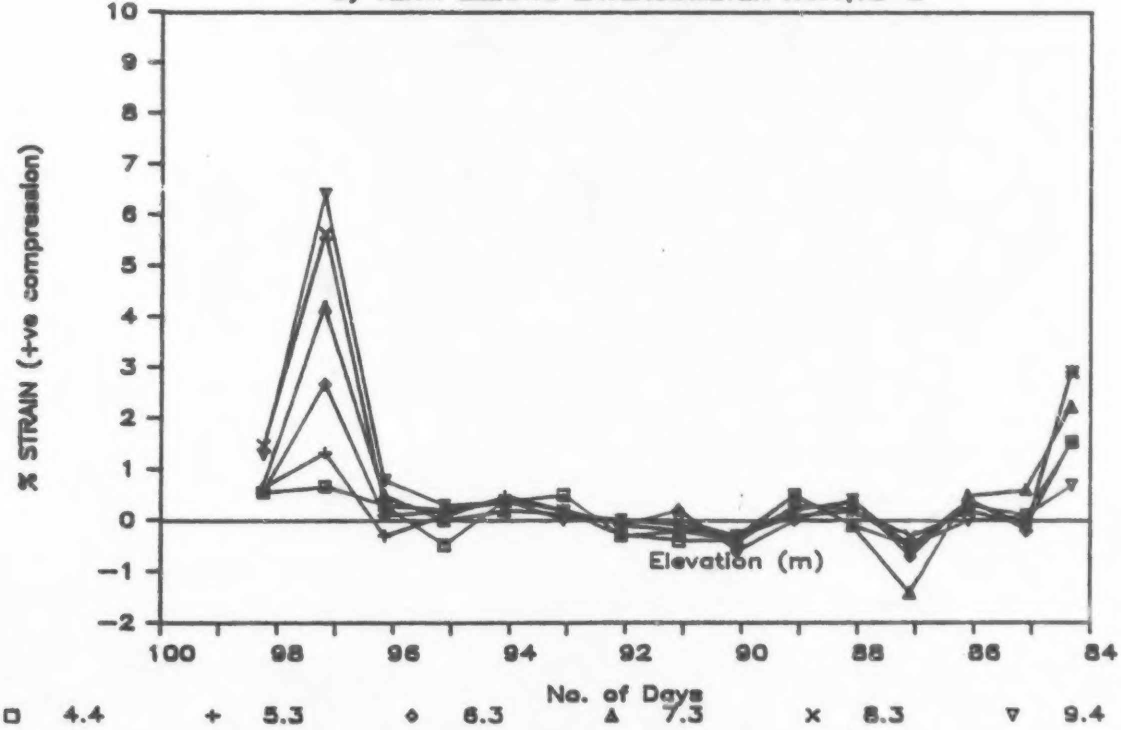

FIGURE 8.8 VERTICAL ELECTRICAL EXTENSOMETERS NO.1, VE–1 AND 2

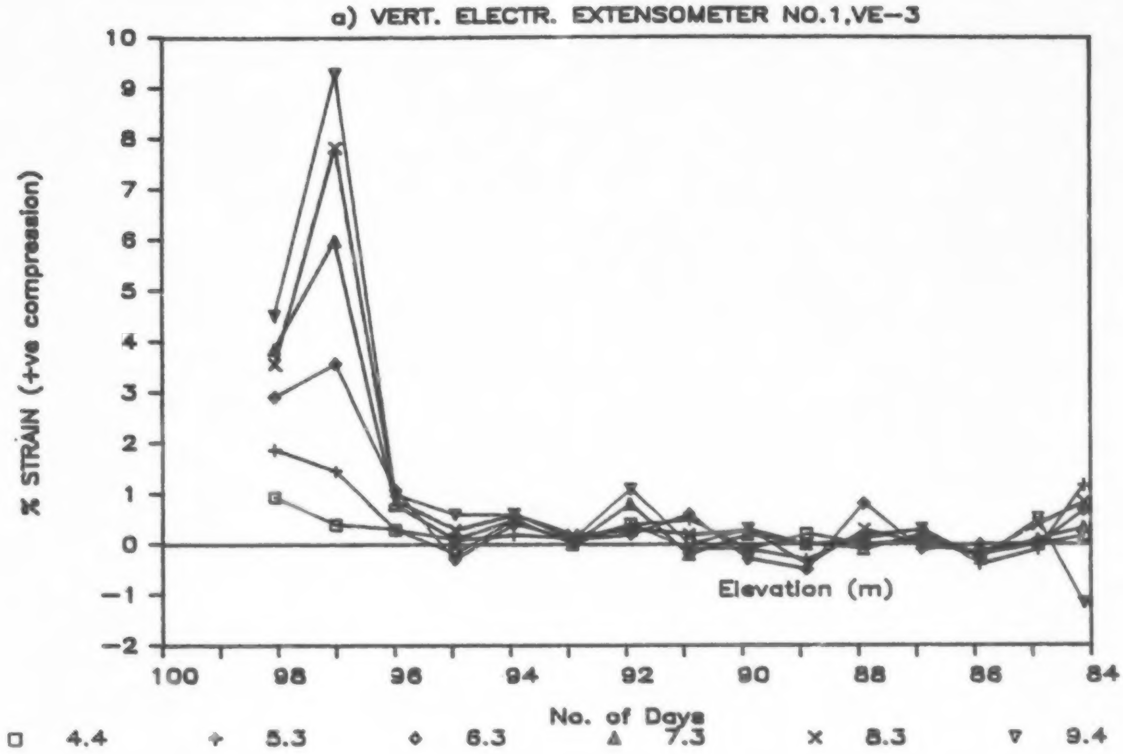

a) VERT. ELECTR. EXTENSOMETER NO.1,VE-3

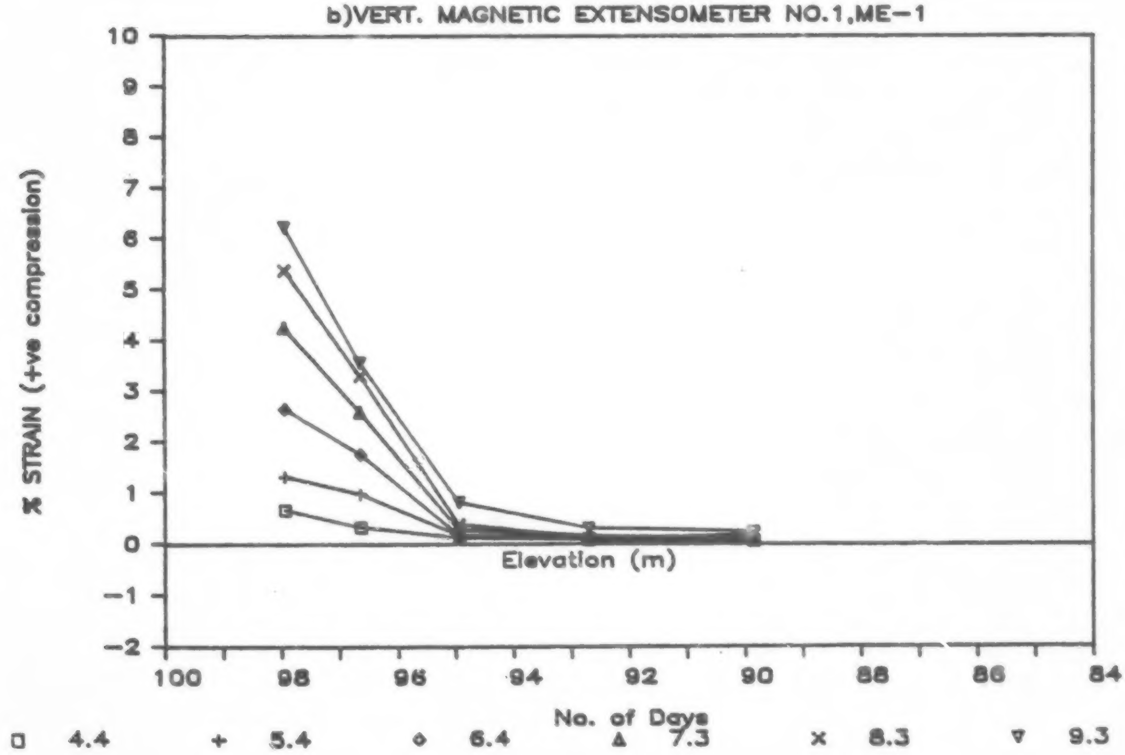

b)VERT. MAGNETIC EXTENSOMETER NO.1,ME-1

FIGURE 8.9 VERTICAL ELECTRICAL AND MAGNETIC EXTENSOMETERS NO.1, VE-3 AND ME-1

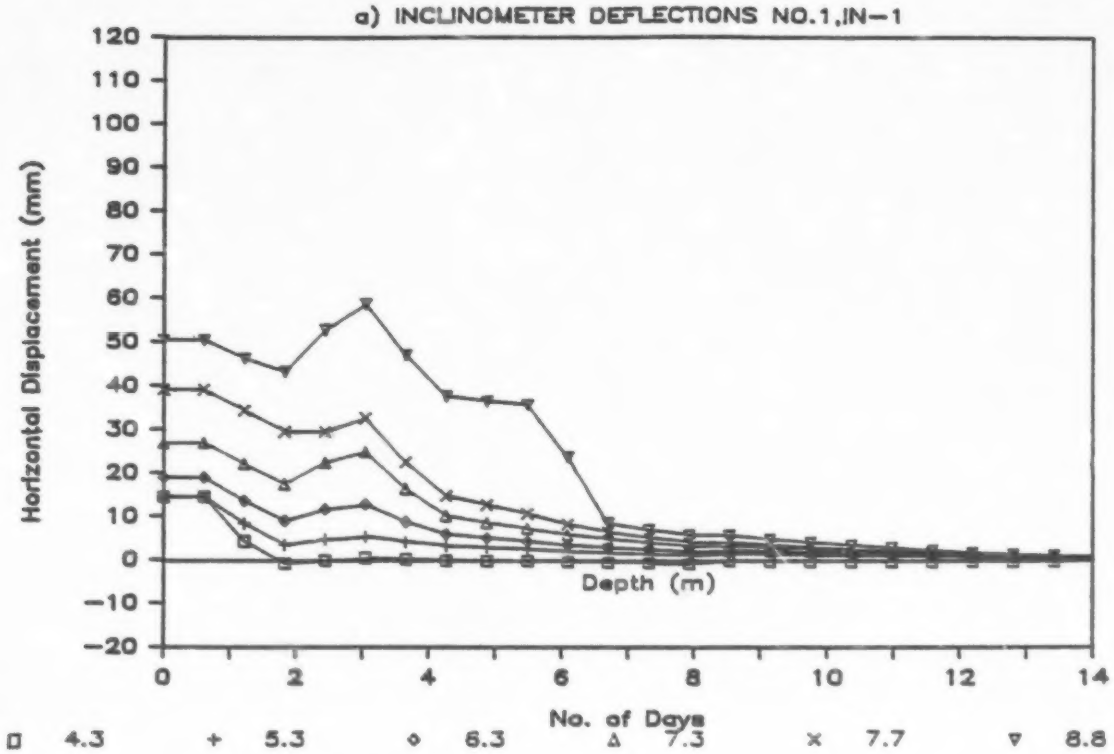

a) INCLINOMETER DEFLECTIONS NO.1,IN-1

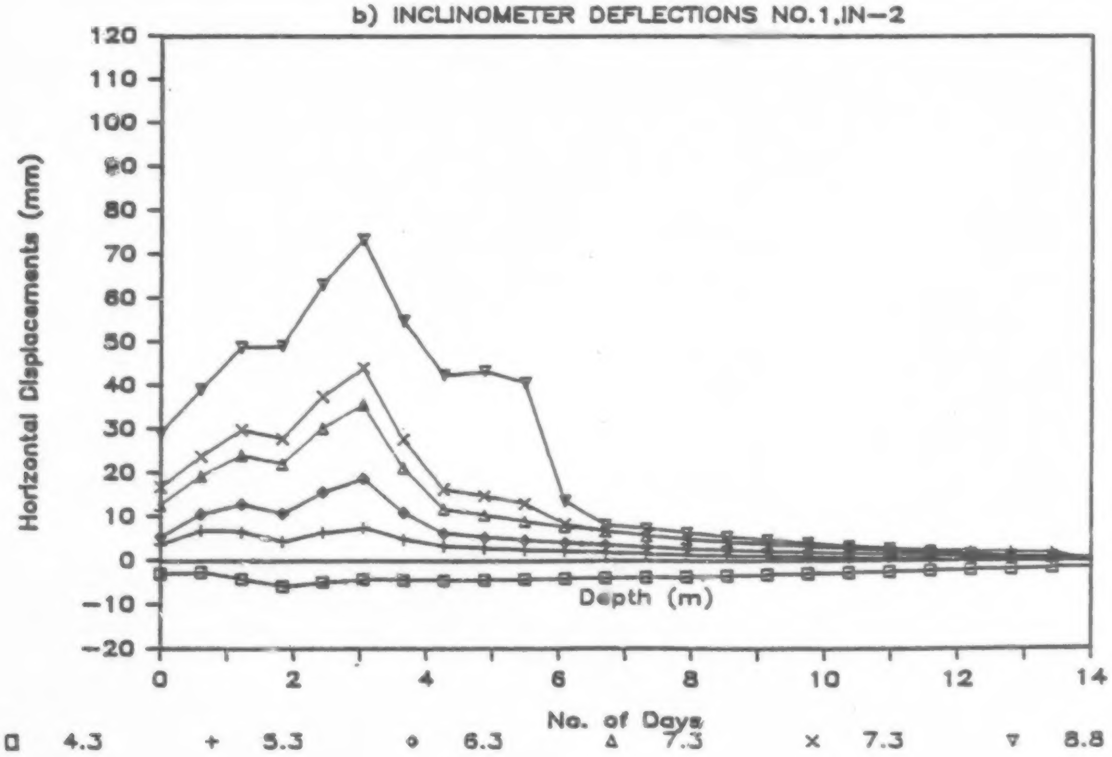

b) INCLINOMETER DEFLECTIONS NO.1,IN-2

FIGURE 8.10 INCLINOMETER DEFLECTIONS NO.1, IN-1 AND 2

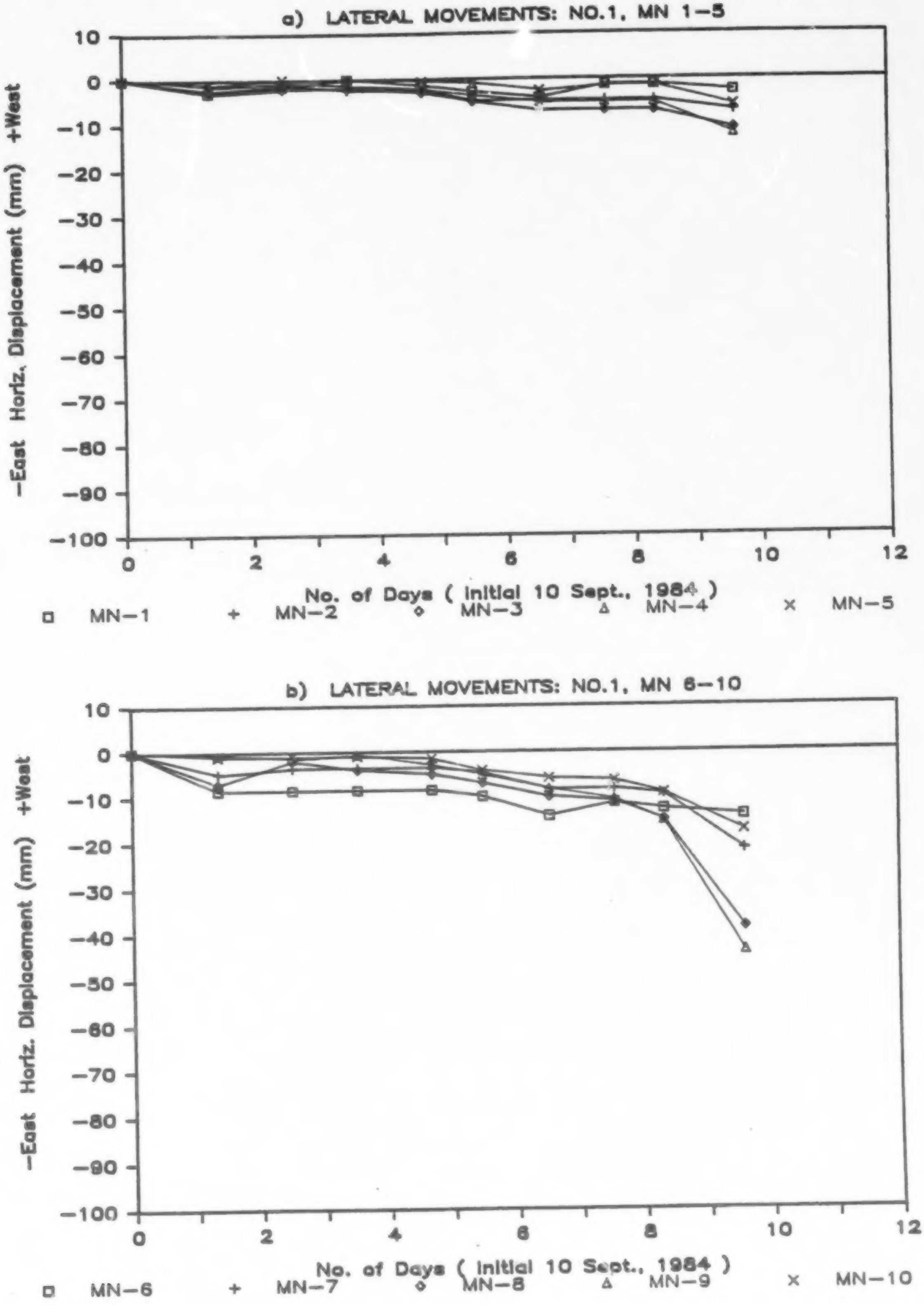

FIGURE 8.11 HORIZONTAL DISPLACEMENT OF MONUMENTS NO.1, MN-1 TO 10

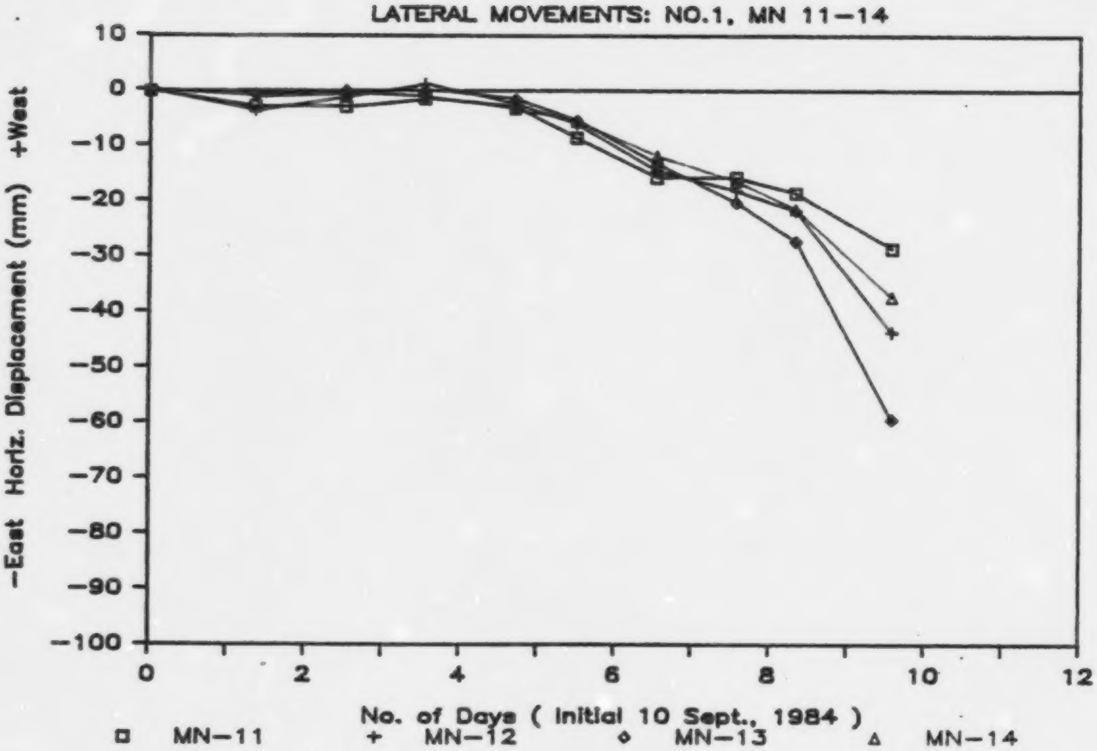

FIGURE 8.12 HORIZONTAL DISPLACEMENT OF MONUMENTS NO.1, MN-11 TO 14

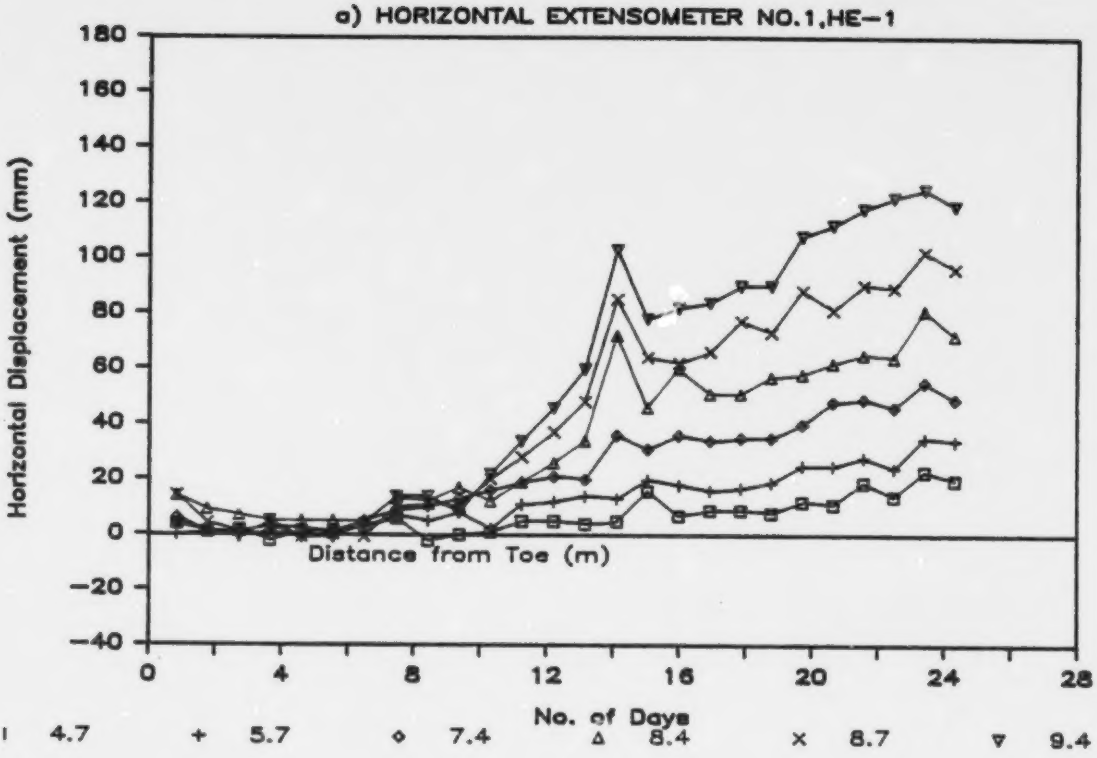

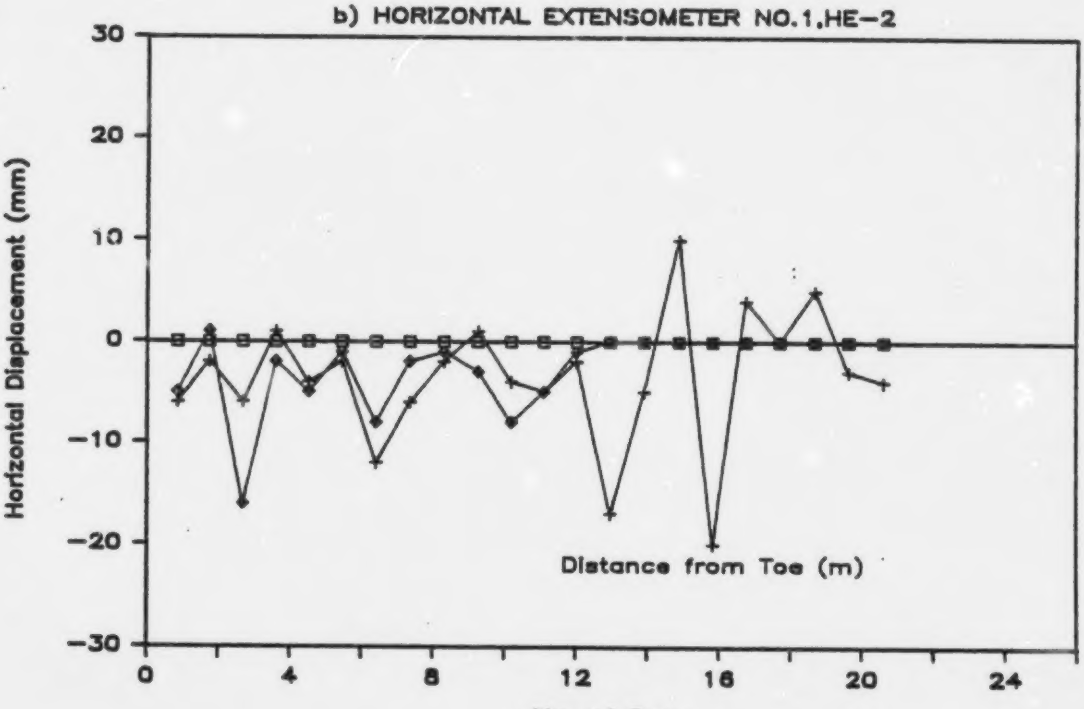

FIGURE 8.13 HORIZONTAL EXTENSOMETERS NO.1, HE-1 AND 2

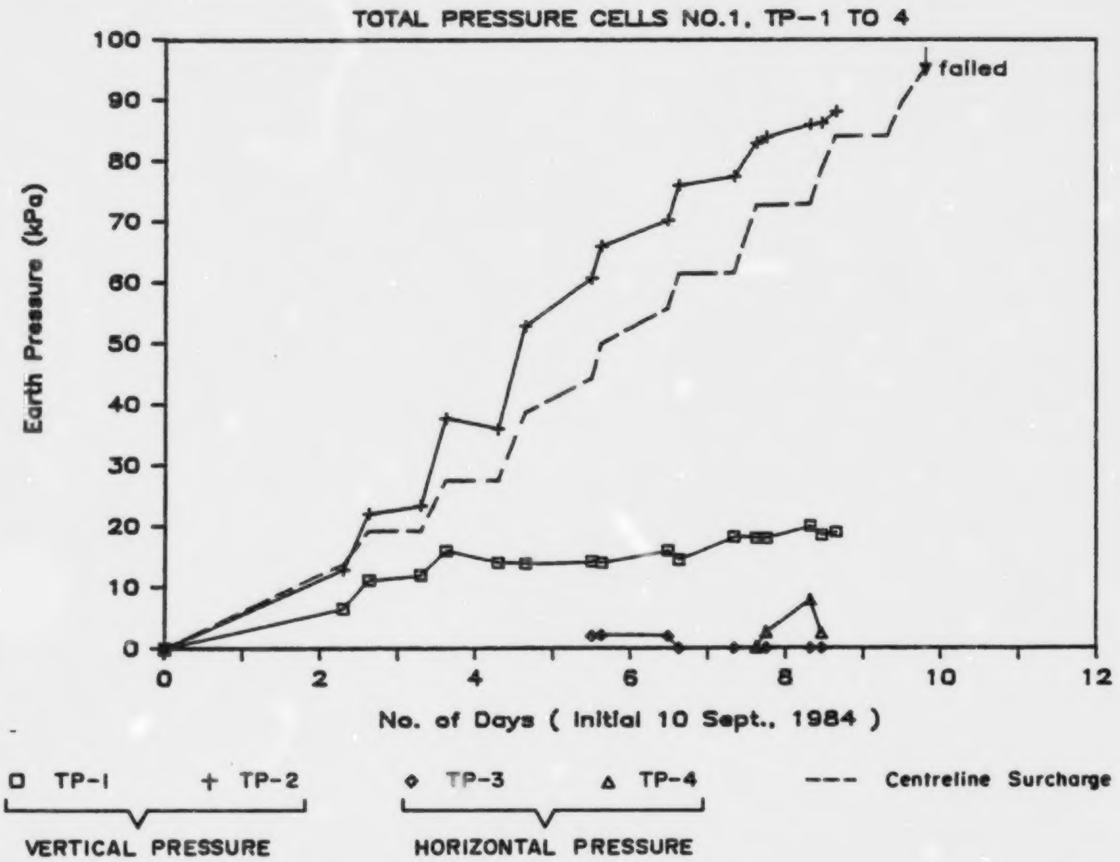

FIGURE 8.14 TOTAL PRESSURE CELLS NO.1, TP-1 TO 4

a) PNEUMATIC PIEZOMETERS NO.2,PN-1 TO 4

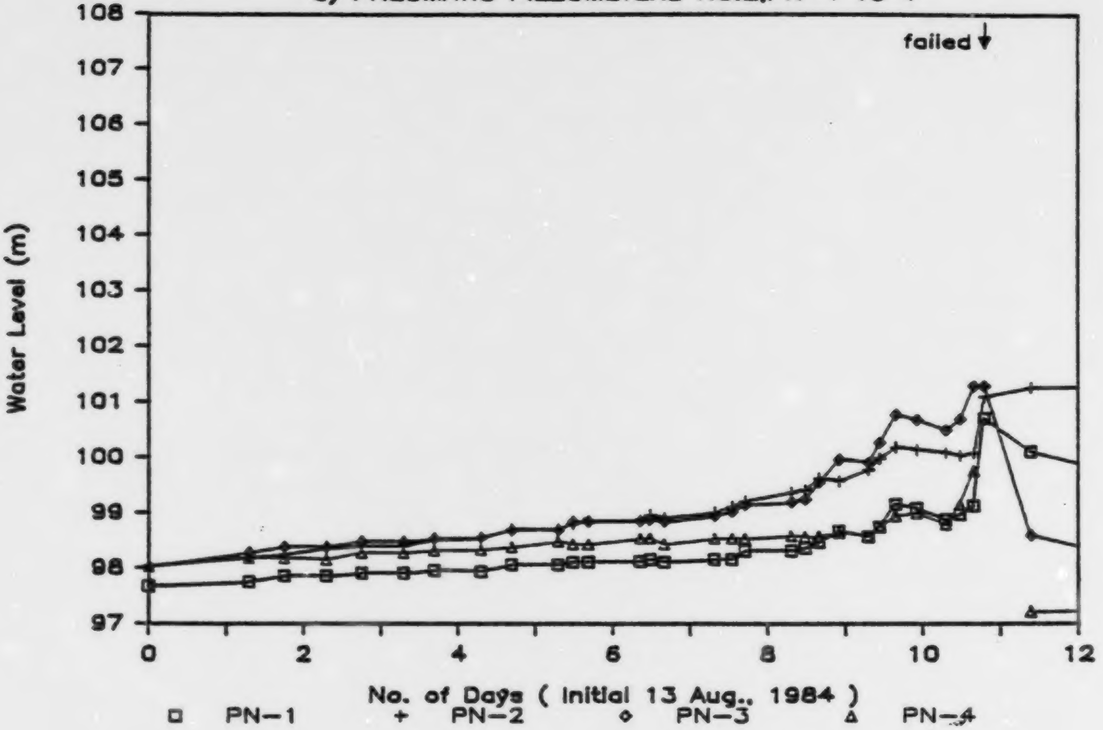

b) PNEUMATIC PIEZOMETERS NO.2,PN-5 TO 8

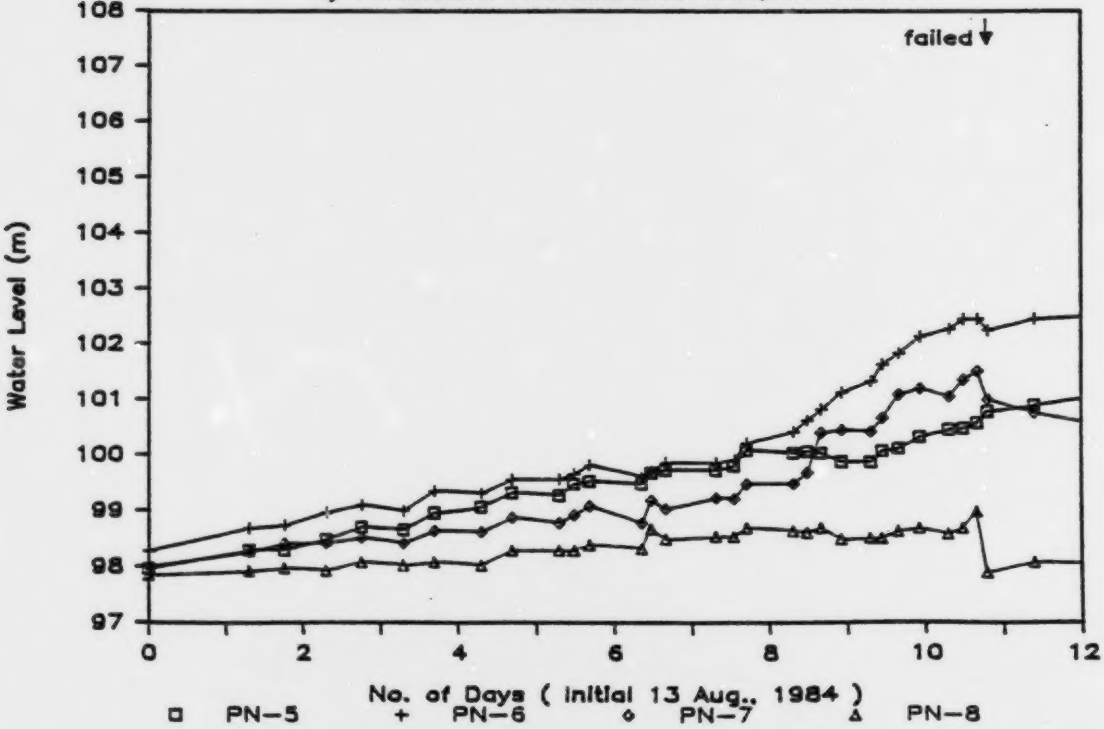

FIGURE 8.15 PNEUMATIC PIEZOMETERS NO.2, PN-1 TO 8

a) PNEUMATIC PIEZOMETERS NO.2,PN 9–12

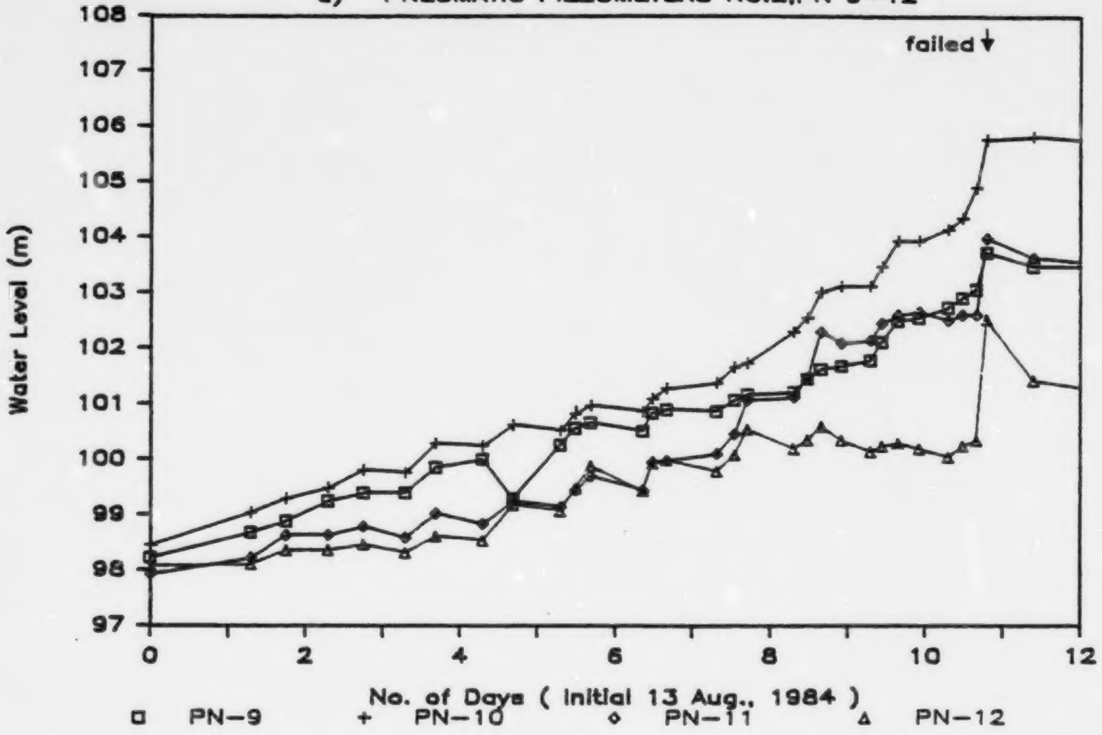

b) PNEUMATIC PIEZOMETERS NO.2,PN 13–16

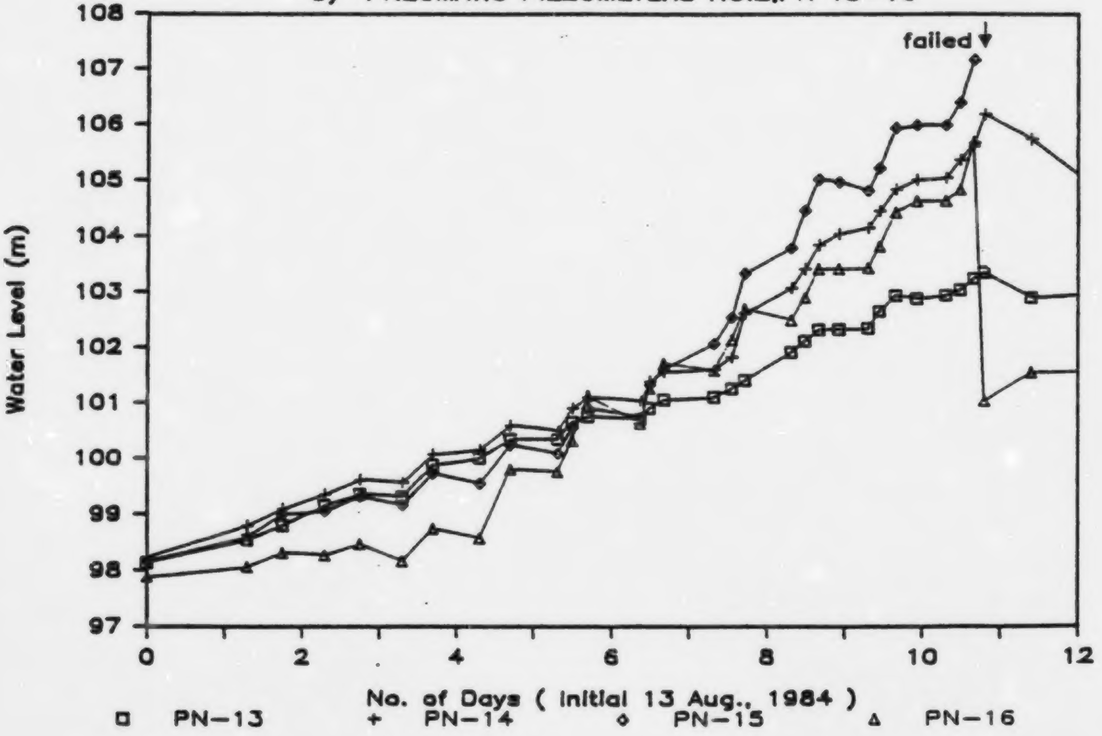

FIGURE 8.16 PNEUMATIC PIEZOMETERS NO.2. PN–9 TO 16

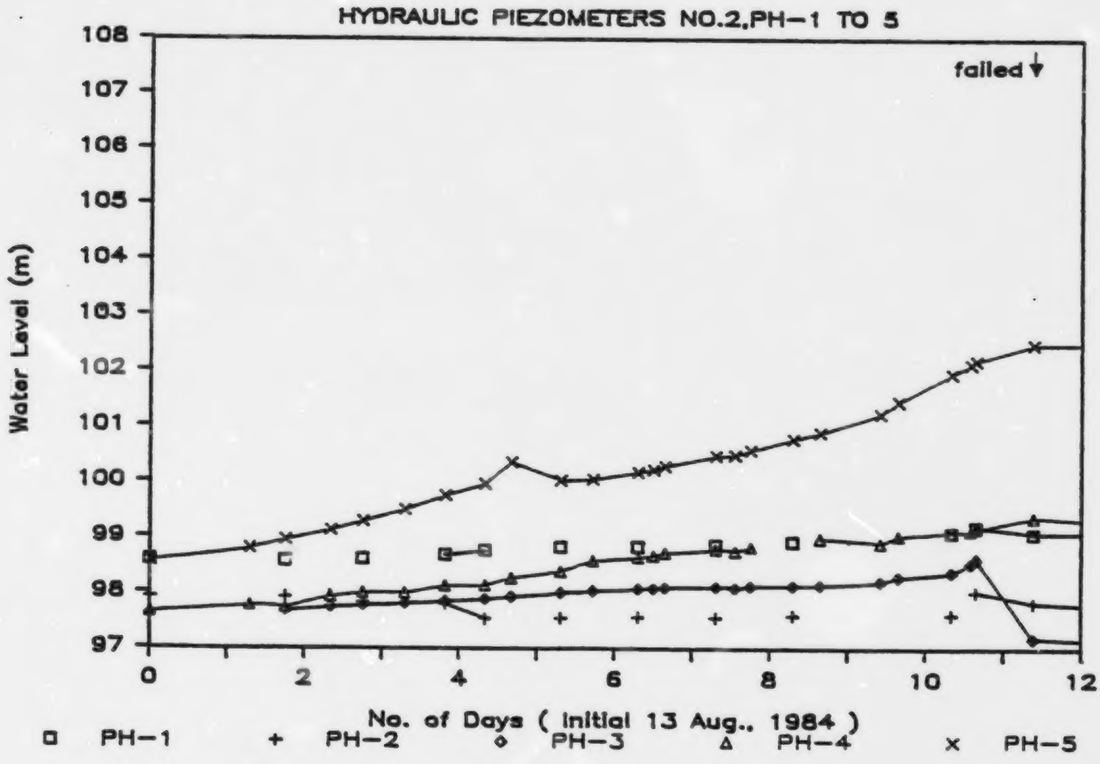

FIGURE 8.17 HYDRAULIC PIEZOMETERS NO.2, PH-1 TO 5

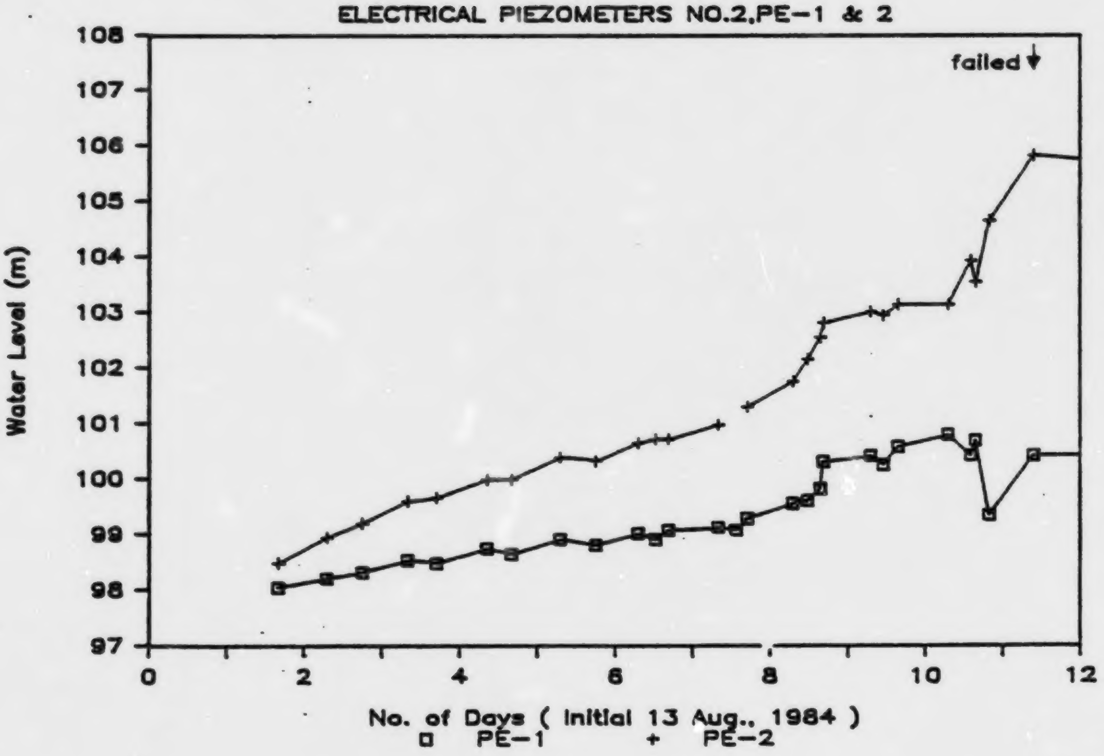

FIGURE 8.18 ELECTRICAL PIEZOMETERS NO.2, PE-1 AND 2

a) SETTLEMENT PLATES NO.2,SP–1 TO 6

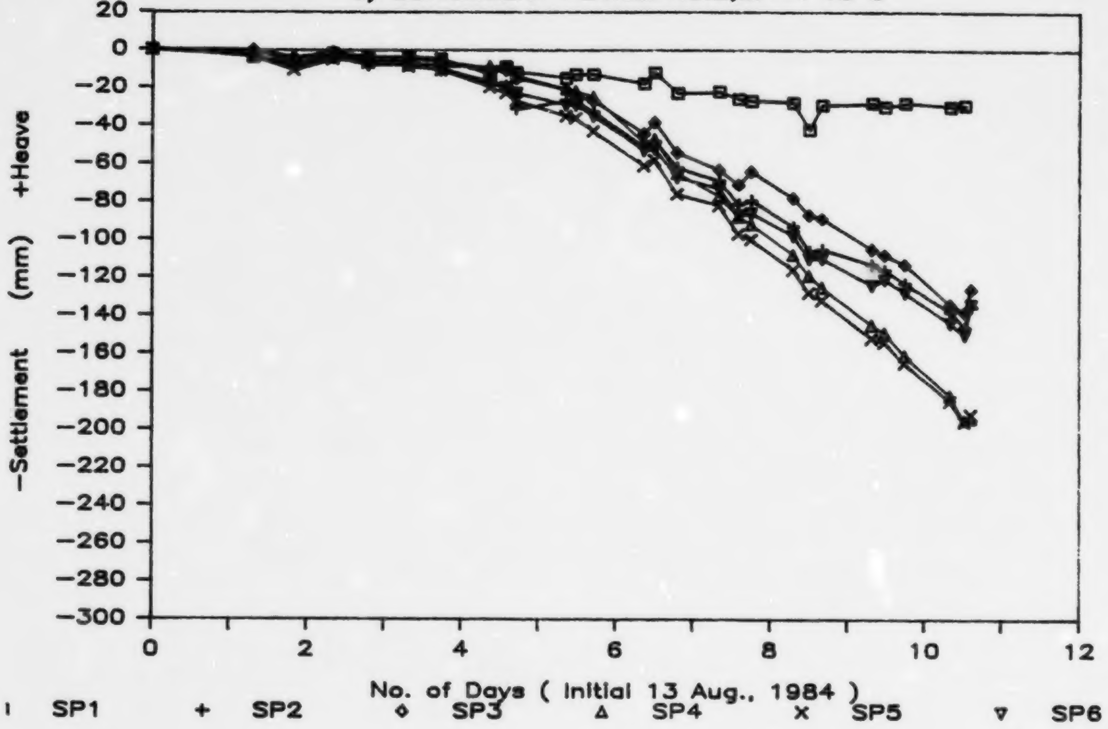

b) SETTLEMENT PLATES NO.2,SP–7 TO 11

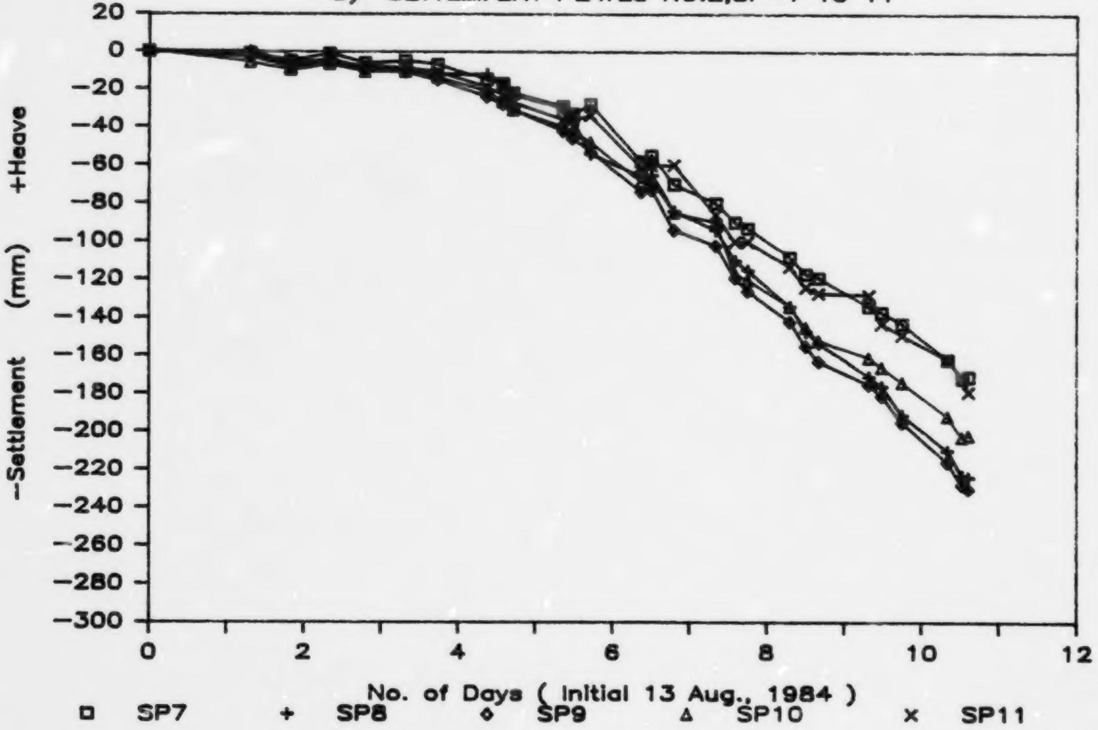

FIGURE 8.19 SETTLEMENT PLATES NO.2. SP–1 TO 11

a) SETTLEMENT OF MONUMENTS NO.2,MN 6–10

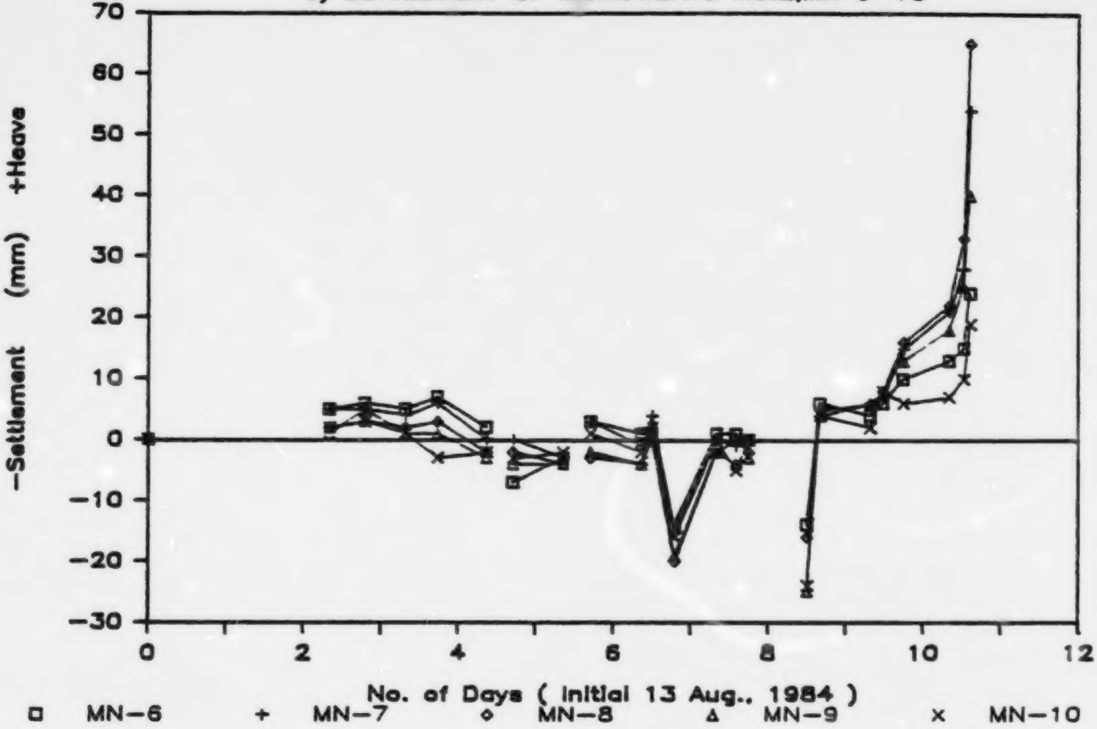

b)SETTLEMENT OF MONUMENTS NO.2,MN 11–14

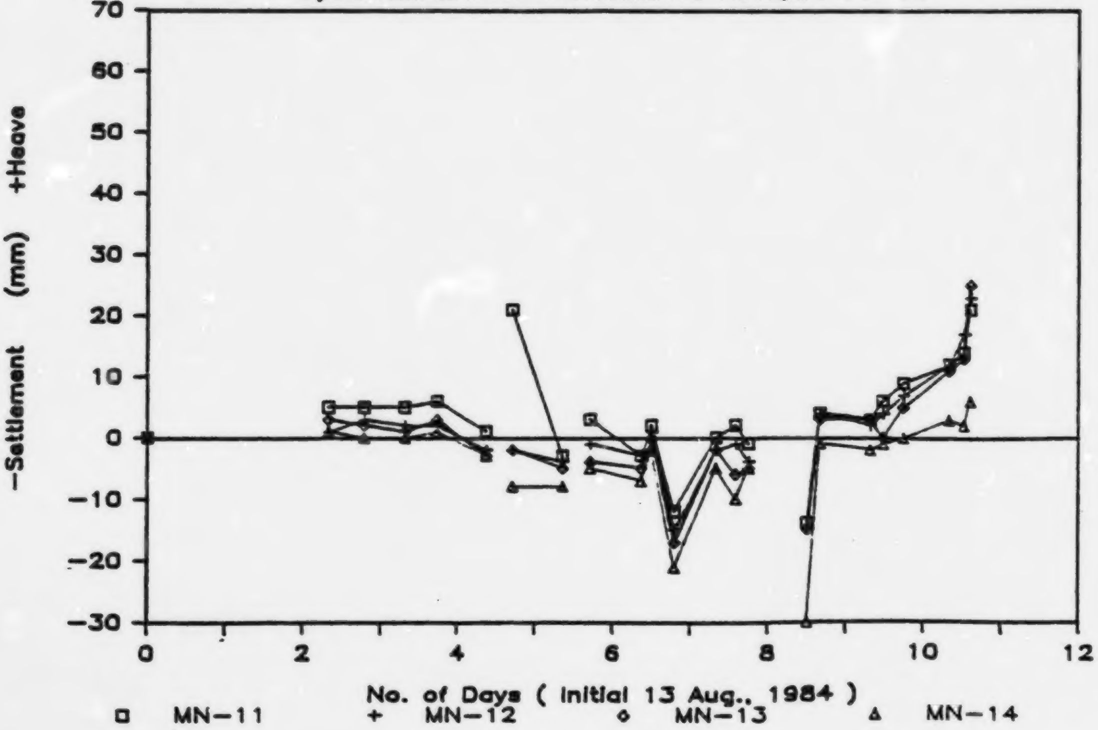

FIGURE 8.20 SETTLEMENT OF MONUMENTS NO.2, MN-6 TO 14

a) VERT. ELECTR. EXTENSOMETER NO.2,VE-1

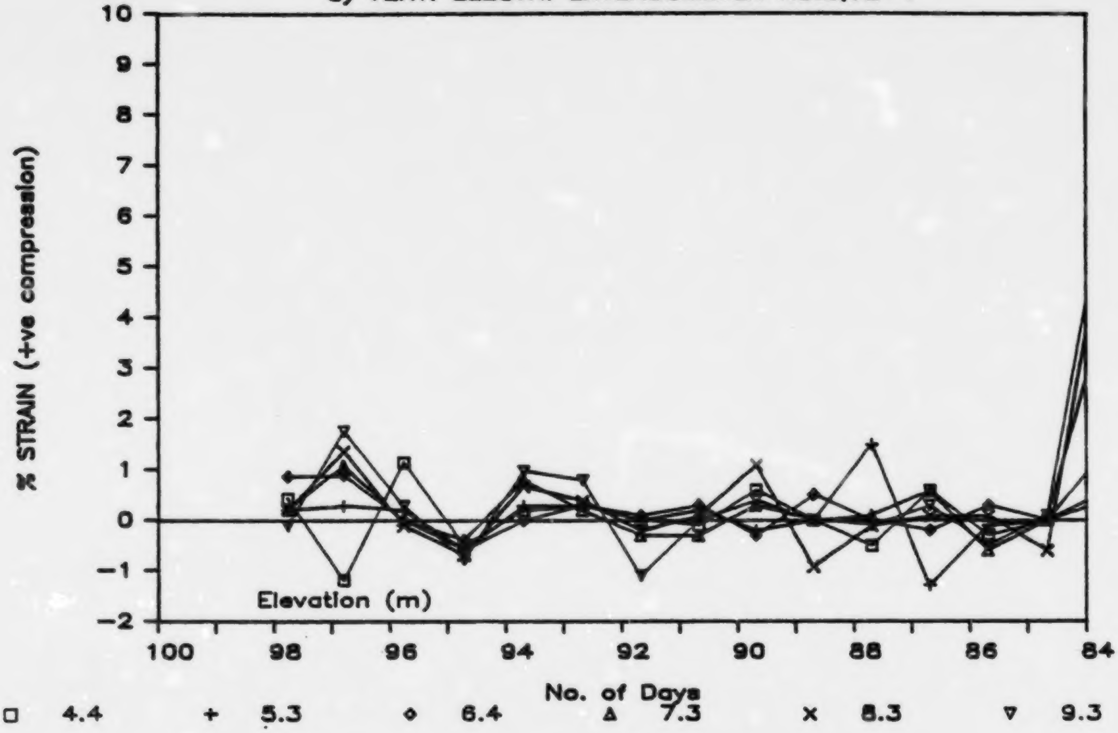

b) VERT. ELECTR. EXTENSOMETER NO.2,VE-2

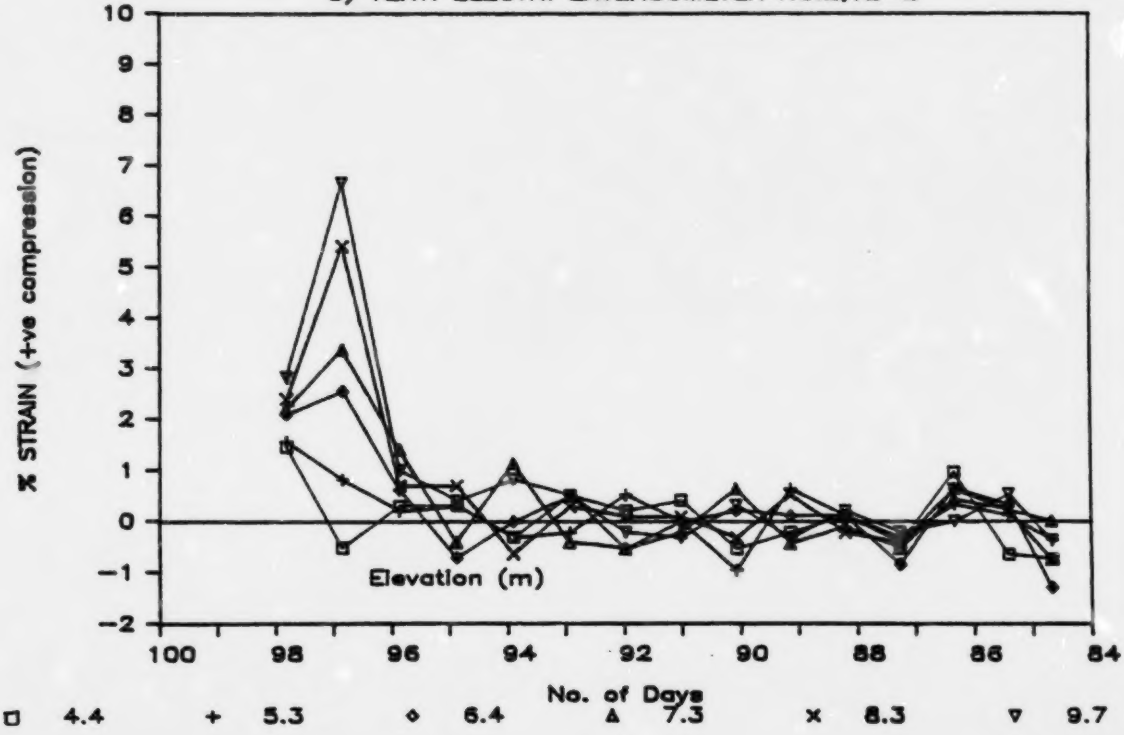

FIGURE 8.21 VERTICAL ELECTRICAL EXTENSOMETERS NO.2, VE-1 AND 2

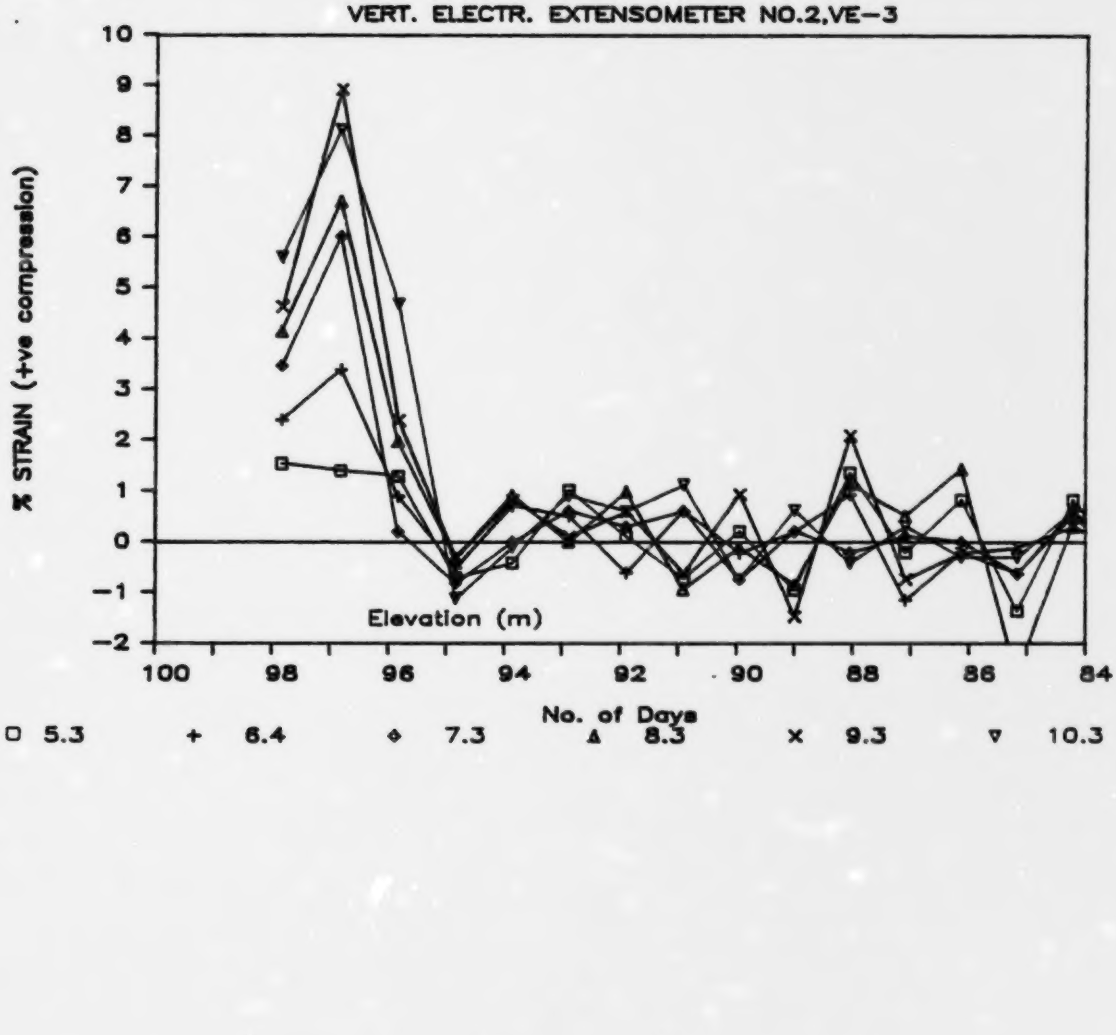

FIGURE 8.22 VERTICAL ELECTRICAL EXTENSOMETER NO.2, VE-3

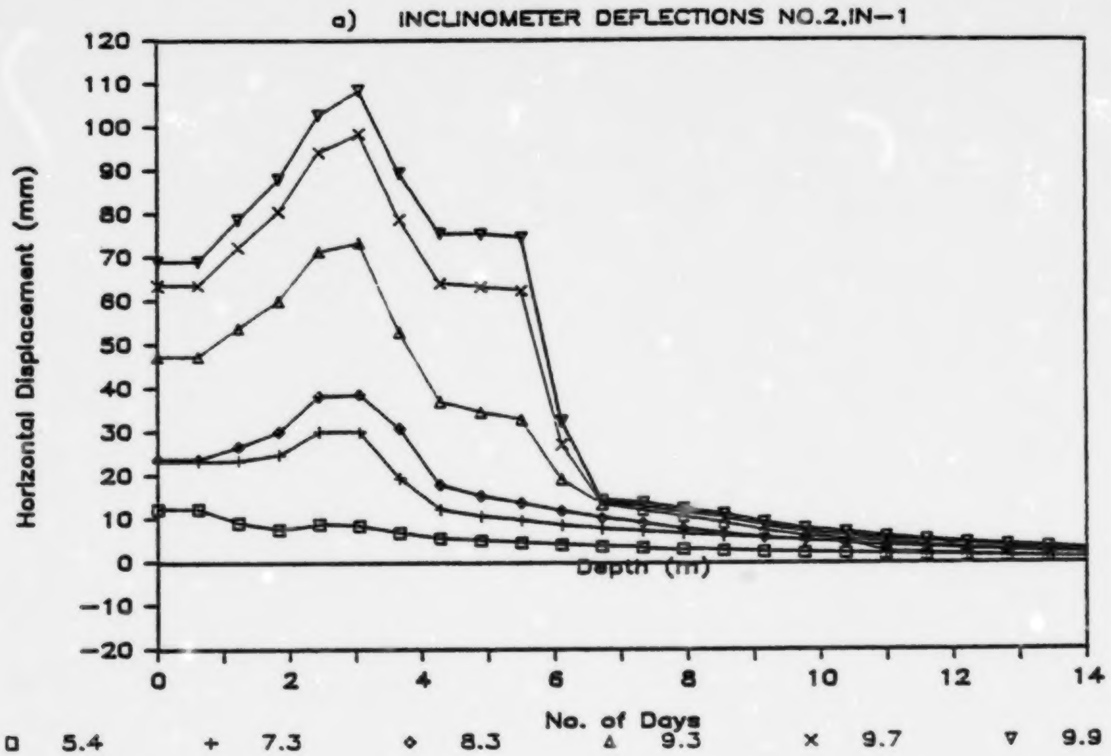

a) INCLINOMETER DEFLECTIONS NO.2,IN-1

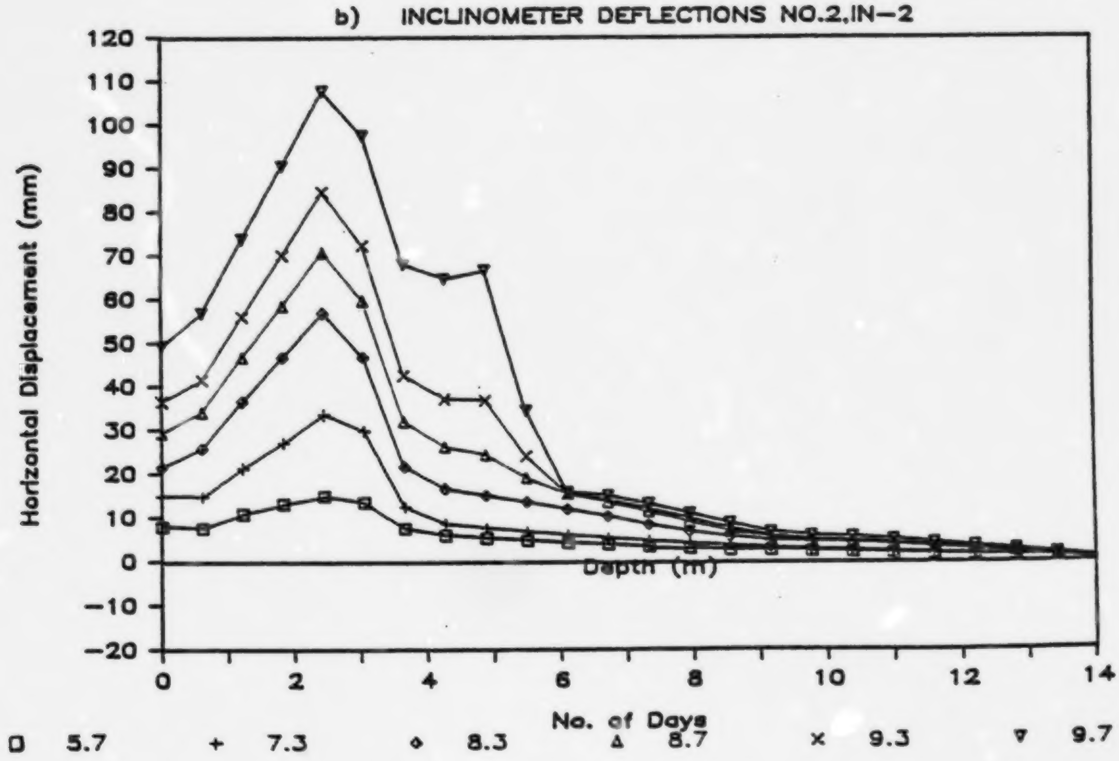

b) INCLINOMETER DEFLECTIONS NO.2,IN-2

FIGURE 8.23 INCLINOMETER DEFLECTIONS NO.2, IN-1 AND 2

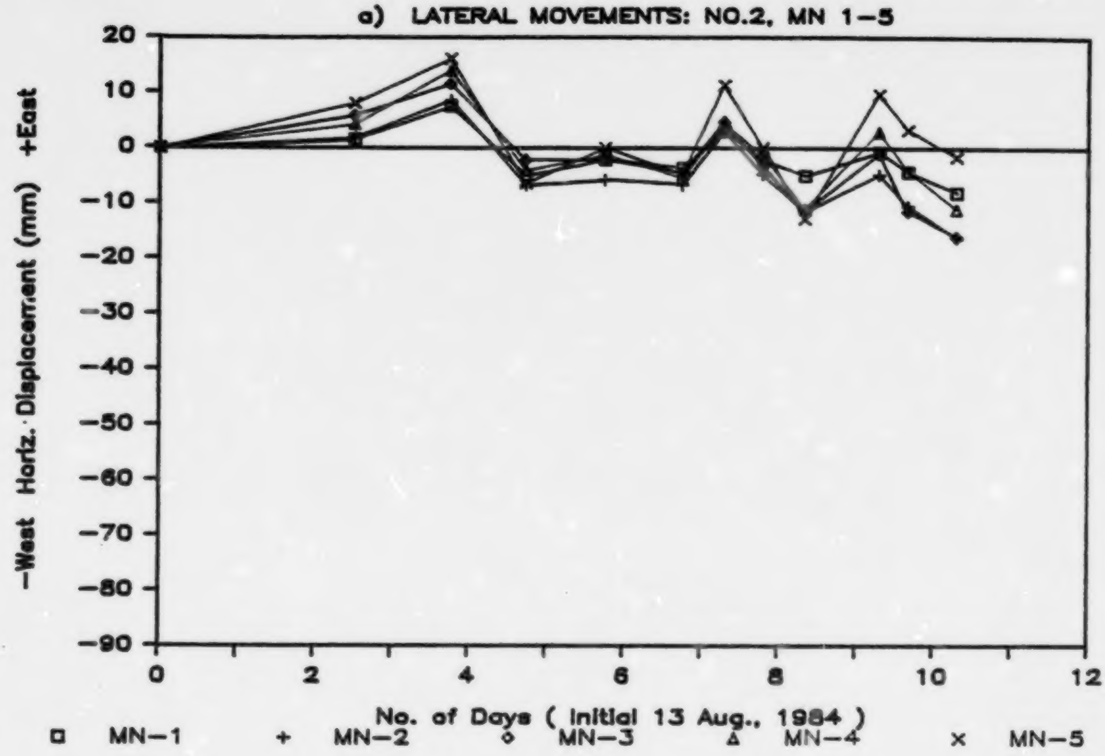

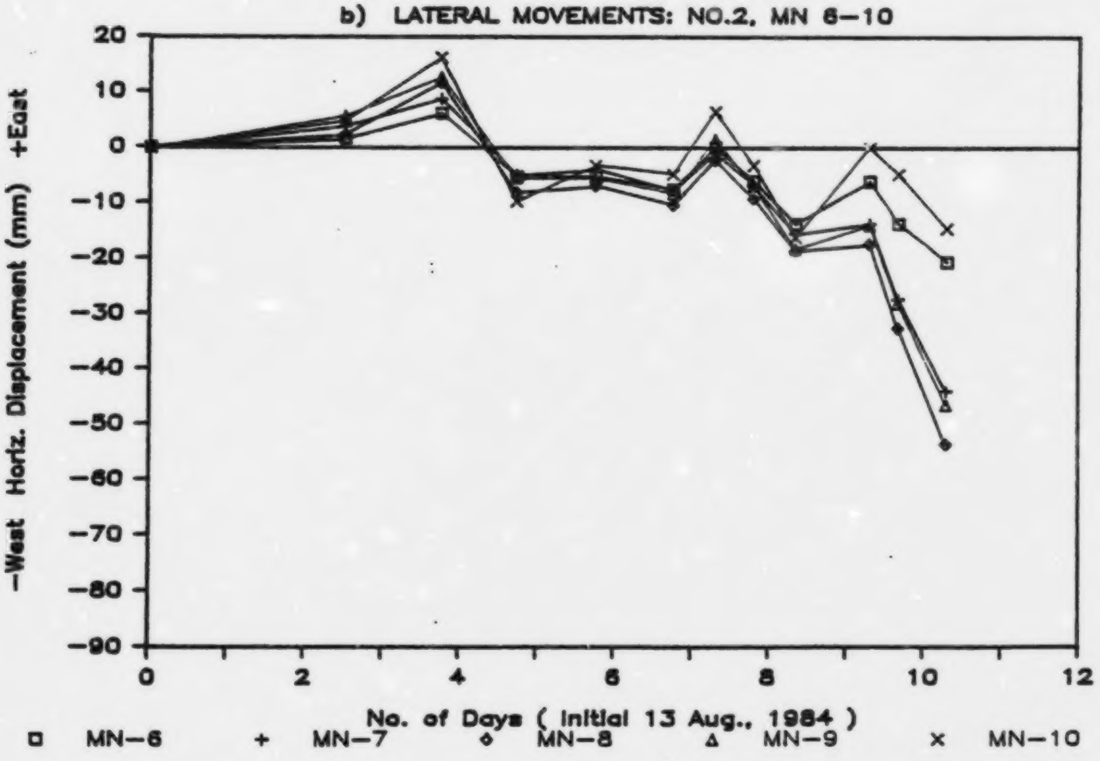

FIGURE 8.24 HORIZONTAL DISPLACEMENT OF MONUMENTS NO.2, MN-1 TO 10

8

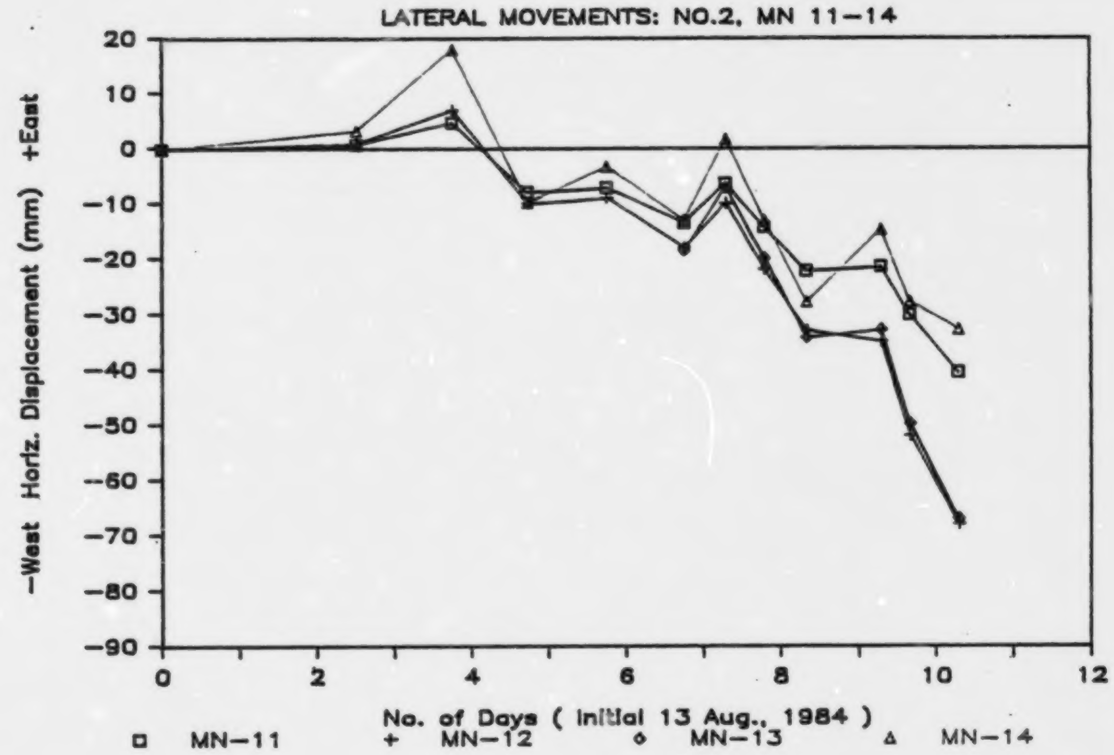

FIGURE 8.25 HORIZONTAL DISPLACEMENT OF MONUMENTS NO.2, MN-11 TO 14

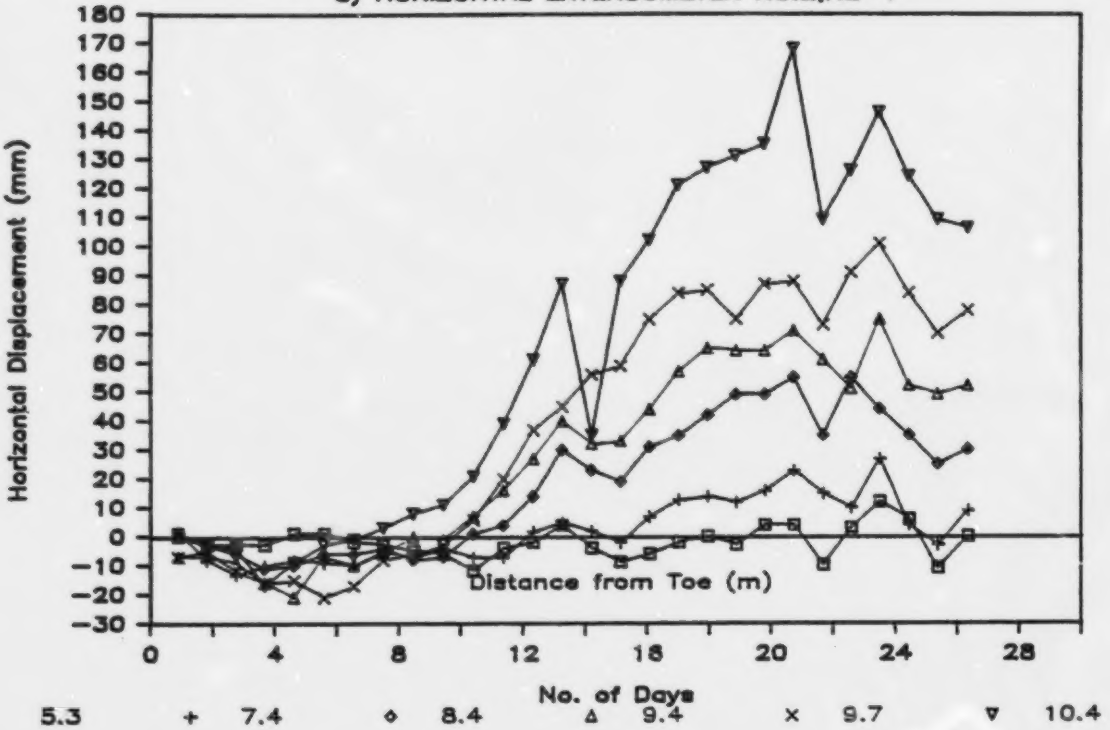
a) HORIZONTAL EXTENSOMETER NO.2,HE-1

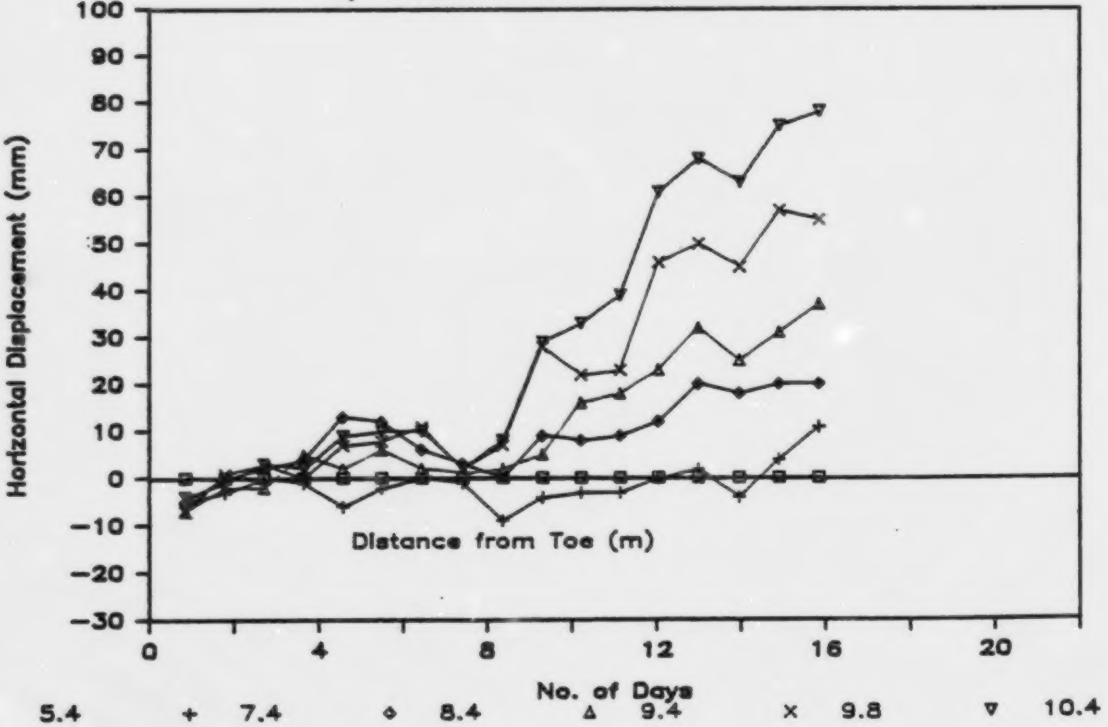
b) HORIZONTAL EXTENSOMETER NO.2,HE-2

FIGURE 8.26 HORIZONTAL EXTENSOMETERS NO.2, HE-1 AND 2

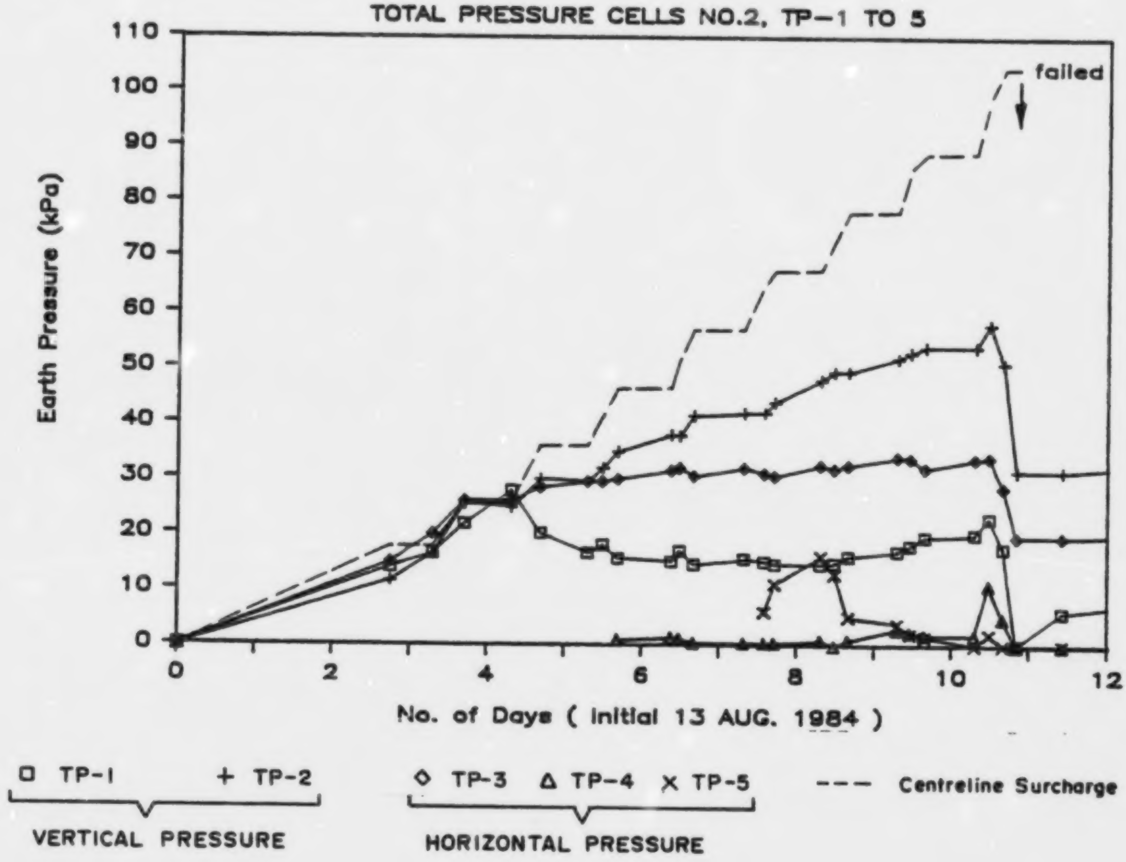

FIGURE 8.27 TOTAL PRESSURE CELLS NO.2, TP-1 TO 5

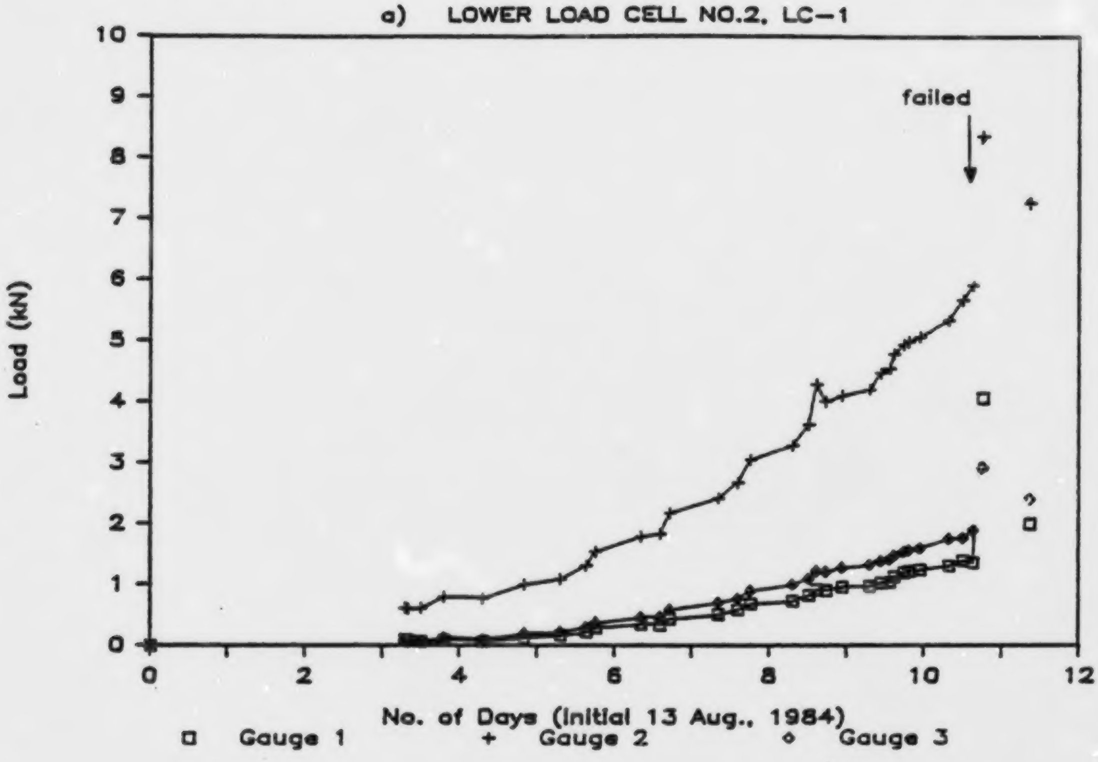

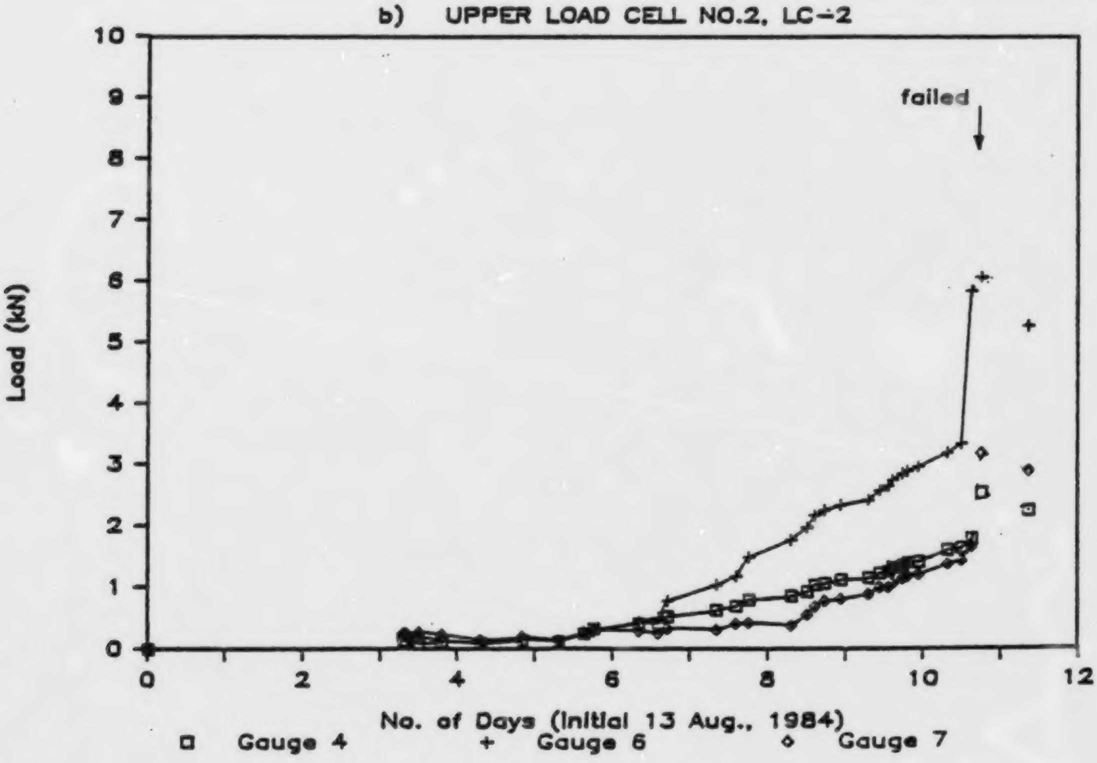

FIGURE 8.28 TENSAR LOAD CELLS NO.2, LC-1 AND 2

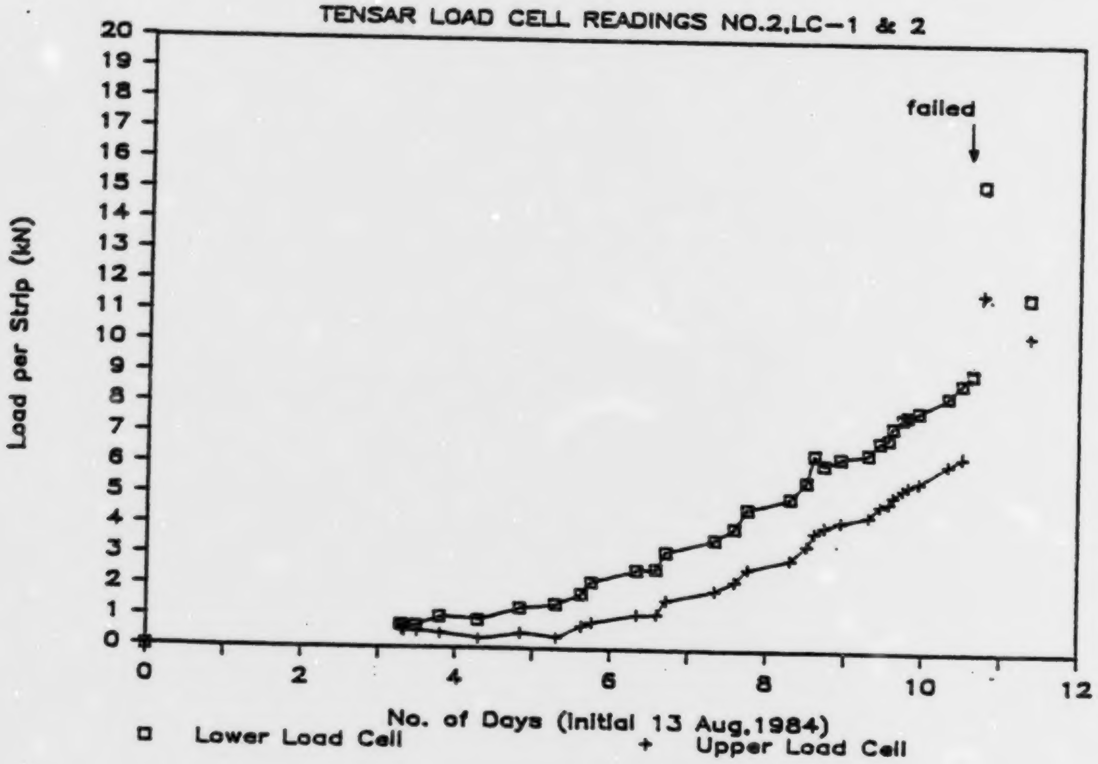

FIGURE 8.29 TENSILE LOAD MEASURED IN STRIP REINFORCEMENTS

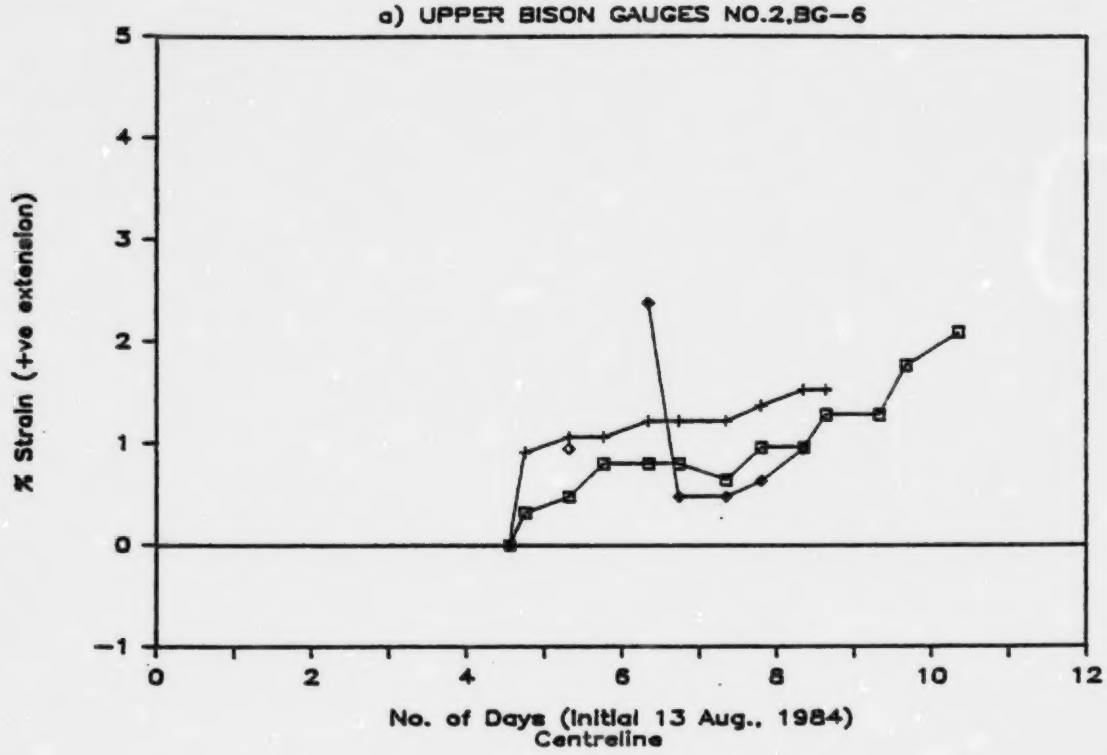

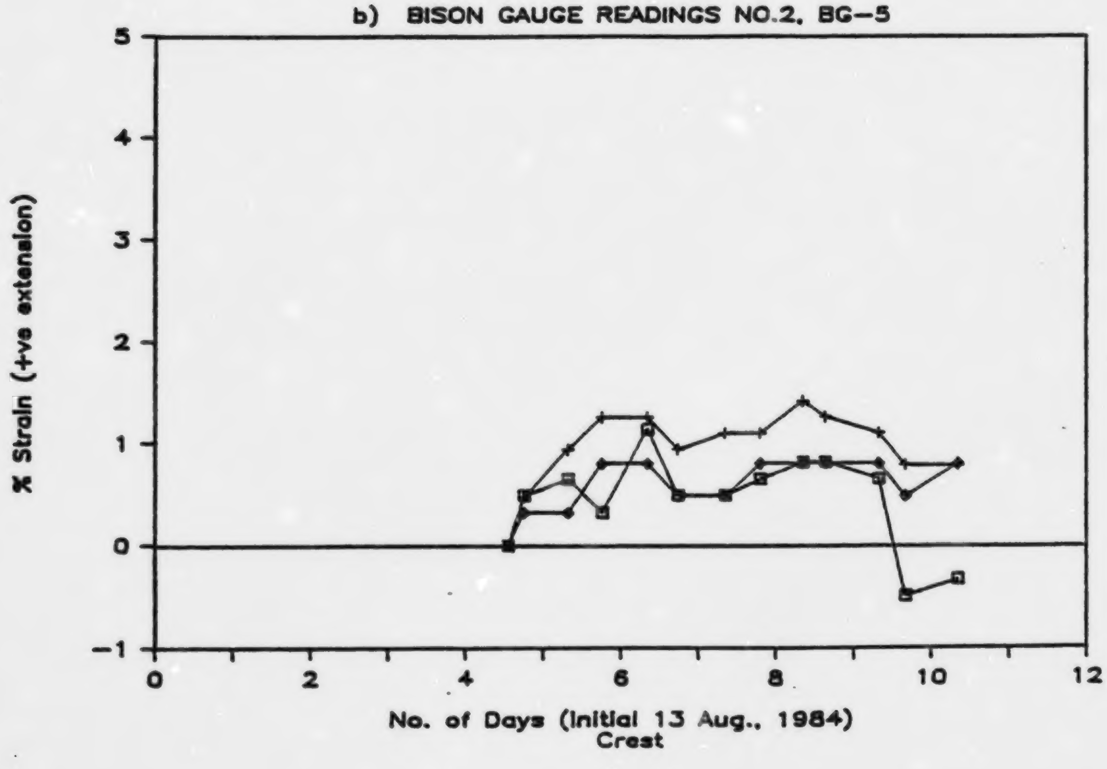

FIGURE 8.30 STRAIN MEASUREMENTS ON UPPER LAYER OF STRIP REINFORCEMENT

a) PNEUMATIC PIEZOMETERS NO.3,PN 1-4

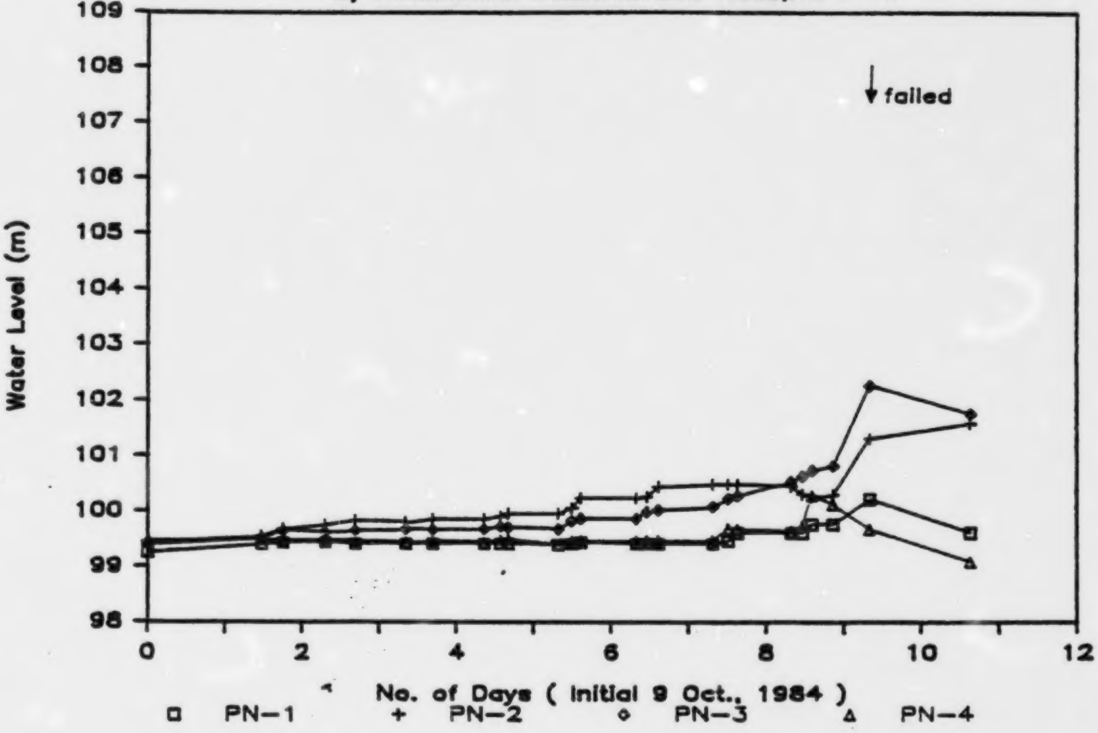

b) PNEUMATIC PIEZOMETERS NO.3,PN 5-8

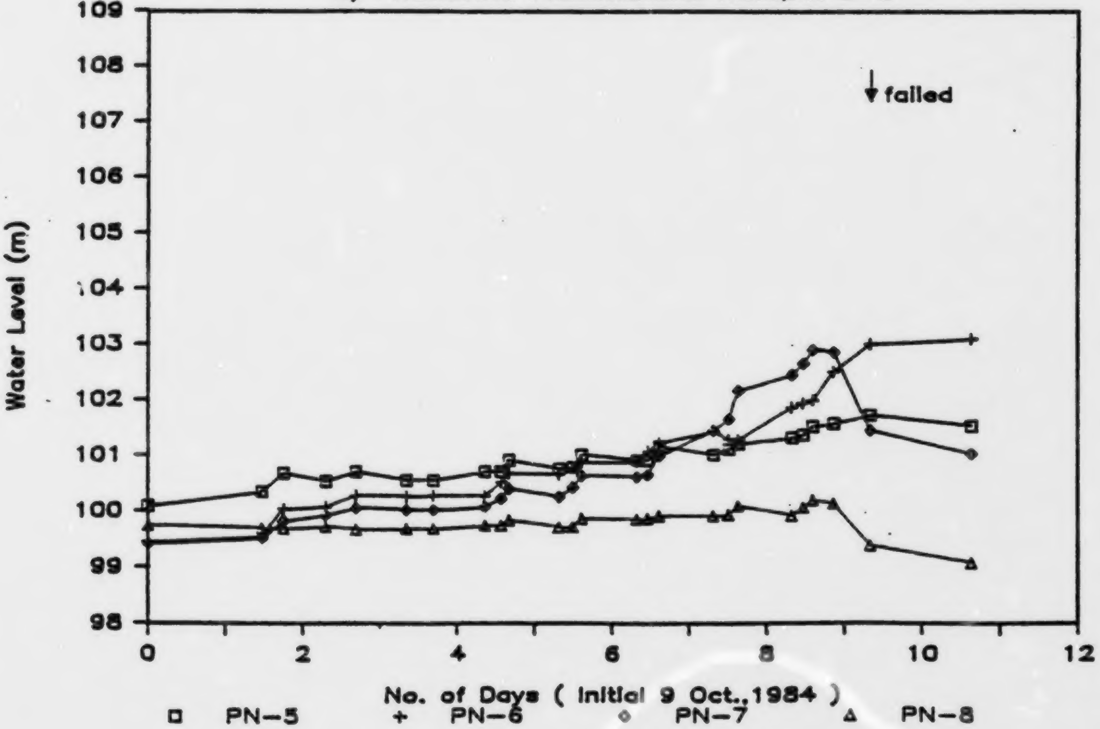

FIGURE 8.31 PNEUMATIC PIEZOMETERS NO.3, PN-1 TO 8

a) PNEUMATIC PIEZOMETERS NO.3,PN 9–12

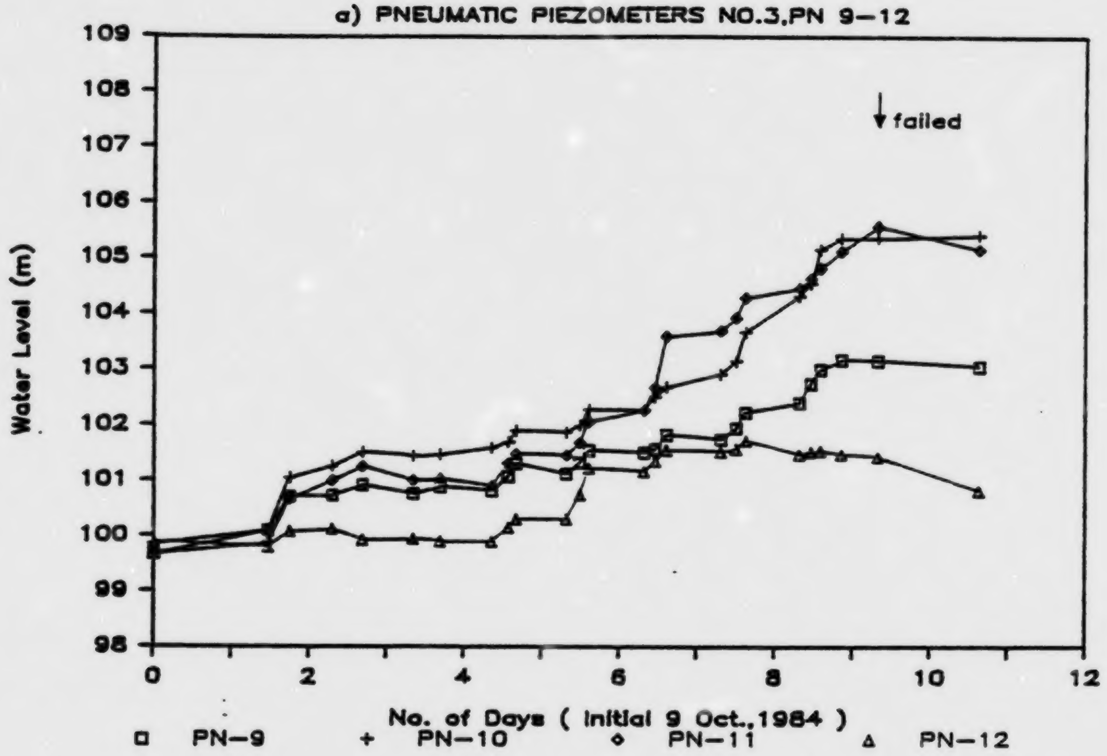

b) PNEUMATIC PIEZOMETERS NO.3,PN 13–16

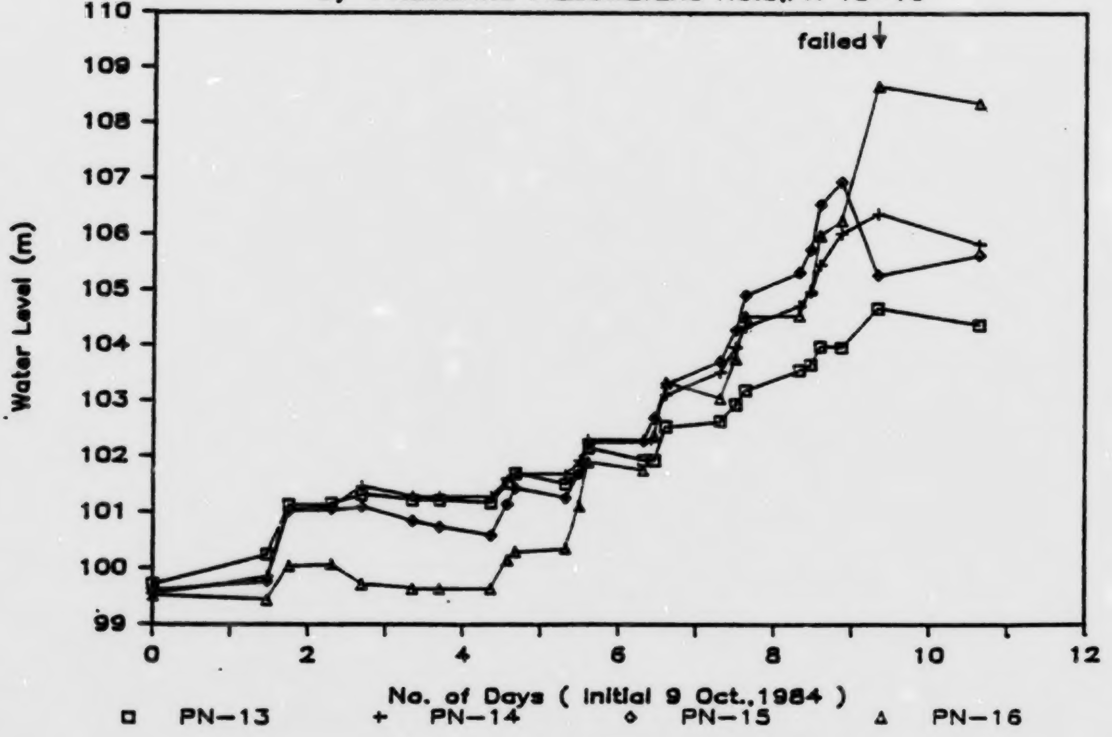

FIGURE 8.32 PNEUMATIC PIEZOMETERS NO.3. PN-9 TO 16

a) HYDRAULIC PIEZOMETERS NO.3,PH 1–5

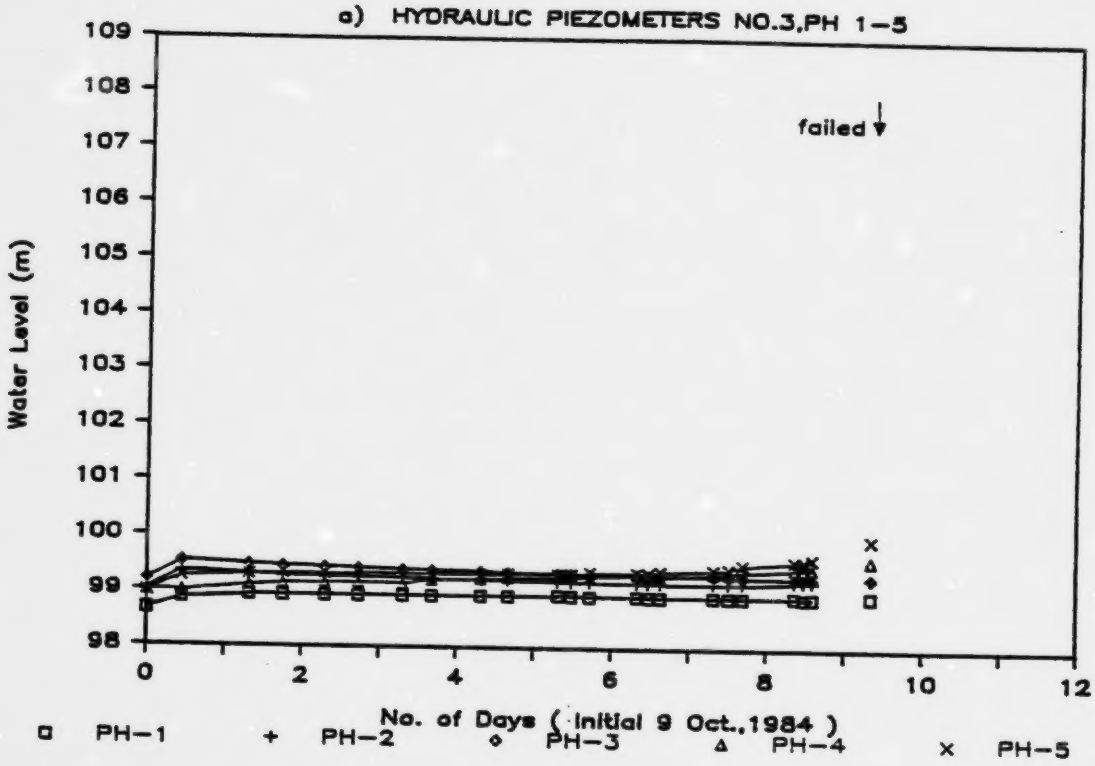

b) HYDRAULIC PIEZOMETERS NO.3,PH 6–10

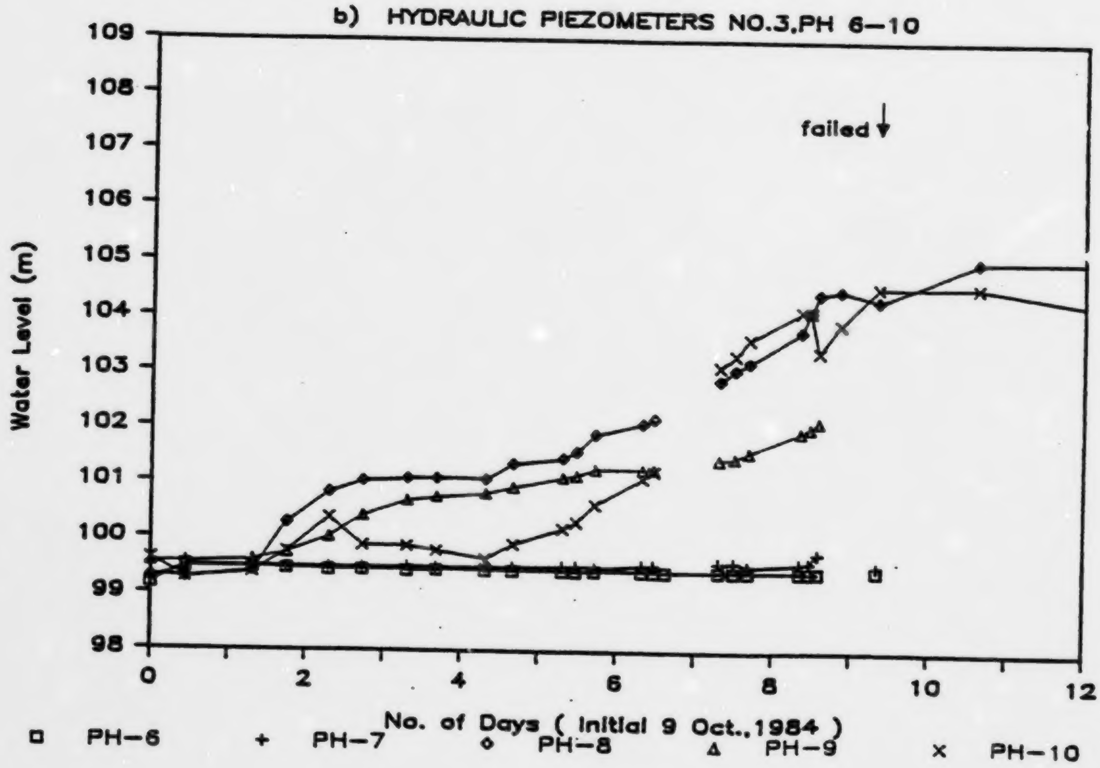

FIGURE 8.33 HYDRAULIC PIEZOMETERS NO.3. PH–1 TO 10

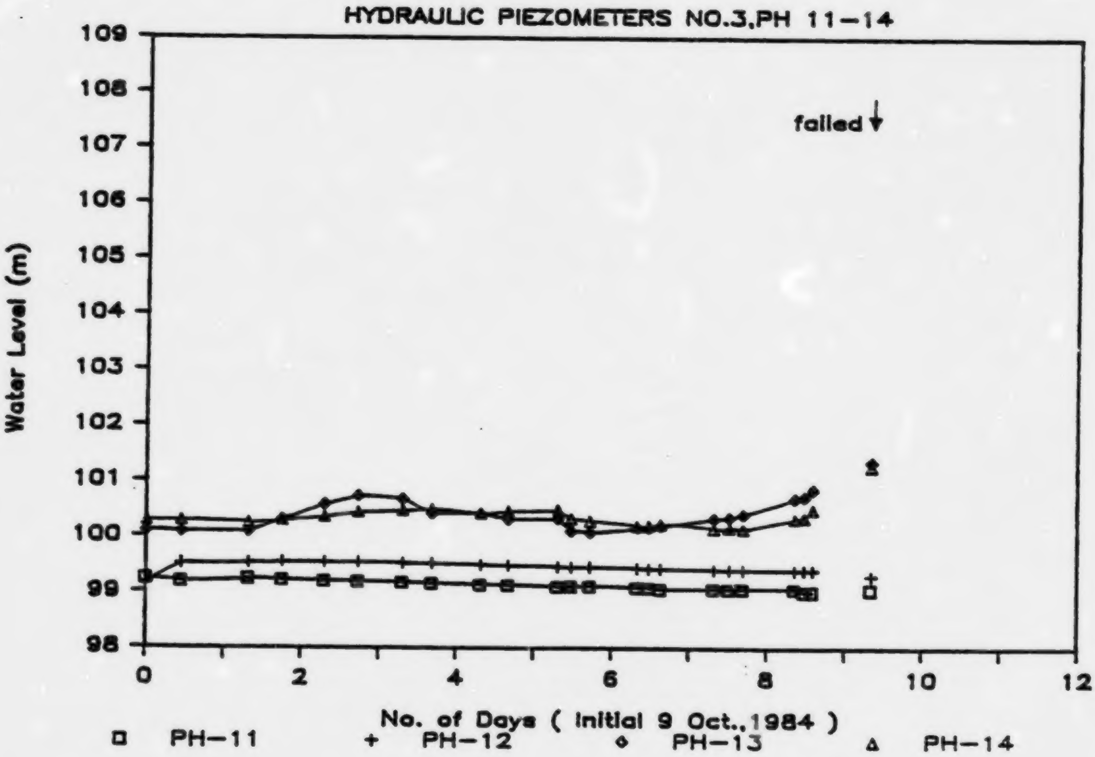

FIGURE 8.34 HYDRAULIC PIEZOMETERS NO.3. PH-11 TO 14

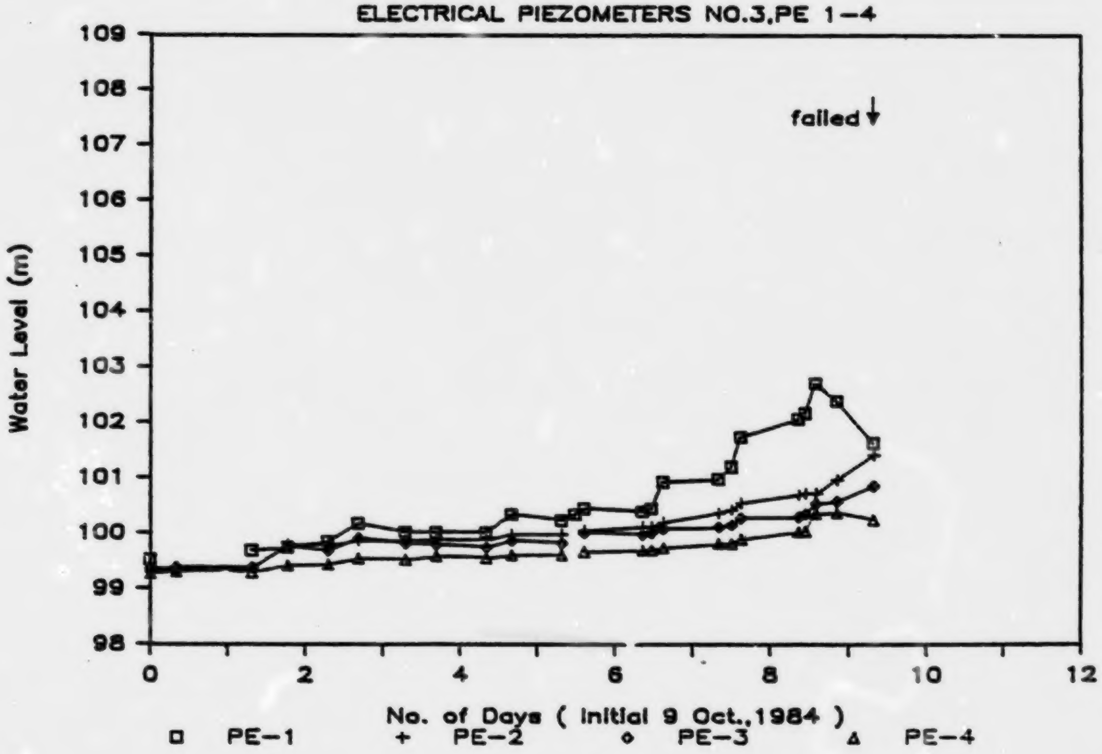

FIGURE 8.35 ELECTRICAL PIEZOMETERS NO.3. PE-1 TO 4

a) SETTLEMENT PLATES NO.3,SP-1 TO 6

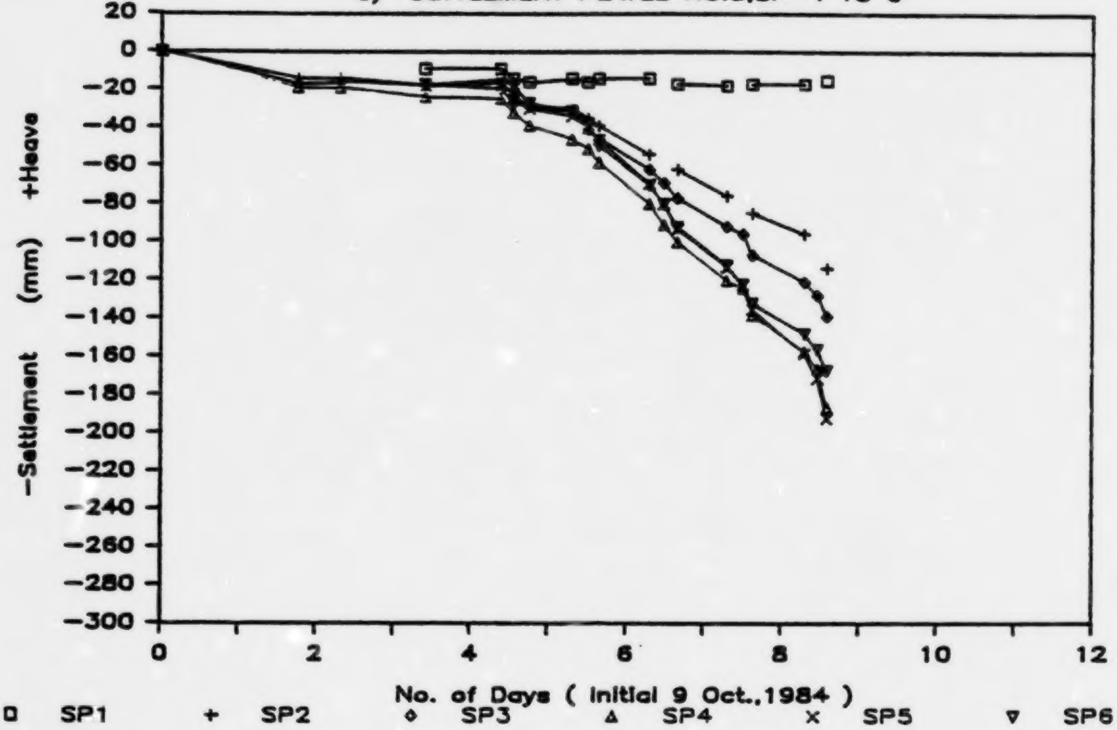

b) SETTLEMENT PLATES NO.3,SP-7 TO 11

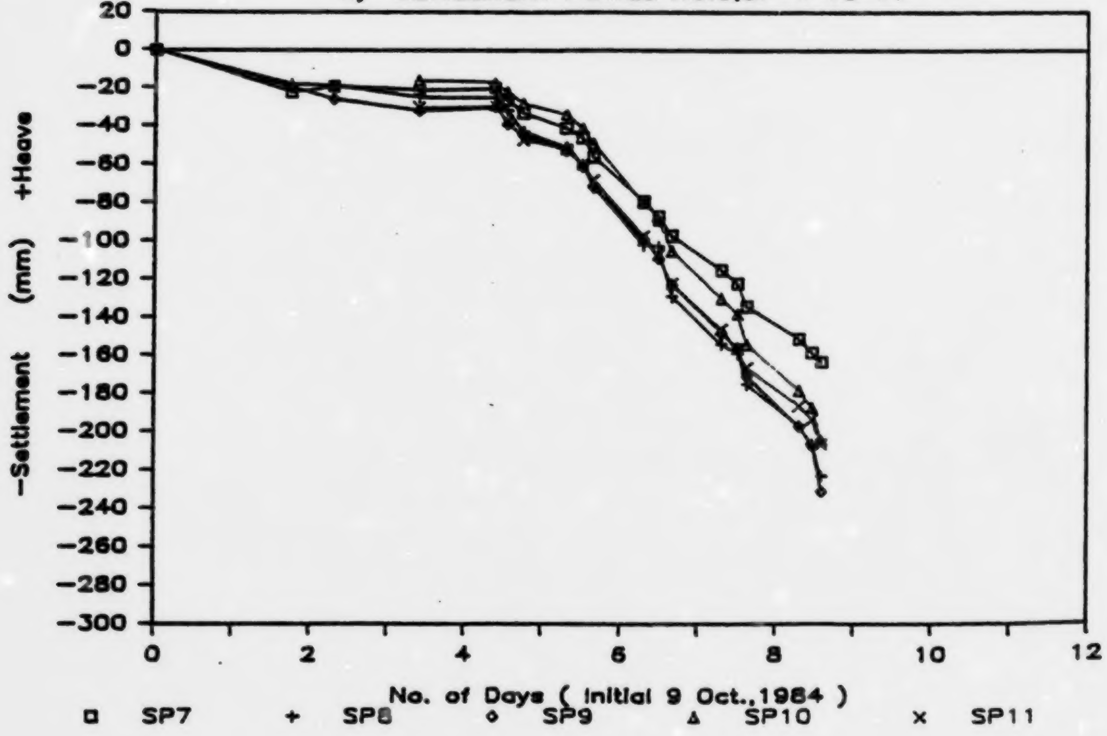

FIGURE 8.36 SETTLEMENT PLATES NO.3, SP-1 TO 11

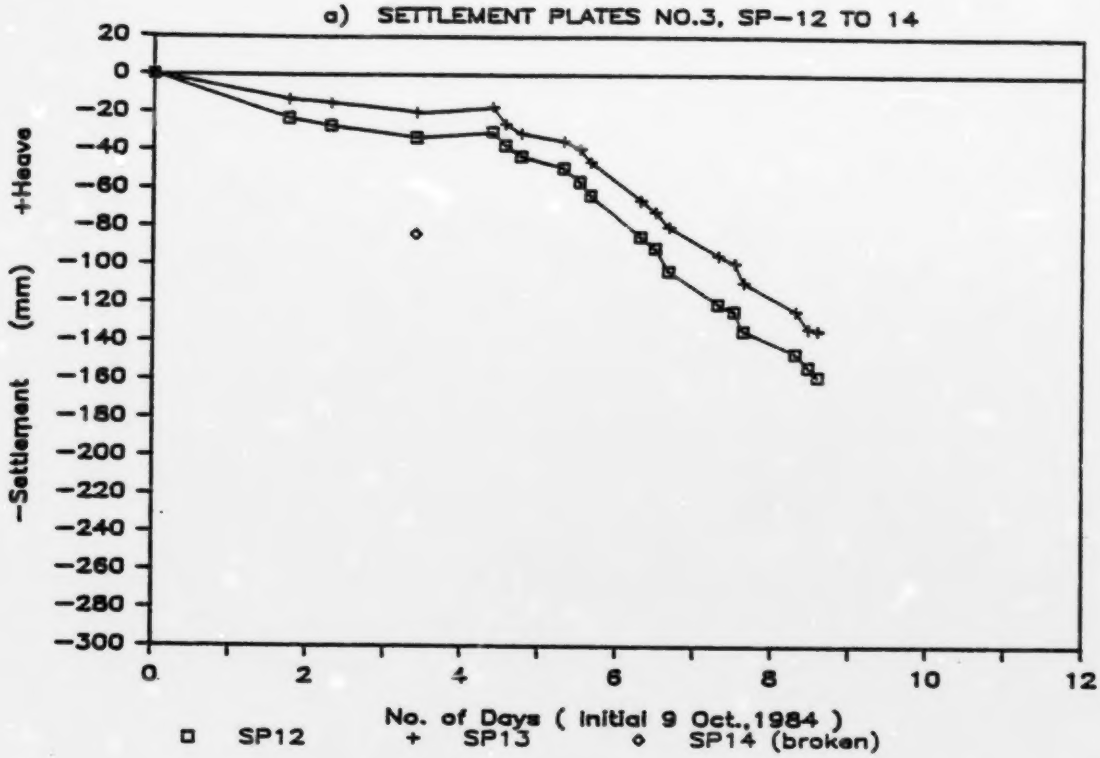

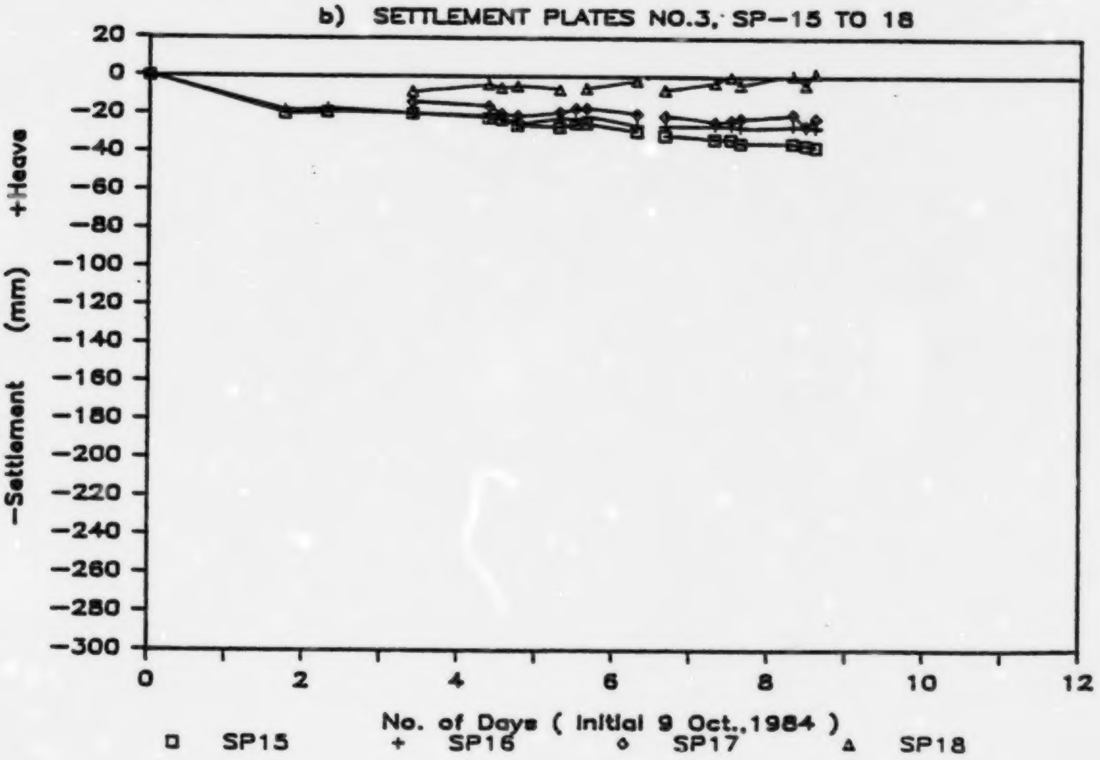

FIGURE 8.37 SETTLEMENT PLATES NO.3, SP-12 TO 18

a) SETTLEMENT OF MONUMENTS NO.3,MN 1-5

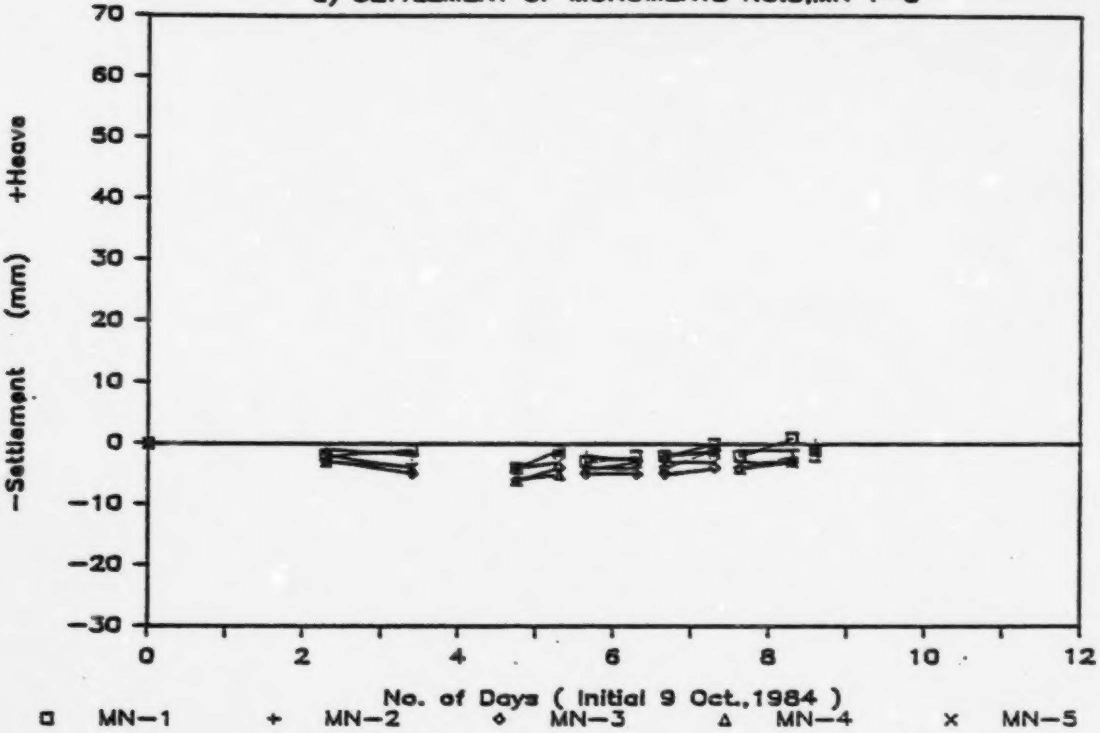

b) SETTLEMENT OF MONUMENTS NO.3,MN 6-10

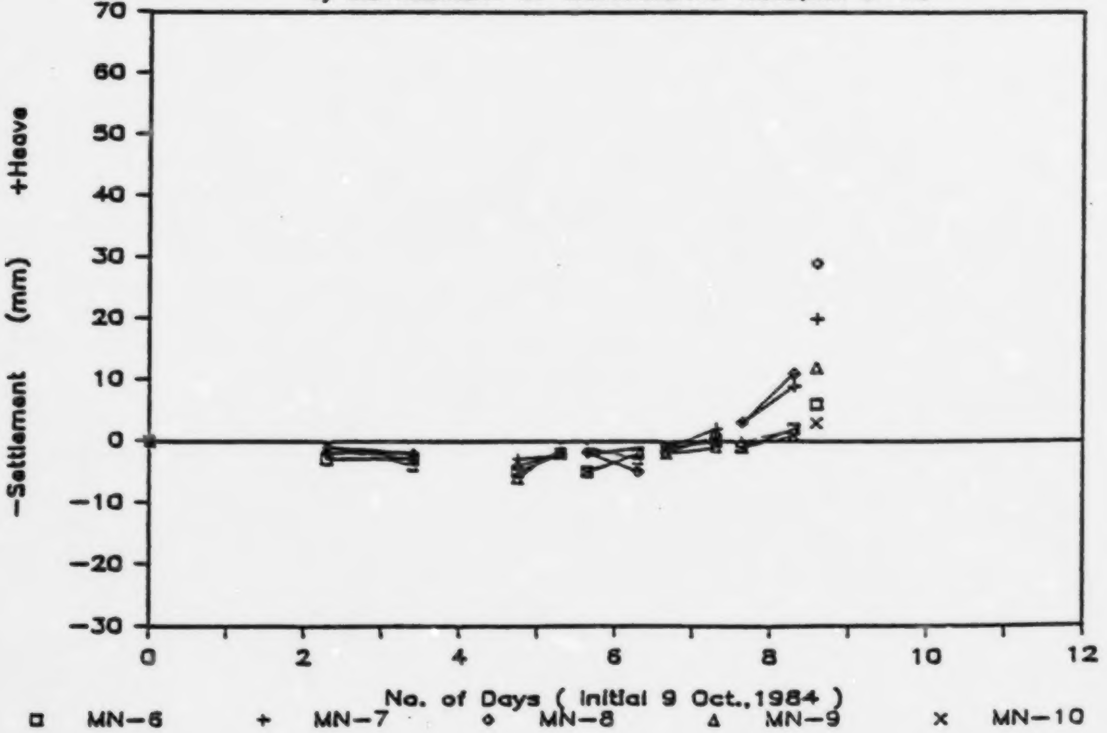

FIGURE 8.38 SETTLEMENT OF MONUMENTS NO.3, MN-1 TO 10

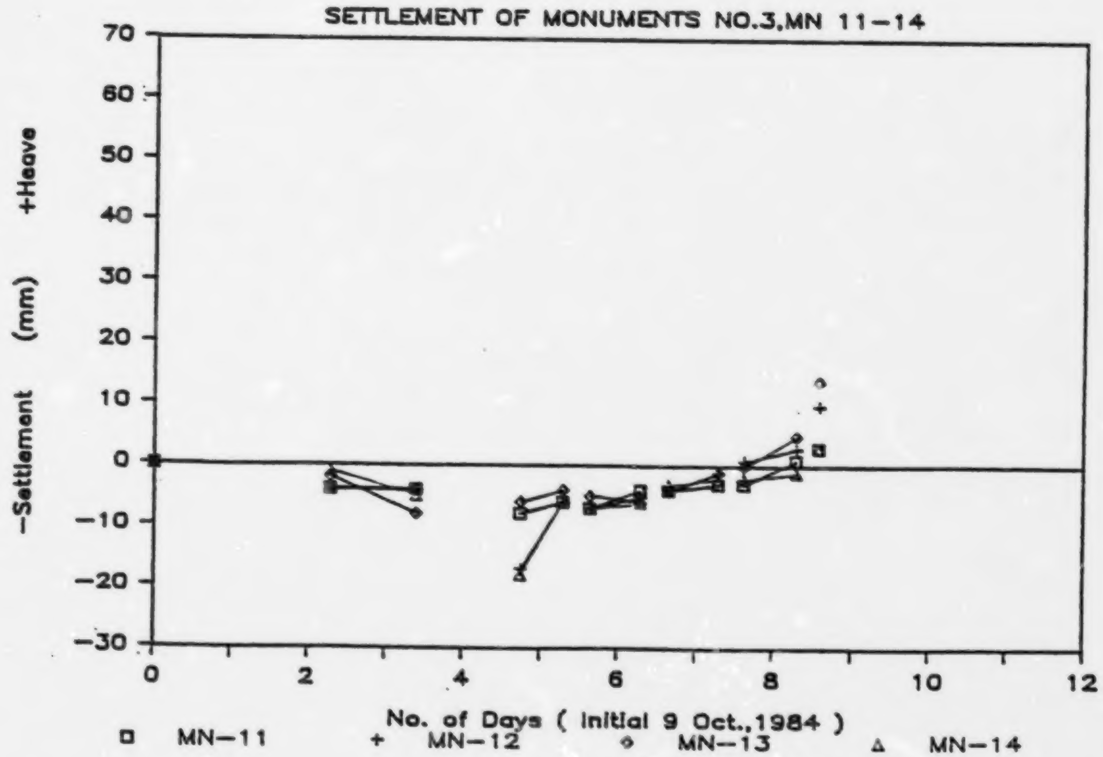

FIGURE 8.39 SETTLEMENT OF MONUMENTS NO.3, MN-11 TO 14

a) VERT. ELECTR. EXTENSOMETER NO.3,VE-1

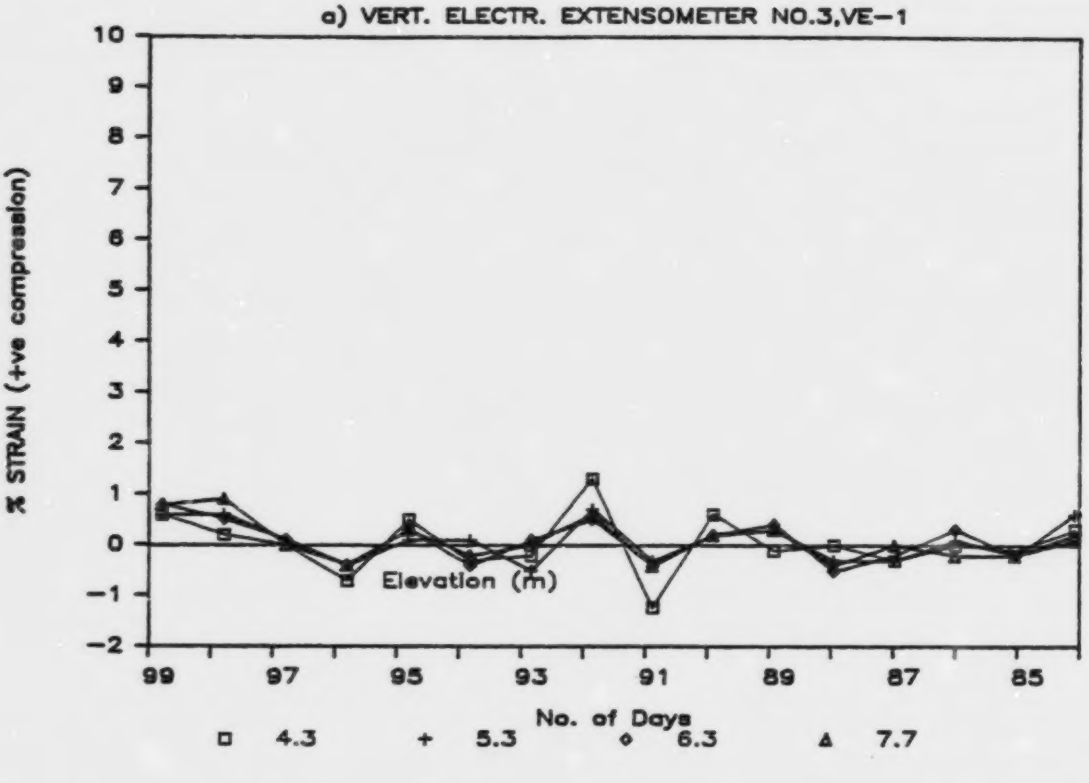

b) VERT. ELECTR. EXTENSOMETER NO.3,VE-2

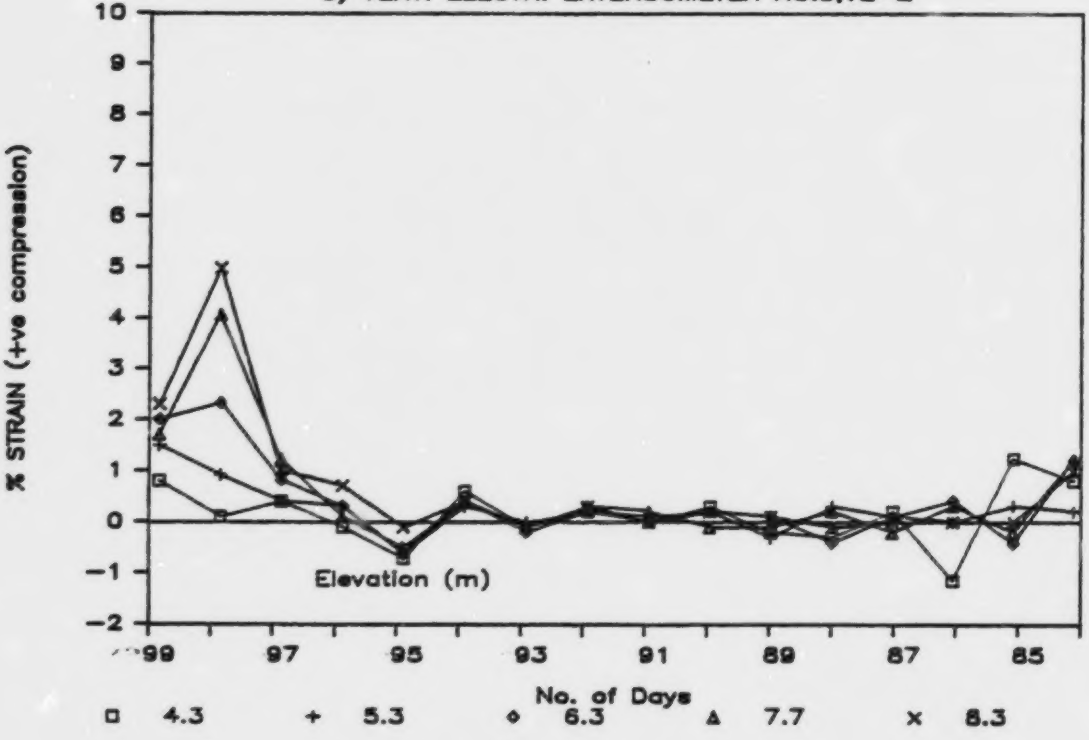

FIGURE 8.40 VERTICAL ELECTRICAL EXTENSOMETERS NO.3, VE-1 AND 2

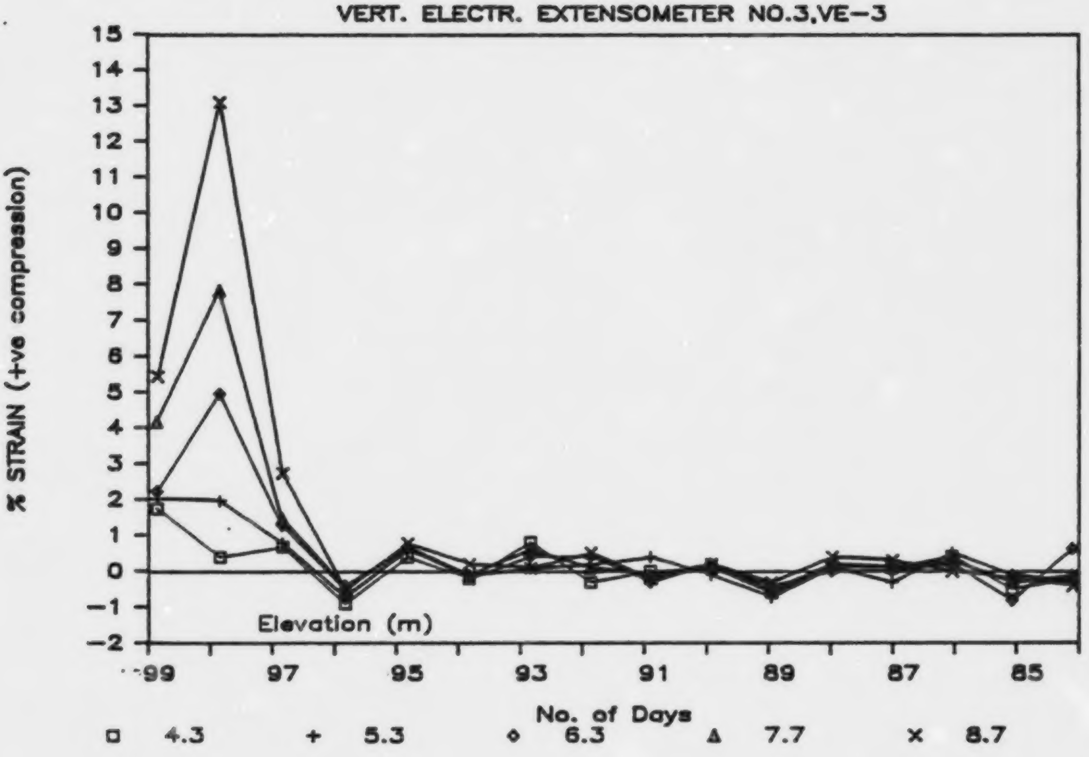

FIGURE 8.41 VERTICAL ELECTRICAL EXTENSOMETER NO.3, VE-3

a) INCLINOMETER DEFLECTIONS NO.3,IN-1

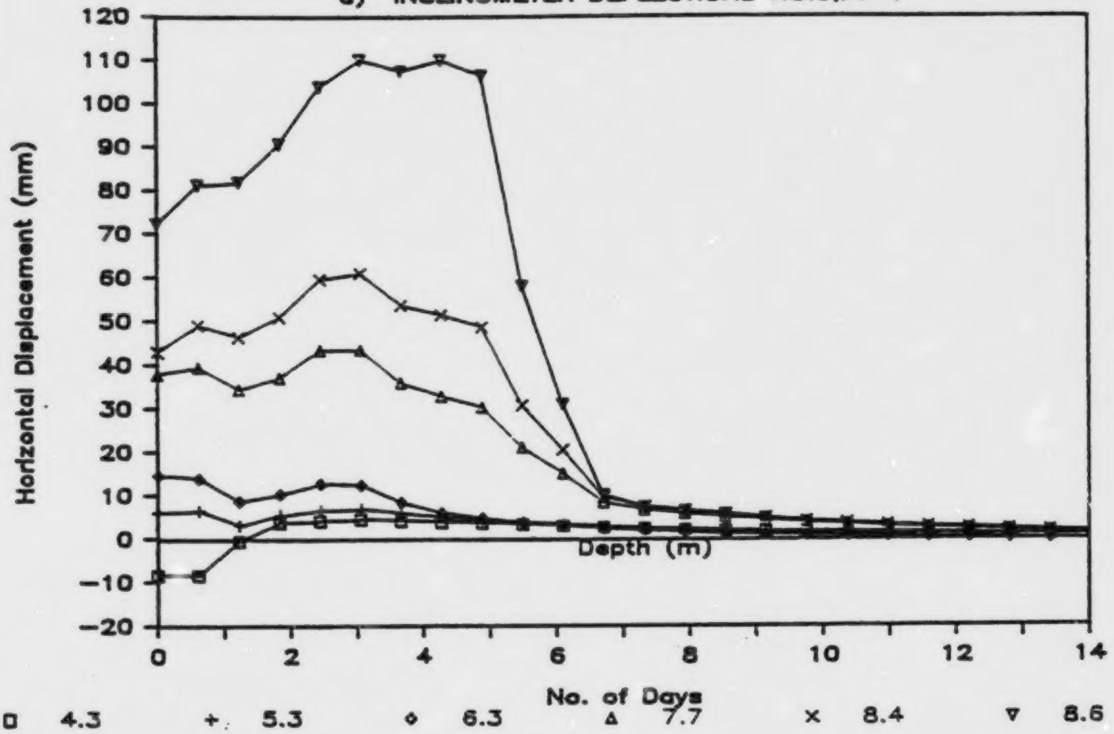

b) INCLINOMETER DEFLECTIONS NO.3,IN-2

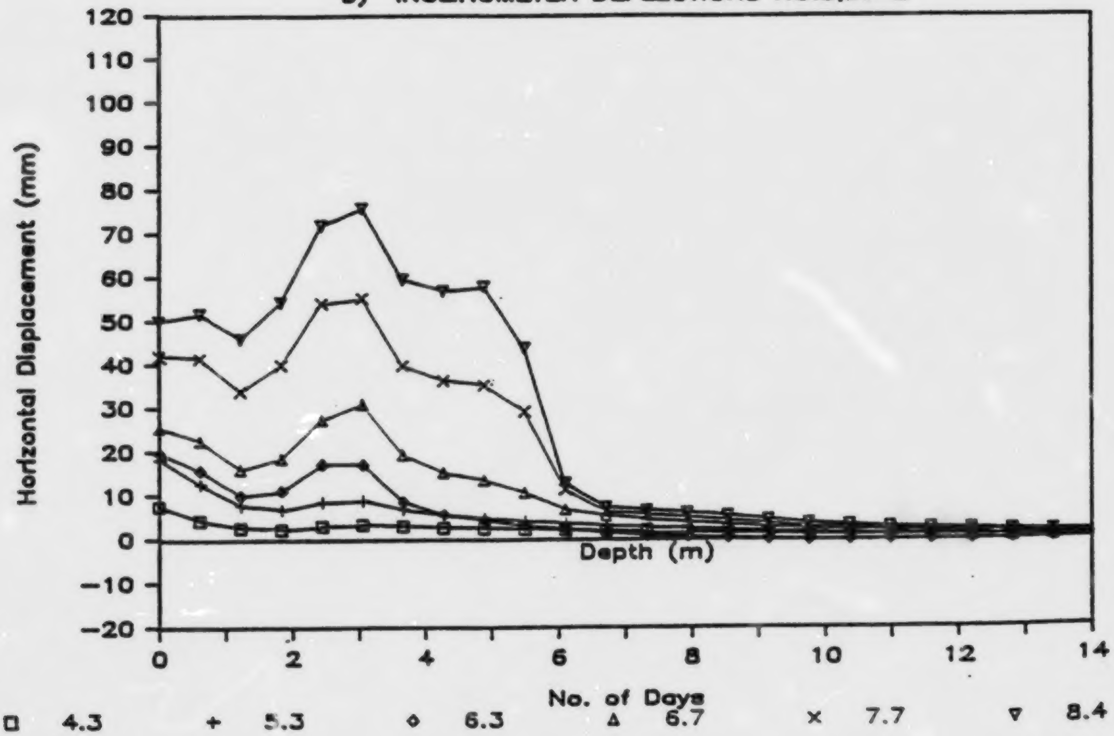

FIGURE 8.42 INCLINOMETER DEFLECTIONS NO.3, IN-1 AND 2

a) LATERAL MOVEMENTS: NO.3, MN 1–5

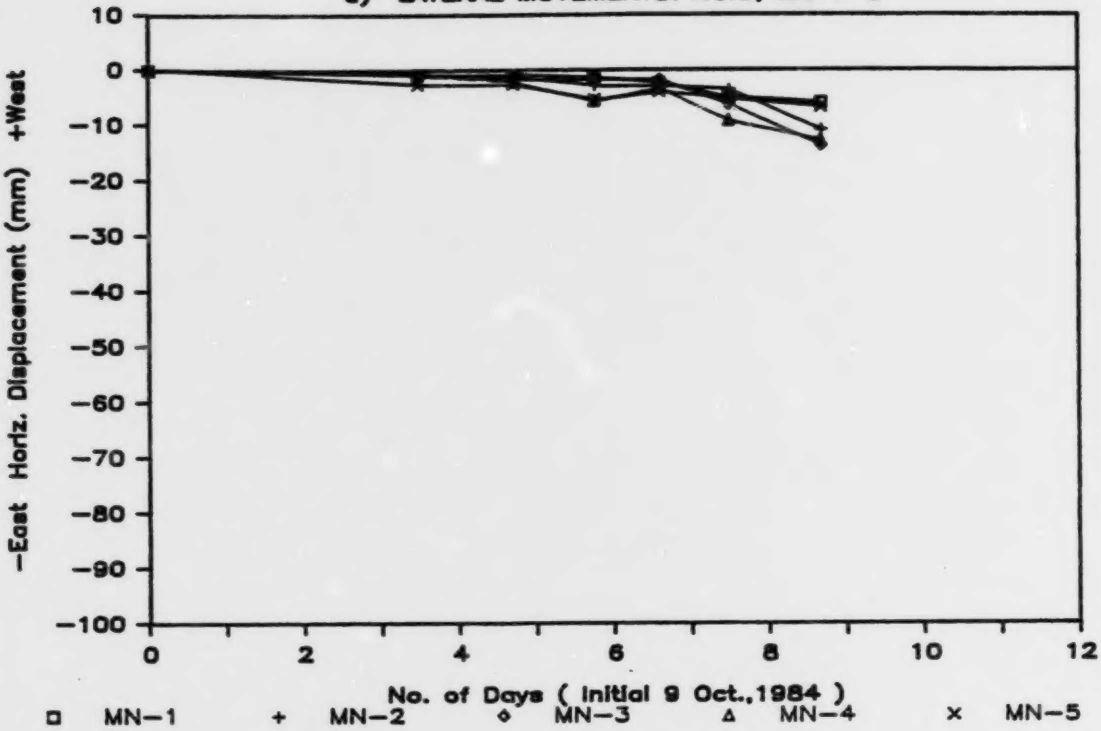

b) LATERAL MOVEMENTS: NO.3, MN 6–10

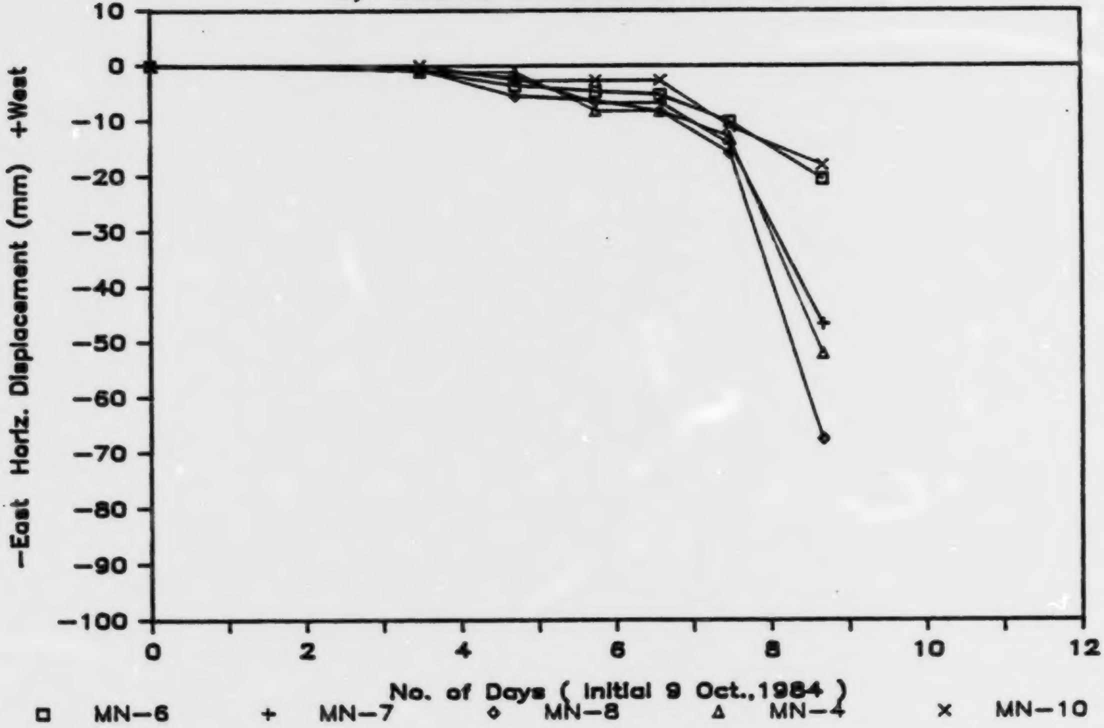

FIGURE 8.43 HORIZONTAL DISPLACEMENT OF MONUMENTS NO.3, MN-1 TO 10

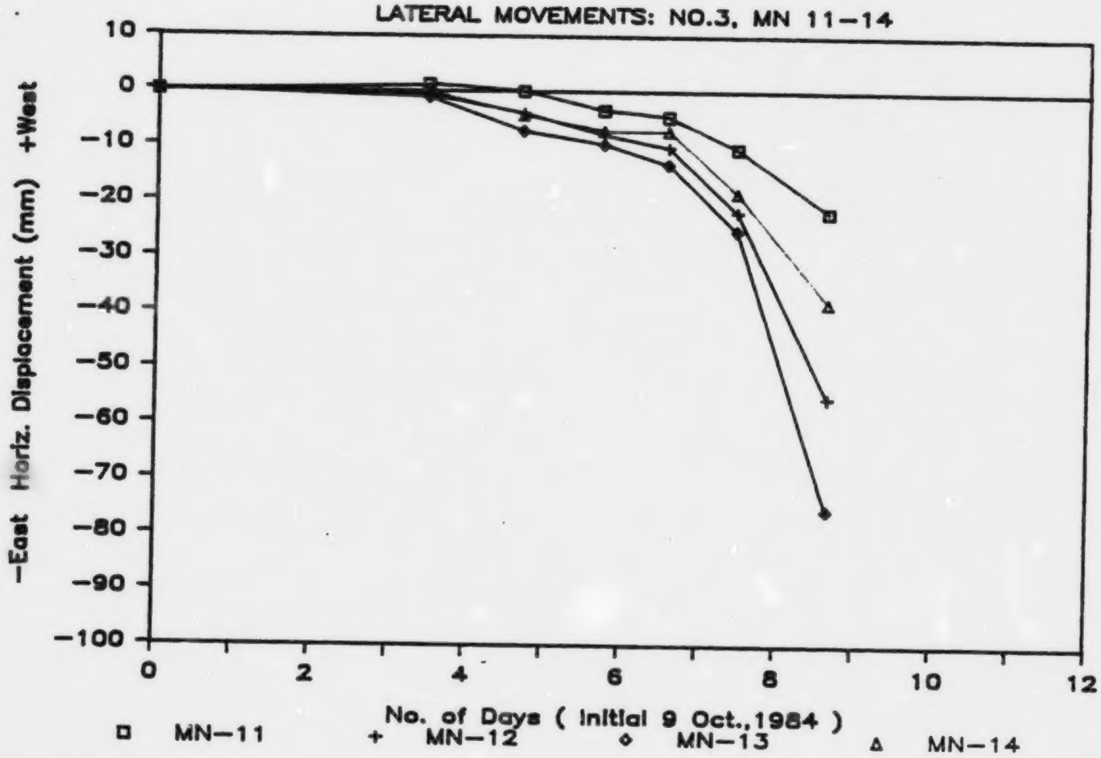

FIGURE 8.44 HORIZONTAL DISPLACEMENT OF MONUMENTS NO.3, MN-11 TO 14

a) HORIZONTAL EXTENSOMETER NO.3,HE-1

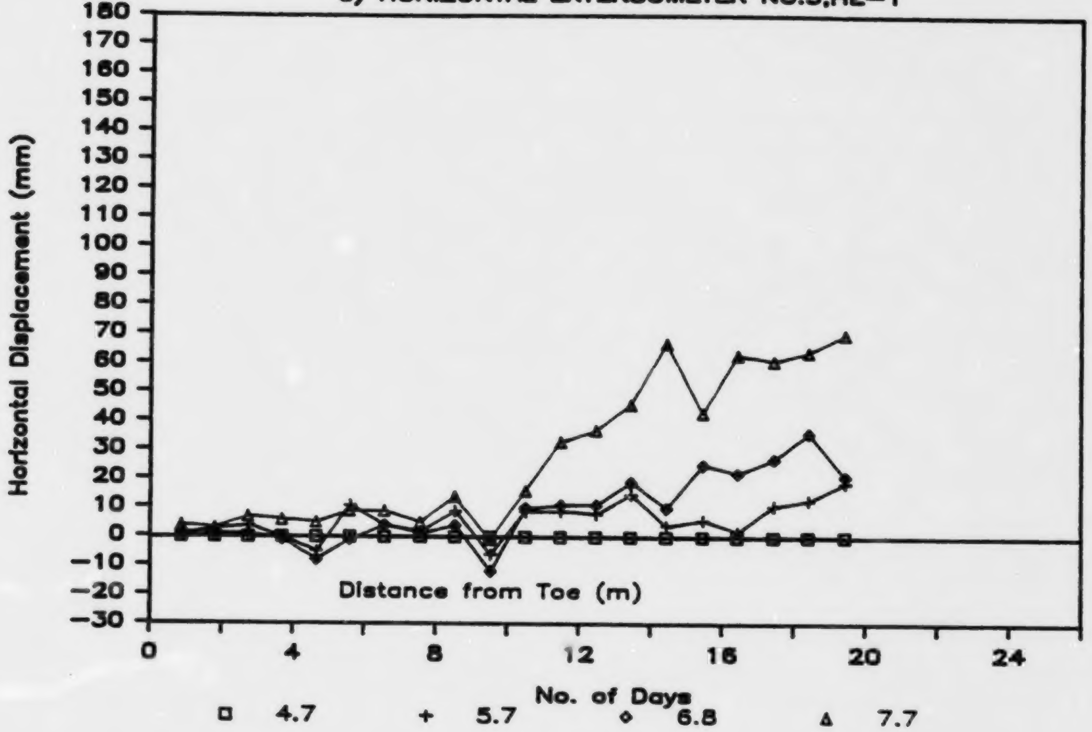

b) HORIZONTAL EXTENSOMETER NO.3,HE-2

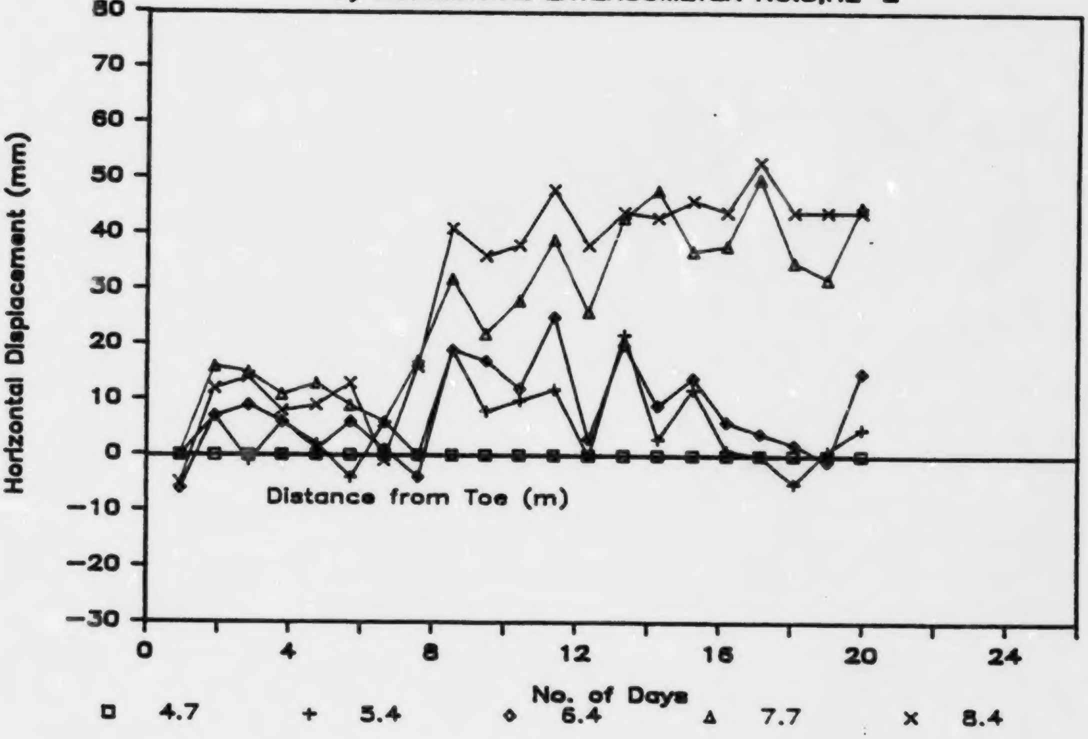

FIGURE 8.45 HORIZONTAL EXTENSOMETERS NO.3, HE-1 AND 2

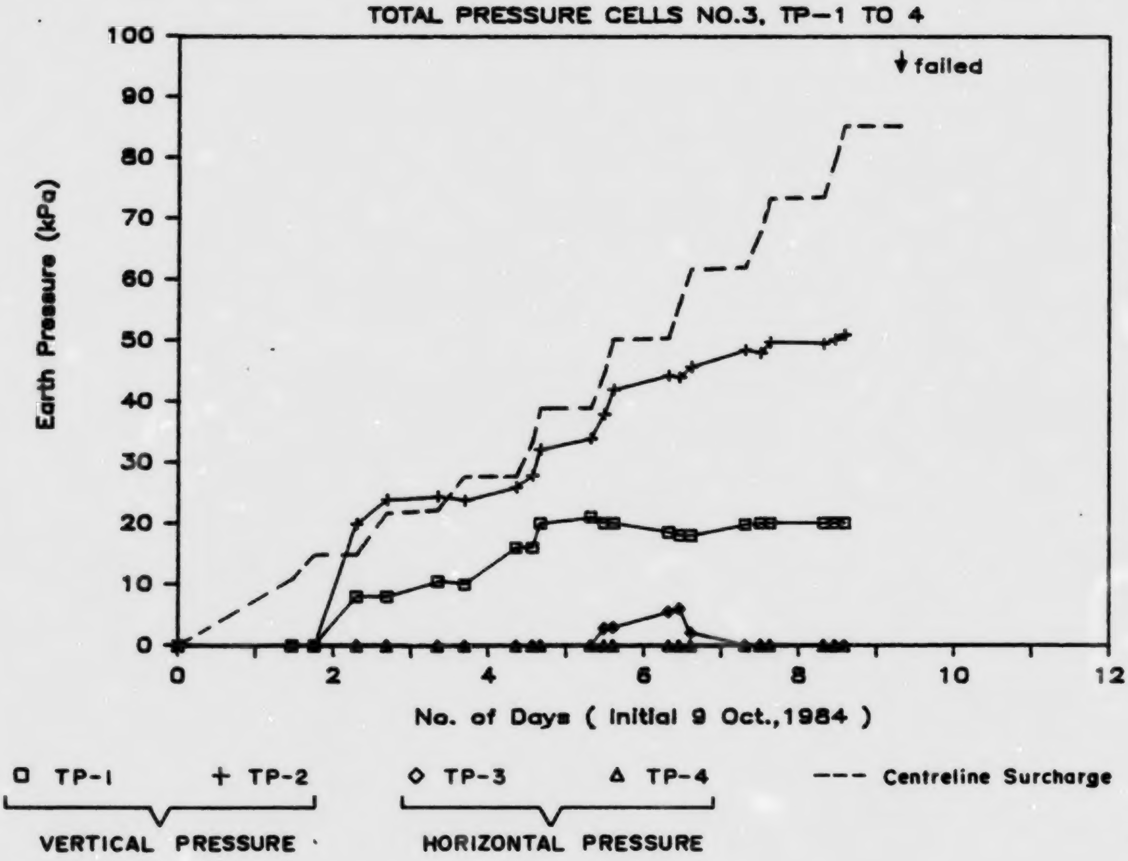

FIGURE 8.46 TOTAL PRESSURE CELLS NO.3, TP-1 TO 4

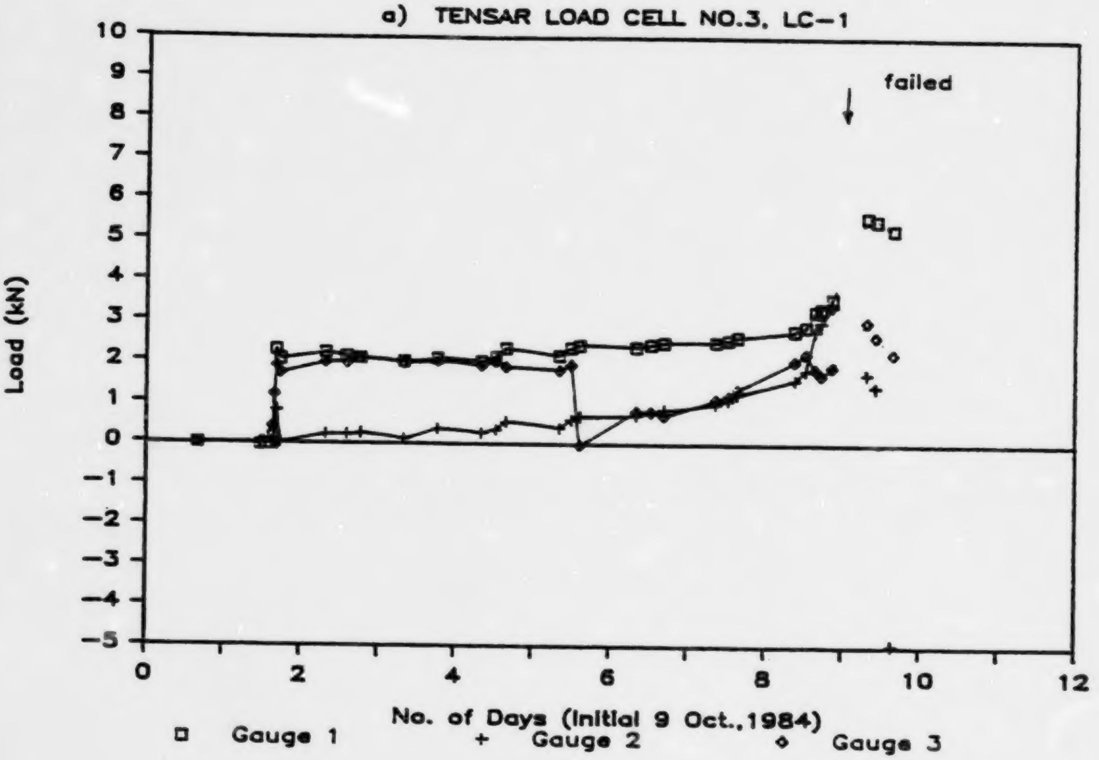

a) TENSAR LOAD CELL NO.3, LC-1

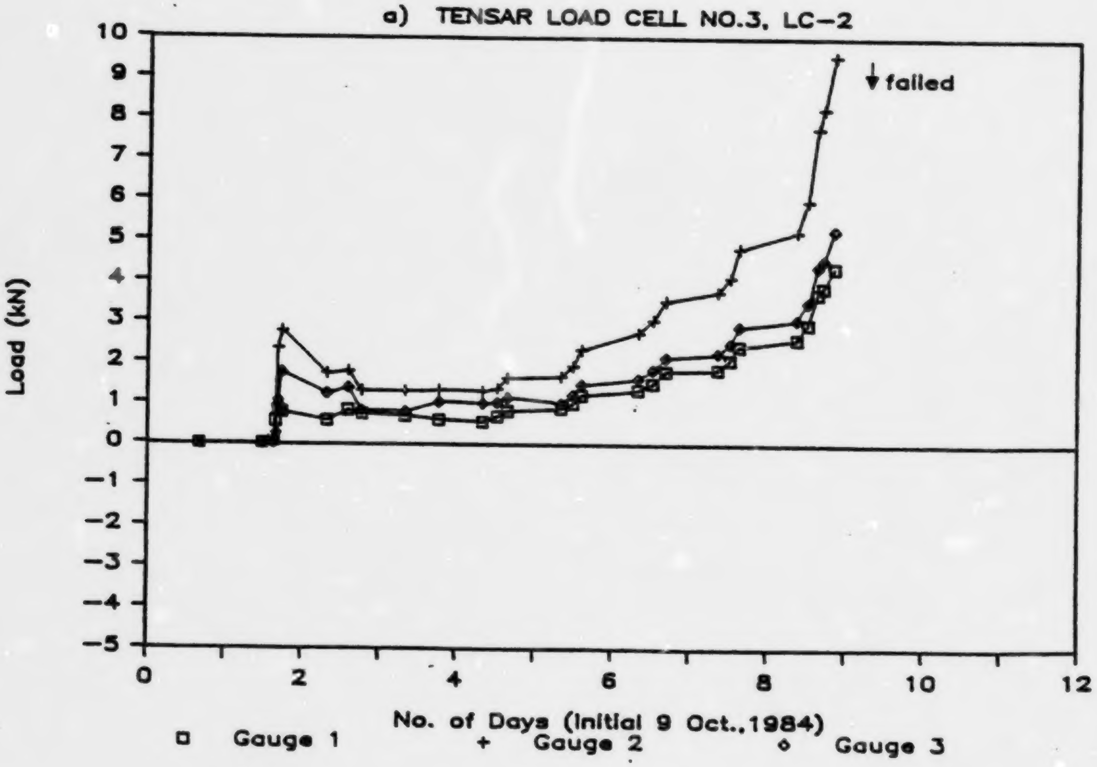

a) TENSAR LOAD CELL NO.3, LC-2

FIGURE 8.47 TENSAR LOAD CELLS NO.3, LC-1 AND 2

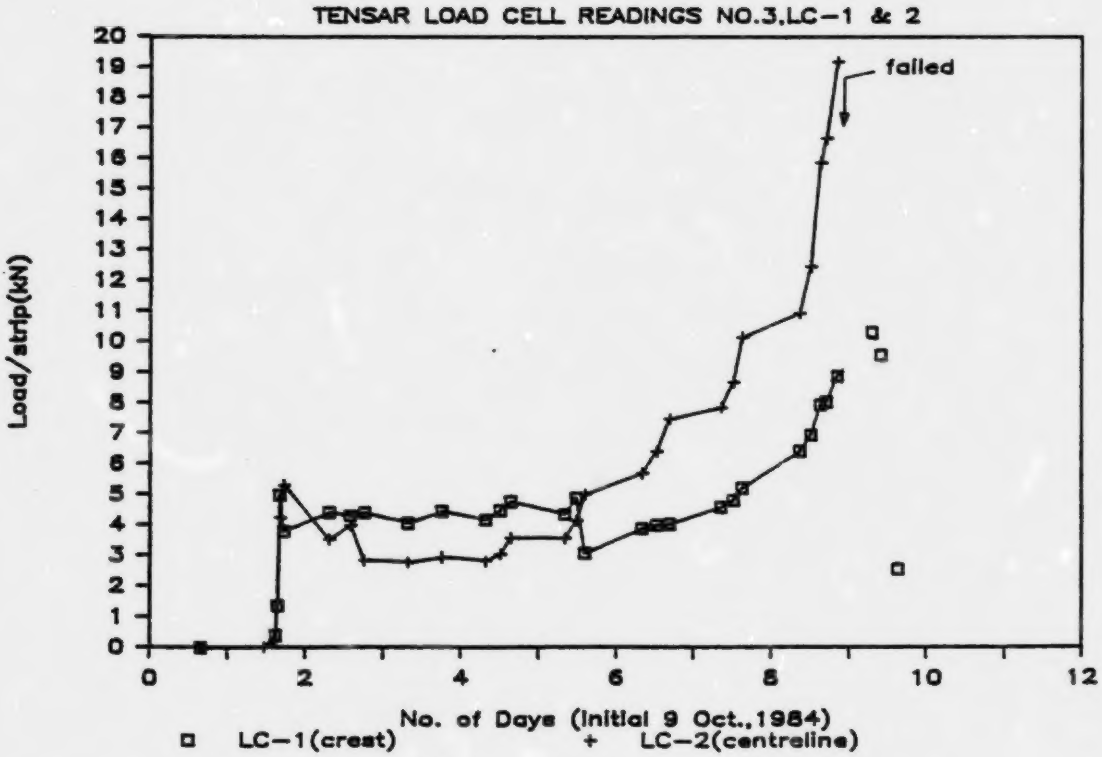

FIGURE 8.48 TENSILE LOADS IN GEOCELL REINFORCEMENT

a) BISON GAUGES NO.3:BG-1,5, CENTRELINE

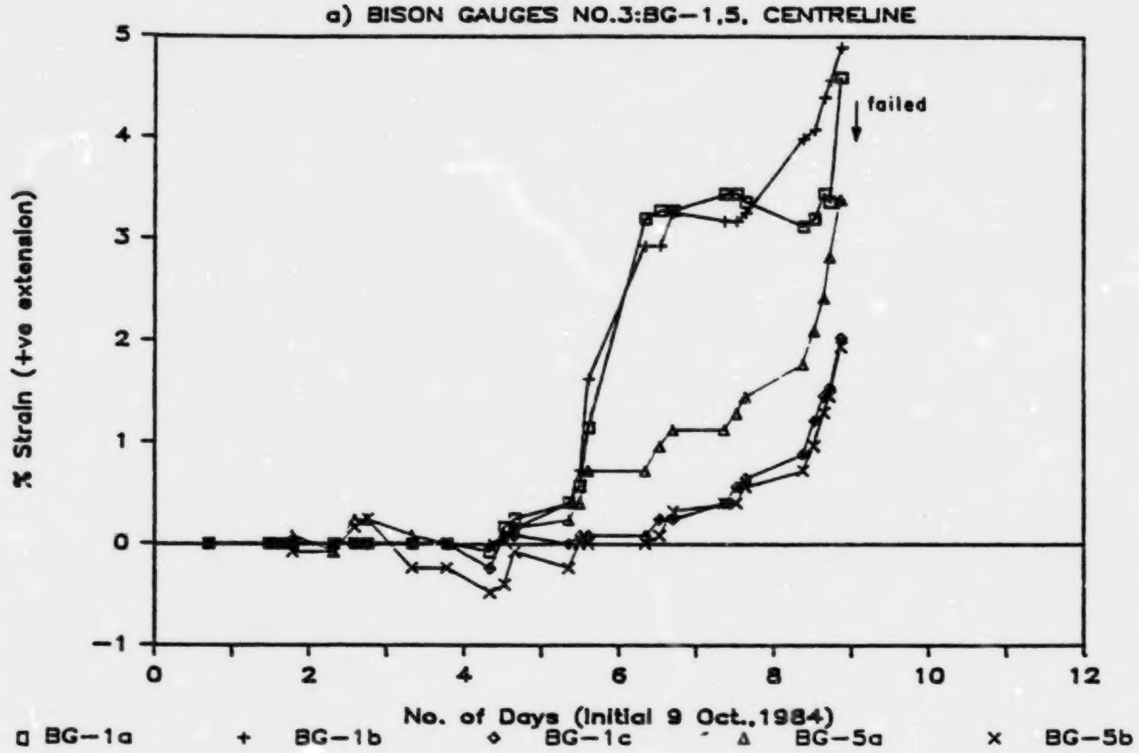

b) BISON GAUGES NO.3, BG-2 & 3

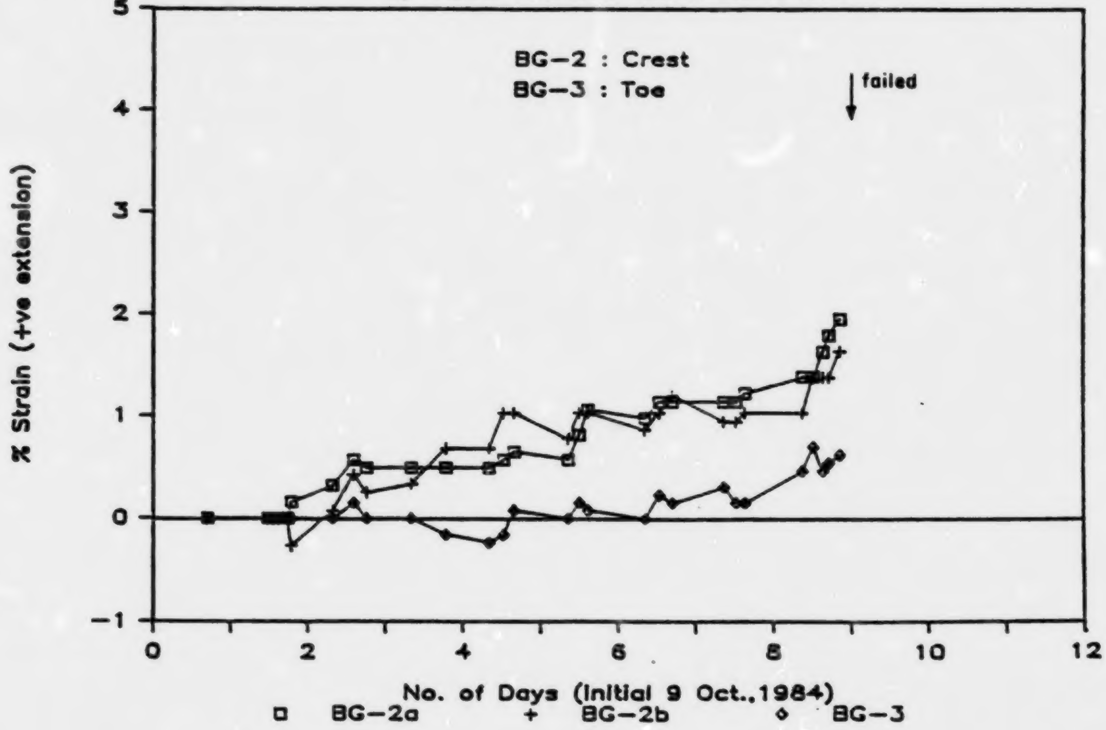

FIGURE 8.49 STRAIN MEASUREMENTS IN GEOCELL REINFORCEMENT

a) BISON GAUGES NO.3: BG-4, DIAGONAL

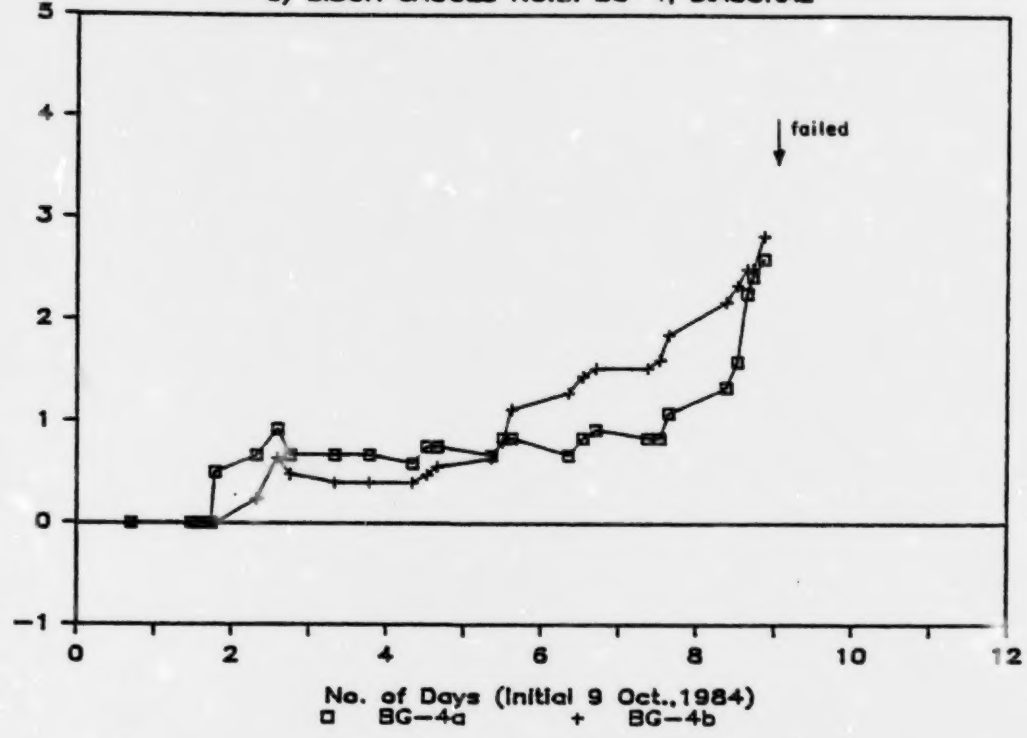

b) AVERAGE BISON GAUGE READINGS, NO.3

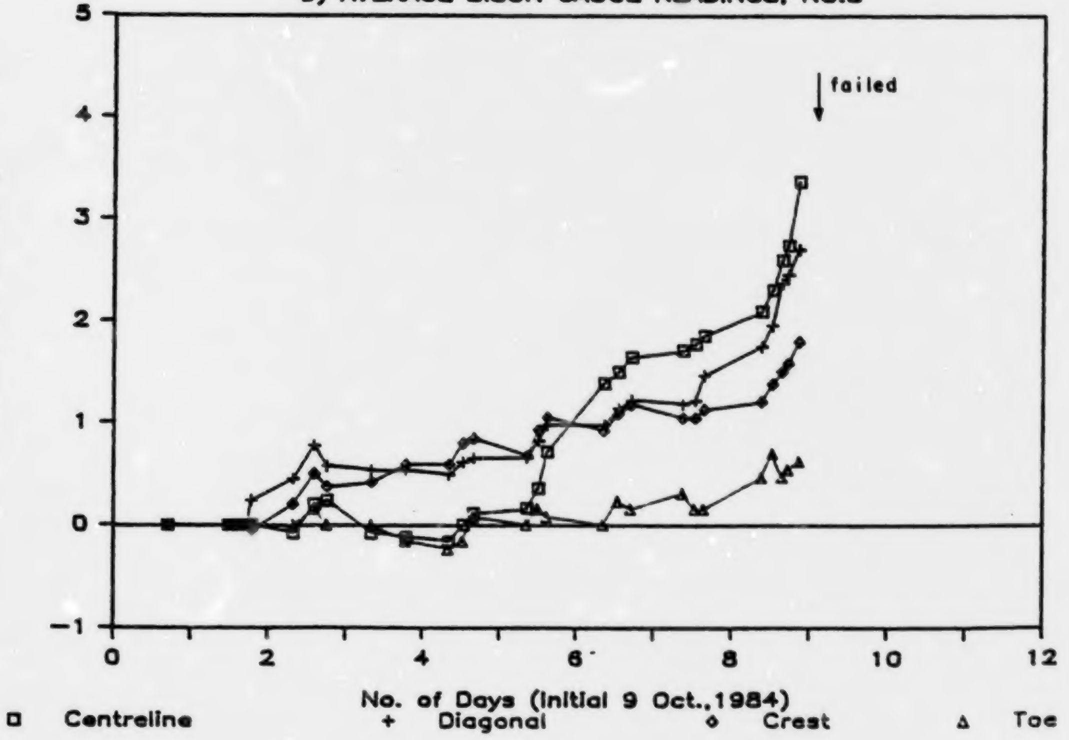

FIGURE 8.50 STRAIN MEASUREMENTS IN GEOCELL REINFORCEMENT

a) TYPICAL PORE PRESSURE RESPONSE UNDER EMBANKMENT CENTRE

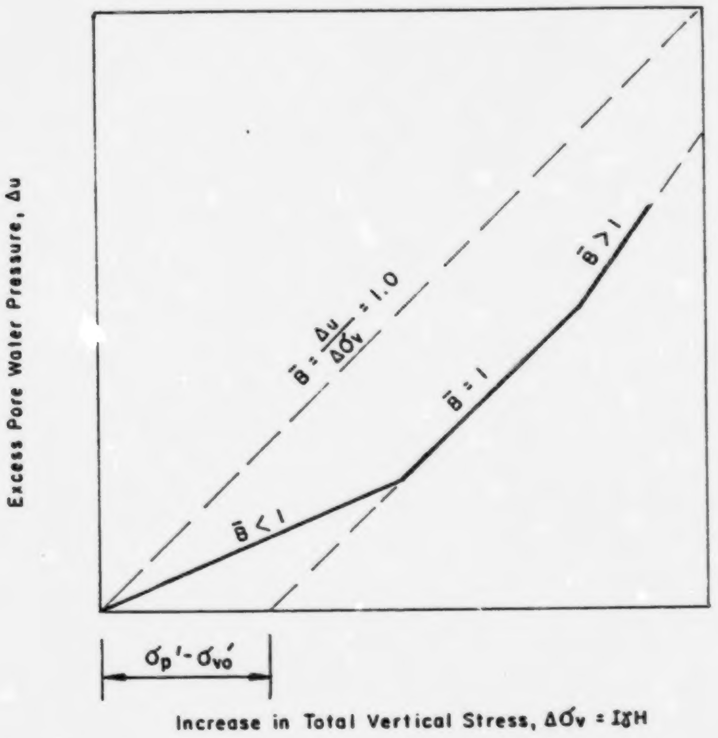

b) PORE PRESSURE RESPONSE, PN-15

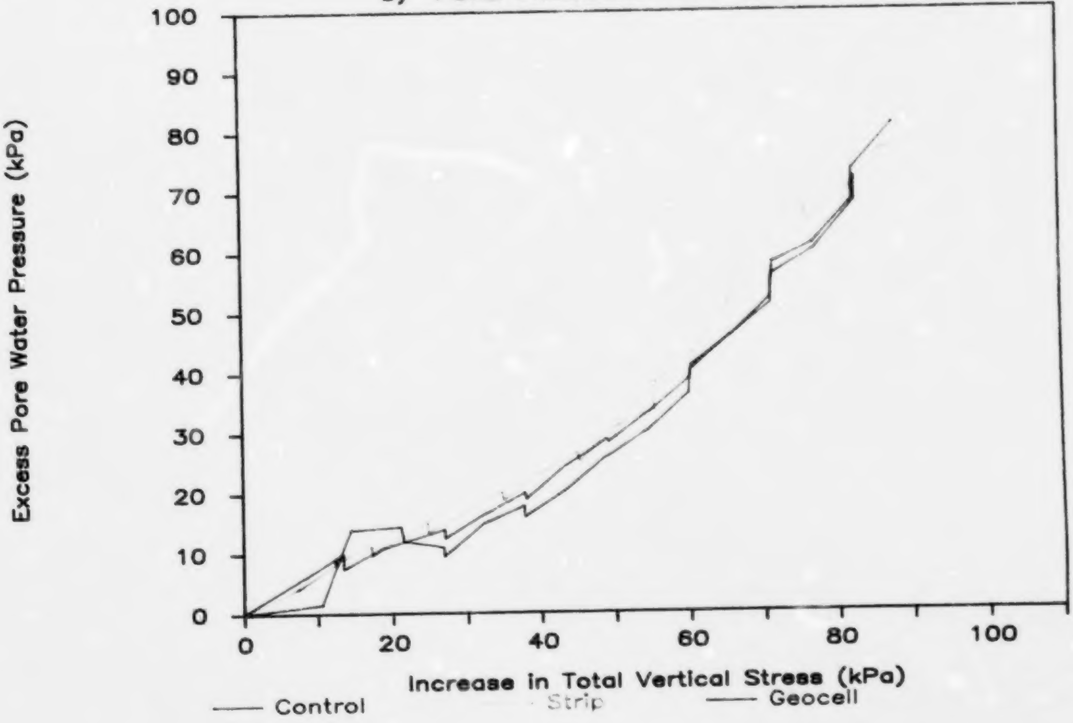

FIGURE 8.51 VARIATION OF PORE PRESSURE UNDER EMBANKMENT CENTRE

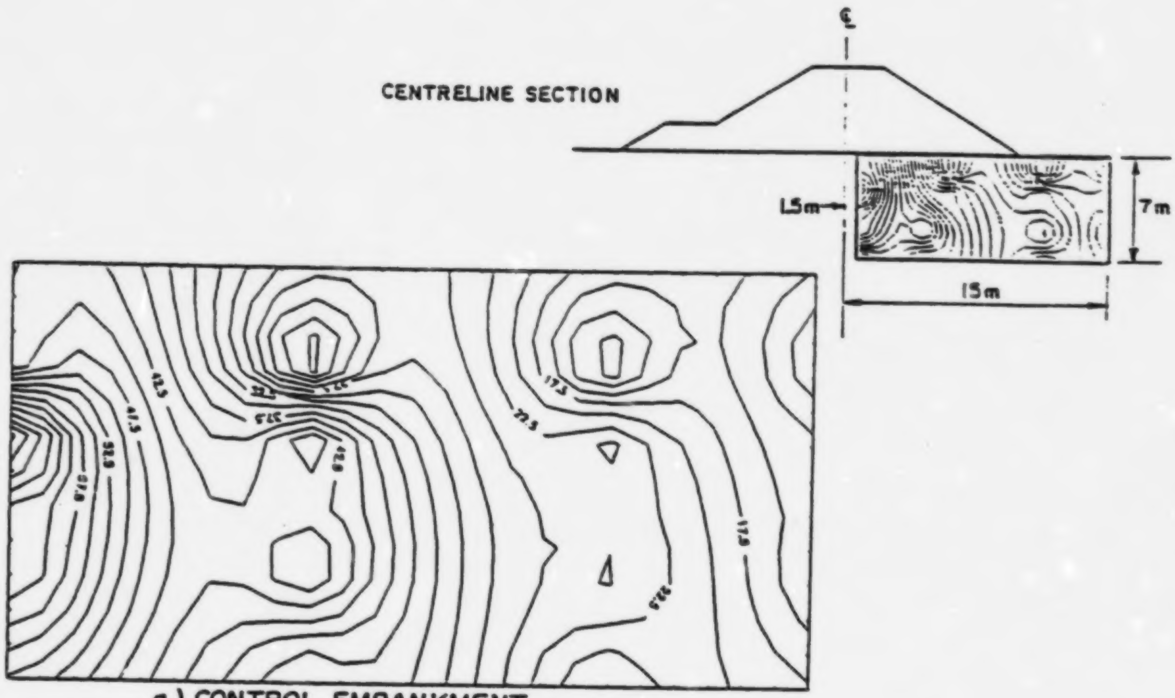

a) CONTROL EMBANKMENT

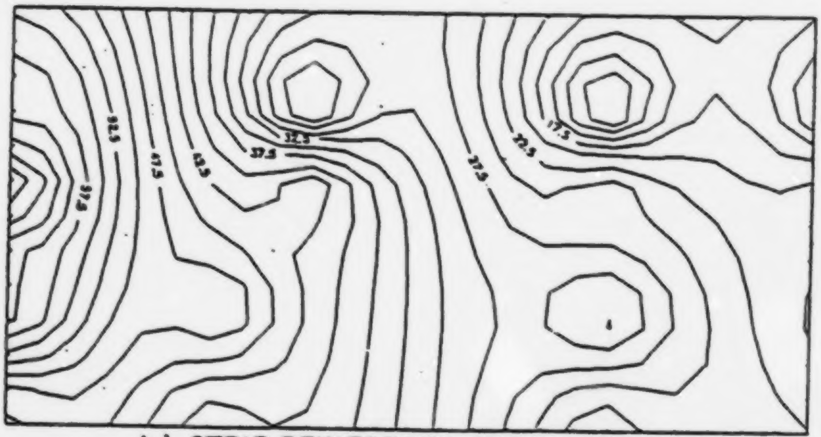

b) STRIP REINFORCED EMBANKMENT

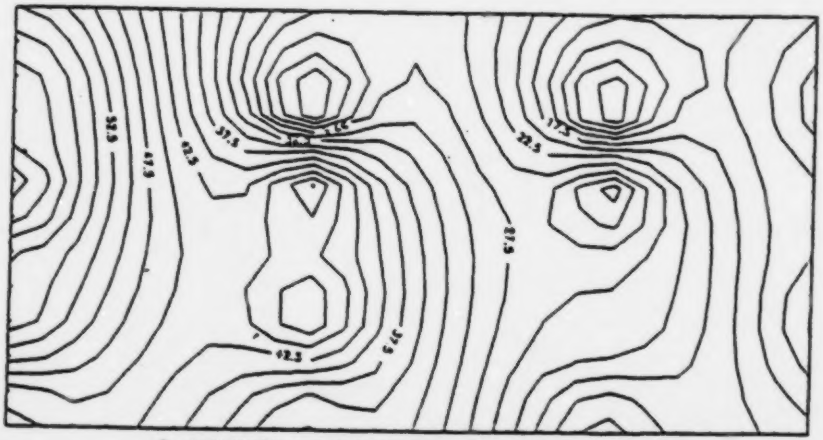

c) GEOCELL REINFORCED EMBANKMENT

FIGURE 8.52 EXCESS PORE PRESSURE CONTOURS AT SURCHARGE OF 84 kPa

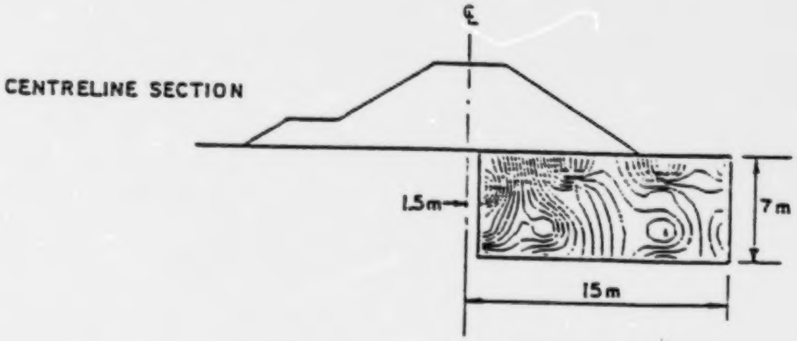

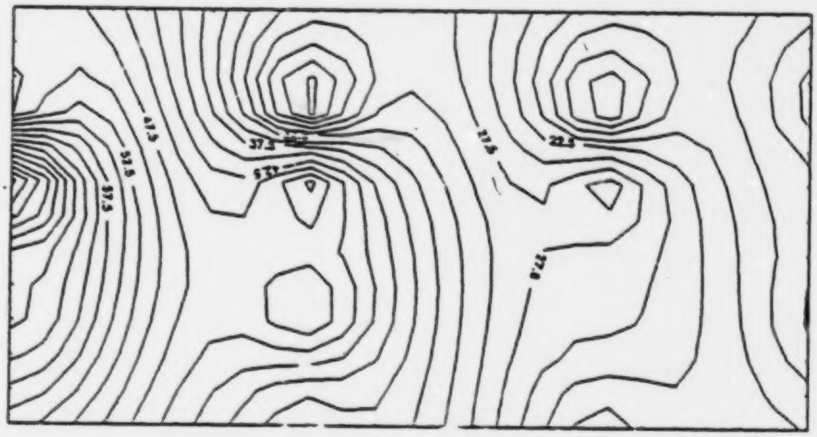

a) CONTROL EMBANKMENT

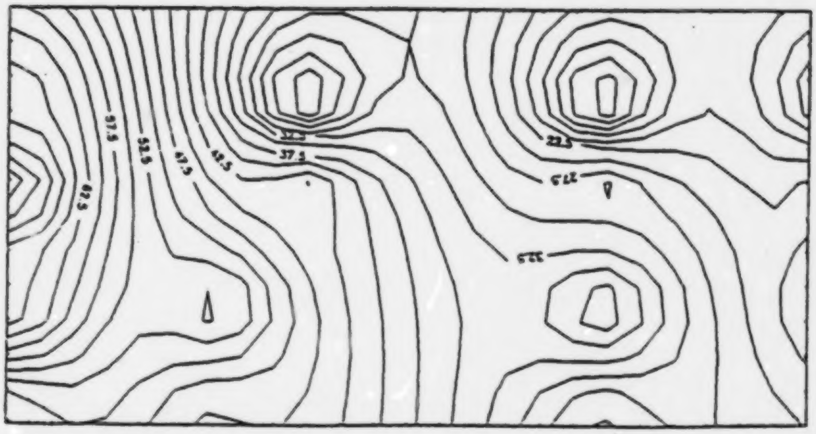

b) STRIP REINFORCED EMBANKMENT

FIGURE 8.53 EXCESS PORE PRESSURE CONTOURS AT SURCHARGE OF 90 kPa

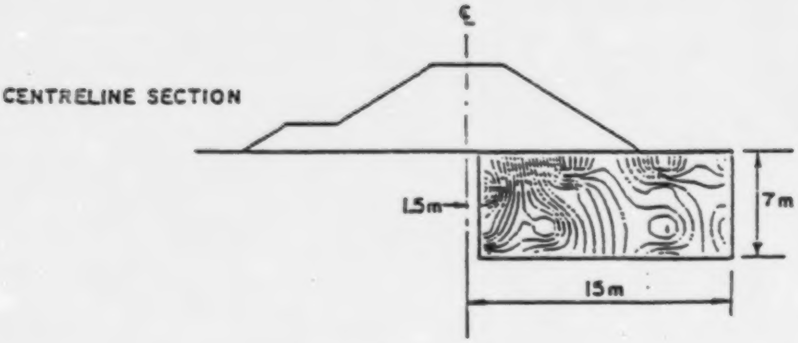

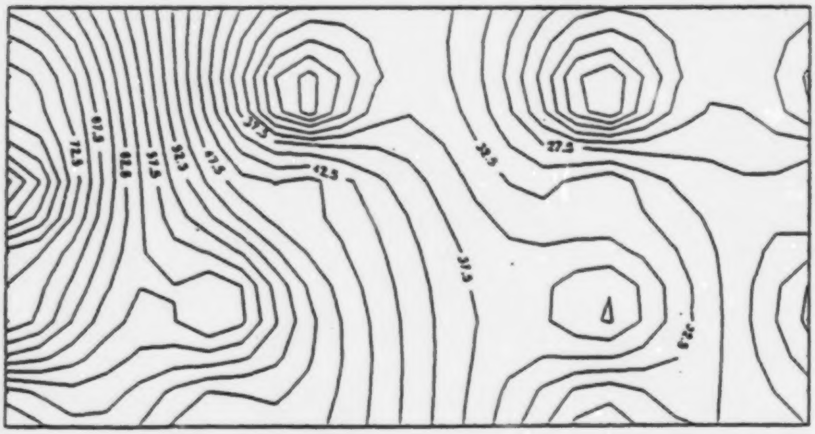

STRIP REINFORCED EMBANKMENT

FIGURE 8.54 EXCESS PORE PRESSURE CONTOURS AT SURCHARGE OF 104 kPa

a) EXCESS PORE PRESSURE, PN-6

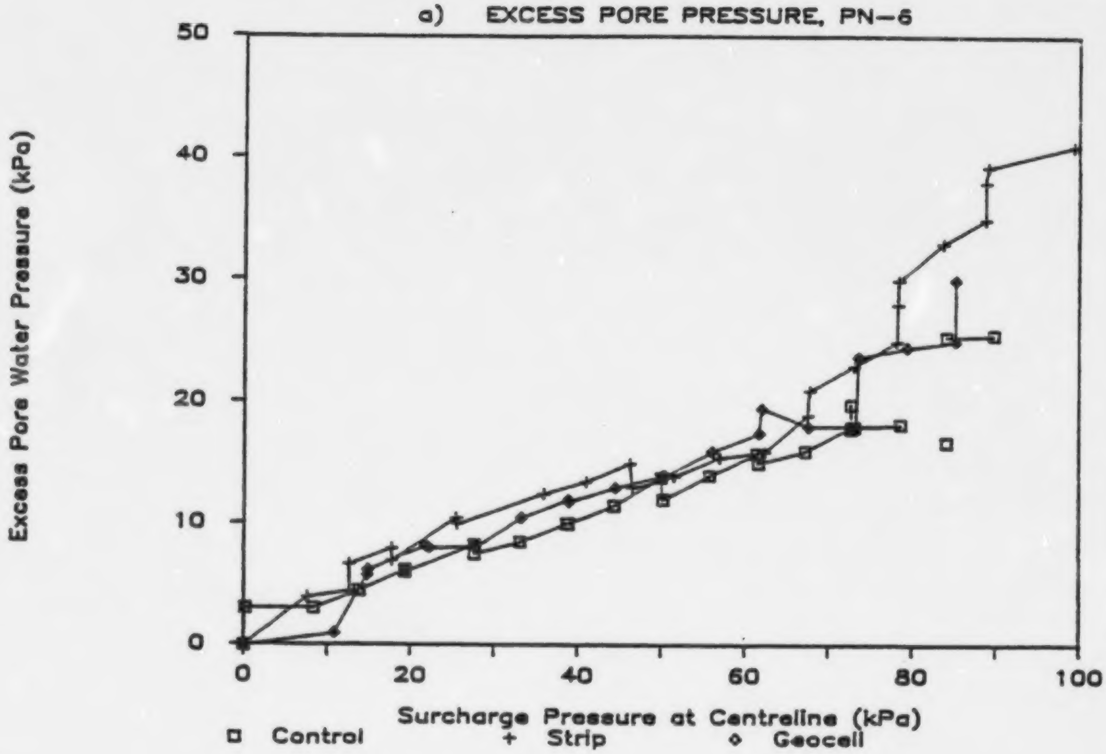

b) EXCESS PORE PRESSURE, PN-7

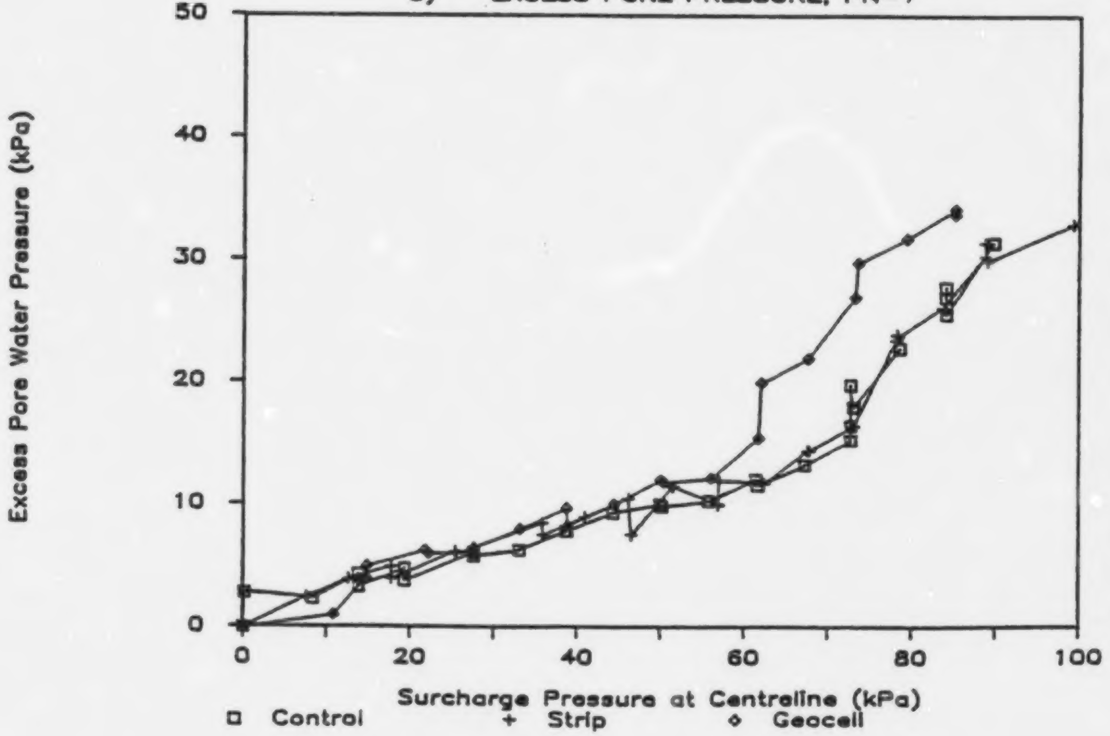

FIGURE 8.55 PORE PRESSURE RESPONSE OF PIEZOMETERS PN-6 AND 7

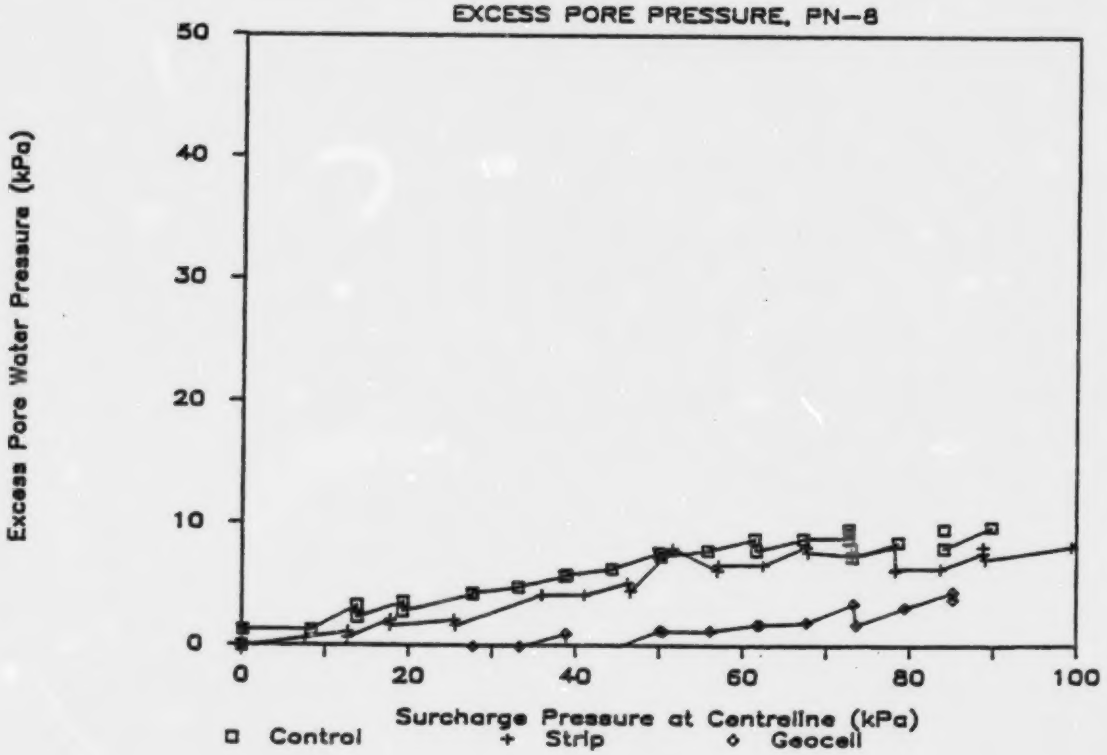

FIGURE 8.56 PORE PRESSURE RESPONSE OF PIEZOMETER PN-8

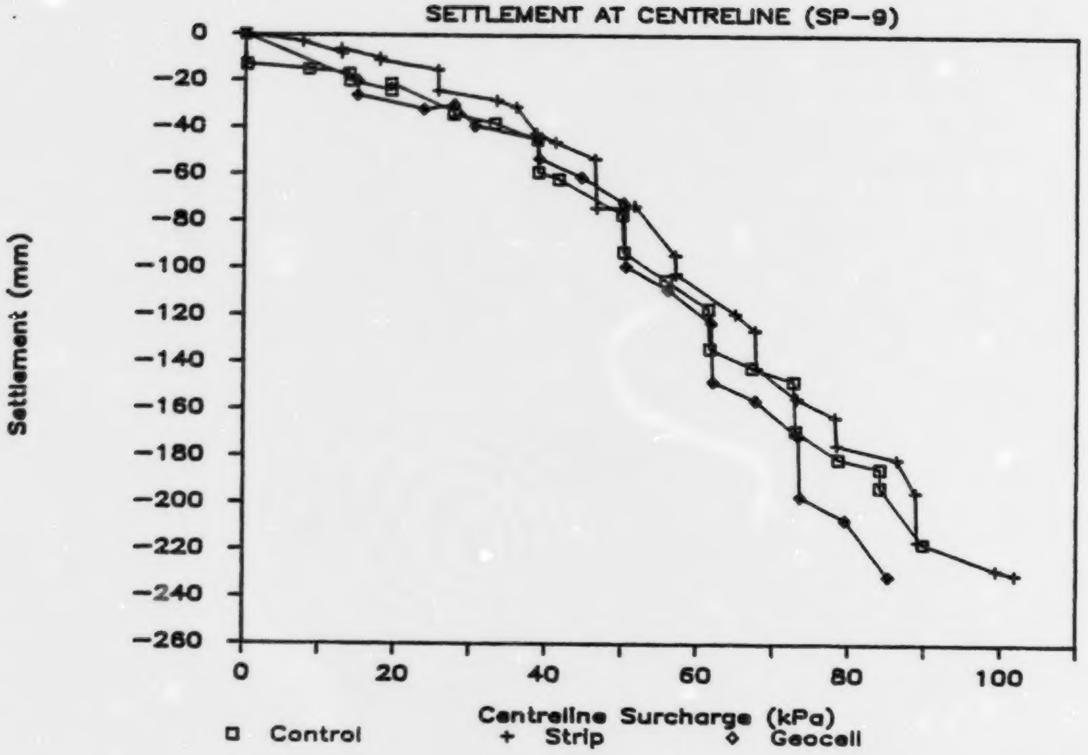

FIGURE 8.57 COMPARISON OF SETTLEMENTS AT CENTRELINE (SP-9)

a) DEFLECTION PROFILE OF IN-1

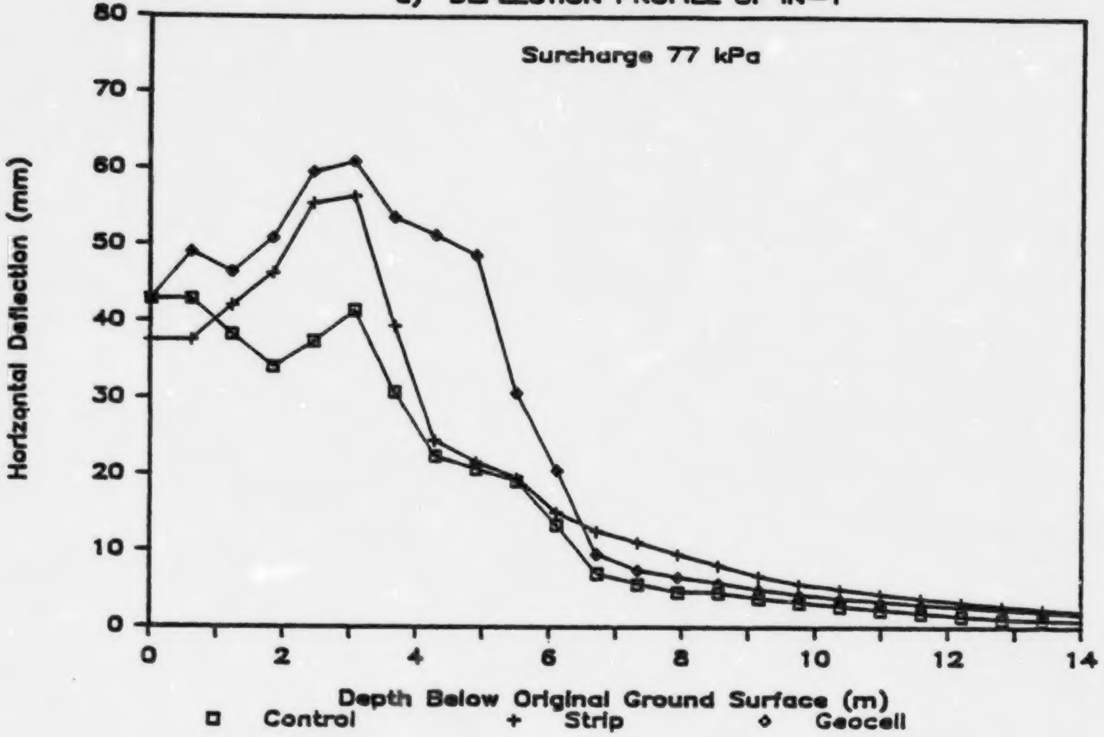

b) DEFLECTION PROFILE OF IN-2

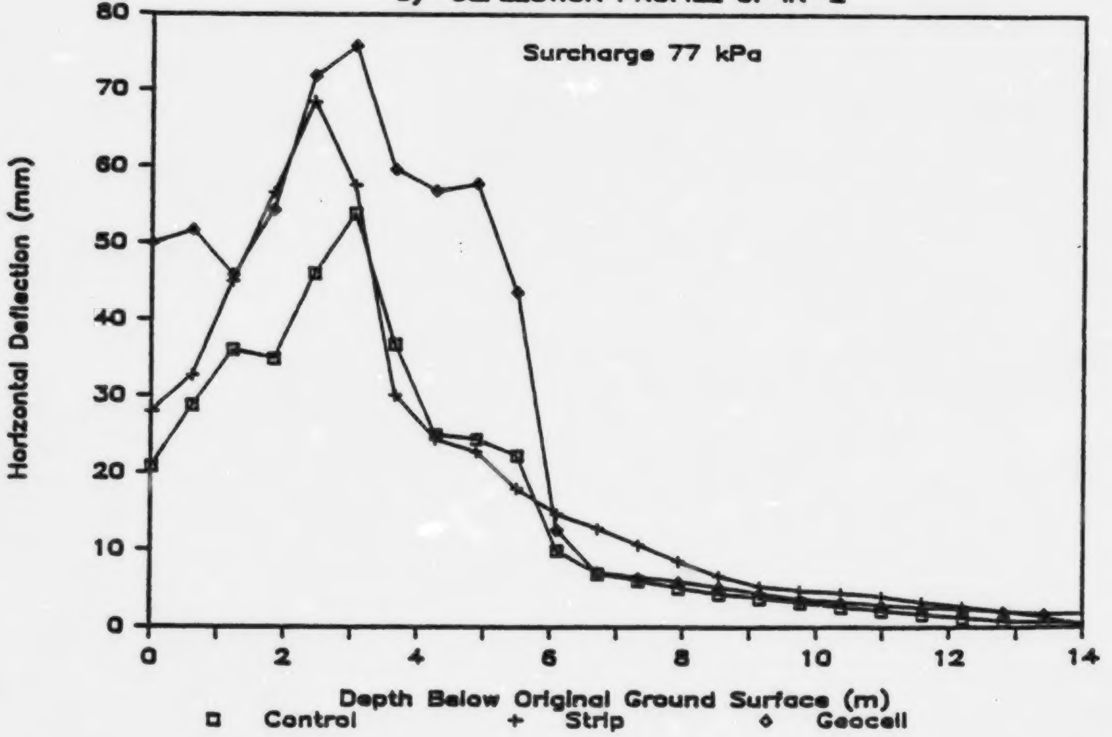

FIGURE 8.58 COMPARISON OF DEFLECTION PROFILES AT SURCHARGE OF 77 kPa

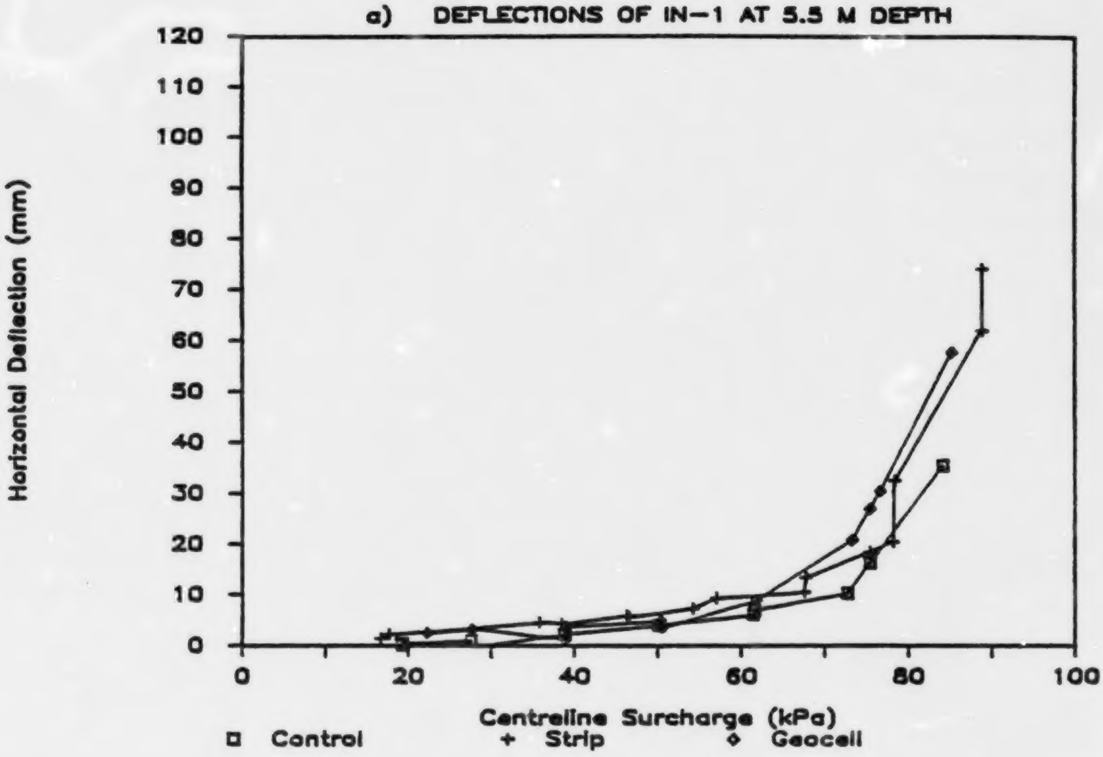

a) DEFLECTIONS OF IN-1 AT 5.5 M DEPTH

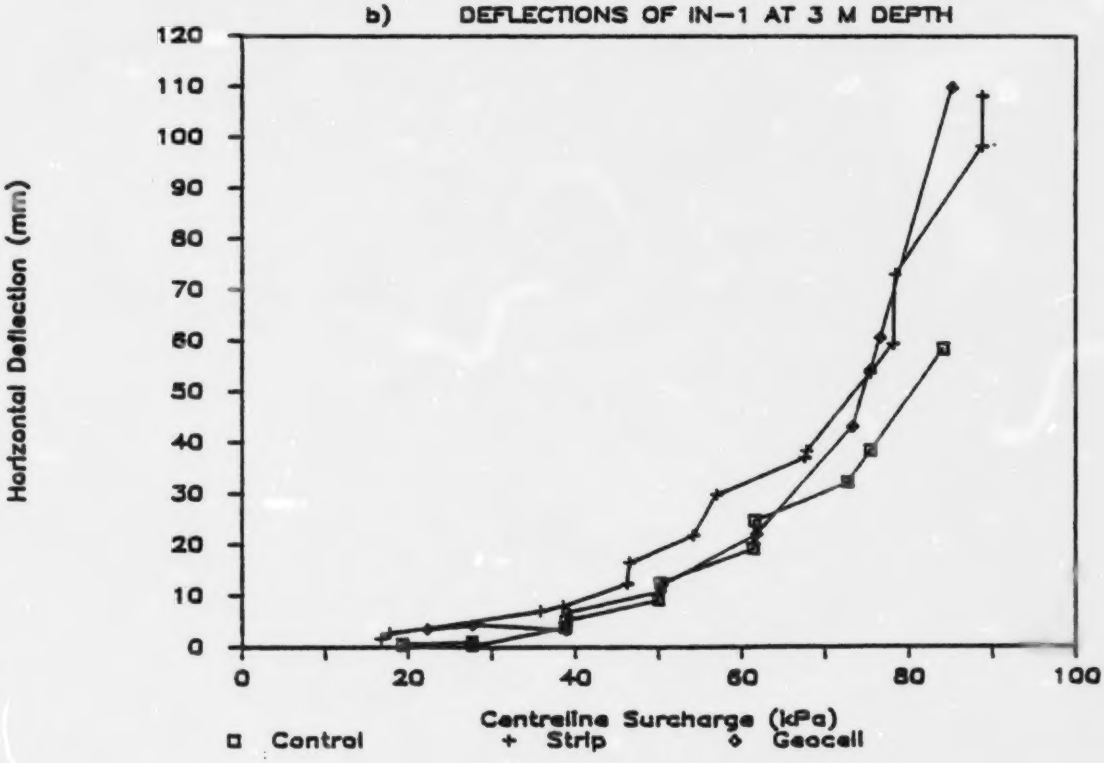

b) DEFLECTIONS OF IN-1 AT 3 M DEPTH

FIGURE 8.59 SURCHARGE VERSUS DEFLECTION AT 5.5m AND 3m DEPTHS, IN-1

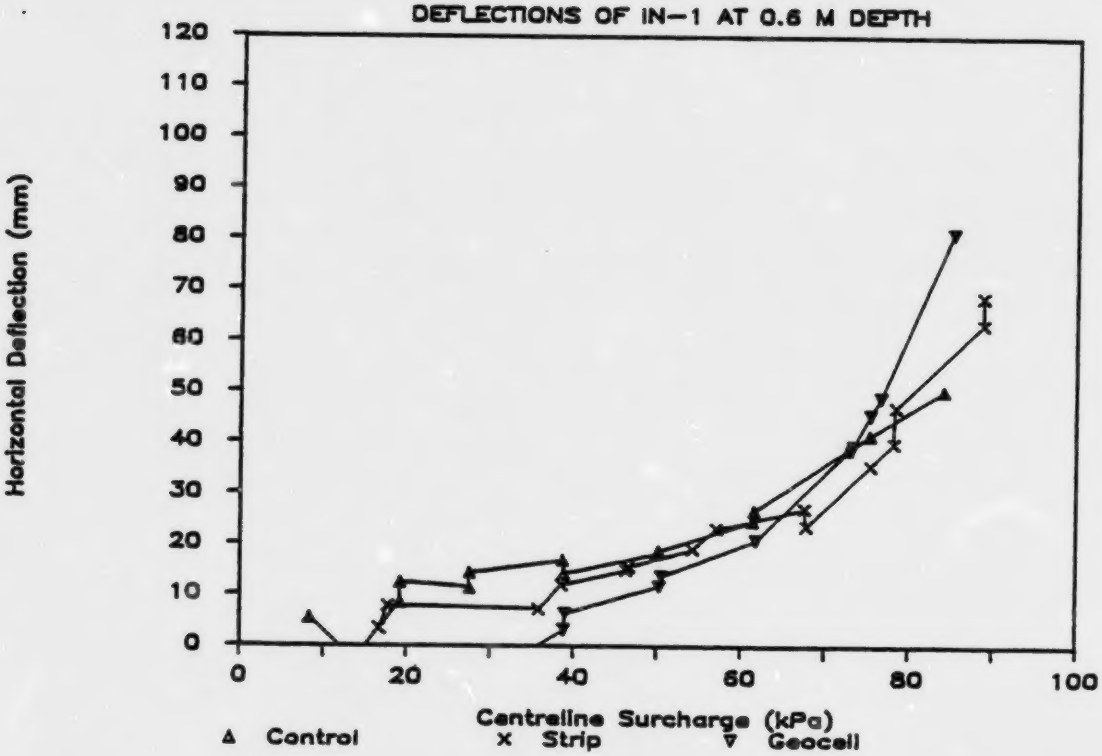

FIGURE 8.60 SURCHARGE VERSUS DEFLECTION AT 0.6m DEPTH, IN-1

SECTION 9

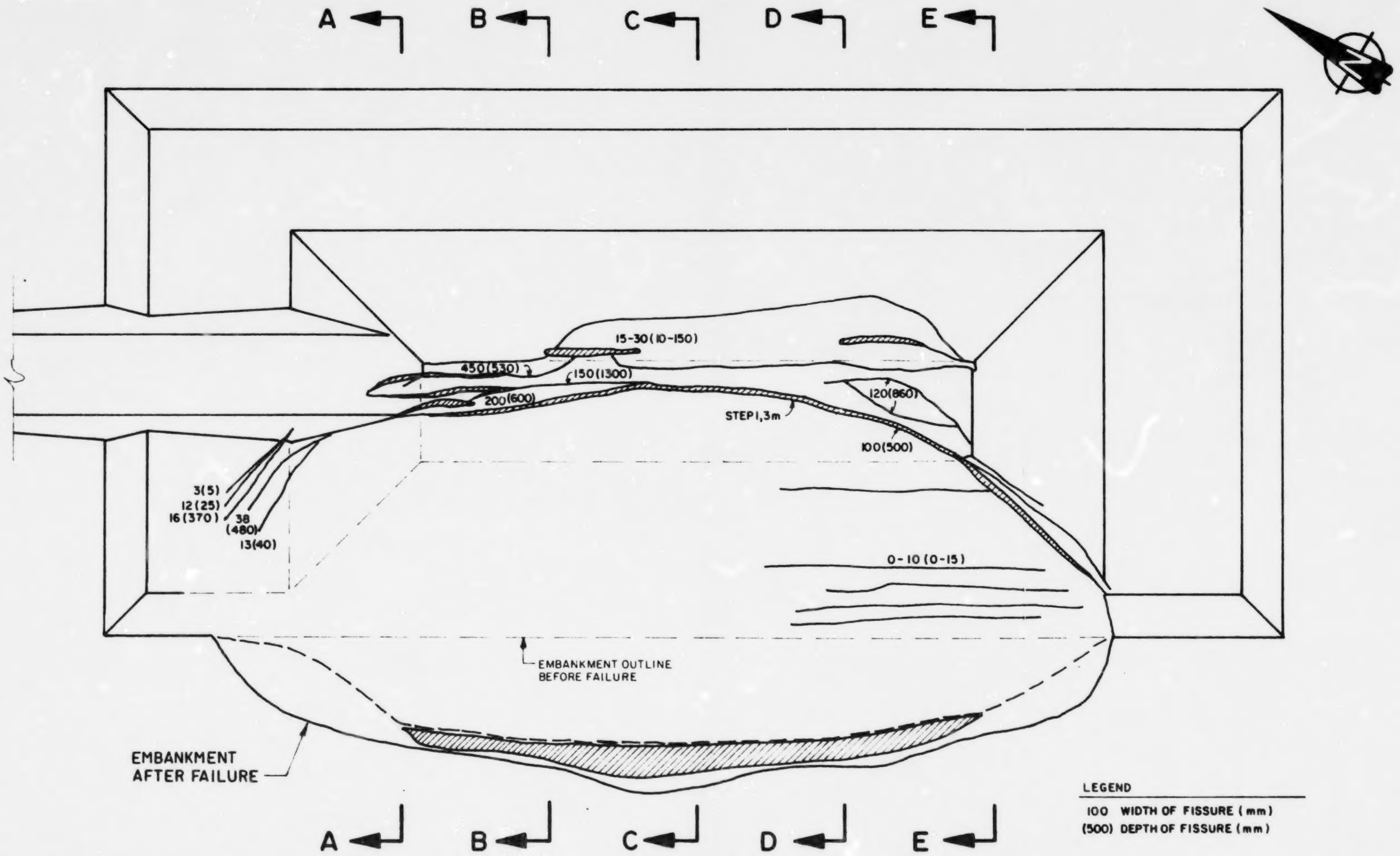

PLAN

SHOWING PATTERN OF FISSURES

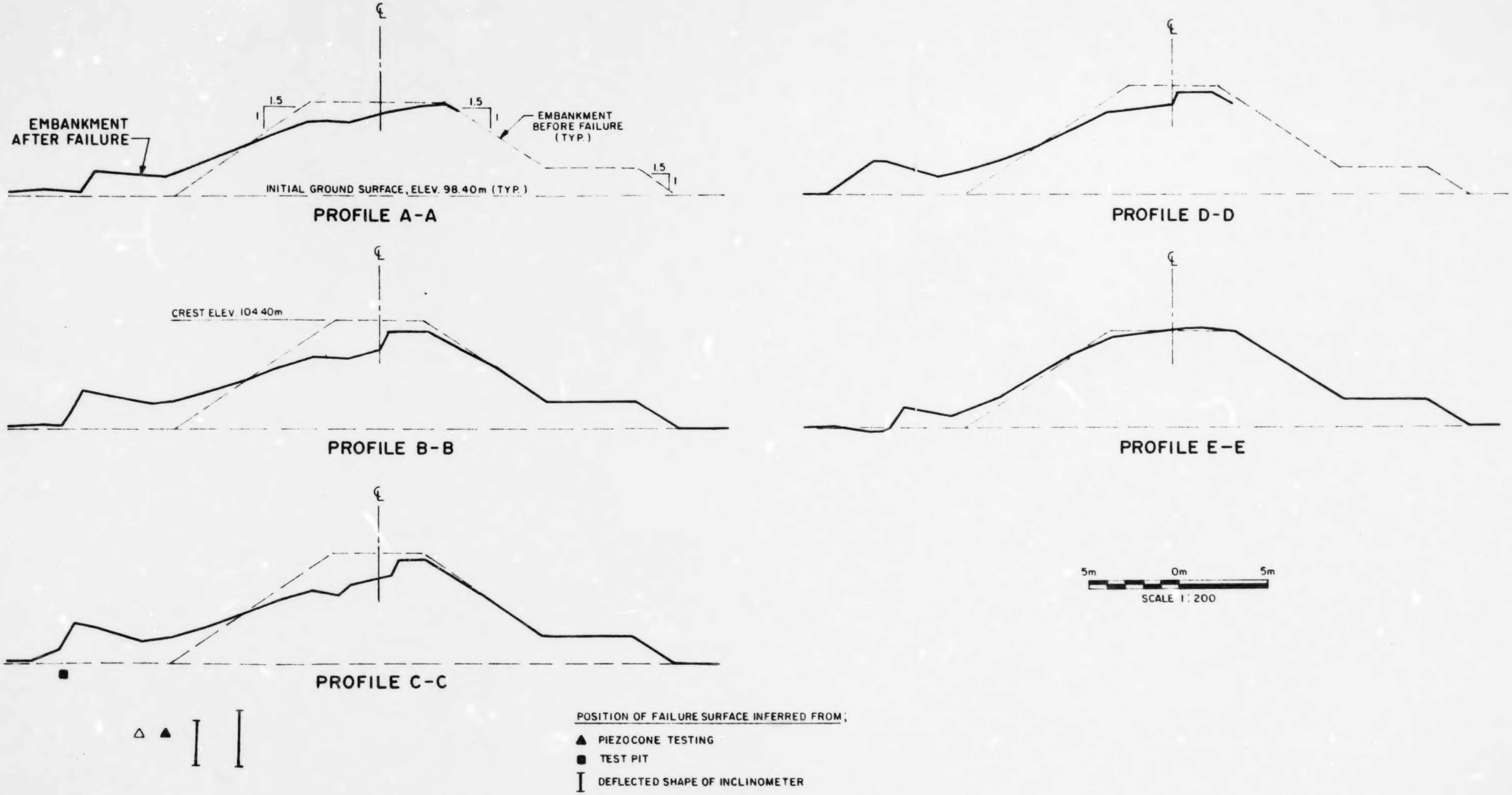

FIGURE 9·1 OBSERVATIONS OF FAILURE, STRIP REINFORCED EMBANKMENT (No. 2)

Golder Associates - Université Laval

FIGURE 9.2 FAILURE OF STRIP REINFORCED EMBANKMENT (NO.2)

a) PIEZOCONE TEST NO. P-2.1

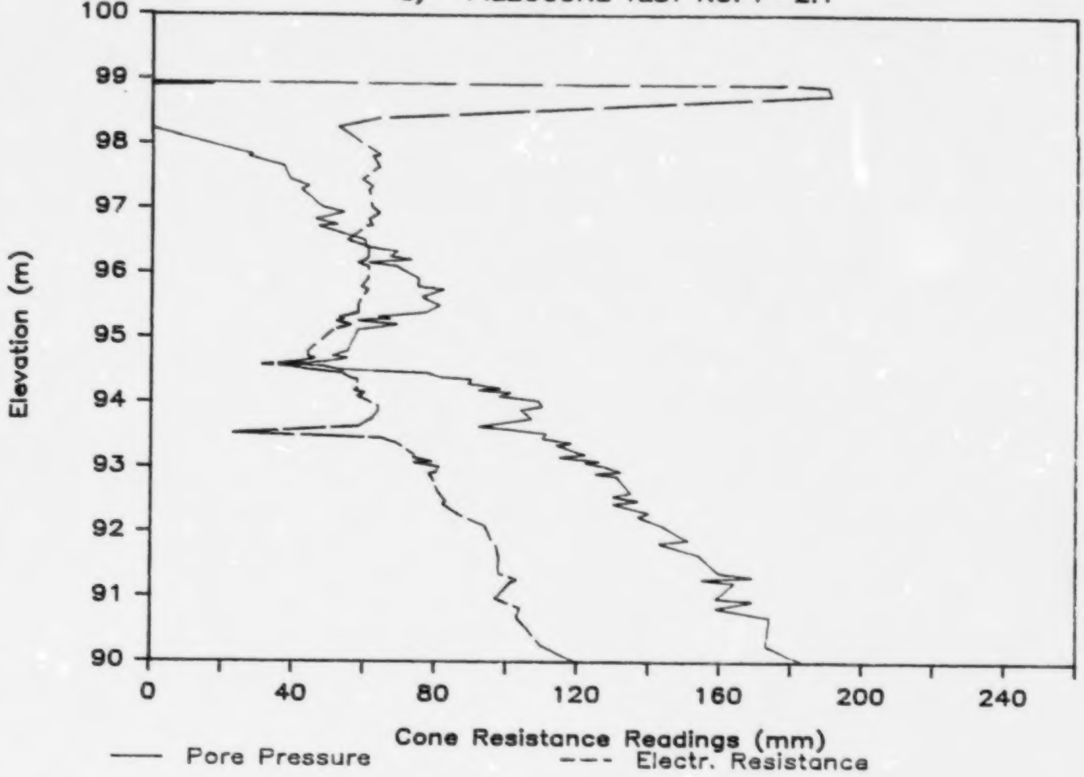

b) PIEZOCONE TEST NO. P-2.2

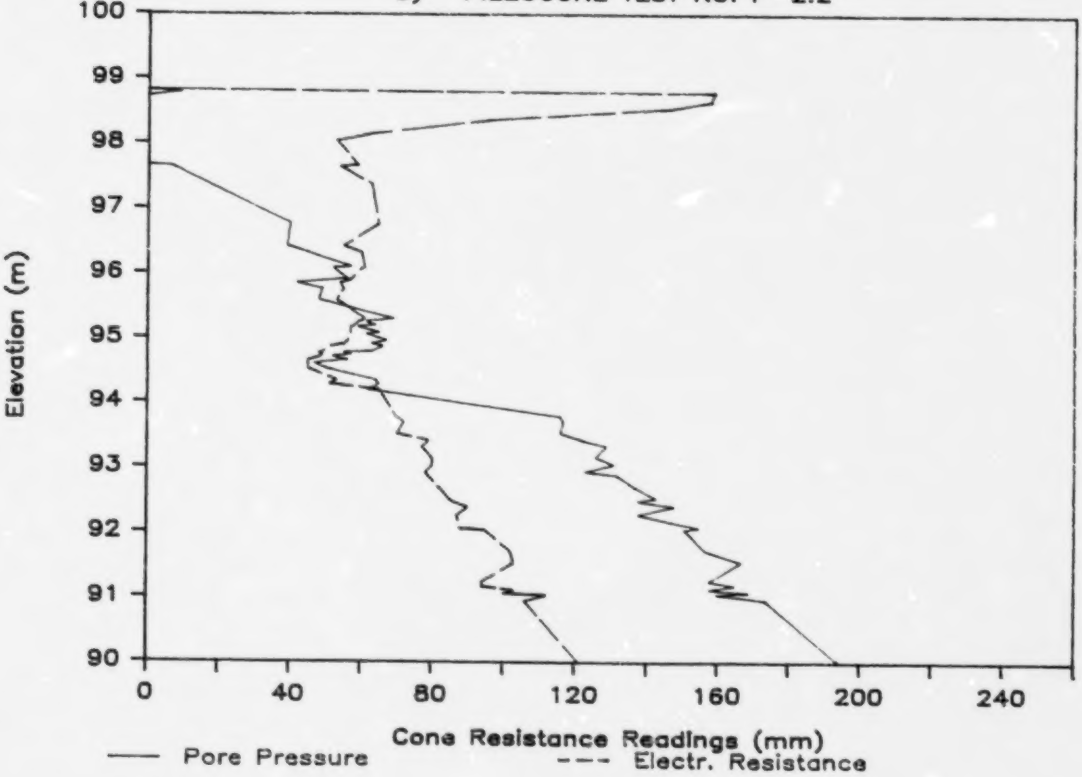

FIGURE 9.3 PIEZOCONE TEST RESULTS (P-2.1 AND P-2.2)

a) PIEZOCONE TEST NO. P-2.3

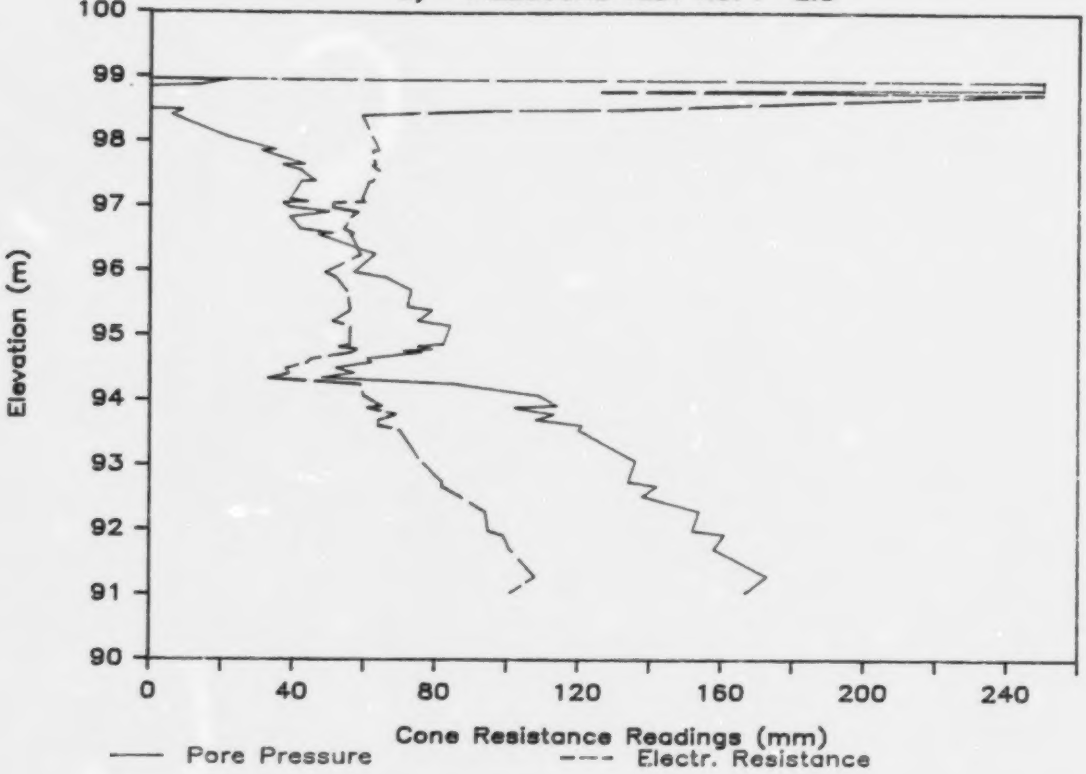

b) PIEZOCONE TEST NO. P-2.4

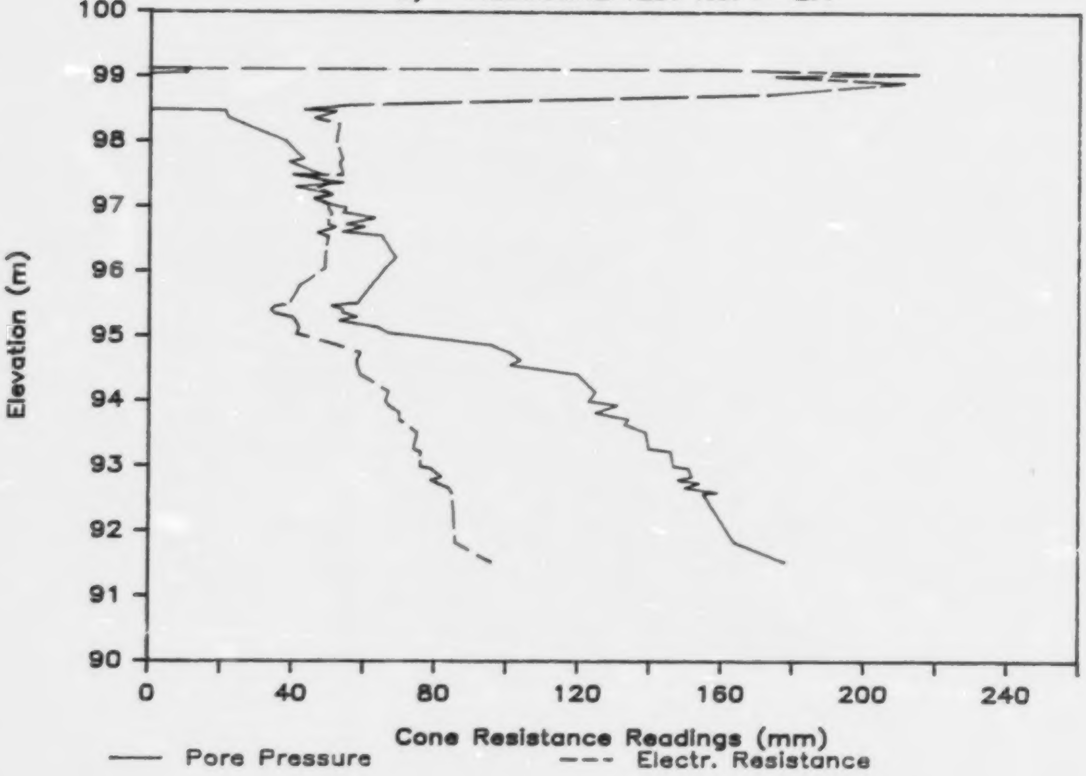

FIGURE 9.4 PIEZOCONE TEST RESULTS (P-2.3 AND P-2.4)

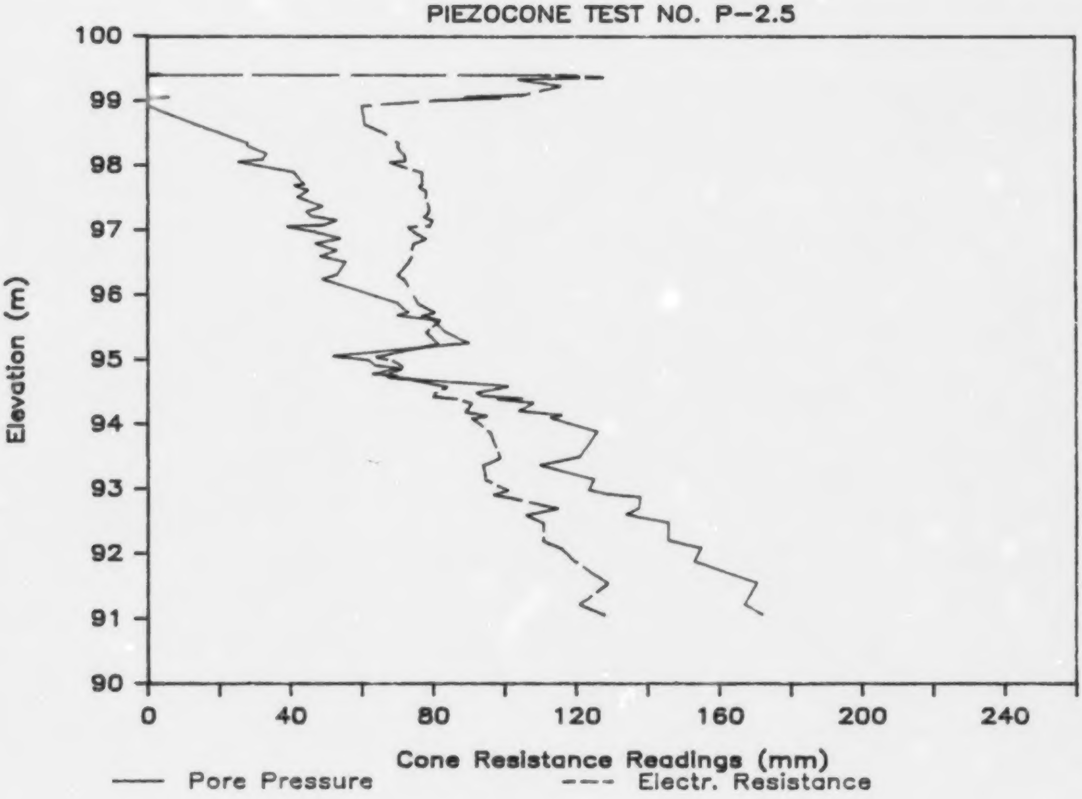

FIGURE 9.5 PIEZOCONE TEST RESULTS (P-2.5)

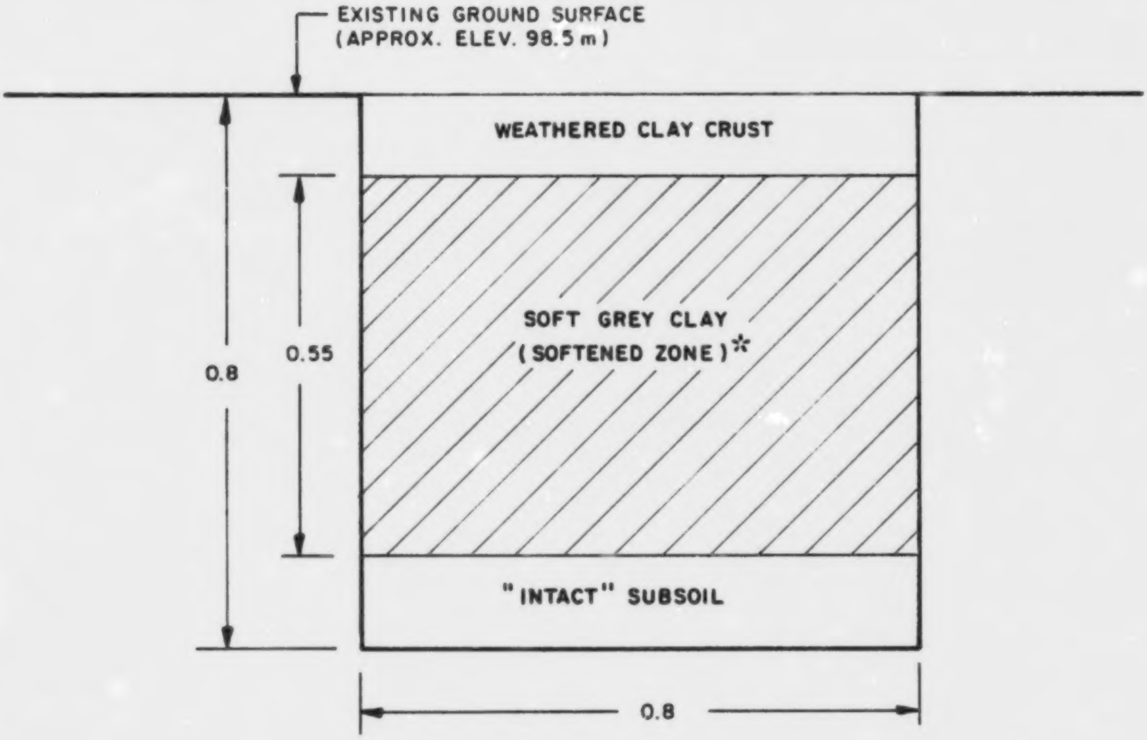

ALL DIMENSIONS IN METRES

*FAILURE ZONE

FIGURE 9.6 CROSS SECTION OF TEST PIT, STRIP REINFORCED EMBANKMENT

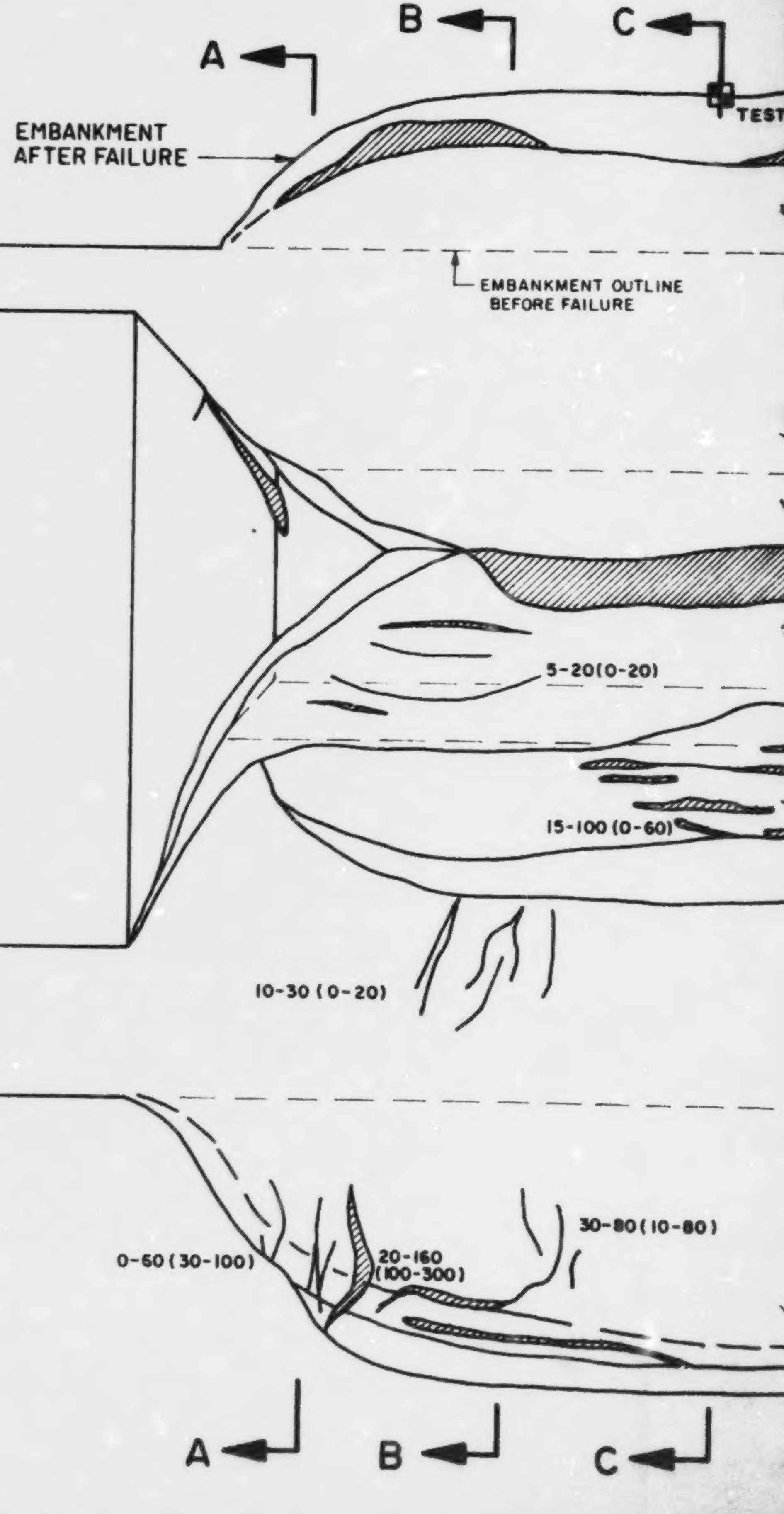
A
B
C
TEST
EMBANKMENT AFTER FAILURE
EMBANKMENT OUTLINE BEFORE FAILURE
5-20(0-20)
15-100 (0-60)
10-30 (0-20)
0-60 (30-100)
20-160 (100-300)
30-80(10-80)
A
B
C

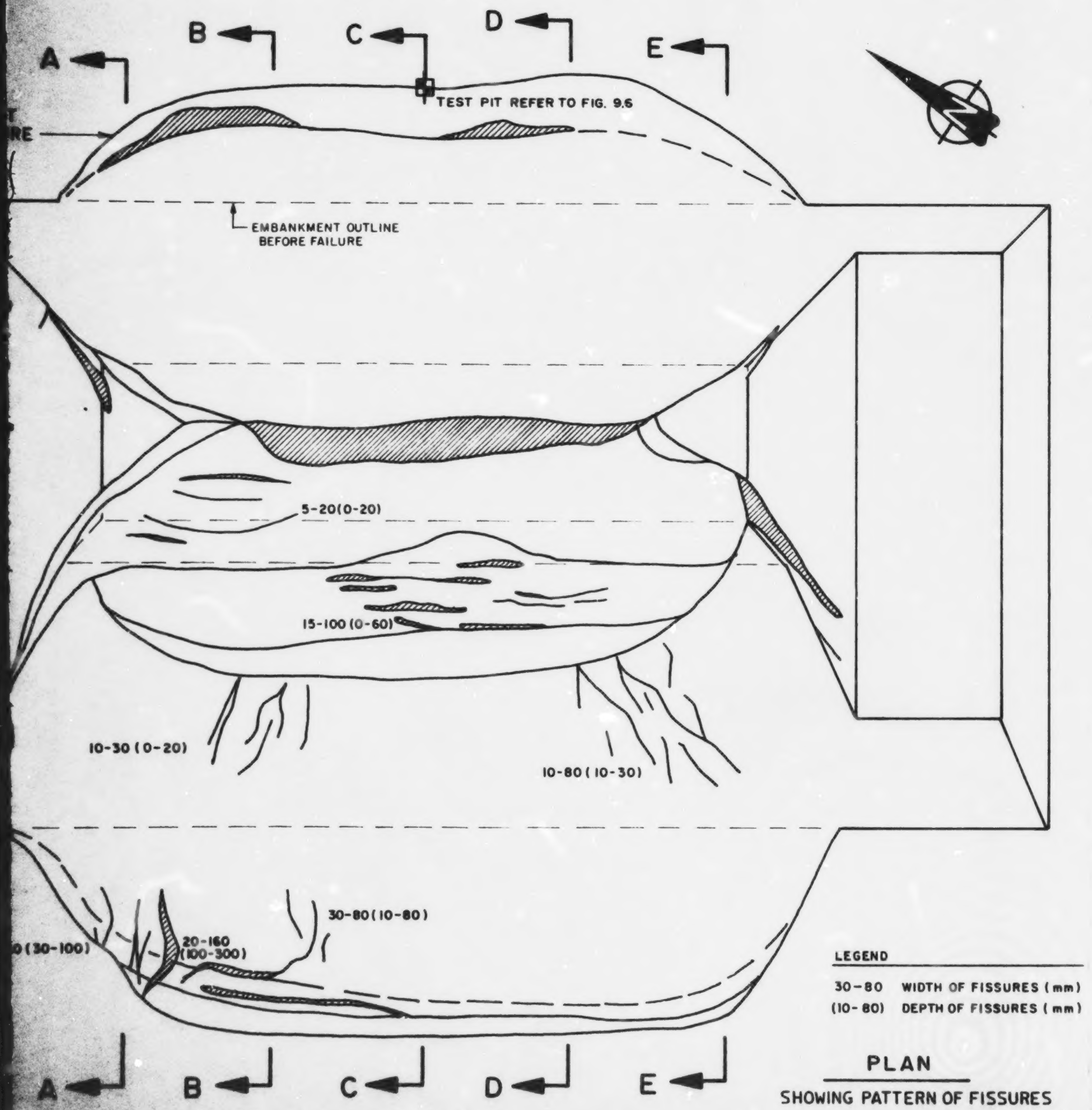

LEGEND

30-80 WIDTH OF FISSURES (mm)
(10-80) DEPTH OF FISSURES (mm)

PLAN
SHOWING PATTERN OF FISSURES

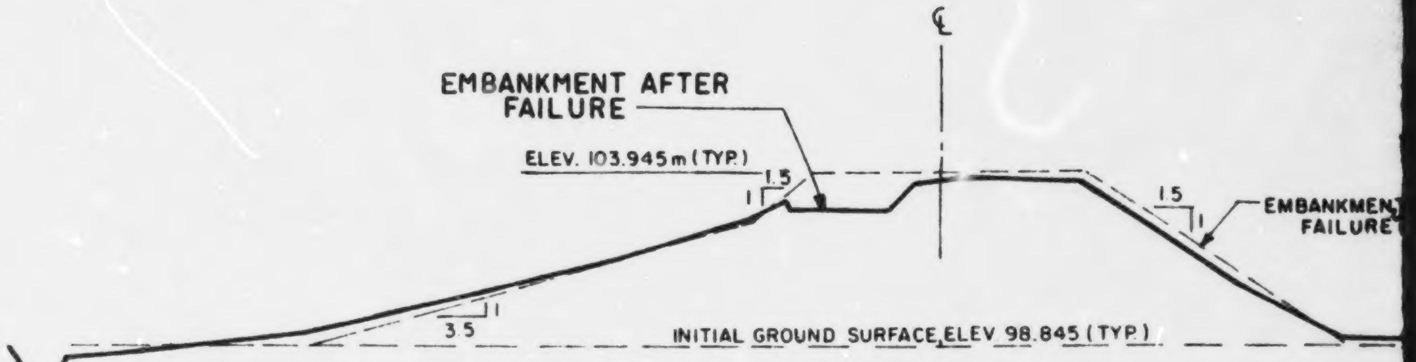

PROFILE A-A

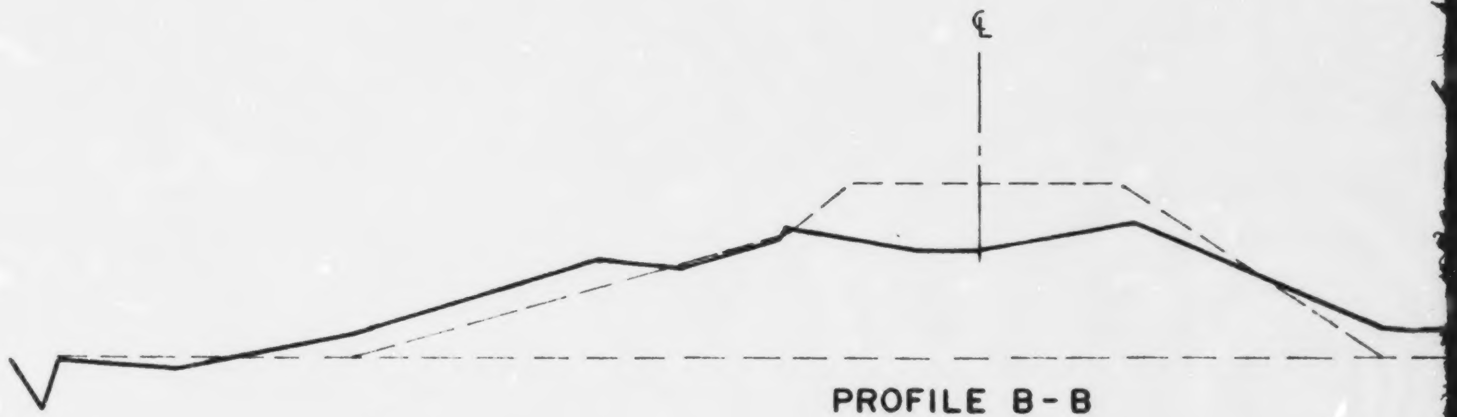

PROFILE B-B

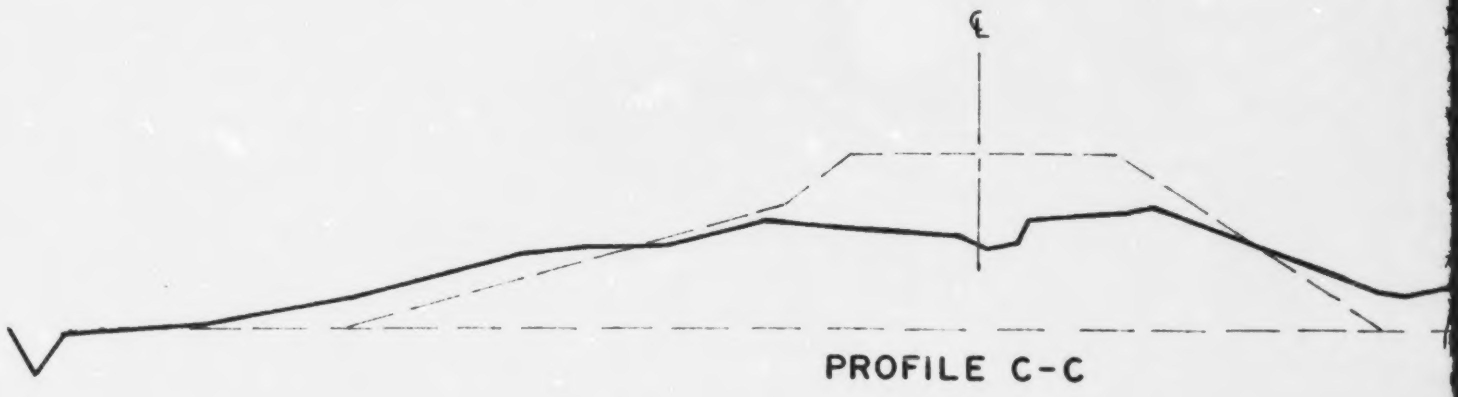

PROFILE C-C

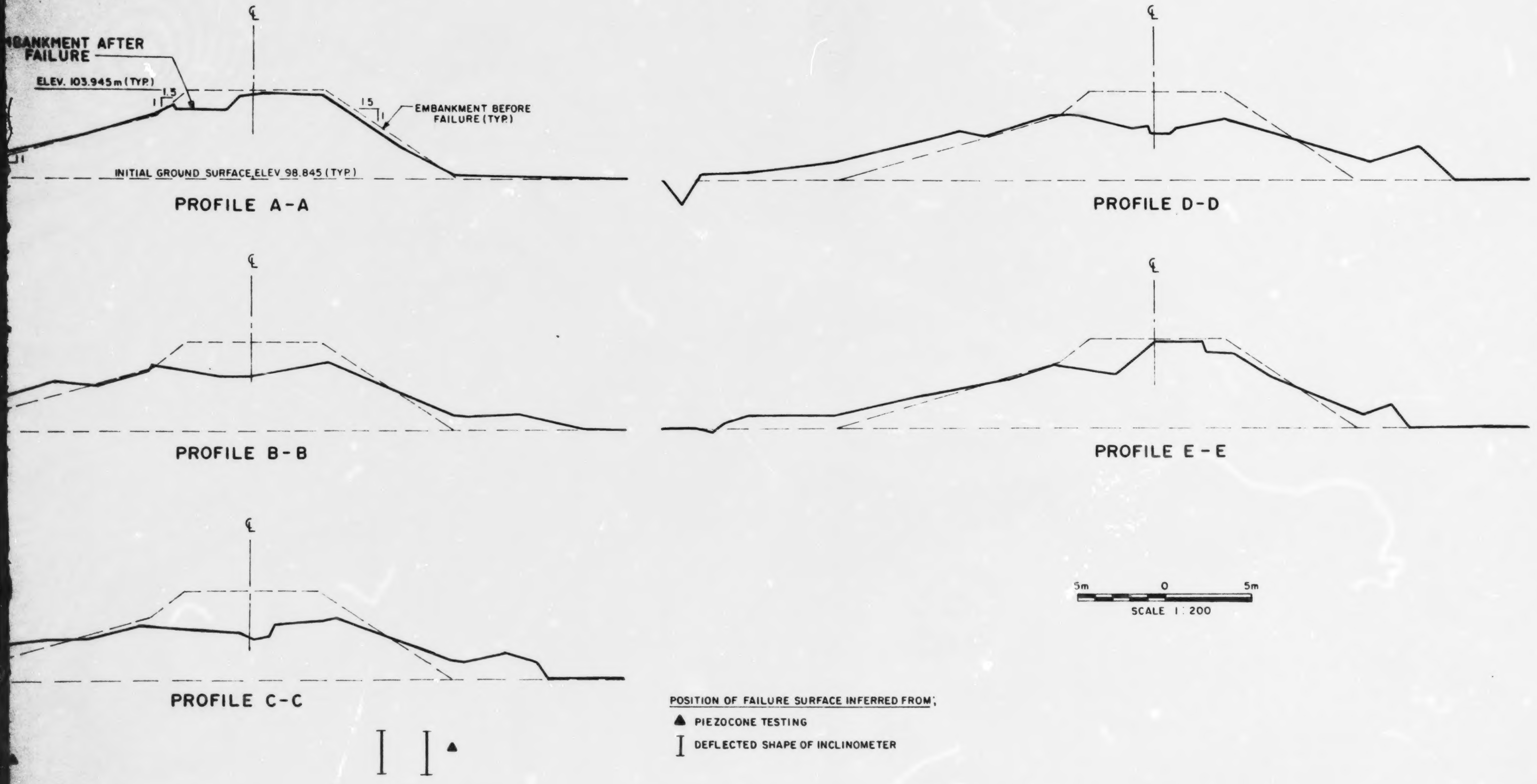

MBANKMENT AFTER FAILURE
ELEV. 103.945 m (TYP.)
1.5
1
1.5
1
EMBANKMENT BEFORE FAILURE (TYP.)
INITIAL GROUND SURFACE ELEV 98.845 (TYP.)
℄
PROFILE A-A
PROFILE D-D
PROFILE B-B
PROFILE E-E
PROFILE C-C
5m
0
5m
SCALE 1:200
POSITION OF FAILURE SURFACE INFERRED FROM;
▲ PIEZOCONE TESTING
I DEFLECTED SHAPE OF INCLINOMETER

FIGURE 9·7 OBSERVATIONS OF FAILURE, CONTROL EMBANKMENT (No.1)

FIGURE 9.8 FAILURE OF CONTROL EMBANKMENT (NO.1)

FIGURE 9.9 FAILURE AT BACK OF CONTROL EMBANKMENT (NO.1)

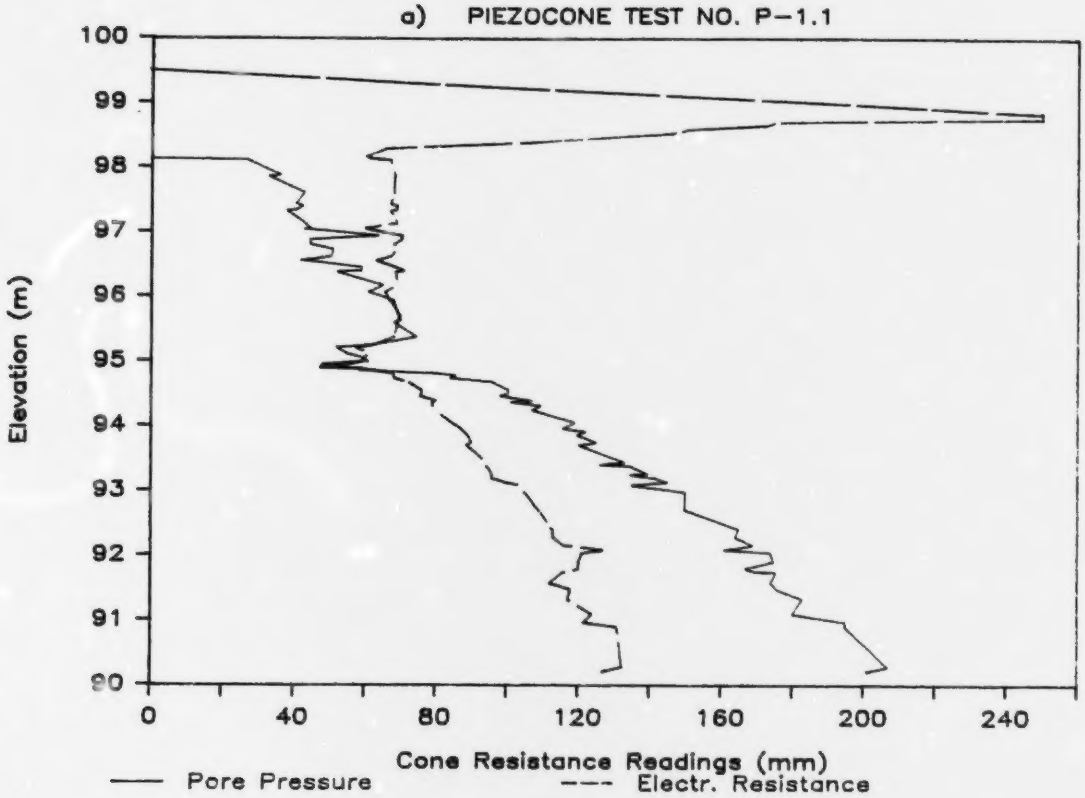

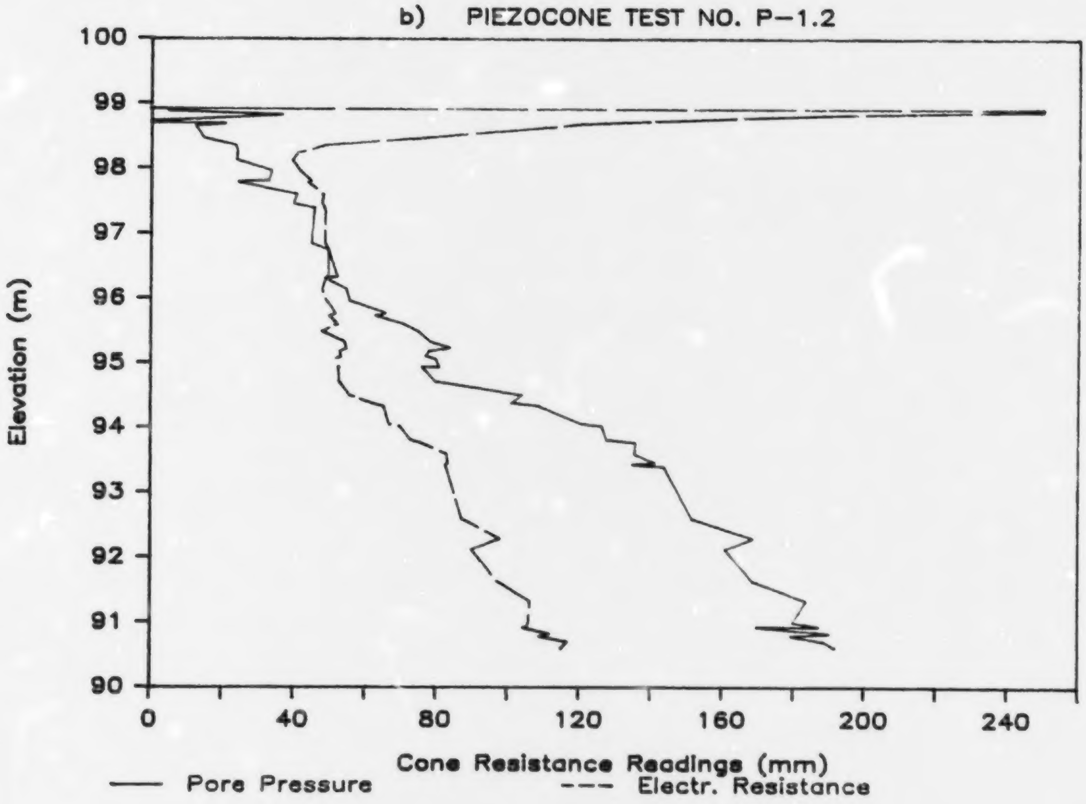

FIGURE 9.10 PIEZOCONE TEST RESULTS (P-1.1 AND P-1.2)

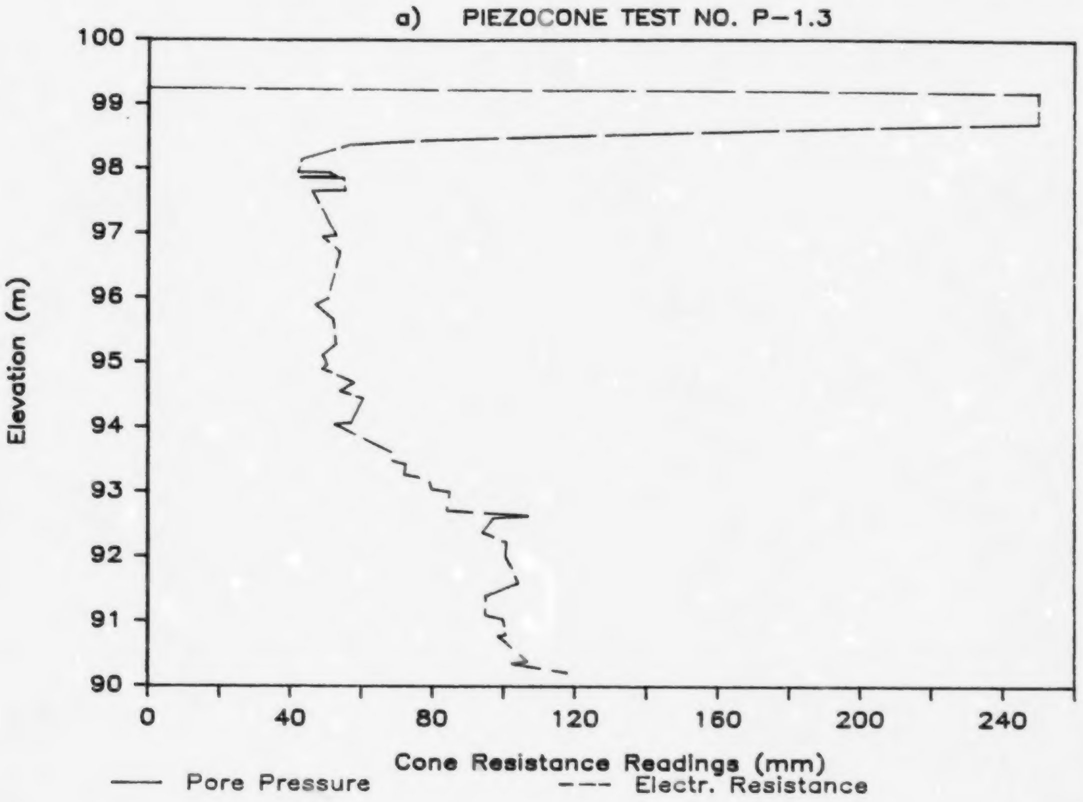

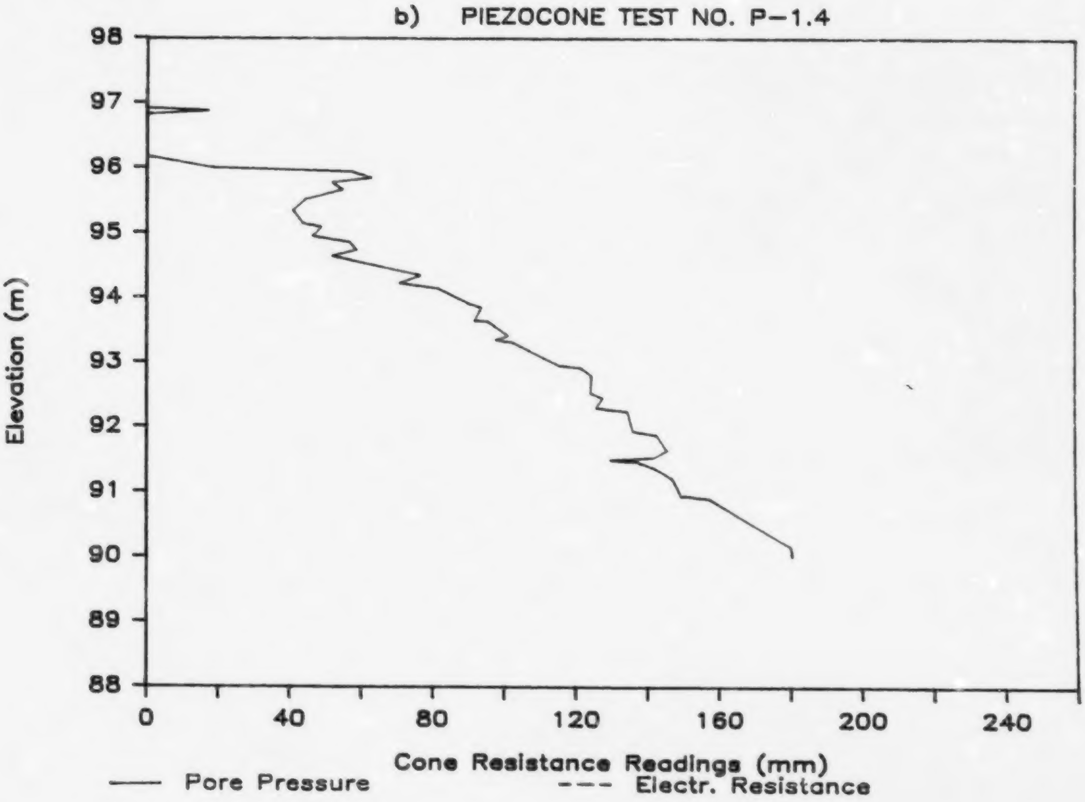

FIGURE 9.11 PIEZOCONE TEST RESULTS (P-1.3 AND P-1.4)

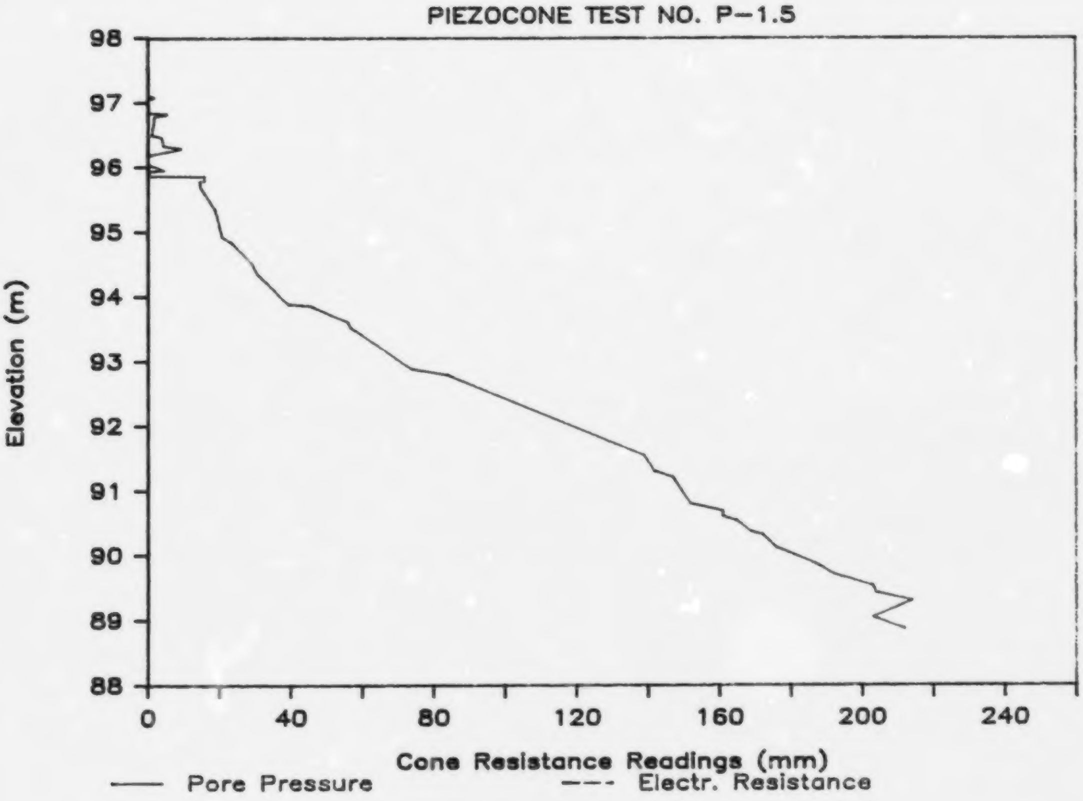

FIGURE 9.12 PIEZOCONE TEST RESULTS (P-1.5)

a) PIEZOCONE TEST NO. P-2.6

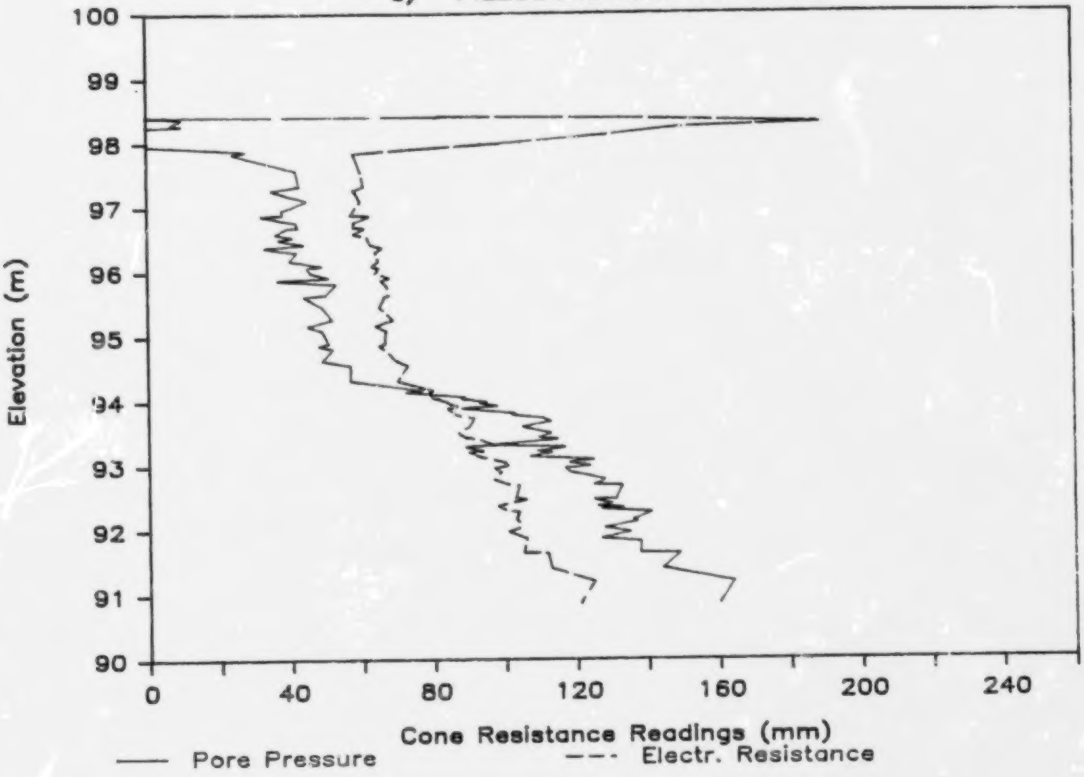

b) PIEZOCONE TEST NO. P-2.7

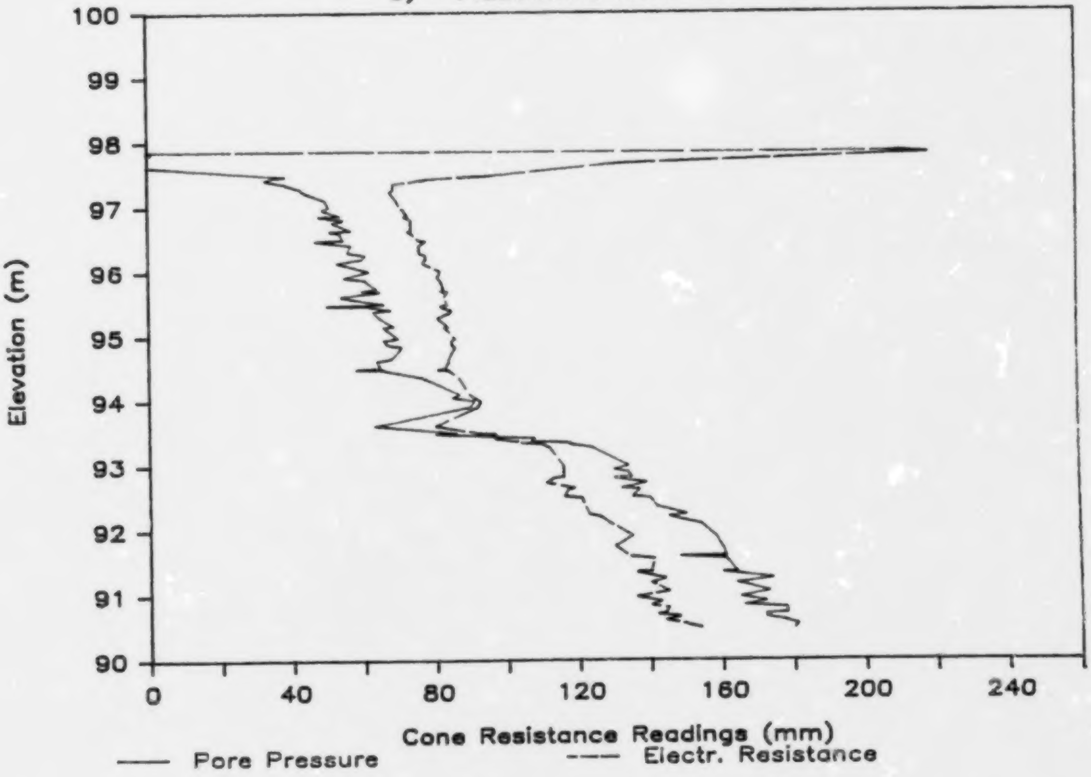

FIGURE 9.13 PIEZOCONE TEST RESULTS (P-2.6 AND P-2.7)

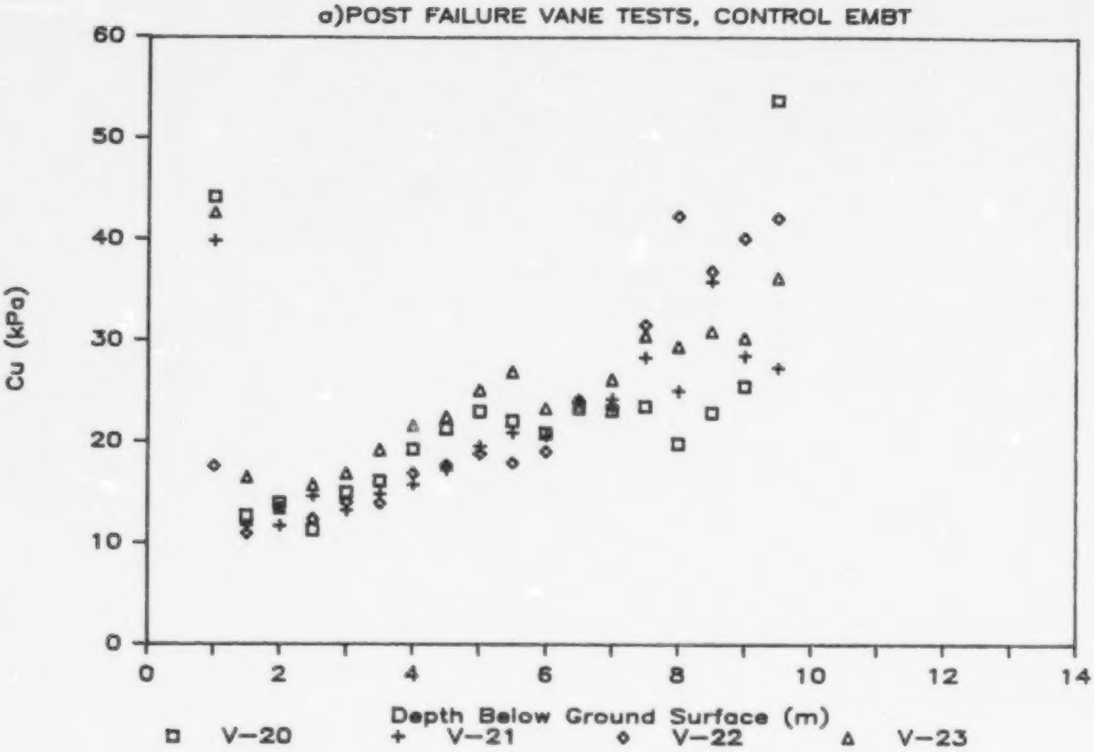

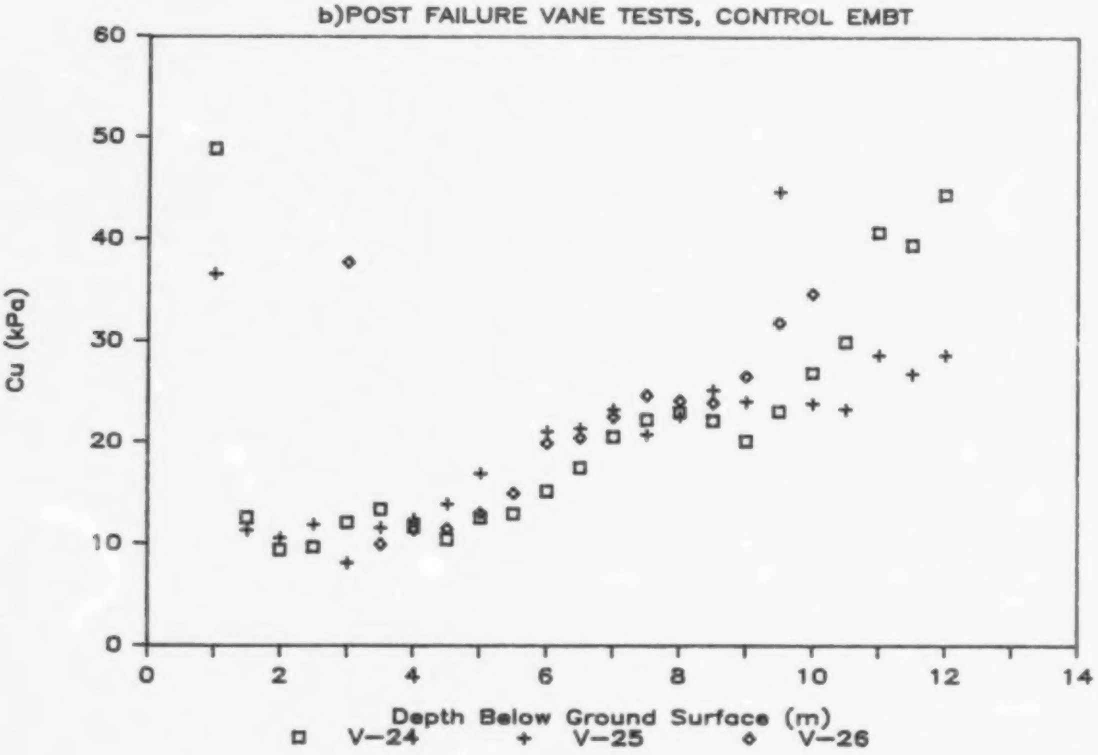

FIGURE 9.14 POST-FAILURE VANE TESTS FOR CONTROL EMBANKMENT (NO. 1)

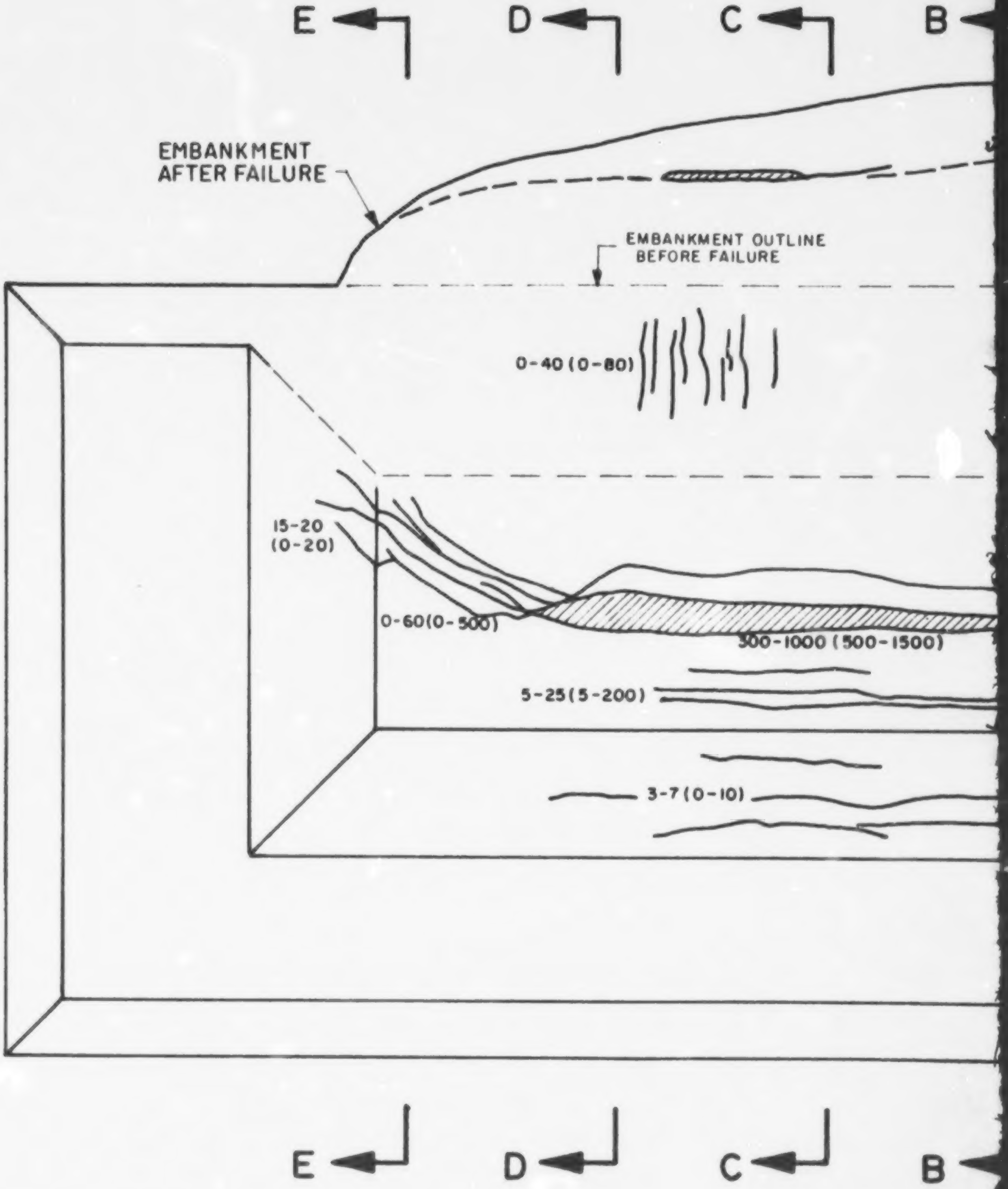

PLAN

SHOWING PATTERN OF FISSU

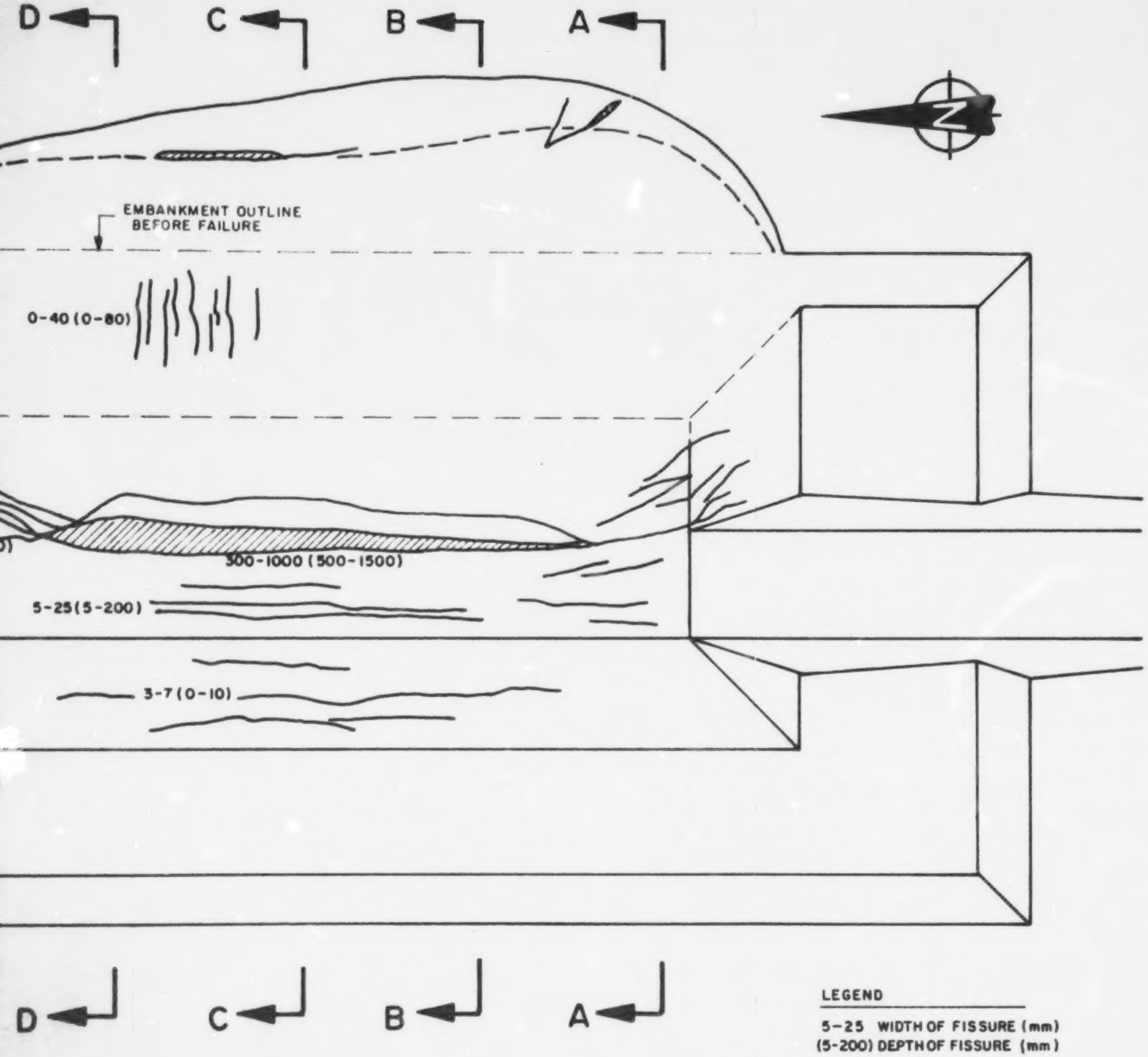
D
C
B
A
N
EMBANKMENT OUTLINE BEFORE FAILURE
0-40 (0-80)
300-1000 (500-1500)
5-25(5-200)
3-7 (0-10)
LEGEND
5-25 WIDTH OF FISSURE (mm)
(5-200) DEPTH OF FISSURE (mm)

PLAN

SHOWING PATTERN OF FISSURES

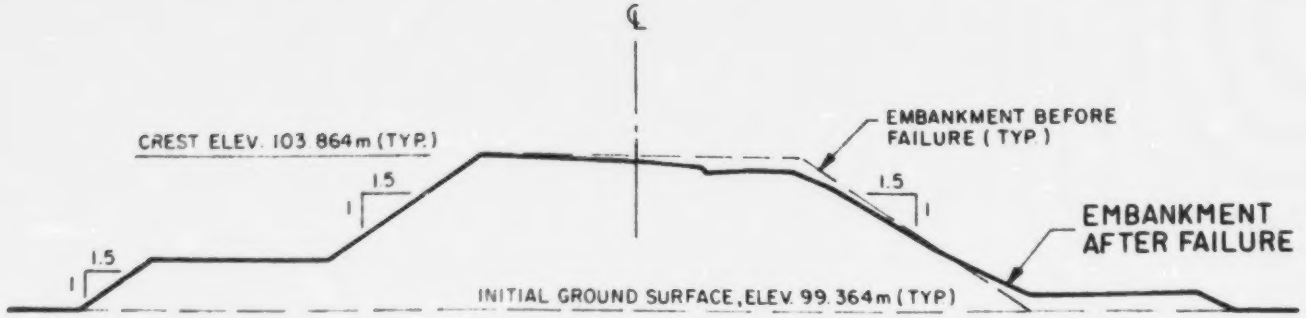
℄
CREST ELEV. 103.864m (TYP.)
EMBANKMENT BEFORE FAILURE (TYP.)
1.5
1
EMBANKMENT AFTER FAILURE
INITIAL GROUND SURFACE, ELEV. 99.364m (TYP)

PROFILE A-A

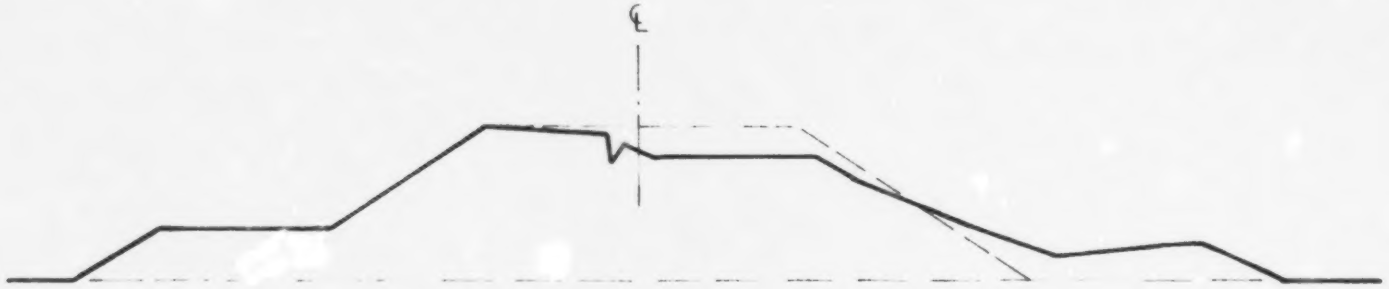

PROFILE B-B

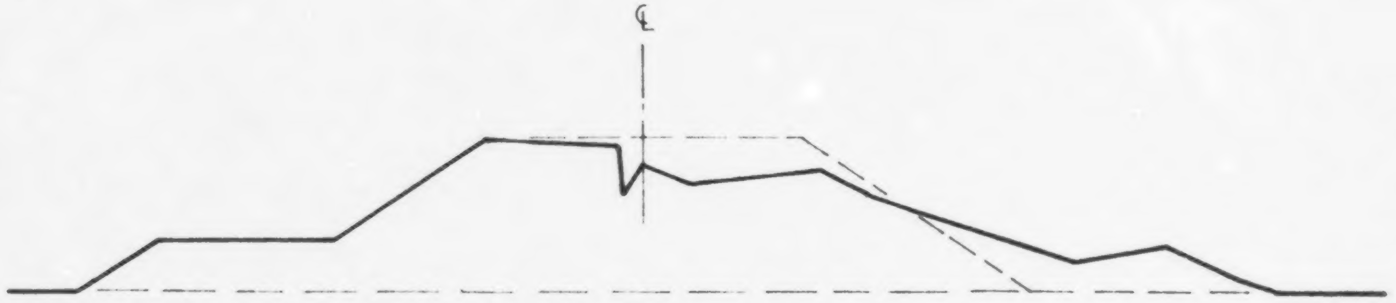

PROFILE C-C

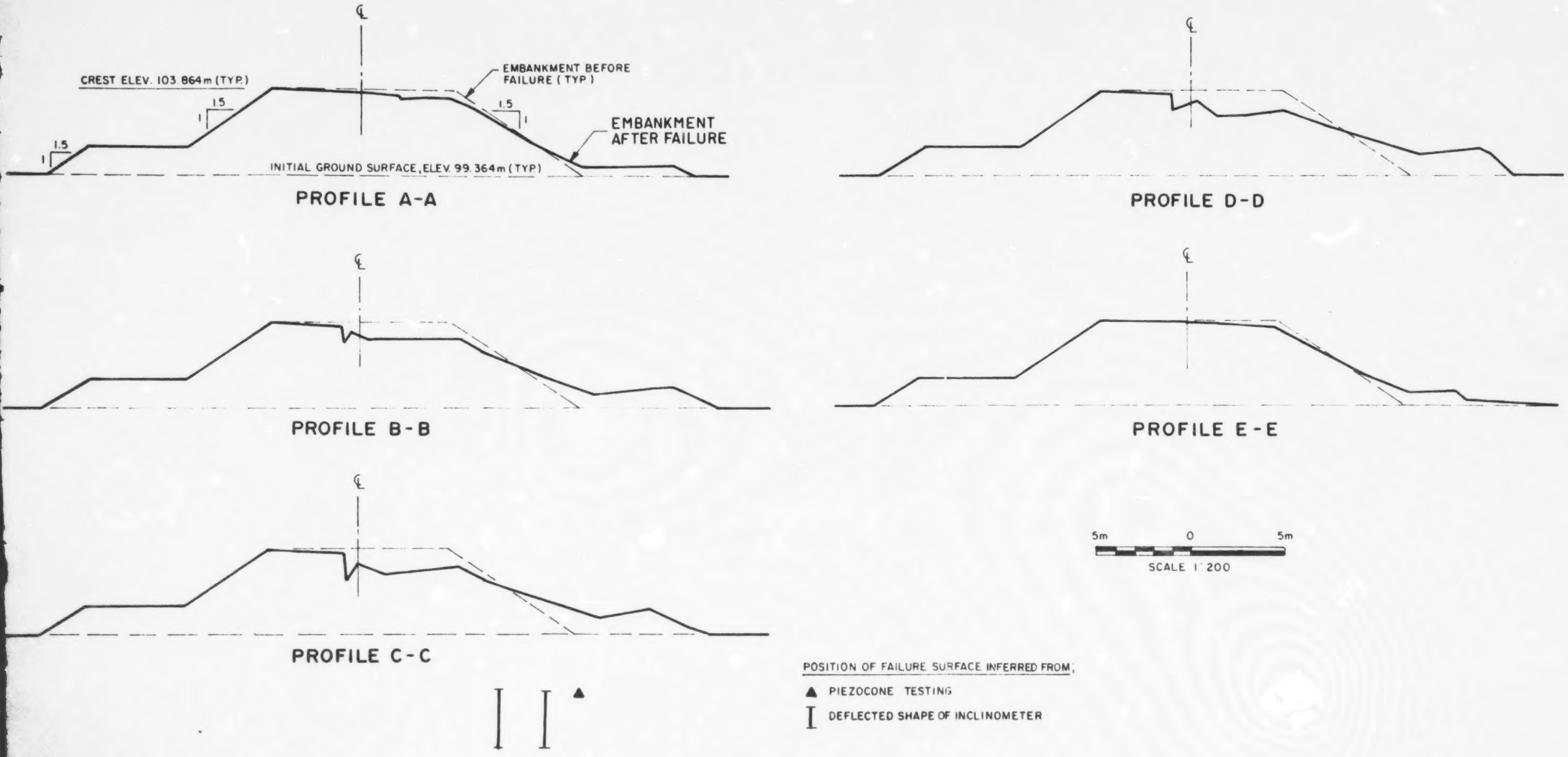
℄
CREST ELEV. 103.864m (TYP.)
1.5
1
EMBANKMENT BEFORE FAILURE (TYP)
EMBANKMENT AFTER FAILURE
INITIAL GROUND SURFACE, ELEV. 99.364m (TYP)
PROFILE A-A
PROFILE B-B
PROFILE C-C
PROFILE D-D
PROFILE E-E
5m
0
5m
SCALE 1:200
POSITION OF FAILURE SURFACE INFERRED FROM;
▲ PIEZOCONE TESTING
I DEFLECTED SHAPE OF INCLINOMETER

FIGURE 9.15 OBSERVATIONS OF FAILURE, GEOCELL REINFORCED EMBANKMENT (No.3)

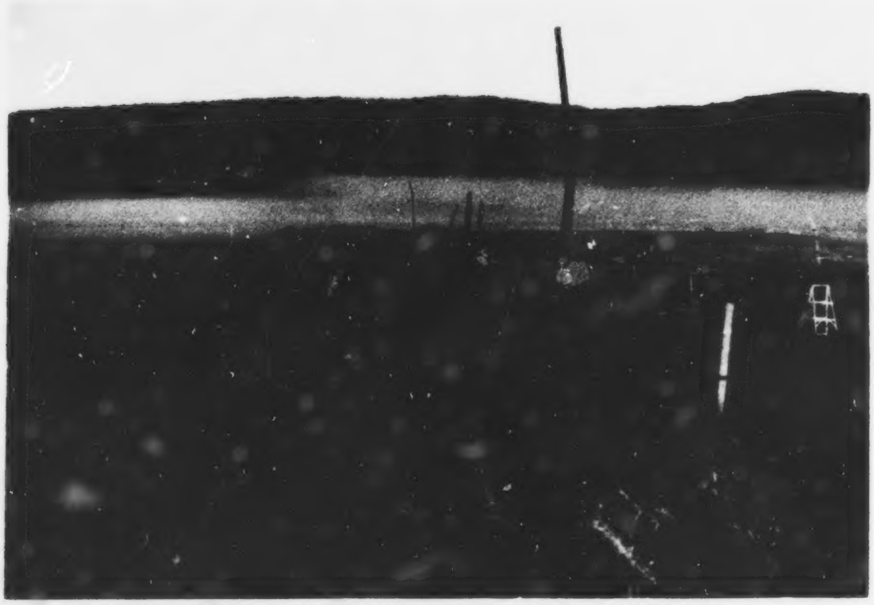

FIGURE 9.16 FAILURE OF GEOCELL REINFORCED EMBANKMENT (NO.3)

a) PIEZOCONE TEST NO. P-3.1

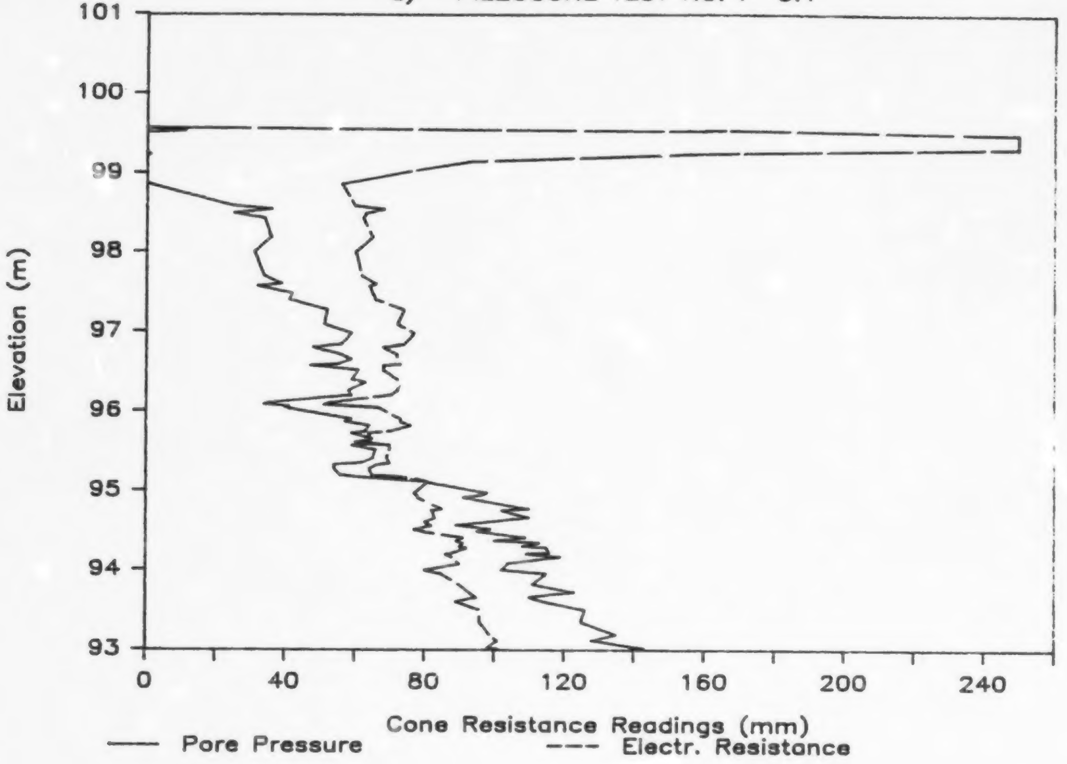

b) PIEZOCONE TEST NO. P-3.2

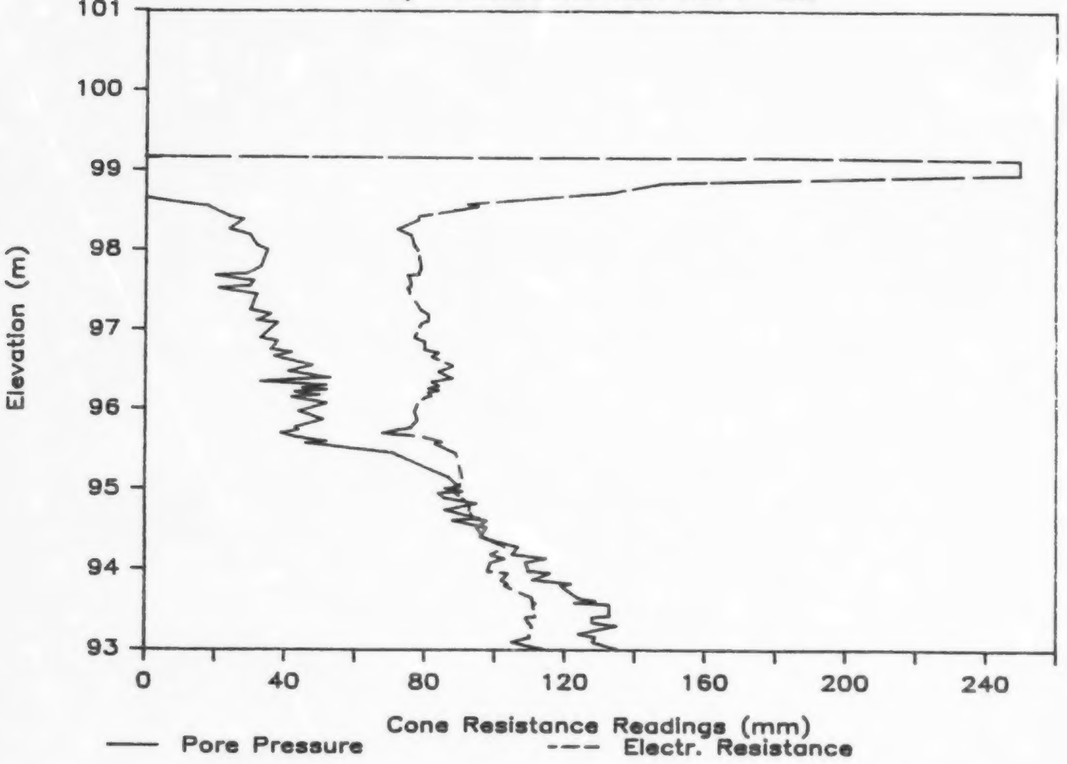

FIGURE 9.17 PIEZOCONE TEST RESULTS (P-3.1 AND P-3.2)

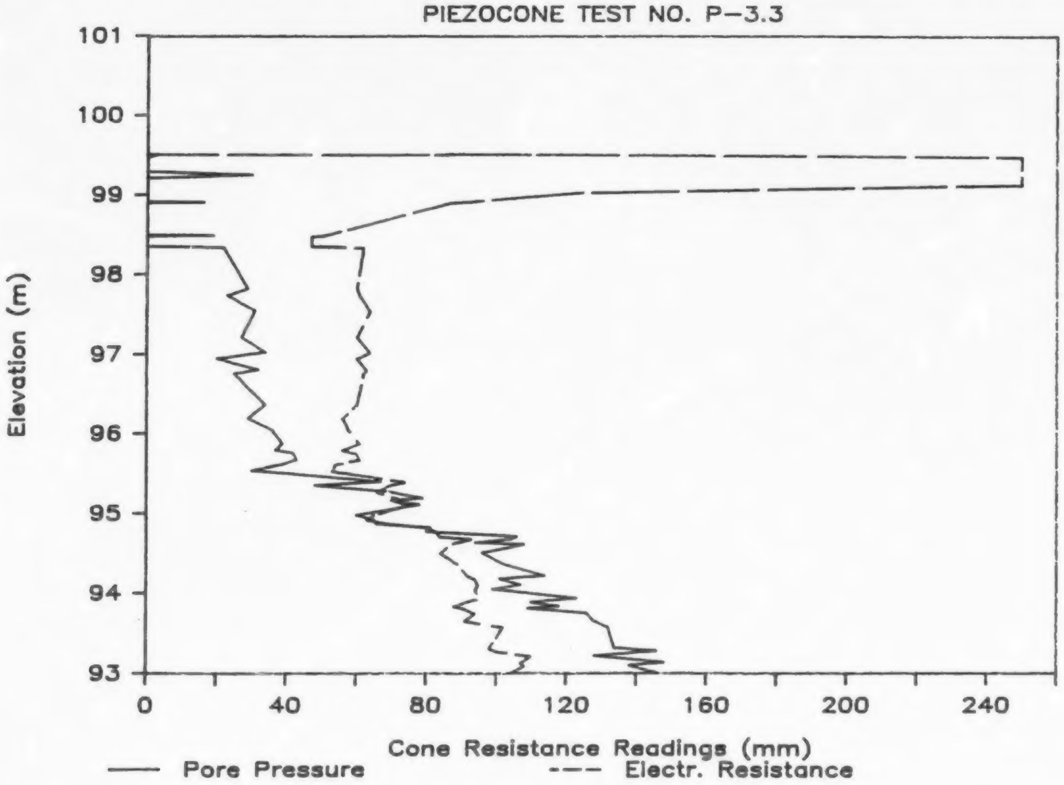

FIGURE 9.18 PIEZOCONE TEST RESULTS (P-3.3)

SECTION 10

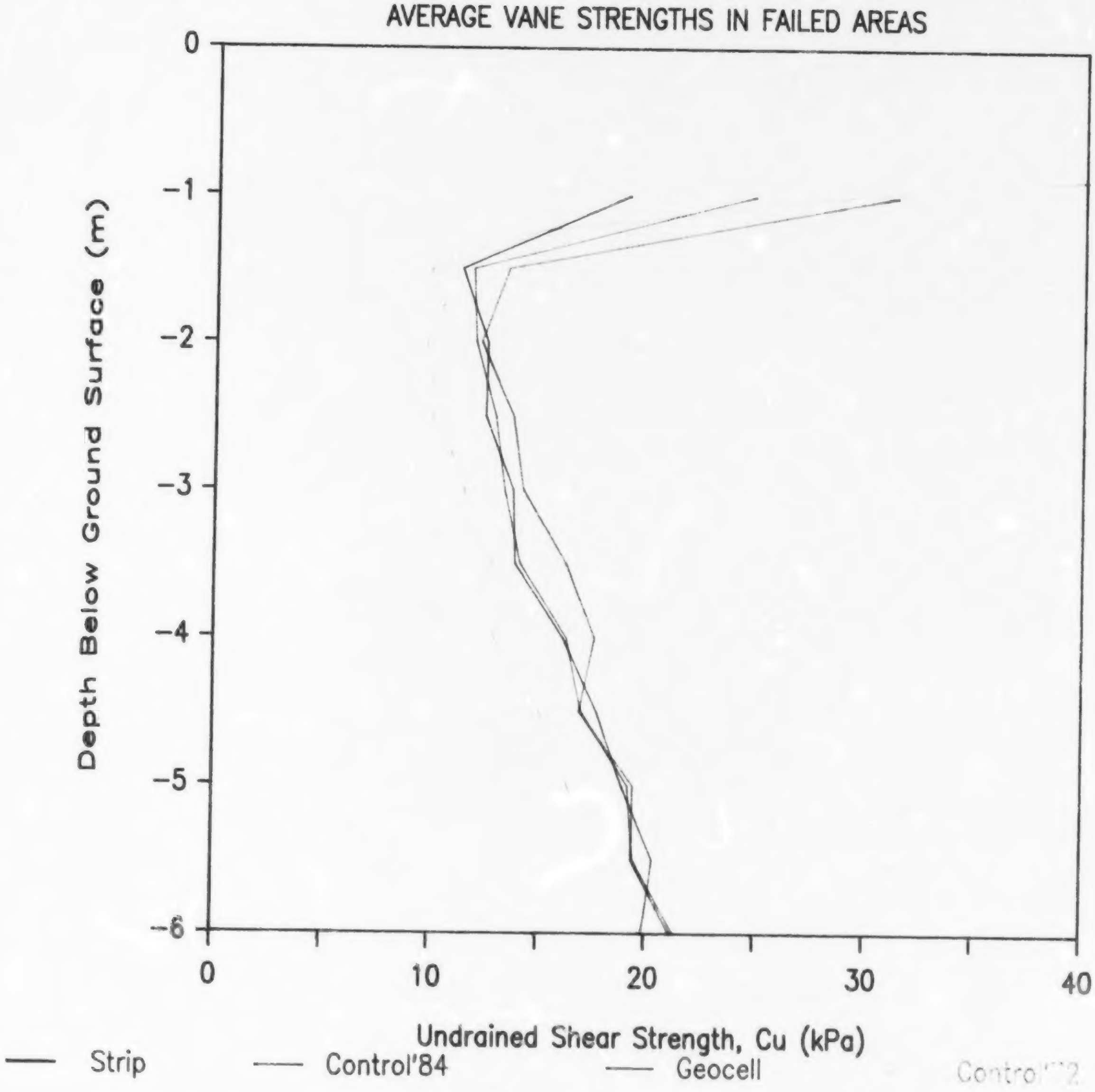

FIGURE 10.1 AVERAGE VANE STRENGTH PROFILE IN FAILED AREAS

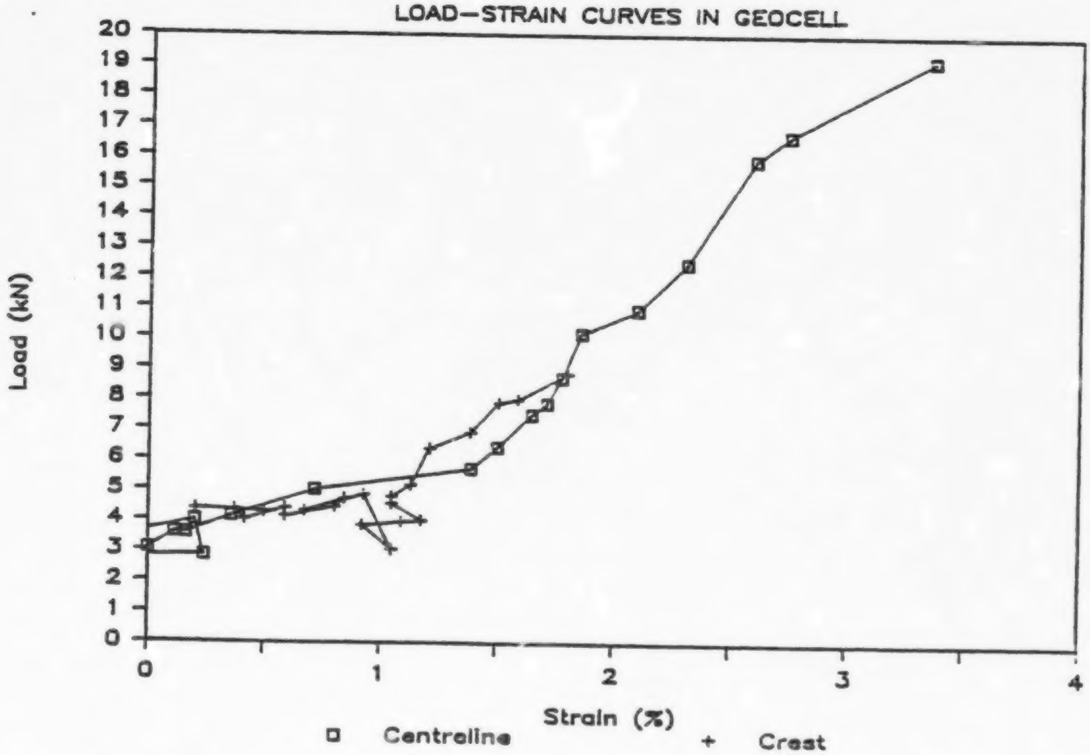

FIGURE 10.2 LOAD-STRAIN CHARACTERISTICS OF GEOCELL MATTRESS

841-1083

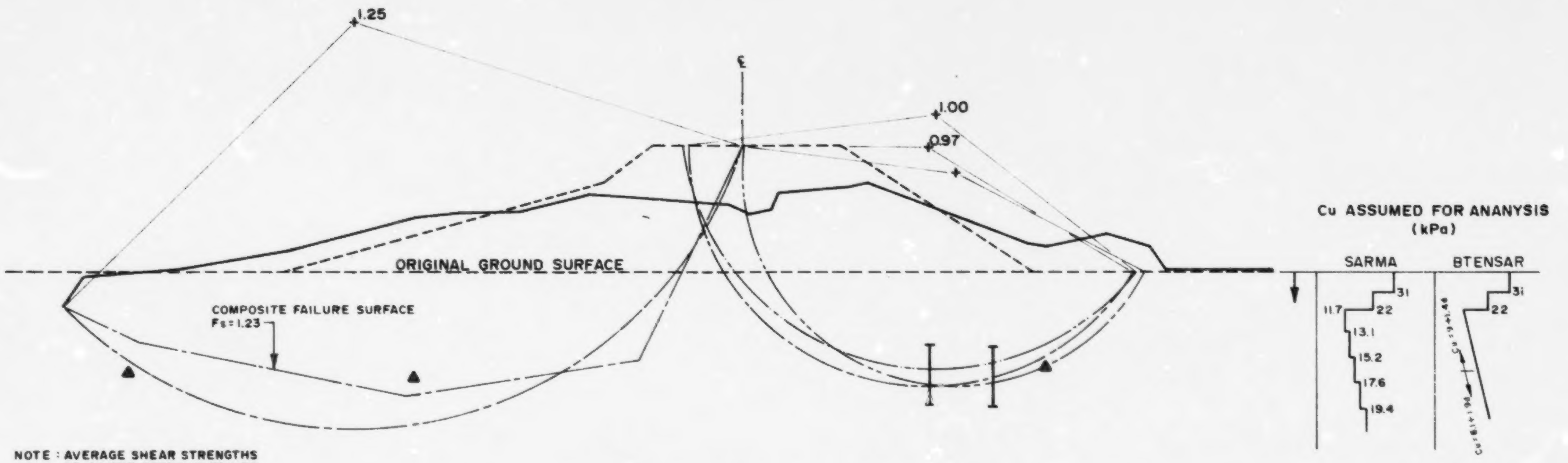

NOTE : AVERAGE SHEAR STRENGTHS
OF 4 VANE TESTS IN FAILED
AREA TAKEN FOR SLOPE
STABILITY ANALYSIS.

AXIS PROFILE

CONTROL EMBANKMENT (Nº 1)

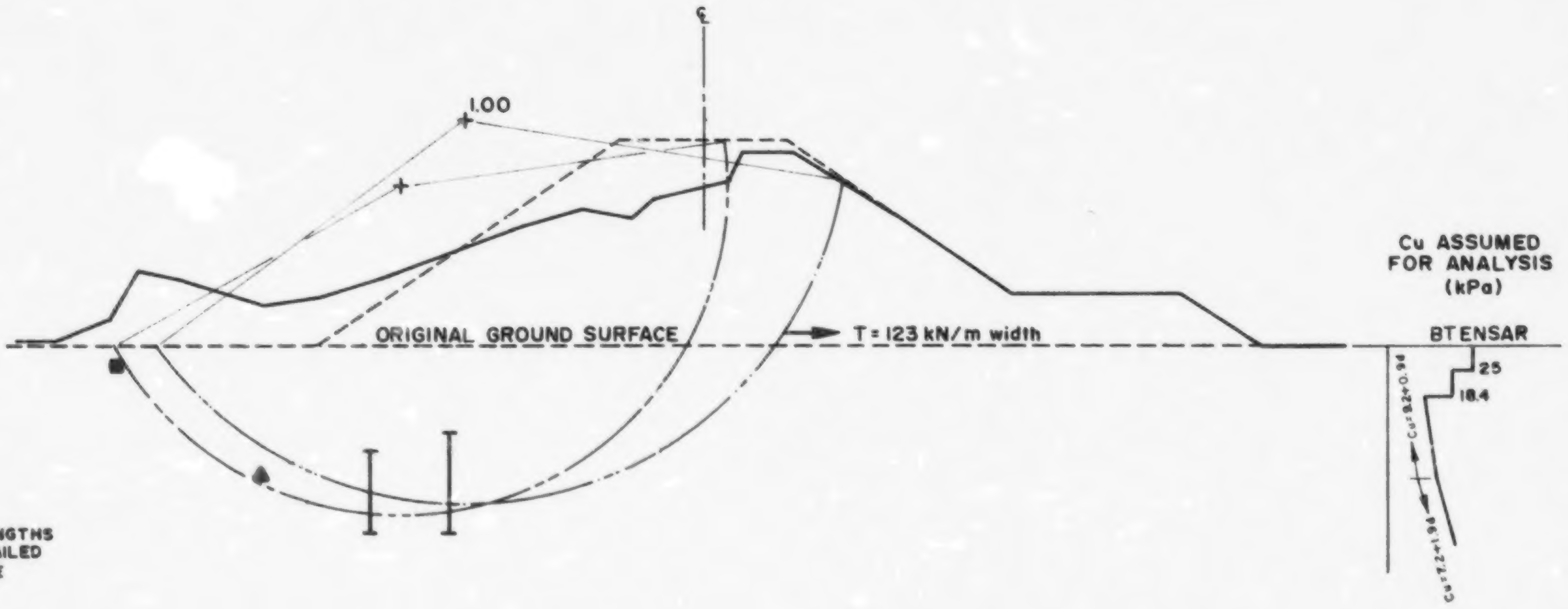

NOTE : AVERAGE SHEAR STRENGTHS
OF 2 VANE TESTS IN FAILED
AREA TAKEN FOR SLOPE
STABILITY ANALYSIS.

AXIS PROFILE

STRIP REINFORCED EMBANKMENT (Nº 2)

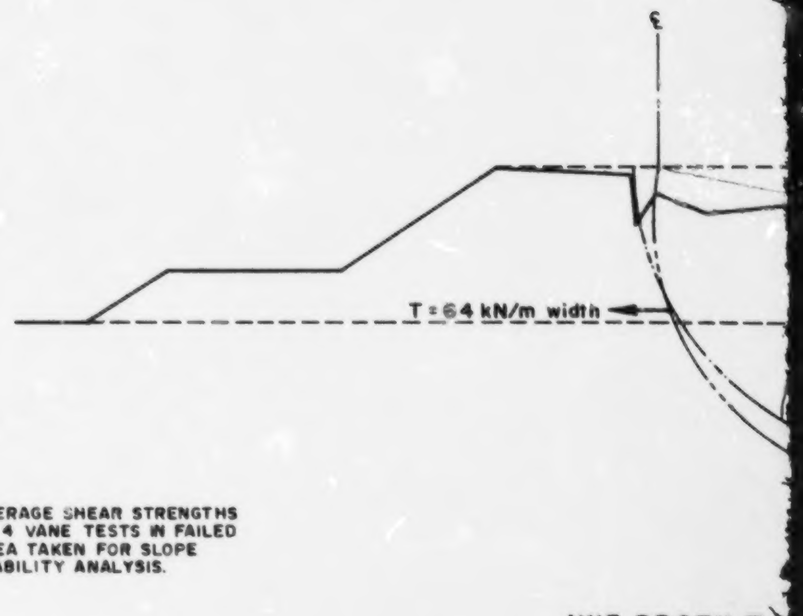

NOTE : AVERAGE SHEAR STRENGTHS
OF 4 VANE TESTS IN FAILED
AREA TAKEN FOR SLOPE
STABILITY ANALYSIS.

AXIS PROFILE

GEOCELL REINFORCED EMBAN

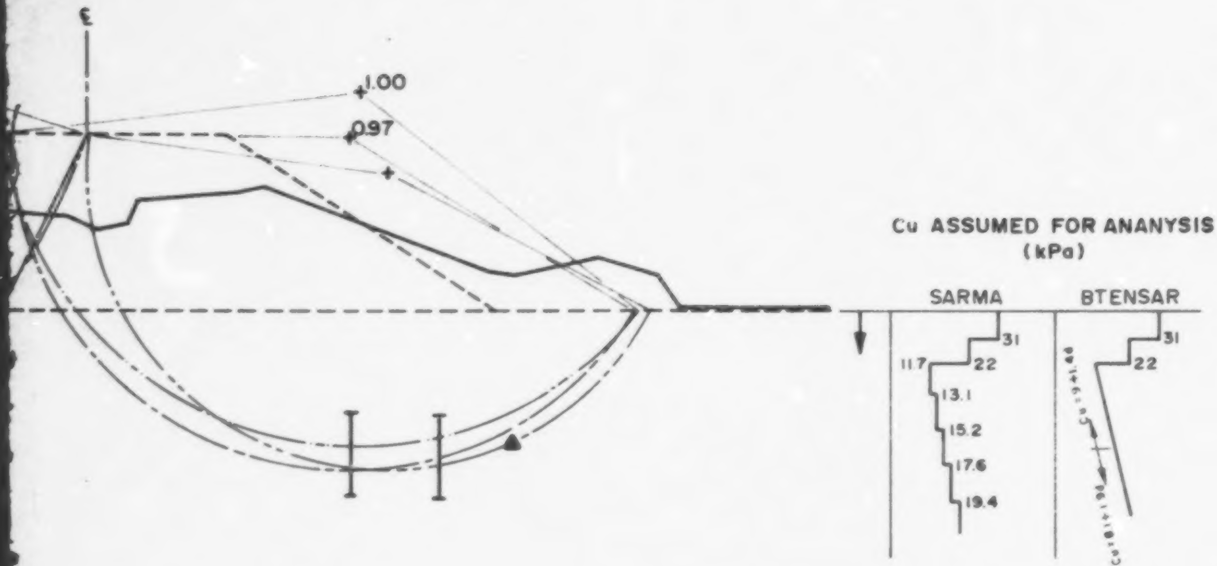

S PROFILE

BANKMENT (Nº 1)

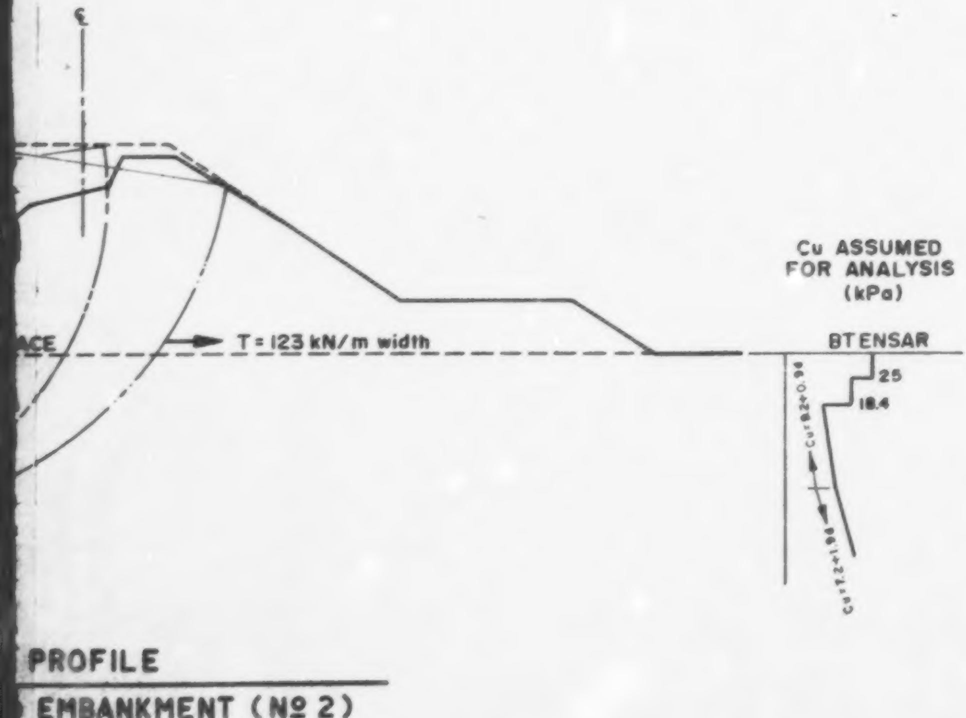

NOTE : AVERAGE SHEAR STRENGTHS OF 4 VANE TESTS IN FAILED AREA TAKEN FOR SLOPE STABILITY ANALYSIS.

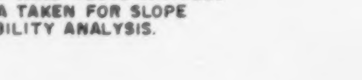

PROFILE

EMBANKMENT (Nº 2)

GE

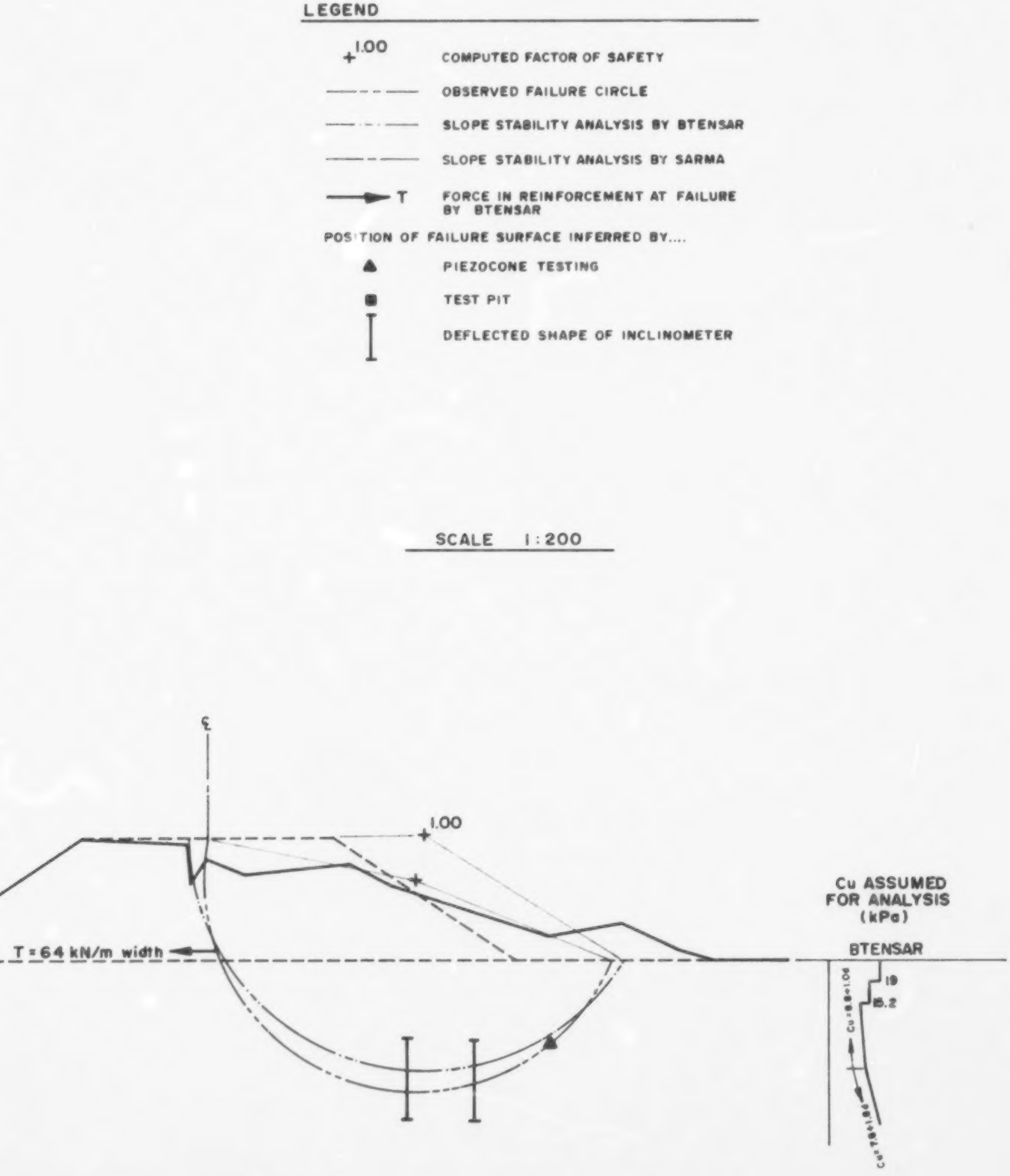
LEGEND
+1.00 COMPUTED FACTOR OF SAFETY
OBSERVED FAILURE CIRCLE
SLOPE STABILITY ANALYSIS BY BTENSAR
SLOPE STABILITY ANALYSIS BY SARMA
T FORCE IN REINFORCEMENT AT FAILURE BY BTENSAR
POSITION OF FAILURE SURFACE INFERRED BY....
PIEZOCONE TESTING
TEST PIT
DEFLECTED SHAPE OF INCLINOMETER
SCALE 1:200
℄
1.00
T = 64 kN/m width
Cu ASSUMED FOR ANALYSIS (kPa)
BTENSAR
19
15.2
Cu=8.8+1.0d
Cu=7.8+1.0d

AXIS PROFILE

CELL REINFORCED EMBANKMENT (Nº 3)

FIGURE 10.3 SUMMARY OF SLOPE STABILITY ANALYSES

Golder Associates - Université Laval

APPENDIX A

FINITE ELEMENT ANALYSIS

A.1 FINITE ELEMENT METHOD

Finite element analyses were carried out in order to consider the relative propagation of the overstressed zone under reinforced and unreinforced embankments. While this method cannot be used to predict failure, it gives an indication of the stress distribution and progressive movements under the embankments.

For the analyses, the program FINELM developed by Professor Clough of Duke University was used. Parameters for the foundation subsoil are the same as those used by Trak (1974) to analyze the behaviour of the test embankment, constructed to failure at St. Alban in 1972. For this study, an analysis of an unreinforced embankment was carried out and the results were compared with those for an embankment with reinforcement introduced at its base.

The finite element program adopted calculates stresses and displacements of both foundation and fill for arbitrary sequences of loading. A hyperbolic stress-strain relationship for the soil elements was employed.

An overstressed element is defined to be an element having a stress level greater or equal to 1, with the stress level (SL) defined as:

$$SL = \frac{(\sigma_1 - \sigma_3)}{(\sigma_1 - \sigma_3)\ \text{failure}}$$

The main parameters used are:

1. The coefficients of earth pressure at rest (K_o) proposed by Tavenas et al (1974) were used for the St. Alban site. These were obtained by hydraulic fracture techniques suggested by Bjerrum and Anderson (1972);

2. The shear strength of the foundation was taken to be the undrained strength at large strains (USALS) as given by Trak et al (1980) (Figure 4.4.);

3. Poisson's ratio for undrained conditions equal to 0.49 was assumed;

4. Young's moduli E for the foundation were taken equal to the average secant modulus E_s obtained from unconsolidated undrained triaxial tests;

5. Parameters for the geogrid were based on those provided by the manufacturer. In the computer model the geogrid was simulated by two 6 mm thick soil layers. Relevant assumed properties are shown in Table A.1.

	Foundation	Fill	Geogrid (6 mm thick)
Unit Weight (kN/m^3)	15 to 19	17.2-18.1	3.0
Friction angle (degrees)	-	44	44
Initial tangent modulus (kPa)	2000 to 24000	20270	2.3×10^6
Shear strength (kPa)	10 to 50	-	2.3×10^5

Table A.1 Typical Values for Finite Element Analysis

The deformed meshes for the reinforced and the unreinforced embankments are shown on Figure A-1. This mesh for the reinforced embankment is made up of 289 elements and 326 nodal points while the mesh for the reinforced embankment consists of 349 elements and 390 nodal points.

A.2 RESULTS OF THE ANALYSES

The results of the calculations obtained from the finite element analyses are presented in the following sections. Section A.2.1 present the calculated propagation of failure under the unreinforced and reinforced embankments; while Sections A.2.2 and A.2.3 present a comparison of the computed and observed pore pressures and displacements in the foundation. For the purpose of the comparisons, the test embankments have been compared at similar heights. Because of the difference in unit weight of the fill, the height does not accurately reflect the surcharge on the foundation. This has been considered in the main body of the report. Where it is significant for the comparisons made in this appendix, comment is included.

A.2.1 DISTRIBUTION OF THE OVERSTRESSED ZONE

The analyses indicated that the reinforcement has a beneficial effect in restricting the propagation of failure in the foundation. For the same surcharge, the reinforced embankment had a smaller overstressed zone. It was found that at centreline surcharges of 105 kPa and 94 kPa for the reinforced and the unreinforced embankment respectively, the failure zone was extensively developed to approximately the same extent under both embankments (Figure A-2). From the same figure, the stabilizing effect of the berm is apparent.

A.2.2 PORE PRESSURES

In the program used by Trak (1974), the formula proposed by Henkel (1960) for the prediction of pore pressure was modified to account for observed pore pressure response at stresses beyond the preconsolidation pressure (σ_p'). The method assumes the intermediate principal stress to equal the minor principal stress (Leroueil et al (1978)). Following this empirical approach and taking account of the preconsolidation pressure of the St. Alban clay (Figure 4.3), the excess pore pressure was calculated from:

$$\Delta u = \frac{\Delta\sigma_1 + 2\Delta\sigma_3}{3} \quad \text{for } \sigma_1' < \sigma_p' \qquad (1)$$

$$\Delta u = \Delta\sigma_1 \quad \text{for } \sigma_1' \geq \sigma_p' \qquad (2)$$

The excess pore pressures calculated at 3 m depth under the centreline at element 105 (Figure A-1) for the reinforced and the unreinforced embankments are presented in Figure A-3. The observed pore pressures at the same location as measured by piezometer PN-15 are also shown in the same figure. The general trend of the curves is very similar; the calculated pore pressures increase in a similar manner to those recorded in the field.

A.2.3 DISPLACEMENTS

The calculated displacements of the nodal points for the unreinforced embankment are shown on Figure A-4a, while the corresponding values for the reinforced embankment are shown on Figure A-4b. The comparison is made for surcharges that allowed the same propagation of failure in the reinforced and unreinforced embankments, as shown in Figure A-2.

The displacements at a similar stage of failure propagation appear to be quite similar and this will be discussed further in the following sections.

A.2.3.1 Vertical Displacements

The observed settlements recorded at settlement plates SP-1 and SP-9, at 1.5 m from the toe and at the centreline, respectively, have been plotted on Figure A-5. The vertical displacement computed at these locations (nodal points 182 and 189, respectively) are also presented on the same figure.

At the toe, the calculation indicated upward heave in both cases, with the heave of the unreinforced embankment greater than that of the other embankment. These calculated movements were significant only after the embankment height exceeded about 3.4 m and 4.0 m in the case of the unreinforced and the reinforced embankments, respectively.

Under the centreline, the calculated settlements are higher for the unreinforced embankment. As calculated at the toe, the displacement at the centreline is less for the reinforced embankment than for the unreinforced embankment at the same height of fill. The rate of settlement with respect to the height of the embankment again shows a marked increase at heights of 3.4 m and 4.0 m for the unreinforced and the reinforced embankments, respectively.

Comparing the calculated vertical displacements with the observations made, it appears that the calculations consistently underestimate the magnitude of settlement, even to the extent of predicting heave instead of settlement, close to the toe of the embankment.

A.2.3.2 Horizontal Displacements

The horizontal displacements of nodal points 126 and 100 correspond to the readings of inclinometer IN-1 at 2.4 m depth and inclinometer IN-2 at 4.0 m depth. The horizontal displacements calculated at these nodal points, together with the observations made in the inclinometer installations, are shown in Figure A-6. The computed values show a significant reduction in horizontal displacement under the reinforced embankment. In the test embankments the geocell reinforced embankment showed the greatest horizontal displacement at the same height. If the embankments are compared at the same surcharge, as in Figure 8.58 in the main report, it can be seen that the strip reinforced embankment also showed greater displacement compared to the unreinforced (control) embankment.

LIST OF REFERENCES

BJERRUM, L., ANDERSON, K.H. (1972). In Situ Measurement of Lateral Pressures in Clay, Proc. Eur. Conf. Soil Mech. Found. Eng., Madrid, Spain 1, pp.11-20.

HENKEL, O.J. (1960). The Shear Strength of Saturated Remoulded Clays, Proceedings, ASCE Specialty Conference on Shear Strength of Cohesive Soils, Boulder, pp 533-544.

TRAK, B. (1974). Contribution a l'etude de la stabilite a court terme des remblais sur fondations argileuses Master's Thesis, Department of Civl Engineering, Universite Laval, Quebec.

TRAK, B., LA ROCHELLE, P., TAVENAS, F., LEROUEIL, S., Roy, M. (1980). A New Approach to the Stability Analysis of Embankments on Sensitive Clays, Canadian Geotechnical Journal Vol. 17, No. 4, pp 526-544.

a) DEFORMED MESH OF UNREINFORCED EMBANKMENT AT SURCHARGE OF 94 kPa

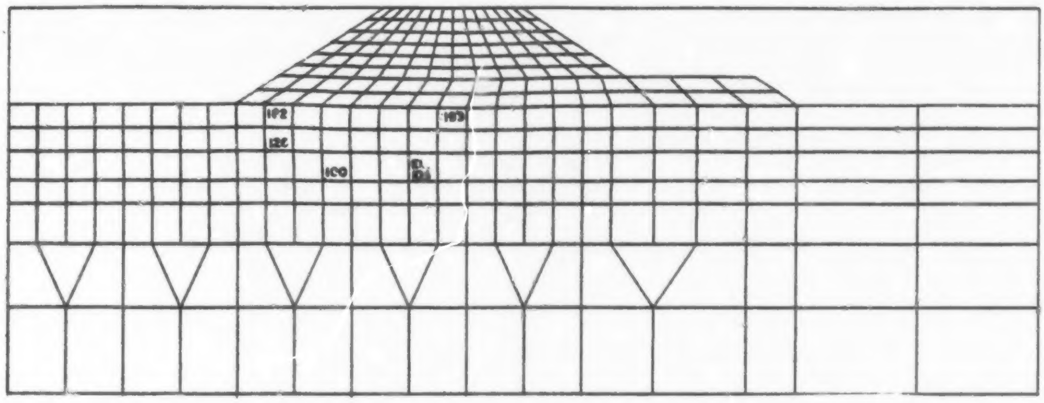

b) DEFORMED MESH OF REINFORCED EMBANKMENT AT SURCHARGE OF 105 kPa

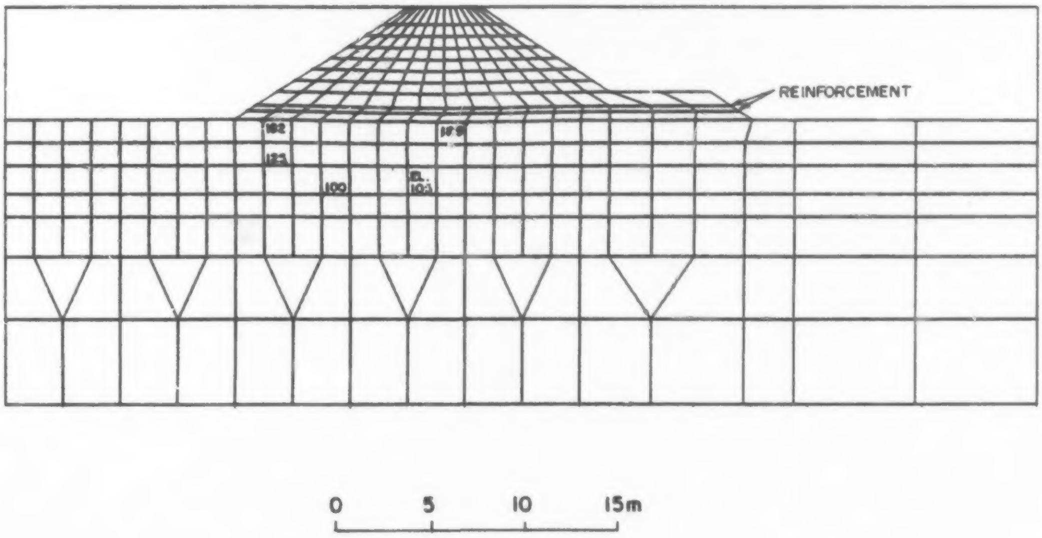

FIGURE A-1 FINITE ELEMENT MESHES

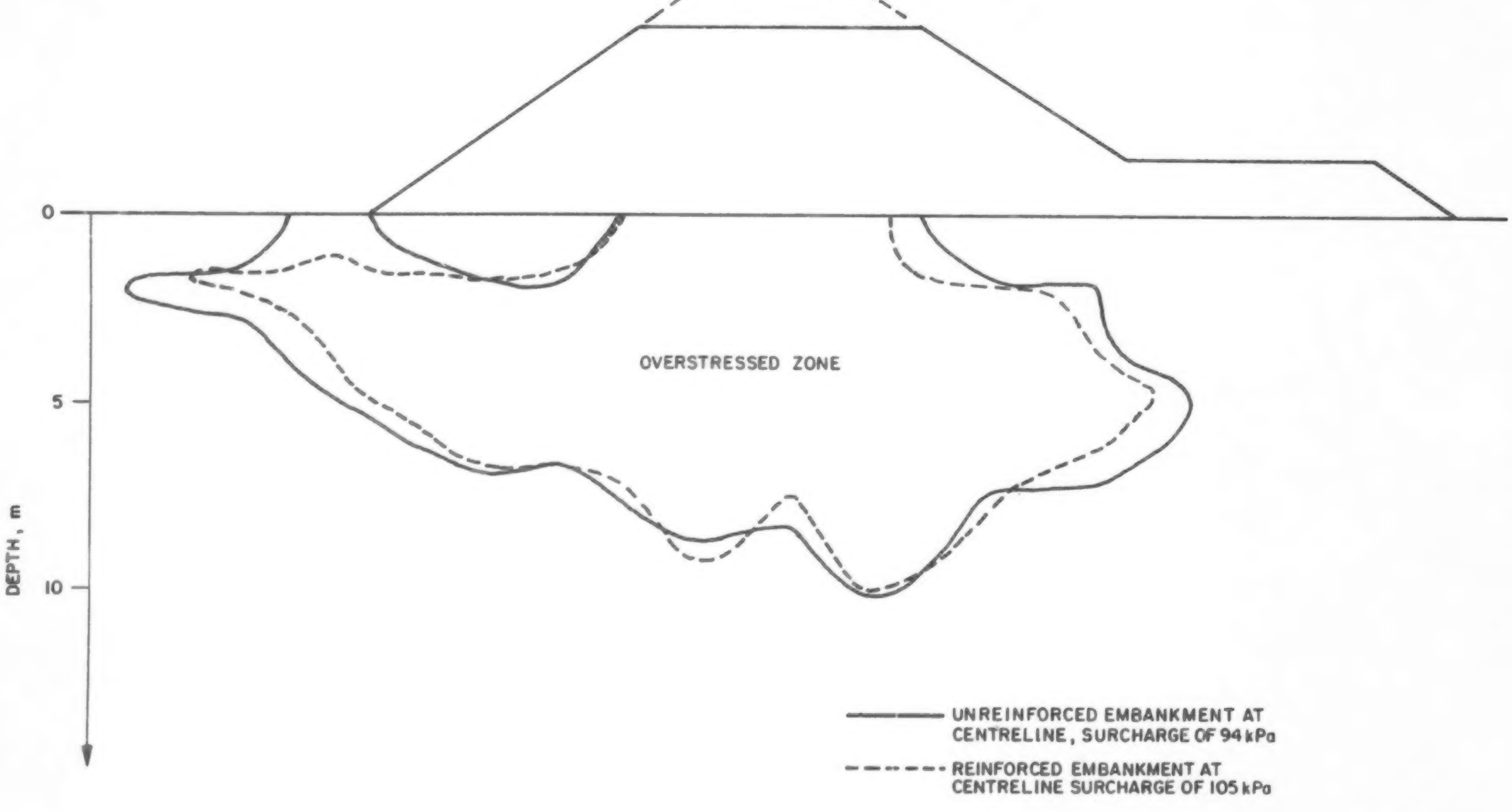
0
5
10
DEPTH, m
OVERSTRESSED ZONE
UNREINFORCED EMBANKMENT AT CENTRELINE, SURCHARGE OF 94 kPa
REINFORCED EMBANKMENT AT CENTRELINE SURCHARGE OF 105 kPa

FIGURE A-2 COMPARISON OF CENTRELINE SURCHARGES AT FAILURE

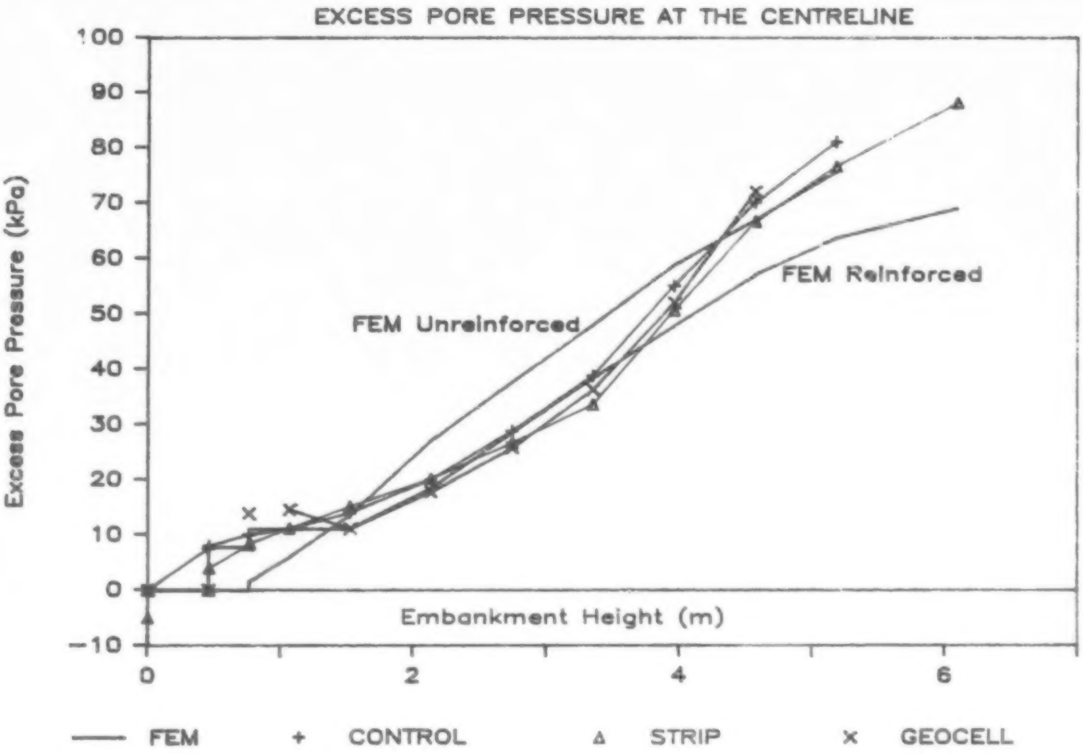

FIGURE A-3 PORE PRESSURES UNDER EMBANKMENT CENTRELINE a) DISPLACEMENT OF NODAL POINTS, UNREINFORCED EMBANKMENT

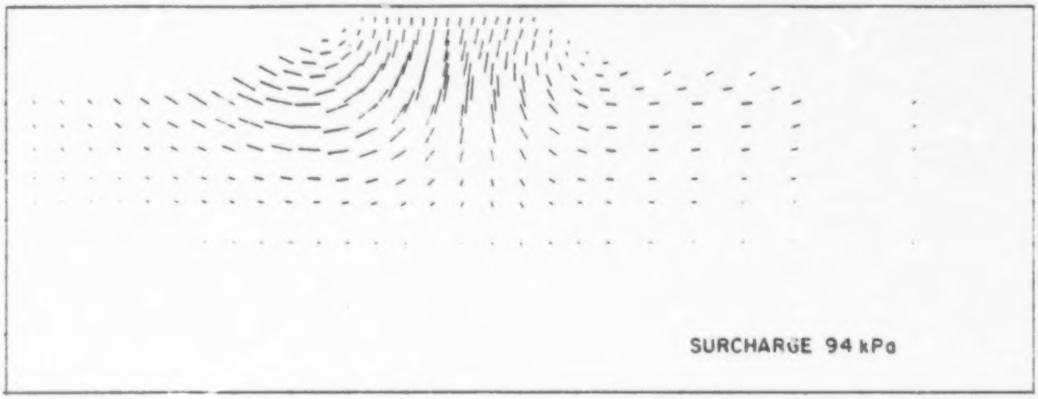

b) DISPLACEMENT OF NODAL POINTS, REINFORCED EMBANKMENT

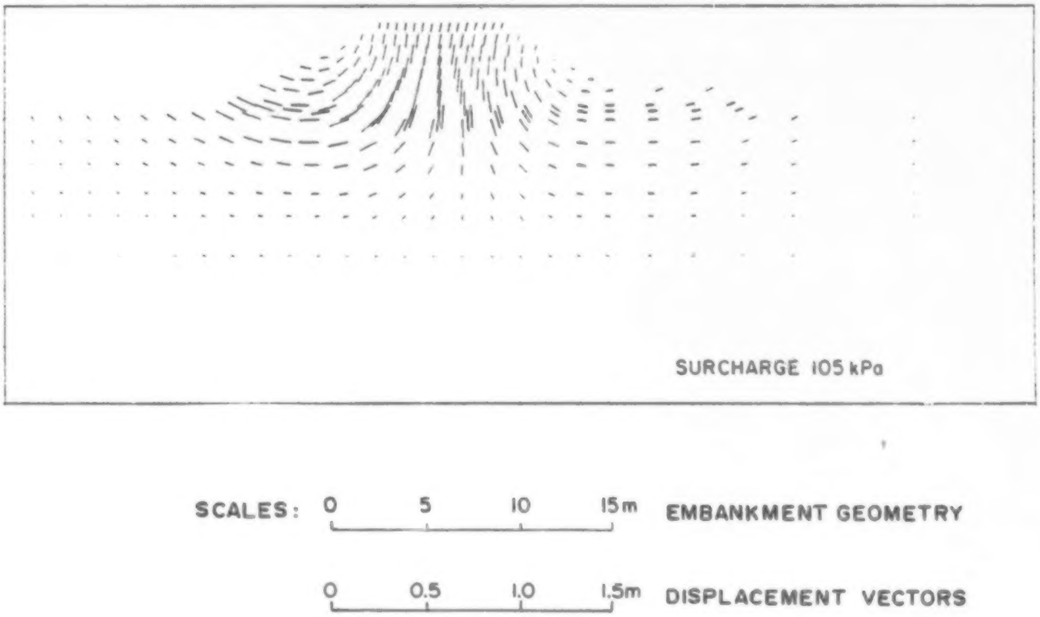

FIGURE A-4 DISPLACEMENT VECTORS AT FAILURE

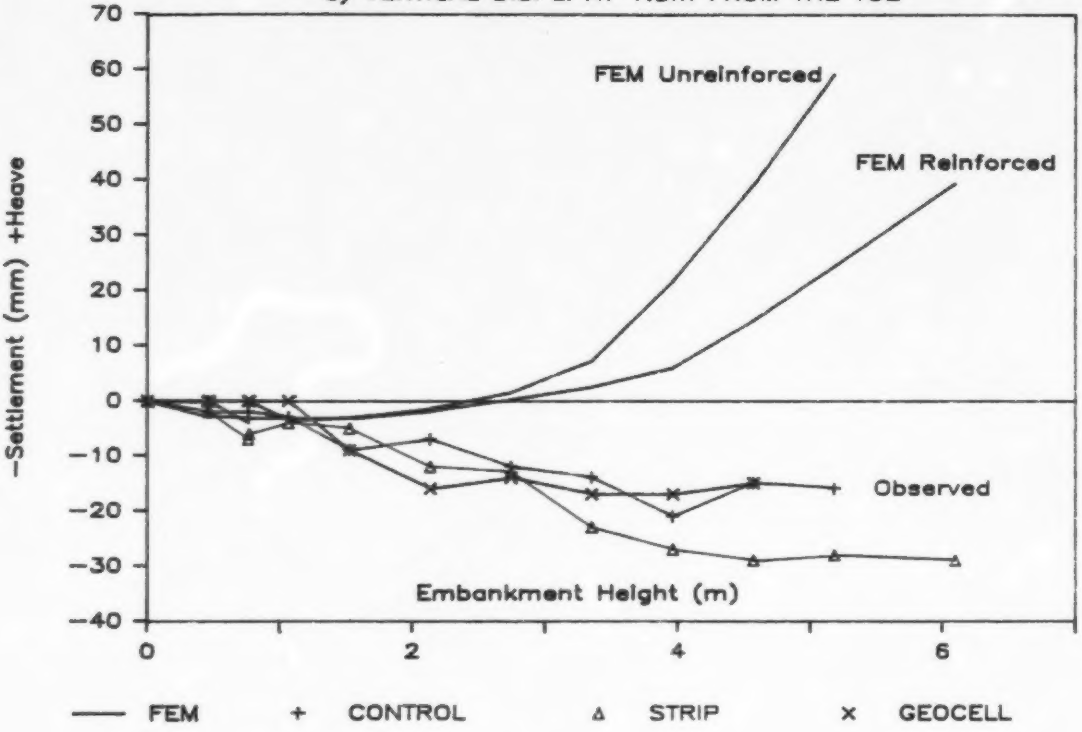
a) VERTICAL DISPL. AT 1.5m FROM THE TOE

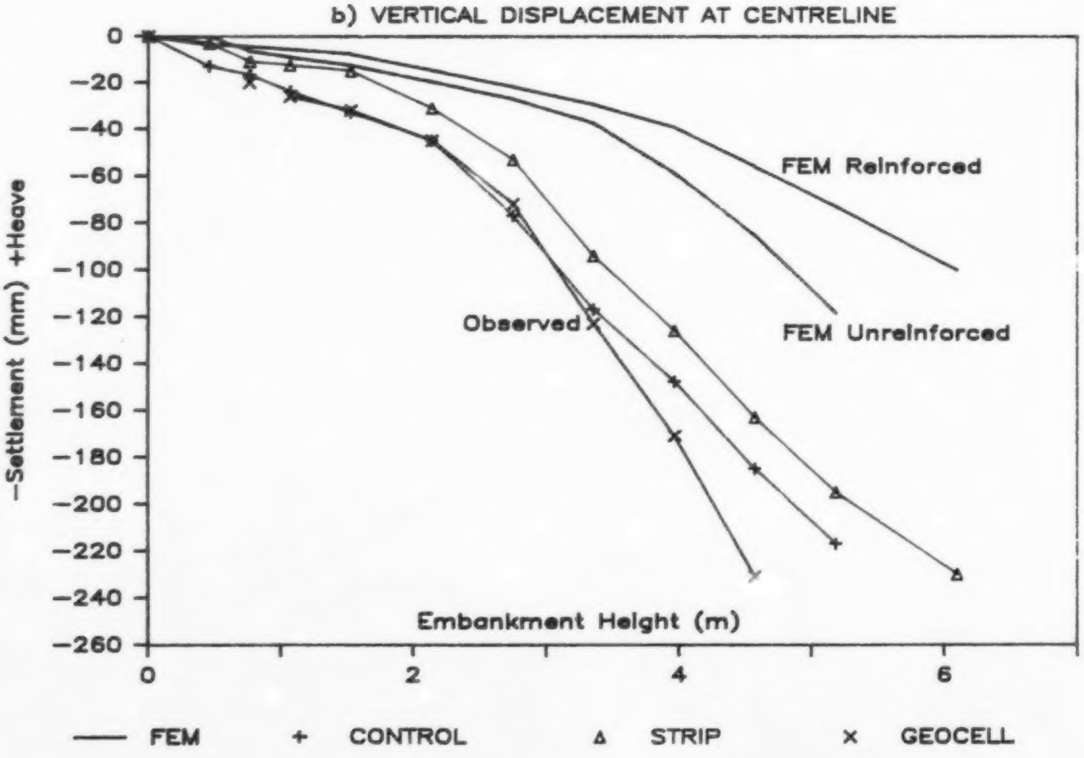
b) VERTICAL DISPLACEMENT AT CENTRELINE

FIGURE A-5 VERTICAL DISPLACEMENTS

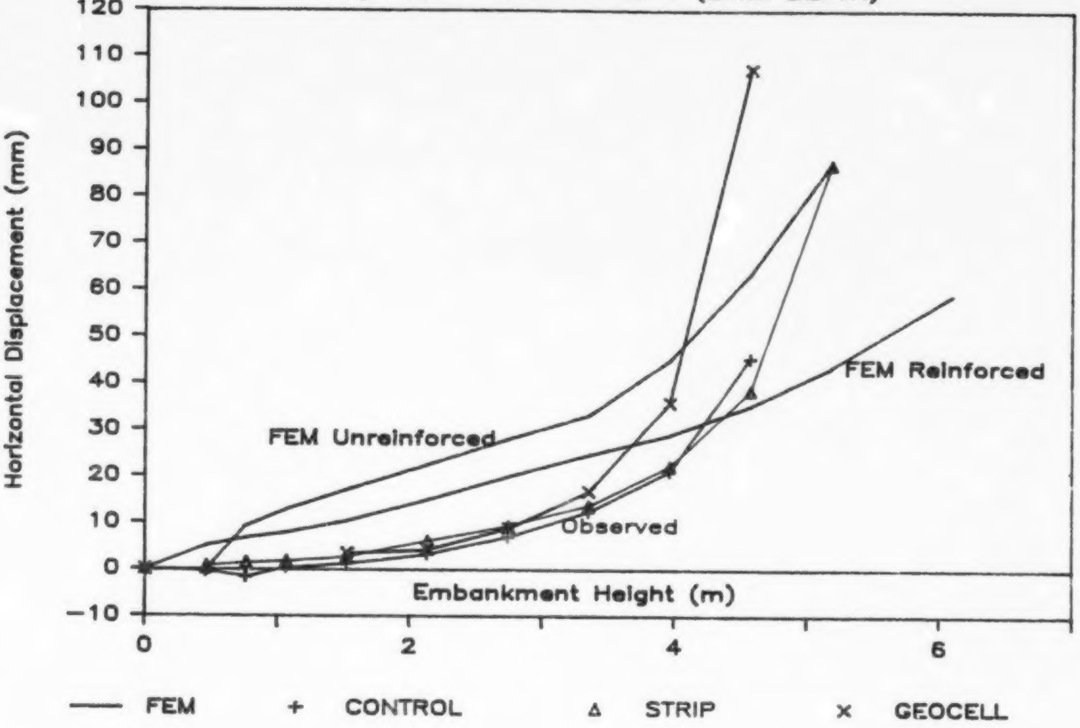
a) HORIZ. DISPL. AT IN-1 (2.4m DEPTH)

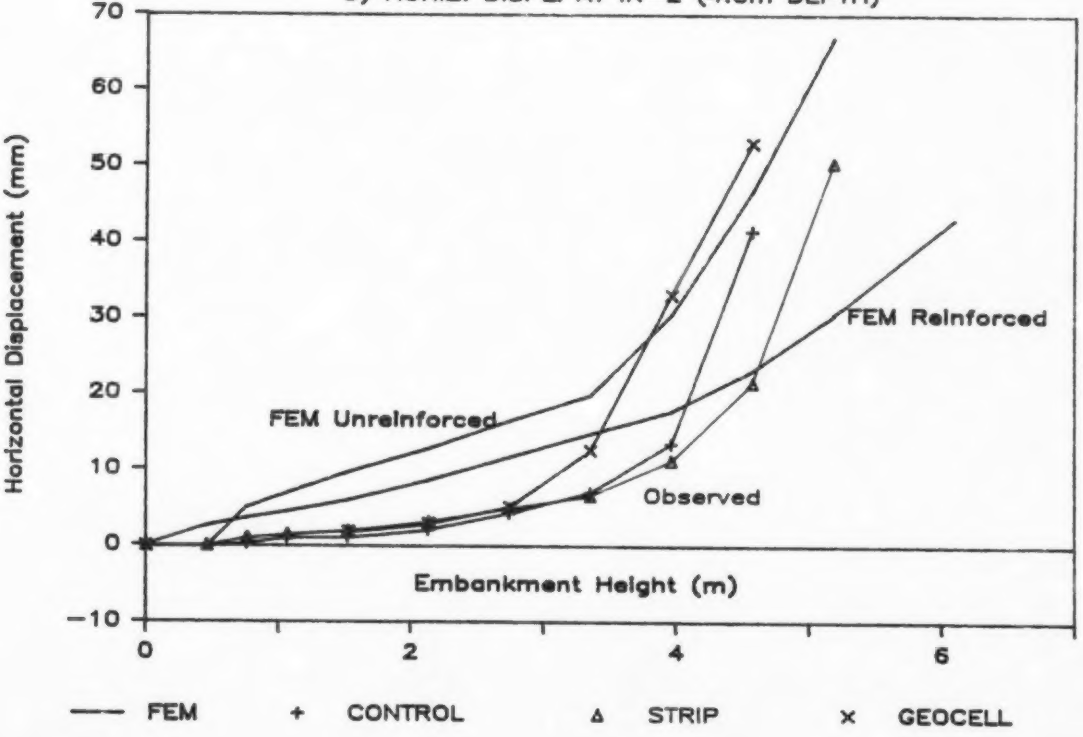
b) HORIZ. DISPL. AT IN-2 (4.0m DEPTH)

FIGURE A-6 HORIZONTAL DISPLACEMENTS

APPENDIX B

TENSAR LOAD CELL

The Tensar load cell can be separated into two basic components; the clamp and the load bridges. The Tensar clamp is illustrated on Figure A-1 and on a cross-section A-A shows that a clamp is manufactured from two strips of mild steel which have a central stepped rectangular groove and are bolted together.

The stepped groove was designed to accommodate the transverse bar and the longitudinal ribs of the geogrid, together with a moulding agent. The moulding agent would fill all spaces between the Tensar SR-2 and the clamp and when hardened, would form an effective connection.

The sequence of events for the preparation of a Tensar clamp was primarily controlled by the short setting time of the moulding agent. Consequently, all the components of the clamp were prepared before the moulding agent is mixed.

The length of Tensar was cut to the predetermined length and its end fitted into the deeper part of the groove within the clamp. Three dummy wooden packers were to be made and fitted at the locations where the load bridges were to be positioned.

All bolts and internal surfaces of the two halves of the clamp was greased. This enabled the clamp to be re-used.

When this preparatory work has been completed, a 0.45 kg container of the moulding agent was mixed and then placed in the two grooves. This was most easily placed by extruding from a small icing bag. The Tensar bar was then placed on top of the moulding agent followed by the upper half of the clamp. The connecting bolts were then fixed to extrude excess moulding agent from all sides of the clamp.

During this stage of tightening the bolts, care had to be taken to ensure that the bolts on the bridge side of the clamp were tightened up hard, whereas the bolts on the Tensar side were sufficiently tightened to bring the edges of the clamp into contact with the ribs of the Tensar SR-2.

The clamp was left for about 24 hours during which the moulding agent hardened. After this period, the wooden packers were removed, the excess moulding agent removed and the load bridges test fitted.

At this stage, the load cell was complete and suitable for installation.

The moulding agent that was found to be most satisfactory is Devcon Plastic Steel. Figure A-3 shows isochronous curves for both the plastic steel and the Tensar SR-2 rib. Though the tests were conducted at different temperatures, the diagram illustrates that the plastic steel is less creep susceptible than the Tensar bars. Consequently, the plastic steel would not cause load shedding.

A load bridge is illustrated on Figure A-2 and shows that it is a 140 mm long instrumented dumb-bell shaped piece of 6.35 mm thick stainless steel.

Two Intertechnology T-Rossette electrical resistance strain gauges (Type CEA-06-250UT-350) were mounted on both sides of the dumb-bell and wired to form a full wheatstone bridge circuit. The gauges were mounted with a 100 per cent epoxy resin (Type M-Bond AE-10) in accordance with the manufacturer's specifications. These were then hermetically sealed with successive coatings of butyl rubber, rubber sheet and aluminium foil (Type M-Coat F).

Specifications of the resistance strain gauges and the protective package are given in Figure A-4.

After the resistance strain gauges had been mounted and sealed, each load bridge was calibrated using a certified tensile testing machine.

The load bridge was secured in the loading frame using two pin jointed connectors. These eliminated the transfer of bending stresses to the bridge. The bridge was then extended at a slow constant rate of strain. During this test, the readings of the tensile loading machine and the load bridge were recorded and compared. The calibration curves generated for bridges 1 to 4, 6 and 7 are illustrated on Figure A-5.

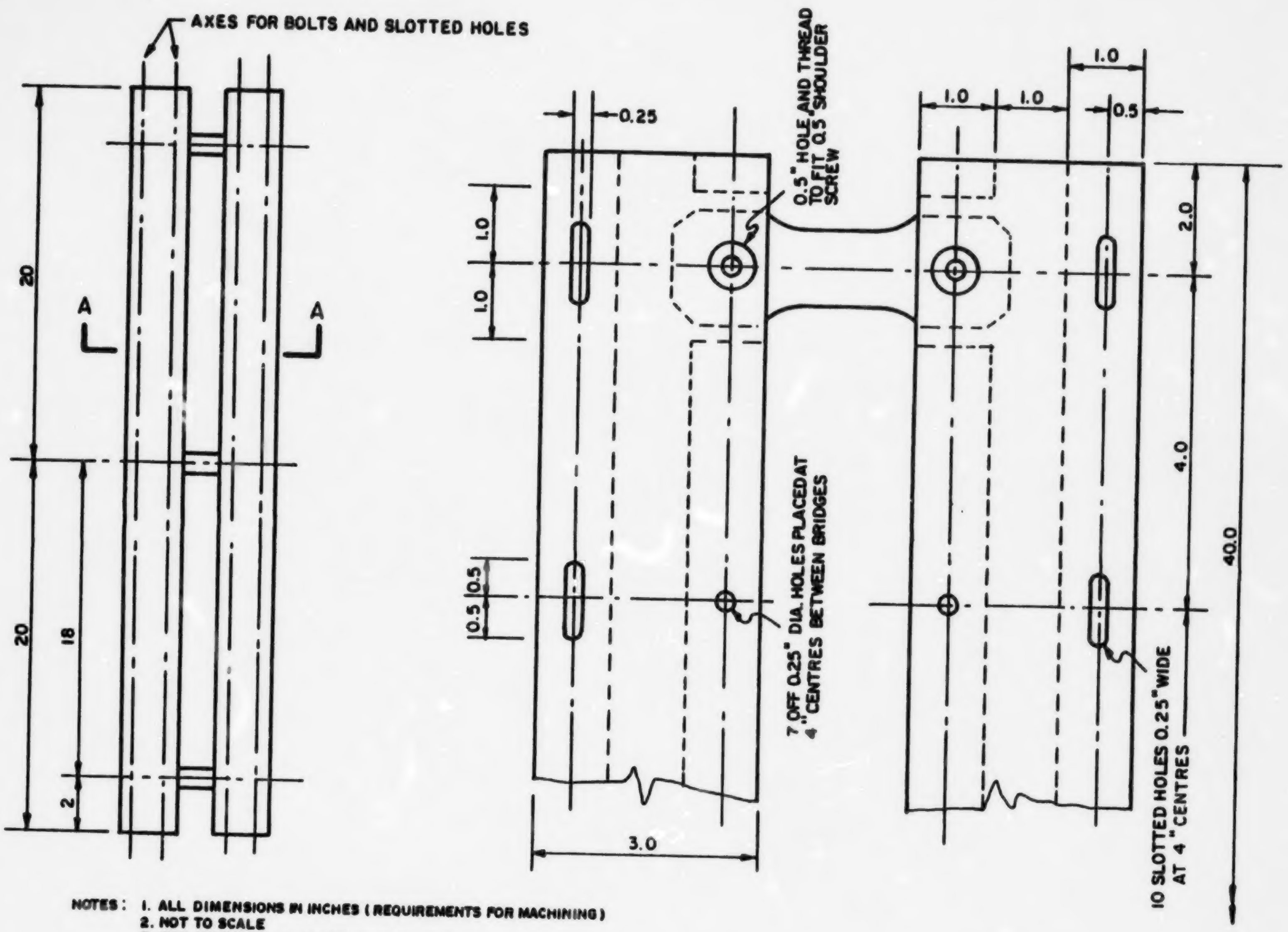
AXES FOR BOLTS AND SLOTTED HOLES
A
A
20
20
18
2
0.25
1.0
1.0
0.5
0.5
3.0
0.5" HOLE AND THREAD TO FIT 0.5" SHOULDER SCREW
7 OFF 0.25" DIA. HOLES PLACED AT 4" CENTRES BETWEEN BRIDGES
1.0
1.0
1.0
0.5
2.0
4.0
40.0
10 SLOTTED HOLES 0.25" WIDE AT 4" CENTRES

NOTES :
1. ALL DIMENSIONS IN INCHES (REQUIREMENTS FOR MACHINING)
2. NOT TO SCALE
3. FOR SECTION A-A, REFER TO FIGURE B-2

FIGURE B-1 ASSEMBLY OF THE TENSAR LOAD CELL

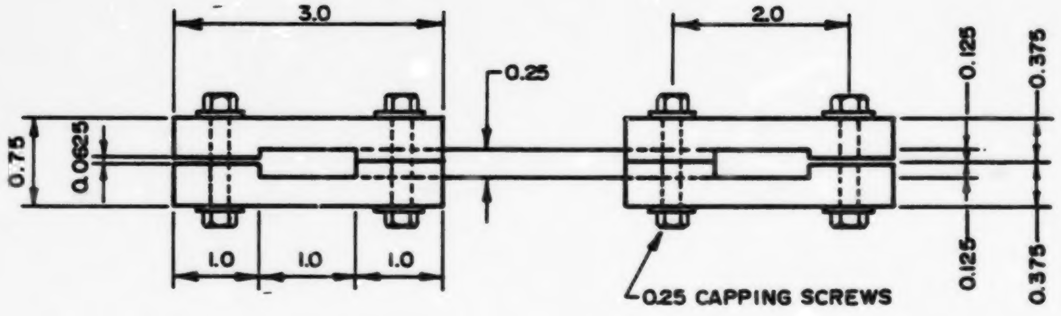

SECTION A-A

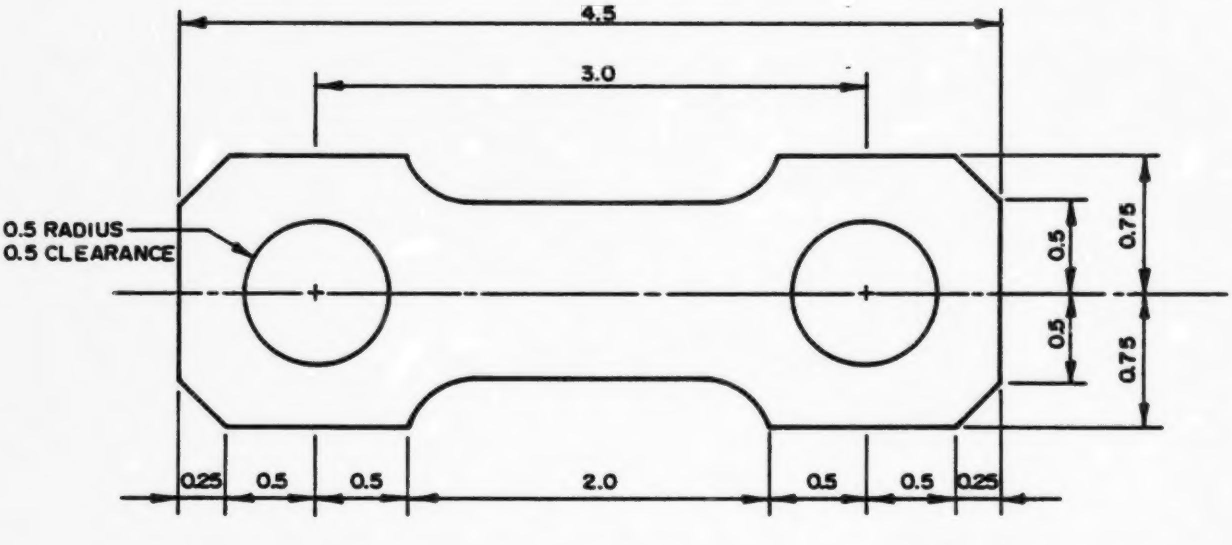

MATERIAL : 0.25 THICK STAINLESS STEEL.

NOTES: 1. ALL DIMENSIONS IN INCHES (REQUIREMENTS FOR MACHINING).
2. NOT TO SCALE.

FIGURE B-2 PLAN OF INSTRUMENTED BRIDGE

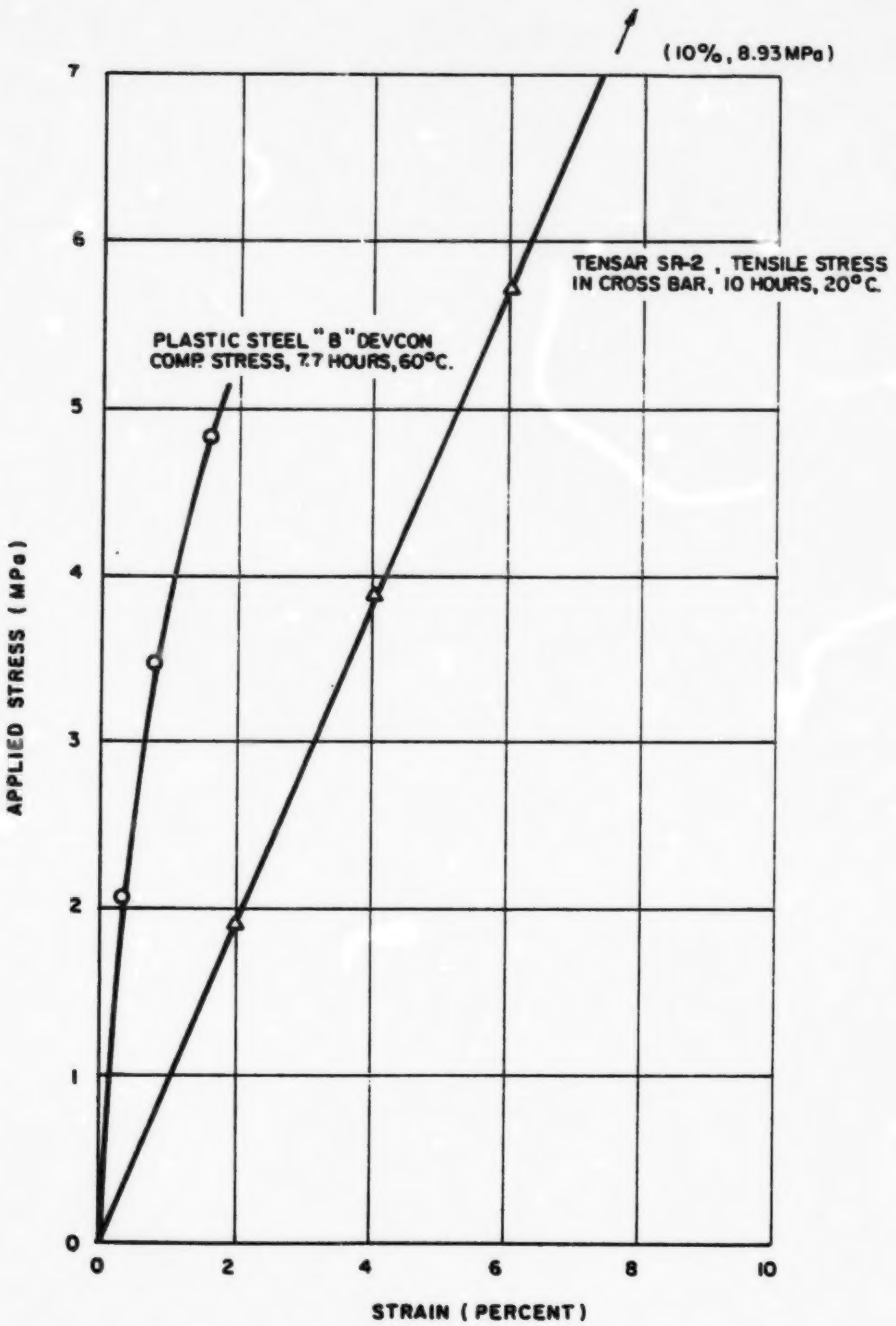

FIGURE B-3 ISOCHRONOUS CURVES FOR TENSAR SR-2 AND PLASTIC STEEL "B" DEVCON

M-COAT DESCRIPTION AND APPLICATIONS	CURE REQUIREMENTS	SHELF LIFE	OPERATING TEMP. RANGE
M-COAT F Kit of selected materials easily applied in various combinations. Provides environmental and mechanical protection. Particularly well-suited to field applications where conditions are not ideal. Typical applications include pipelines, tunnels, bridges, reinforcement bars in concrete structures, heavy machinery, ships, aircraft, motor vehicles, and pressure vessels. **Kit Packaging:** 12 pcs [3-3/4 in (*95 mm*) square, 3/16 in (*4.8 mm*) thick] each M-Coat FB Butyl Rubber Sealant and M-Coat FN Neoprene Rubber Sheets 1 roll [0.003 in (*0.08 mm*) thick x 2 in (*50 mm*) wide x 20 ft (*6 m*) long] M-Coat FA Aluminum Foil Tape 2 brush-cap bottles [1/2 oz (*15 ml*) each] M-Coat BT Air-Drying Nitrile Rubber Coating 1 M-Coat FT 4 x 4 x 0.003 in (*101 x 101 x 0.08 mm*) Teflon Film **Bulk Packaging:** M-Coat FB-2 Butyl Rubber Sealant — 25 pcs M-Coat FN-2 Neoprene Rubber Sheets — 25 pcs M-Coat FA-2 Aluminum Foil Tape — 20 ft (*6 m*) roll M-Coat BT-2 Air-Drying Nitrile Rubber Coating — 4 brush-cap bottles [1 oz (*30 ml*) each]	No mixing or curing required.	2 yr at +75°F (+24°C)	SHORT TERM -70 to +250°F (*-55 to +120°C*) LONG TERM -20 to +175°F (*-30 to +80°C*)

GAGE LISTINGS

GAGE PATTERN (Actual Size) Grids are Vertical Except as Noted	GAGE DESIGNATION Insert Desired S-T-C No. in Spaces Marked XX	† Stock Status	RES. IN OHMS	LIST PKG. PRICE (Five Gages)	‡DIMENSIONS IN INCHES / *MILLIMETRES* — Gage Length	Overall Length	Grid Width	Overall Width	Matrix Length	Matrix Width
250UT 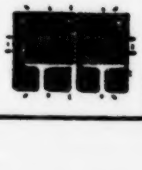	CEA-XX-250UT-120 CEA-XX-250UT-350	A B	120 ±0.4% 350 ±0.4%		0.250 ES *6.35*	0.450 CP *11.43*	0.290 ES *7.37*	0.650 CP *16.51*	0.550 *14.0*	0.740 *18.8*
					Notes: General-purpose two-element 90° "tee" rosette. Exposed solder tab area is 0.13" × 0.10" (3.3mm x 2.5mm).					

ES=Each Section
CP=Complete Pattern

FIGURE B-4

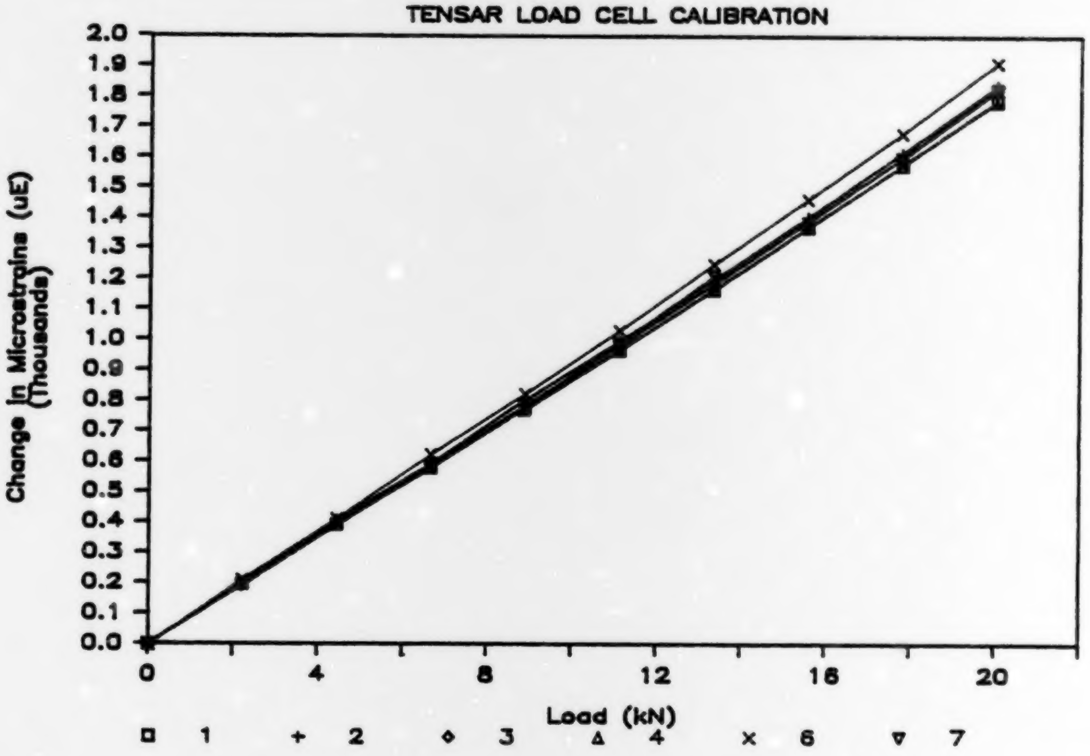

FIGURE 8-5 TENSAR LOAD CELL CALIBRATION CURVES